10:10:54 OCA PAD AMENDMENT - PROJECT HEADER INFORMATION 01/21/92

Active

Project #: E-16-622 Cost share #: E-16-340 Rev #: 9
Center # : R6653-0A0 Center shr #: F6653-0A0 OCA file #:
Work type : RES
Contract#: NAG-1-939 Mod #: ADMIN. Document : GRANT
Prime #: Contract entity: GTRC

Subprojects ? : N CFDA: 43.002
Main project #: PE #: N/A

Project unit: AERO ENGR Unit code: 02.010.110
Project director(s):
CALISE A J AERO ENGR (404)894-7145
HODGES D H AERO ENGR (404)-

Sponsor/division names: NASA / LANGLEY RESEARCH CTR, VA
Sponsor/division codes: 105 / 001

Award period: 881201 to 920331 (performance) 920331 (reports)

Sponsor amount	New this change	Total to date
Contract value	0.00	346,292.00
Funded	0.00	346,292.00
Cost sharing amount		38,477.00

Does subcontracting plan apply ?: N

Title: OPTIMAL GUIDANCE LAW DEVELOPMENT FOR AN ADVANCED LAUNCH SYSTEM

PROJECT ADMINISTRATION DATA

OCA contact: Ina R. Lashley 894-4820

Sponsor technical contact

DR DANIEL D MOERDER, GCD M/S 161
(804)864-6495

NASA LANGLEY RESEARCH CENTER
HAMPTON VA 23665-5225

Sponsor issuing office

ANNE S REED OR BEVERLY THOMAS-BURSE
(804)864-2417

CONTRACTS BRANCH
NASA LANGLEY RESEARCH CENTER
HAMPTON VA 23665-5225

Security class (U,C,S,TS) : U ONR resident rep. is ACO (Y/N): N
Defense priority rating : N/A N/A supplemental sheet
Equipment title vests with: Sponsor GIT X
NONE PROPOSED.
Administrative comments -
ADMIN MOD TO CORRECT DELIVERABLE SCHEDULE BY DELETING SEMI-ANNUAL REPORT DUE 12/15/91.

GEORGIA INSTITUTE OF TECHNOLOGY
OFFICE OF CONTRACT ADMINISTRATION

NOTICE OF PROJECT CLOSEOUT

Closeout Notice Date 06/22/92

Project No. E-16-622 Center No. R6653-0A0

Project Director CALISE A J School/Lab AERO ENGR

Sponsor NASA/LANGLEY RESEARCH CTR, VA

Contract/Grant No. NAG-1-939 Contract Entity GTRC

Prime Contract No.

Title OPTIMAL GUIDANCE LAW DEVELOPMENT FOR AN ADVANCED LAUNCH SYSTEM

Effective Completion Date 920331 (Performance) 920331 (Reports)

Closeout Actions Required:	Y/N	Date Submitted
Final Invoice or Copy of Final Invoice	Y	
Final Report of Inventions and/or Subcontracts	Y	
Government Property Inventory & Related Certificate	Y	
Classified Material Certificate	N	
Release and Assignment	N	
Other	N	

CommentsBILLING VIA LINE-OF-CREDIT.

Subproject Under Main Project No.

Continues Project No.

Distribution Required:

Project Director	Y
Administrative Network Representative	Y
GTRI Accounting/Grants and Contracts	Y
Procurement/Supply Services	Y
Research Property Managment	Y
Research Security Services	N
Reports Coordinator (OCA)	Y
GTRC	Y
Project File	Y
Other	N
	N

NOTE: Final Patent Questionnaire sent to PDPI.

Optimal Guidance Law Development for an Advanced Launch System

INTERIM PROGRESS REPORT

1 December, 1988 – 30 May, 1989

June 1989

Research Supported by NASA Langley Research Center

NASA Grant No. NAG-1-939

Principal Investigators: Anthony J. Calise & Dewey H. Hodges

Research Assistants: Martin S. Leung & Robert R. Bless

NASA Grant Monitor: Dr. Daniel D. Moerder

Georgia Institute of Technology
School of Aerospace Engineering
Atlanta, GA 30332-0150

SUMMARY OF RESEARCH ACCOMPLISHMENTS

Singular Perturbation Analysis

Research during this period has been progressing along two parallel fronts. In the first area we have been examining reduced-order models that are suitable for singular perturbation analysis of optimal launch trajectories. What distinguishes this work from earlier studies on optimal aircraft trajectories is that the small flight path angle approximation is no longer applicable. In particular, we have been considering the dynamics associated with a single-stage vehicle and the problem of optimizing the flight path angle history which minimizes fuel consumption. Thrust is assumed fixed. This reduces the problem to a three-state model in energy, altitude and mass dynamics. While this problem is not analytically tractable, we have uncovered a surprising result. There are two solution possibilities which satisfy the first-order necessary condition on the control, either $\gamma=\pm\pi/2$ or an intermediate solution. We have been able to prove that only the $\gamma=\pm\pi/2$ is a candidate minimizing solution. However, when the problem is further reduced to a two-state problem in energy and mass dynamics, the problem becomes analytically tractable and the optimal profile is one with an intermediate flight path angle history. Through simulation of the full-order dynamics we are able to demonstrate that this solution is superior to a vertical climb solution, which gives rise to a contradiction since one would expect that the conclusion based on the third-order model should be superior. However, further investigation of the third-order model has uncovered the fact that the velocity hodograph is not convex, and that this model allows a relaxed controller whose average behavior is superior and one that approximates flight with an intermediate flight path angle history.

The initial interest in this third-order model was motivated by the parallel research effort in numerical optimization based on finite elements in time. However, based on our current understanding of this model, we have recommended that the finite element based approach use a four-state model in which angle-of-attack is the fundamental control variable.

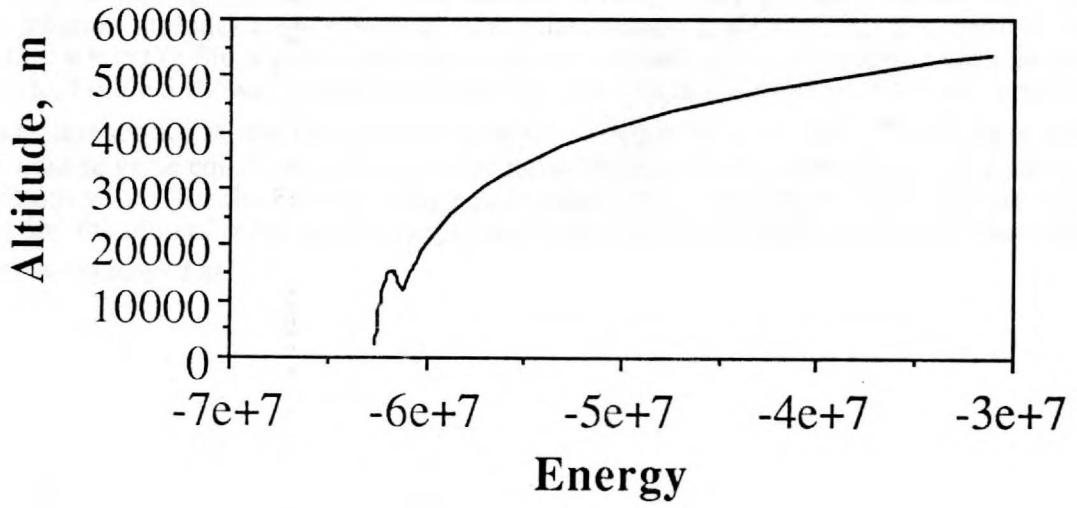

Fig. 1: Reduced solution altitude profile versus energy

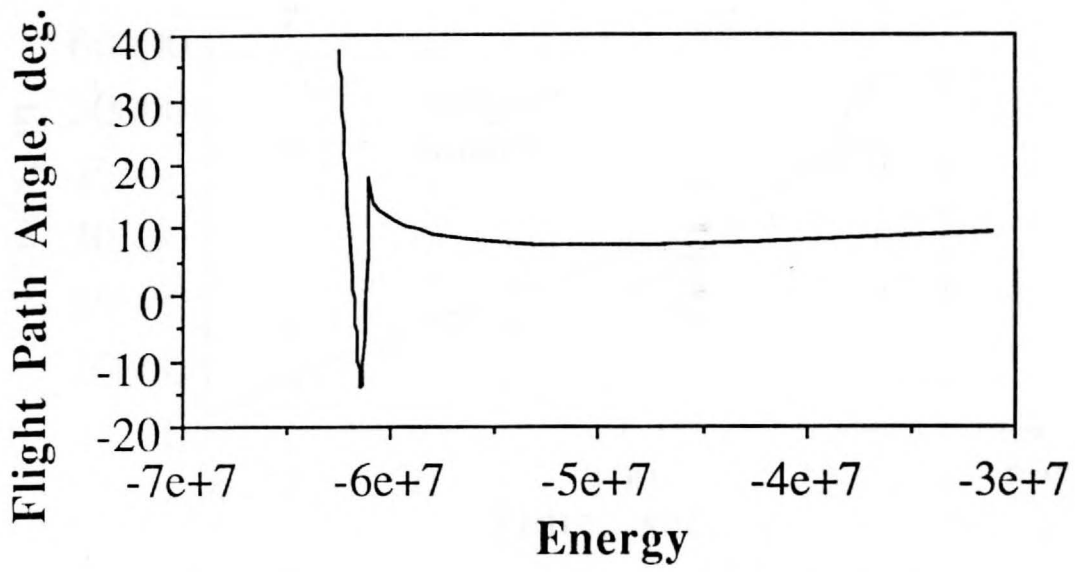

Fig. 2: Reduced solution flight path angle profile versus energy

Figures 1 and 2 show the reduced solution for altitude and flight path angle as a function of vehicle energy. These results were obtained using aerodynamic and propulsion data for the Saturn 1B launch vehicle. Figures 3 and 4 illustrate simulated trajectories for a guided solution derived using the two-state model dynamics. The simulated vehicle dynamics are based on a four-state model, which includes flight path angle dynamics. (It should be noted that the dynamic pressure is extremely high over a portion of the trajectory, and that the trajectory is also unrealistic since we are treating the Saturn 1B as if it were a single-stage vehicle at this point.) Figure 3 compares the guided altitude profile with the actual optimal profile for the four-state model. Figure 4 gives a similar comparison for the flight path angle profiles. The difference in final mass for a guided solution versus the optimal solution is negligible. It is interesting to note that for these data, the guided solution includes a short period where the altitude is decreasing. The optimal solution shows that when the flight path angle dynamics are accounted for, the optimal altitude profile is monotonic. Figure 5 shows the velocity hodograph for a typical altitude and velocity condition for the three-state model, where the lack of convexity is apparent at $\gamma=\pm\pi/2$. This occurs when the altitude costate value equals zero. The implication of this fact is that when the actual altitude is near its optimum value (for the current energy and mass), then to maintain a low altitude rate while maximizing the ratio of mass rate to energy rate, it is desirable to rapidly switch (chatter) the flight path angle between $\pm\pi/2$.

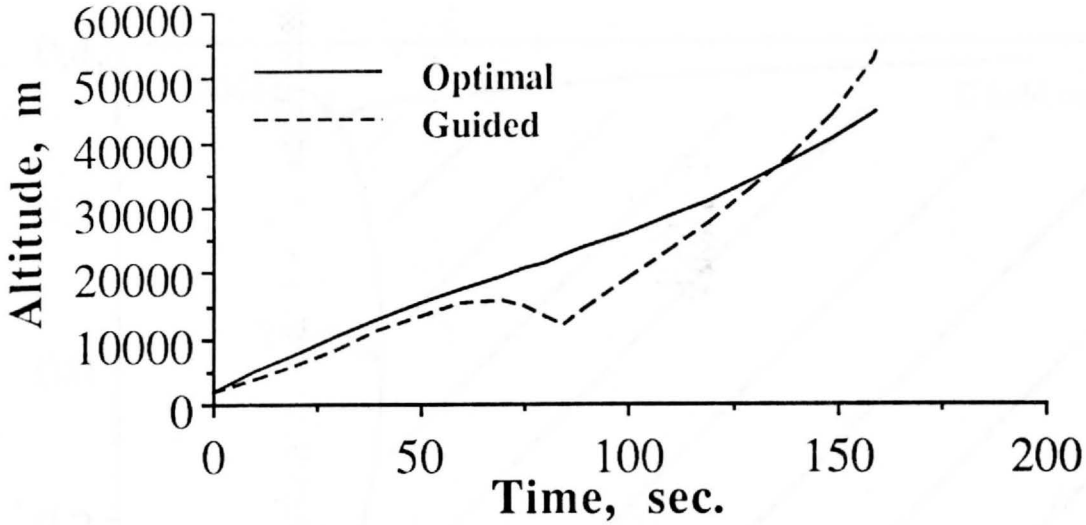

Fig. 3: Comparison of guided and optimal altitude profiles

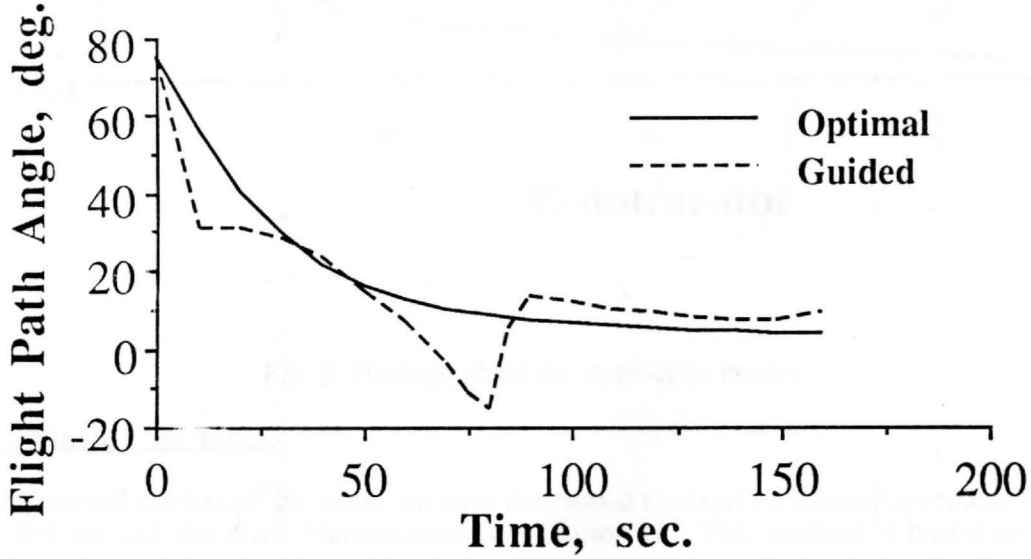

Fig. 4: Comparison of guided and optimal flight path angle profiles

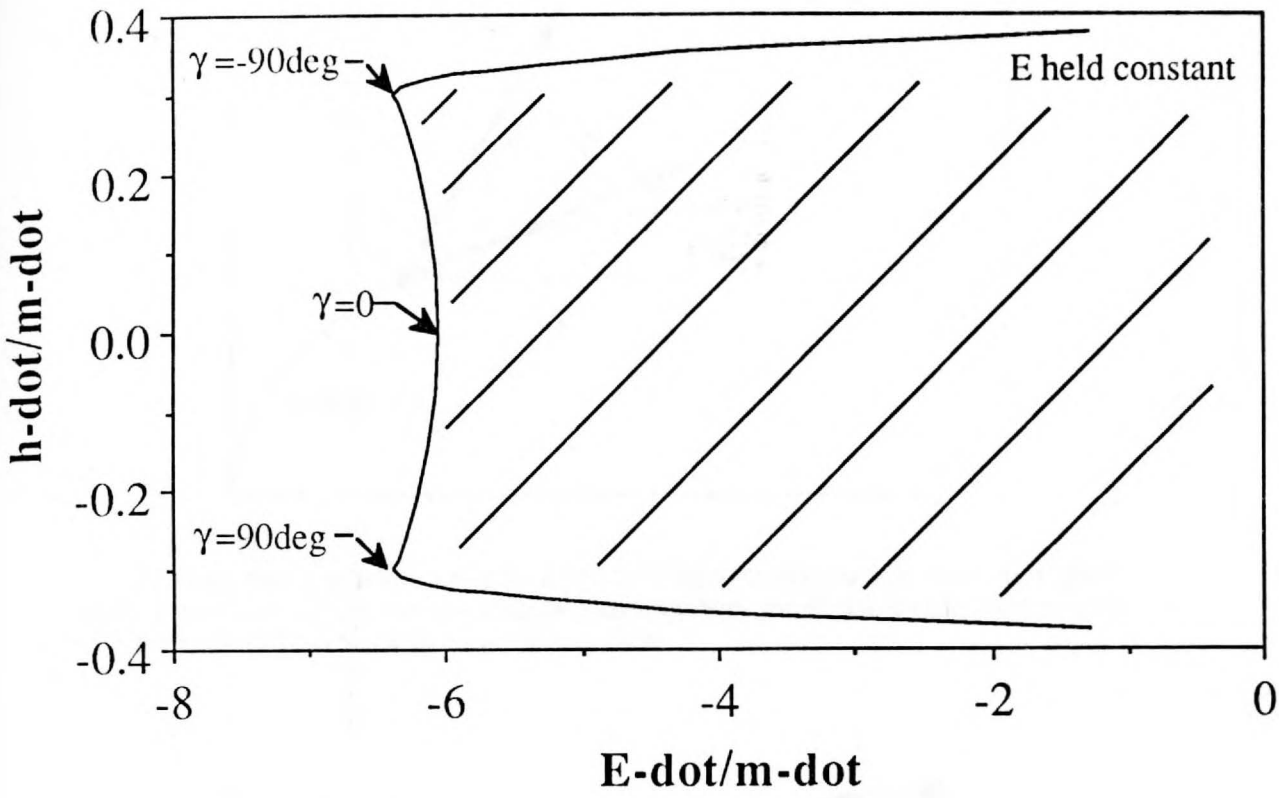

Fig. 5: Hodograph of the three-state model

Finite Elements in Time

For the numerical portion of the work, we have developed a mixed variational approach for optimal control that we call the weak Hamiltonian formulation [1]. This method is based on a similar approach for dynamics problems and facilitates the development of finite element methods in time. We have applied the method to some simple problems in dynamics and optimal control [1,2] and to the present research. Figure 6 illustrates a simple problem in optimal control (see [1] for details). Finite element results are compared with the exact solution in Figures 7 and 8. Note the accuracy of rather crude finite element approximations and the graceful transition between the small number of elements and the larger numbers which are virtually indistinguishable from the exact solution. Although the equations being solved are extremely nonlinear, the method is self-starting. We solve the two-element case with unchanging trivial initial guesses, and the results of this are used as initial guesses for the cases for arbitrary numbers of elements. While we do not claim that this feature will carry over to more difficult problems, we do have evidence that getting the method to converge for a variety of problems is not a serious obstacle.

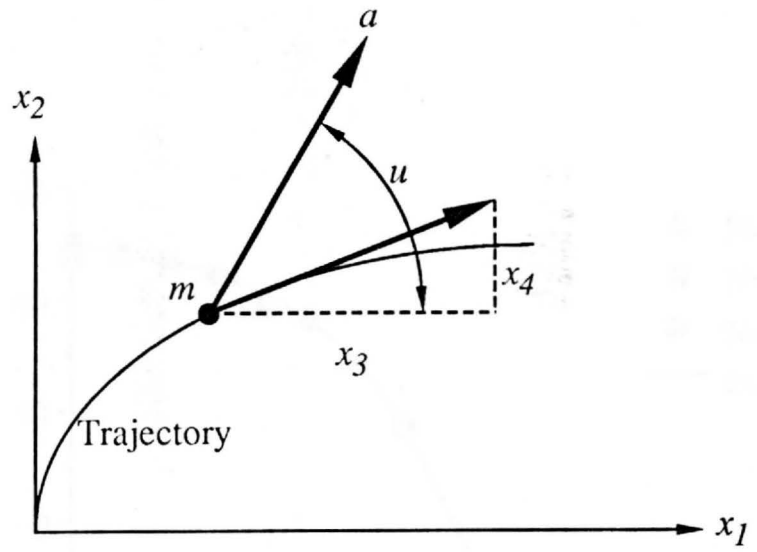

Fig. 6: Mass particle acted upon by a force of magnitude *ma* and with an angle *u* where it is required to achieve a straight line trajectory parallel to the horizontal axis with a specified final velocity in minimum time

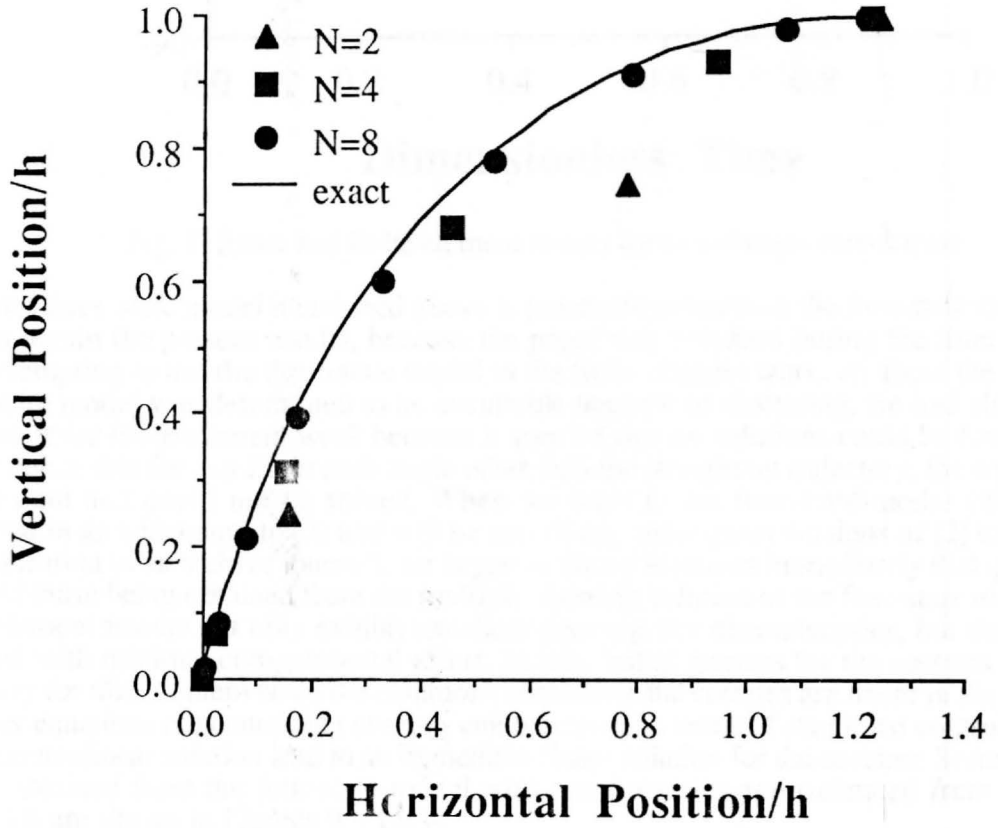

Fig. 7: Exact and finite element results for trajectory profile

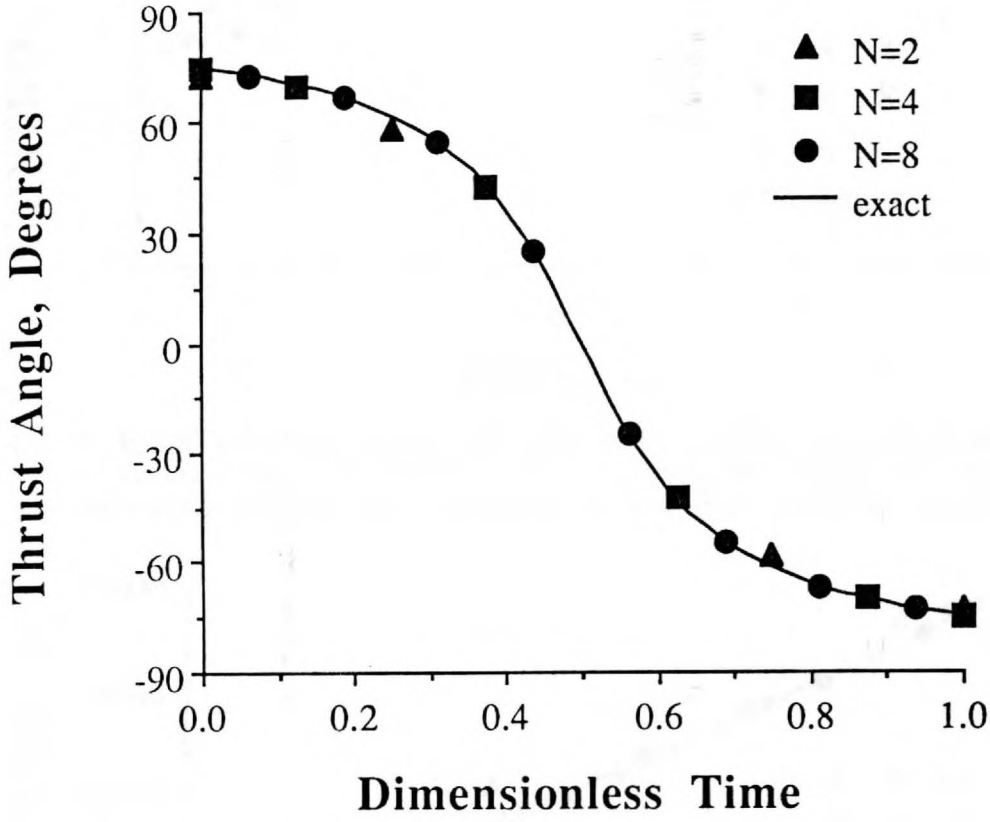

Fig. 8: Exact and finite element results for thrust angle versus time

In [2] the three-state model mentioned above is presented rather than the four-state model actually used to obtain the present results, because the paper was prepared during the time in which we were attempting to use the three-state model in the finite element work. At about the time that the three-state model was determined to be unsuitable because of chattering, we had also decided to abandon it for finite element work because it seemed that no solutions could be found. We even had evidence that for any flight path angle other than the straight up trajectory, the equations were inconsistent and could not be solved. When we went to the four-state model (which will be described in an addendum to [2] and will be part of any subsequent versions of [2] to be prepared for publication in an archive journal), we began to obtain solutions immediately that quantitatively matched those being obtained from the multiple shooting solution of the four-state model. Present finite element results not only exhibit excellent convergence characteristics, but they have been obtained with minimal computational effort. In fact, initial guesses for the costates are not even necessary for this problem since the equations containing the costates are linear in the costates and the other equations not containing costates can be solved in terms of states and control. The results from that nonlinear solution lead to an immediate *linear* solution for the costates. Some preliminary results obtained from the four-state model with aerodynamics approximated from those of the Saturn 1B are shown in Figures 9 – 13.

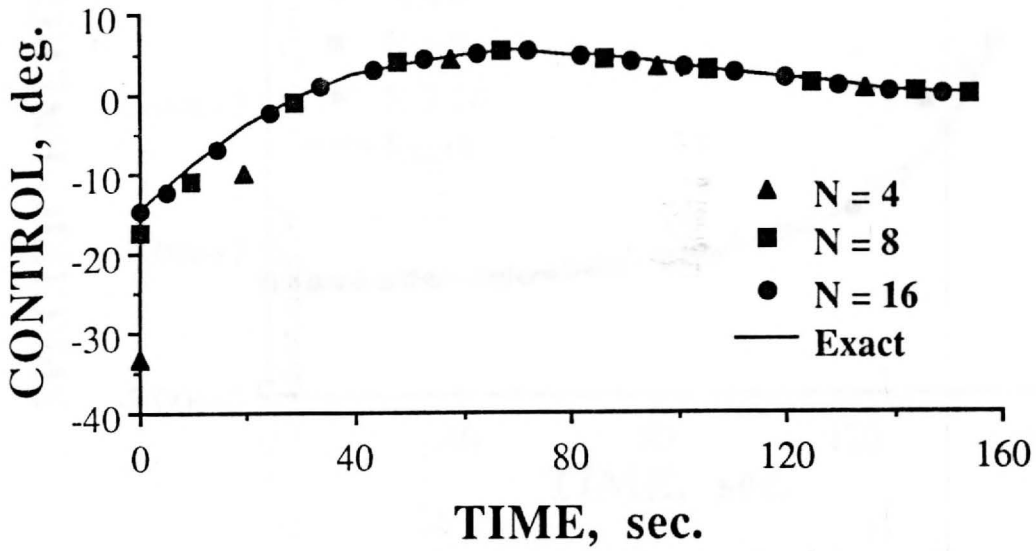

Fig. 9: "Exact" numerical solution and finite element results for control (angle of attack) versus time (ALS model). Here the 16 element results are virtually indistinguishable from the numerical solution obtained from multiple shooting.

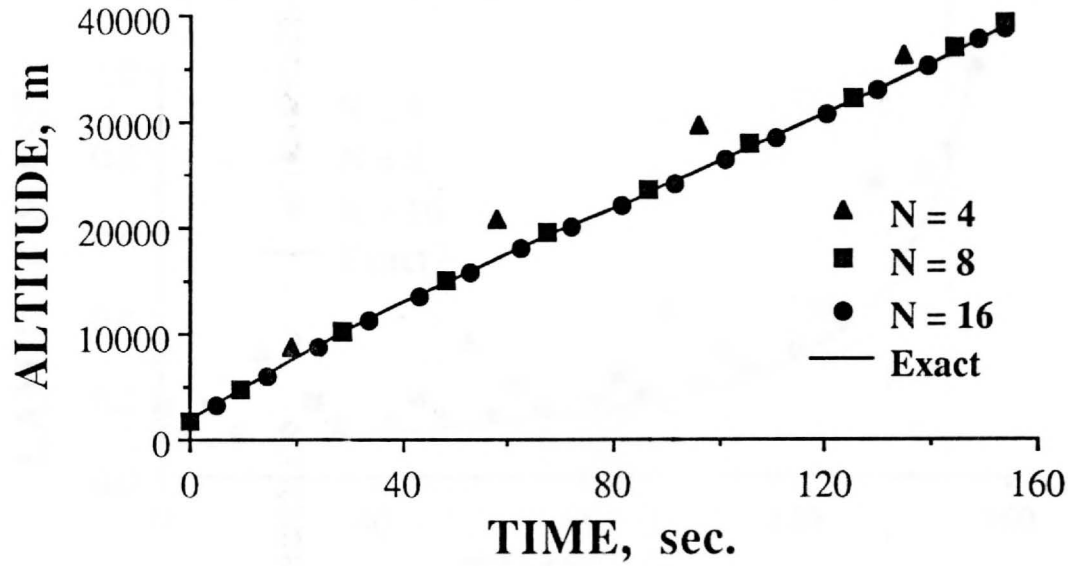

Fig. 10: "Exact" numerical solution and finite element results for altitude versus time (ALS model). Here the 8 element results are virtually indistinguishable from the numerical solution obtained from multiple shooting.

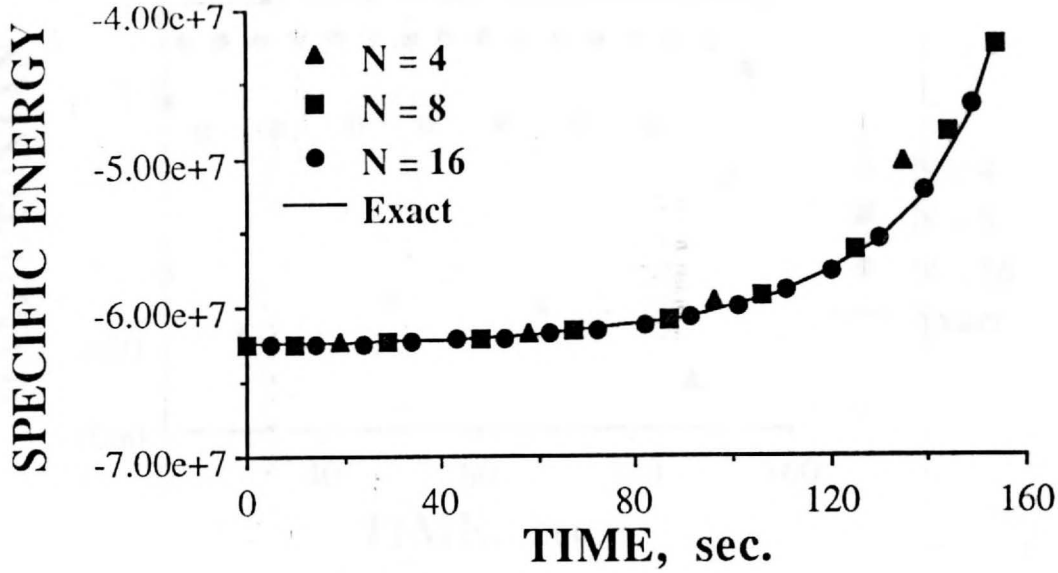

Fig. 11: "Exact" numerical solution and finite element results for specific energy versus time (ALS model). Here the 16 element results are virtually indistinguishable from the numerical solution obtained from multiple shooting. The largest errors are near the end of the trajectory where the rate of increase for the energy is unrealistically high because of the single-stage model.

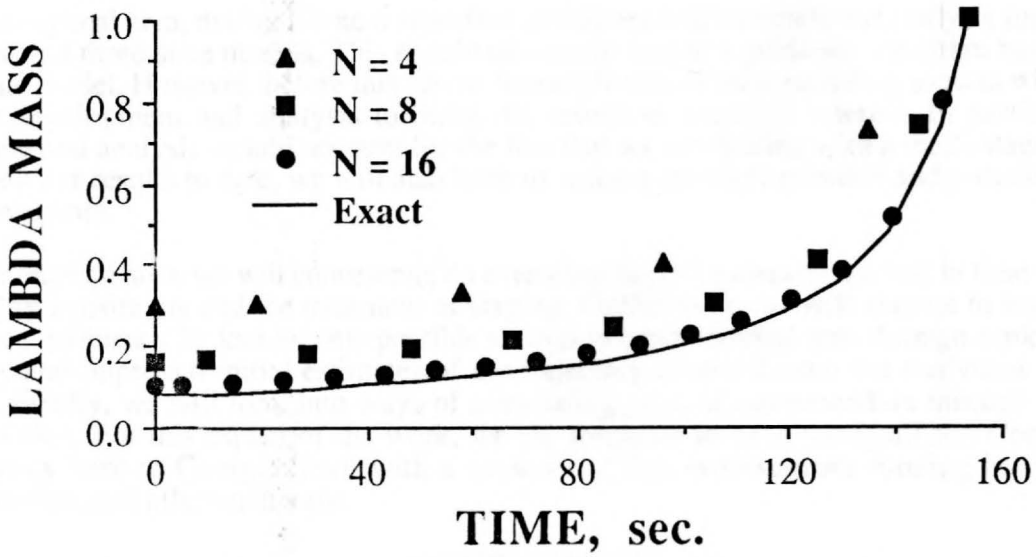

Fig. 12: "Exact" numerical solution and finite element results for mass costate versus time (ALS model). Here even the 16 element results have some observable error near the beginning of the trajectory. However, these results exhibit the worst accuracy of all that we obtained, and they do not seem to have any deleterious effects on the other quantities calculated.

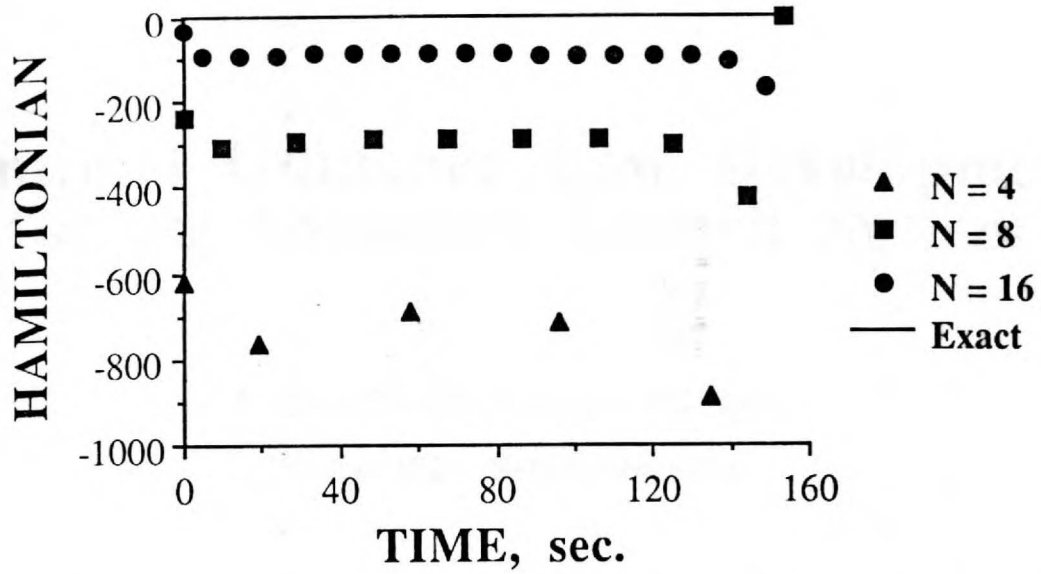

Fig. 13: Exact Hamiltonian and finite element results. Clearly the Hamiltonian is converging rapidly to zero all along the trajectory. The slowest convergence is seen to be taking place near the end where the energy gradients are so large.

FUTURE RESEARCH

In the analytical area, during the next reporting period we will complete our analysis surrounding the two- and three-state models. This should ultimately lead to a guidance algorithm based on the two-state model. However, before this can be accomplished, several modeling aspects will require further development and analysis to make the results of practical interest. In particular, our modeling and analysis should account for the fact that we are dealing with a multi-stage vehicle. Based on our results to date, we will also have to enforce dynamic pressure and possibly heating rate constraints.

In the numerical area, we will concentrate on extending the finite element method in time to include inequality constraints and the treatment of staging. Furthermore, we will attempt to improve the numerical efficiency by looking into possible savings in computational time through exploitation of sparsity and improved initial estimates of the trajectory obtained from the analytical two-state model. Finally, we will look into ways of automating parts of our procedure through symbolic computation. For this aspect of the work, we are fortunate to have the Symbolic Computation Laboratory here at Georgia Tech with a network of Sun workstations running MACSYMA, Mathematica, and other such tools.

REFERENCES

1. Hodges, Dewey H.; and Bless, Robert R.: "A Weak Hamiltonian Finite Element Method for Optimal Control Problems," *Journal of Guidance, Control, and Dynamics*, submitted for publication, 1989.

2. Hodges, Dewey H.; Calise, Anthony J.; Bless, Robert R.; and Leung, Martin: "A Weak Hamiltonian Finite Element Method for Optimal Guidance of an Advanced Launch Vehicle," *Proceedings of the American Control Conference*, Pittsburgh, Pennsylvania, June 21 – 23, 1989.

Optimal Guidance Law Development for an Advanced Launch System

INTERIM PROGRESS REPORT

1 June 1989 – 30 November 1989

December 1989

Research Supported by NASA Langley Research Center

NASA Grant No. NAG-1-939

Principal Investigators: Anthony J. Calise & Dewey H. Hodges

Research Assistants: Martin S. Leung & Robert R. Bless

NASA Grant Monitor: Dr. Daniel D. Moerder

Georgia Institute of Technology
School of Aerospace Engineering
Atlanta, GA 30332-0150

1. SUMMARY

1.1 Singular Perturbation Analysis

During this period we have incorporated the ALS data of September 15 and evaluated the energy state approximation used in our earlier work. Our numerical results indicate that this approach does not result in reasonable profiles that in any way approximate an optimal profile. This is primarily due to the high thrust capability of the ALS vehicle, which invalidates the assumption that energy can be regarded as a slow variable. Optimal solutions obtained numerically via several approaches indicate that the initial and terminal conditions on altitude and flight path angle have a large influence on the shape of the entire trajectory. Thus, we have abandoned this approach in favor of a three state model in velocity, altitude and flight path angle, with mass treated explicitly as a piecewise linear function of time. An analytic solution is possible for this case (including the effect of staging) if we invoke a flat Earth approximation. The effect of the flat Earth approximation has been studied in detail, and an approximation technique has been employed which closely approximates the optimal solution for a spherical Earth.

We have also studied the effect of the non-convexity issue raised in [1], in the context of including bank angle as an additional control variable. Our results show that the velocity hodograph in this case is convex in the absence of control constraints. In the presence of a q-α constraint there is a lack of convexity, but relaxed or chattering solutions are not feasible.

1.2 Finite Elements in Time

In the numerical work based on finite elements in time, several significant items were accomplished. First, our finite element method was extended to include staging and to incorporate control and state constraints. Our ALS finite element code was updated to include the ALS configuration including all vehicle parameters, aerodynamic tables and staging. We have validated the ALS finite element code by comparison of results from it with those from a multiple shooting code in the absence of atmospheric effects.

In addition, the ALS code was transferred to Sun workstations so that we would have easy access to symbolic manipulation software. In the process of changing the code from the Cyber system to run on the Sun, we also incorporated a linear equation solver from Harwell (England) which takes advantage of sparsity. This is significant because our coefficient matrices are about 98% zeros. Because of the savings related to sparsity, we are able to run the code on a desktop machine with less CPU time and far less turn-around time relative to the Cyber system on which we were running before. The actual CPU time to run the code is of the order of 2 – 9 seconds, depending on the number of elements and the quality of the initial guesses. We believe that with further work we can get this time down by a factor of four or so, making the method well suited for online computation.

1.3 Publications

The conference and journal publications that have resulted thus far from this research effort are listed as [2 – 4].

2. RESEARCH ACCOMPLISHMENTS

2.1 Singular Perturbation Analysis

2.1.1 Velocity Hodograph It has been reported in [1] that the velocity hodograph is non-convex due to the reduction in drag over a range of angle of attack that occurs in the speed range corresponding to hypervelocity flight. Also, this effect is only predominant over an altitude range

where the aerodynamic force is sufficiently large. While this is true when angle of attack is the only control variable, it is not true when both angle of attack and bank angle are control variables. In effect, variations in bank angle can be used to fly at an optimum angle of attack while simultaneously controlling flight path angle by dumping the excess lift, thus avoiding the non-convexity issue. In practice, one can think of oscillating the bank angle to maintain flight in a vertical plane, or simply doing a coordinated turn with the net change in heading accounted for at launch.

Fig. 1 shows the velocity hodograph that results for the same flight condition studied in [1], with both angle of attack and bank angle serving as control variables. The $\phi = 0°$ curve is identical to the non-convexity illustrated in [1], taking into account that the velocity in [1] was normalized to the circular velocity at the Earth's surface. Note that the velocity set in this case is convex, with a vertical flat region corresponding to the maximum velocity rate (V-dot) for this flight condition. Flight at maximum V-dot would occur only if the vector representing $[\lambda_\gamma, \lambda_V]$ (when drawn on this figure) intersects this flat region. Hence, the velocity holograph for this flight condition implies that $\phi^* = 0°$ for $\lambda_\gamma/\lambda_V > (0.1/1.7)$, $\phi^* = 180°$ for $\lambda_\gamma/\lambda_V < (-0.95/1.7)$ and that intermediate values of bank angle are optimal for $(-0.95/1.7) < \lambda_\gamma/\lambda_V < (0.1/1.7)$. Note that the optimal bank angle crosses through 90° when $\lambda_\gamma = 0$. The results in this figure are somewhat unrealistic due to the fact that the dynamic pressure (q_{max}) constraint is severely violated for this flight condition.

Fig. 2 illustrates the velocity hodograph for a second flight condition where the q_{max} constraint is satisfied but the alpha-q constraint would be active. Note that the maximum V-dot is now determined by the alpha-q constraint, and that intermediate values of ϕ are optimal for $(-0.59/16.16) < \lambda_\gamma/\lambda_V < (-0.32/16.16)$. Outside this range either $\phi^* = 0°$ or $\phi^* = 180°$ depending on the sign of λ_γ. Chattering solutions are not possible since $\lambda_V > 0$ all along any optimal trajectory. This fact follows from the interpretation of the $\lambda_V(t)$ costate as the sensitivity of performance index to perturbations in the velocity occurring at any time (t) along the trajectory. Thus if the objective is to maximize the final mass, it follows that an incremental increase in V causes an incremental increase in final mass.

It can be seen from Fig. 2 that the maximum performance improvement from the use of bank angle as a control is small. The maximum acceleration improvement is approximately 0.185 m/s^2, or 1% higher than the zero bank angle acceleration, which only occurs if λ_γ is near zero. Also, this improvement can be achieved only over a small portion of the total trajectory (where mach is sufficiently high and aerodynamic forces are sufficiently large). Thus the net effect on fuel consumption to orbit will be negligible.

2.1.2 Energy State Approximation Three energy state models were considered during this period. The first model is the same as that treated in our first progress report. In the energy state approximation we have:

$$dE/dt = [T\cos\gamma - D(r,M,\alpha)]V/m\,, \qquad E = V^2/2 - \mu/r \tag{1}$$

$$dm/dt = -T_{vac}/(g_o I_{sp}) \tag{2}$$

In this model altitude appears as a control variable. Since mass flow is piecewise constant it follows that the optimality condition for maximizing the final mass reduces to finding the altitude at each energy level that maximizes the energy rate. This is equivalent to minimum time to a final energy. Three approximations were tried which differed in the calculation of angle of attack:

$$\alpha = 0, \quad \alpha = \alpha_1, \quad \alpha = \alpha_2 \tag{3}$$

In the second approximation, α_1 is calculated from satisfying:

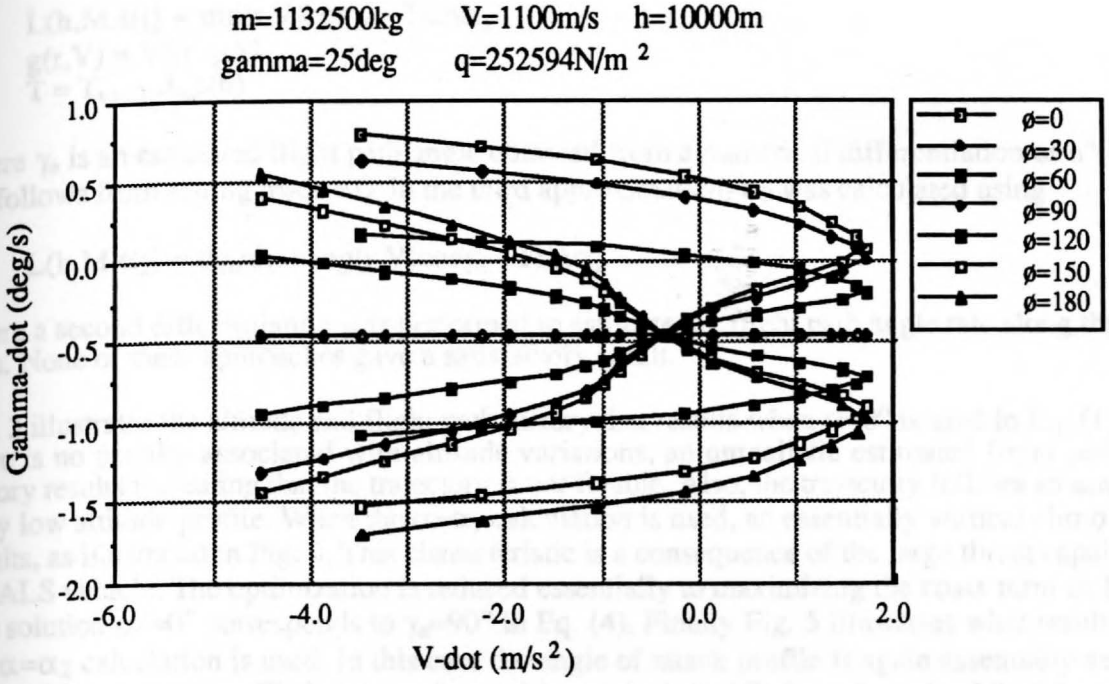

Fig. 1: H=10000m hodograph with Sept. 14 data and no constraints imposed

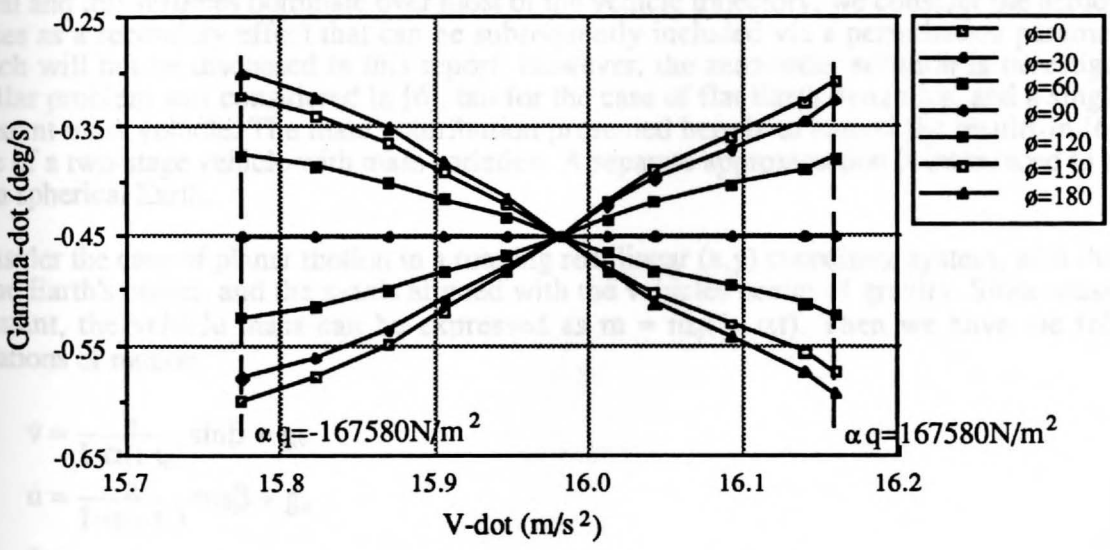

Fig. 2: H=23000m hodograph with Sept. 14 data and αq constraint imposed

$$L(h,M,\alpha_1) = mg(r,V)\cos\gamma_e - T\sin\alpha_1 \quad (4)$$
$$g(r,V) = V^2/r - \mu/r^2 \quad (5)$$
$$T = T_{vac} - A_e p(h) \quad (6)$$

where γ_e is an estimated flight path angle obtained from a numerical differentiation of h*(E). Eq. (4) follows from setting $d\gamma/dt = 0$. In the third approximation, α_2 was calculated using

$$L(h,M,\alpha_2) = d\gamma_e/dt + mg(r,V)\cos\gamma_e - T\sin\alpha_2 \quad (7)$$

where a second differentiation was performed to estimate the flight path angle rate along the climb path. None of these approaches gave a satisfactory result.

Fig. 3 illustrates the altitude and flight path history that results when $\alpha=0°$ is used in Eq. (1). Since there is no penalty associated with altitude variations, an unrealistic estimated flight path angle history results indicating that the trajectory is not flyable. Also, the trajectory follows an unrealistically low altitude profile. When the $\alpha=\alpha_1$ calculation is used, an essentially vertical climb profile results, as illustrated in Fig. 4. This characteristic is a consequence of the large thrust capability of the ALS vehicle. The optimization is reduced essentially to maximizing the $\cos\alpha$ term in Eq. (1). The solution $\alpha_1=0°$ corresponds to $\gamma_e=90°$ in Eq. (4). Finally Fig. 5 illustrates what results when the $\alpha=\alpha_2$ calculation is used. In this case the angle of attack profile is again essentially zero, and the resulting altitude profile is extremely sensitive to the initial flight path angle. All of these results clearly demonstrate that energy state approximations are not useful for vehicles where the thrust is large compared to drag, even if the T/W ratio is small. This is mainly due to the presence of the $\cos\alpha$ term in Eq. (1), which traditionally has been ignored in aircraft analysis.

2.1.3 Analysis of a Three-State Model In wake of the unsatisfactory performance using energy state approximations, a regular perturbation approach was investigated. Since gravitational and thrust forces dominate over most of the vehicle trajectory, we consider the aerodynamic forces as a secondary effect that can be subsequently included via a perturbation parameter [5], which will not be discussed in this report. However, the zero-order solution is investigated. A similar problem was considered in [6], but for the case of flat Earth dynamics, and a single stage constant mass vehicle. The main contribution presented here is to extend the results in [6] to the case of a two-stage vehicle with mass variation. A separate approximation is introduced to account for a spherical Earth.

Consider the case of planar motion in a rotating rectilinear (x,y) coordinate system, with the origin at the Earth's center, and the x-axis aligned with the vehicles center of gravity. Since mass rate is constant, the vehicle mass can be expressed as $m = m_o(1- \alpha t)$. Then we have the following equations of motion:

$$\dot{v} = \frac{a}{1-\alpha(t-t_o)}\sin\beta + g_v \quad (8)$$
$$\dot{u} = \frac{a}{1-\alpha(t-t_o)}\cos\beta + g_u \quad (9)$$
$$\dot{r} = v \quad (10)$$

where v and u are the velocity components along the x and y axes respectively, and r is the radial distance along the x axis. These components are related to the wind frame variables by:

$$v = V\sin\gamma \quad (11)$$
$$u = V\cos\gamma \quad (12)$$

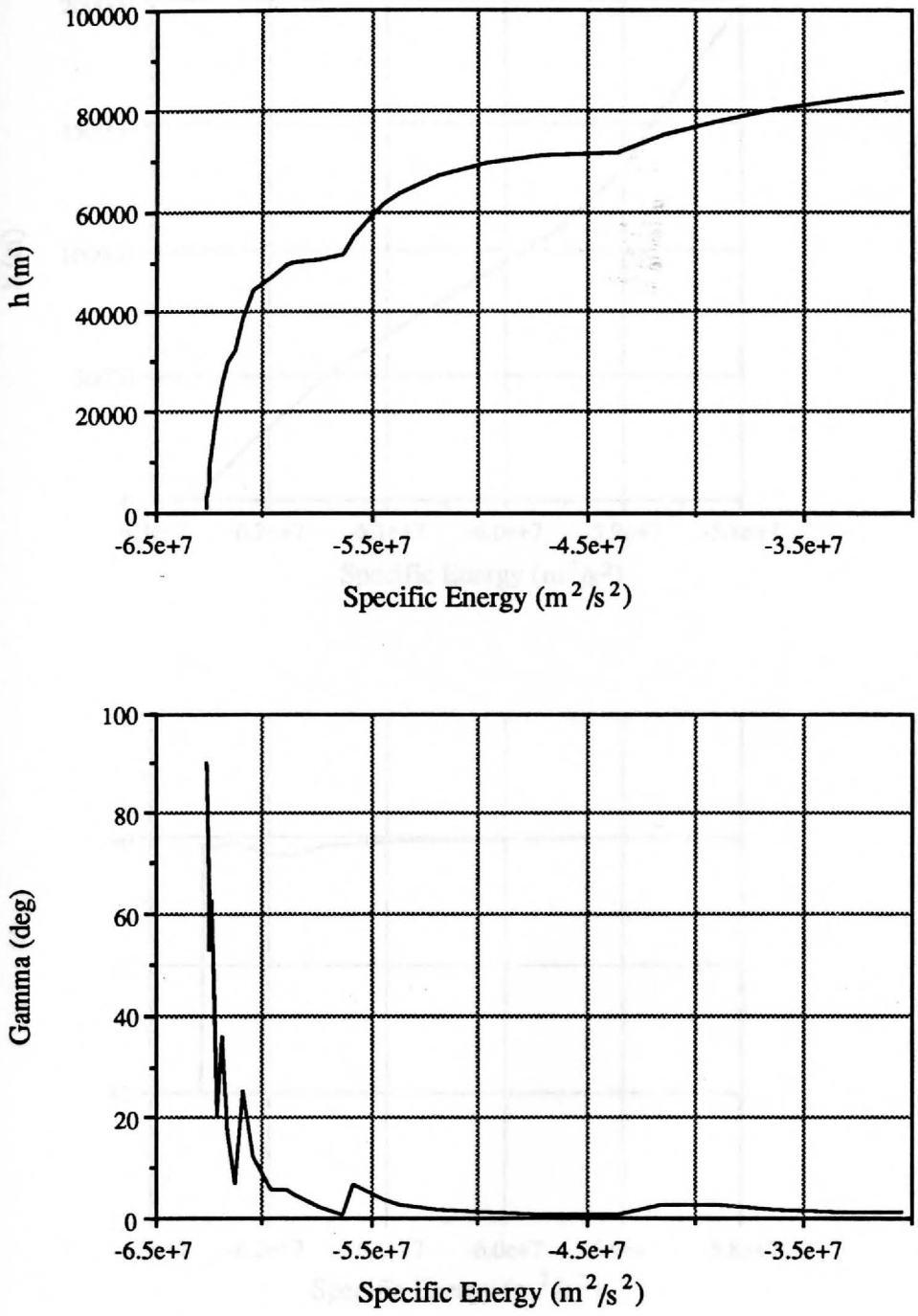

Fig. 3: Reduced solution with L=0

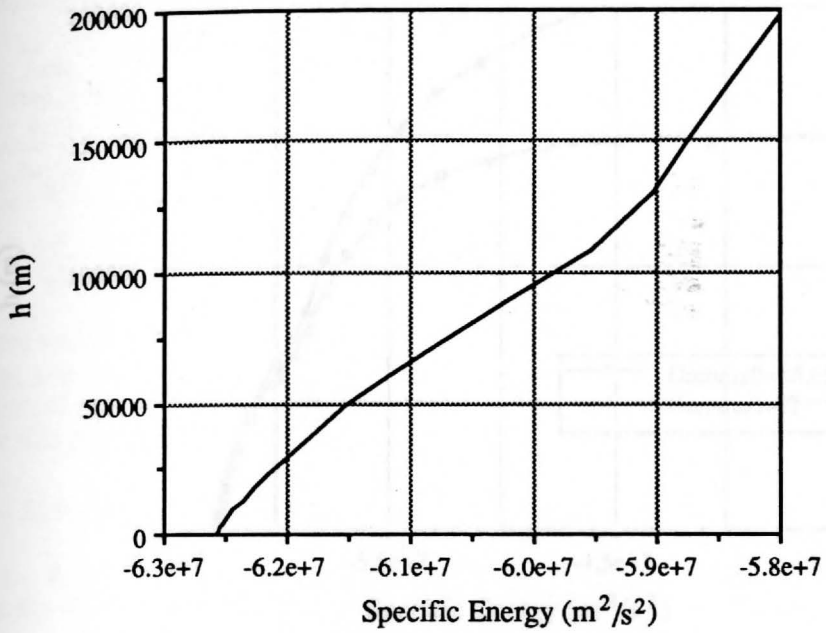

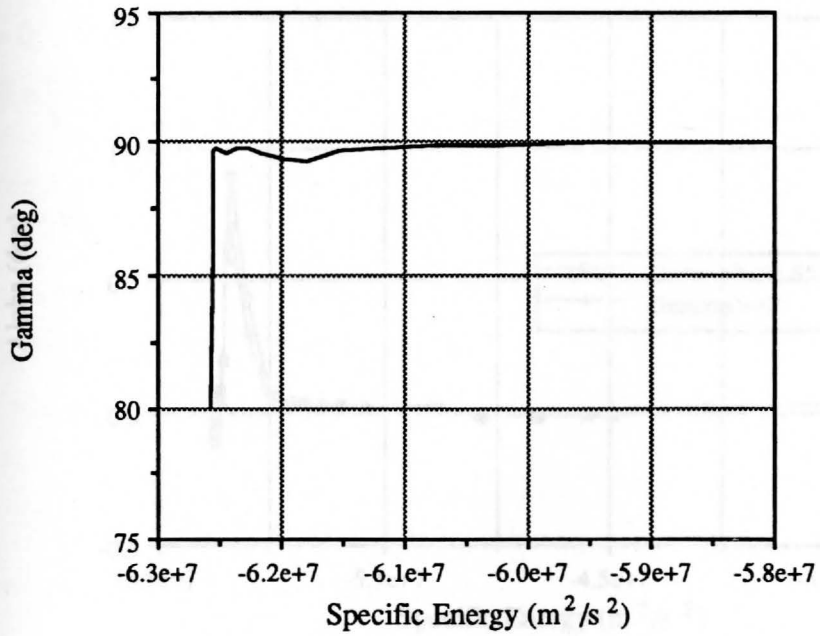

Fig. 4: Reduced solution with $L=mg(r,V)\cos\gamma_e - T\sin\gamma_e$

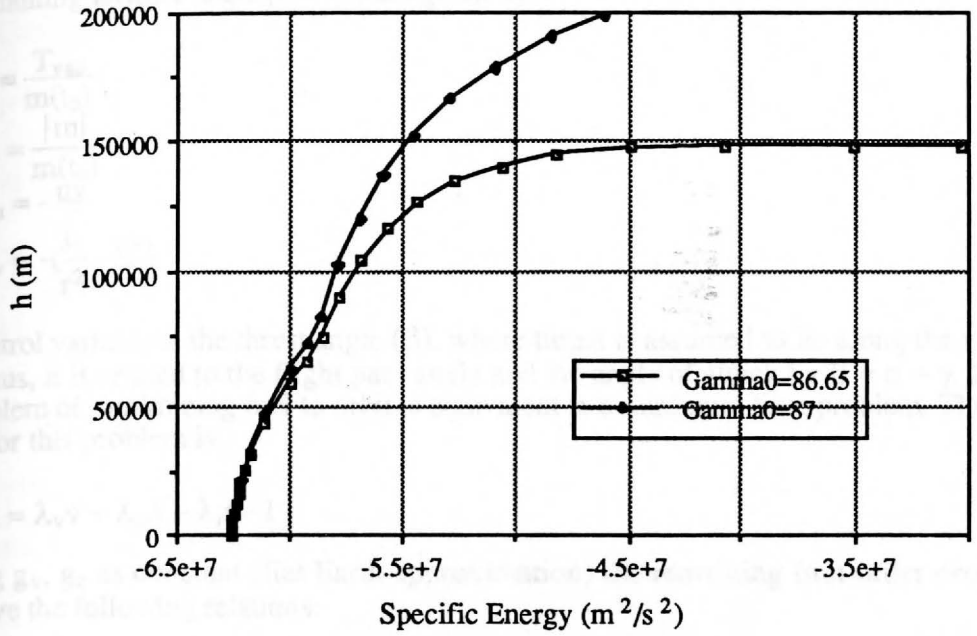

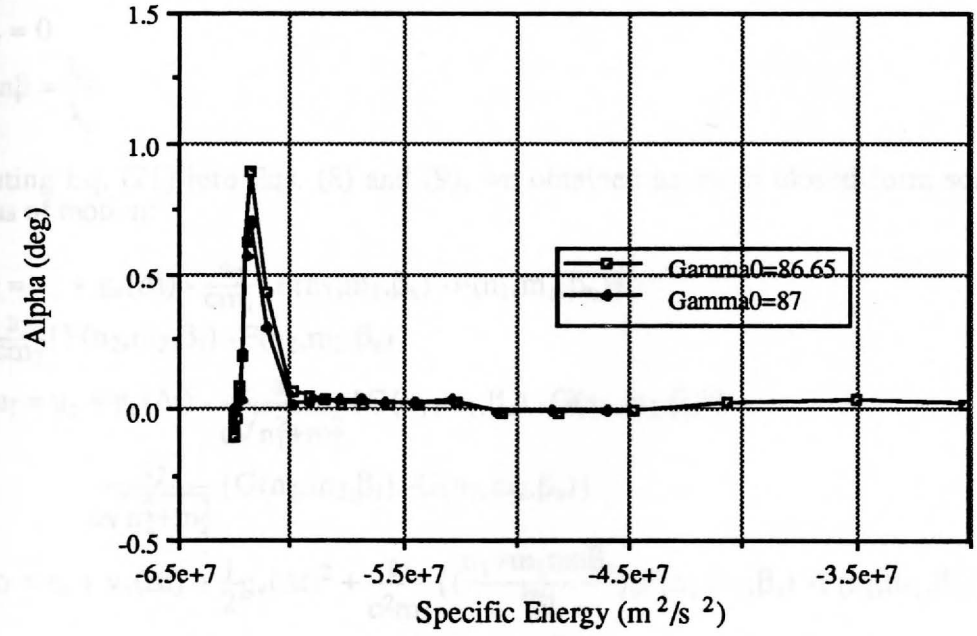

Fig. 5: Reduced solutions with L= γ_e + mg(r,V)cosγ_e - Tsin γ_e

The remaining terms in Eqs. (8 – 10) are given by:

$$a = \frac{T_{vac}}{m(t_o)} \tag{13}$$

$$\alpha = \frac{|\dot{m}|}{m(t_o)} \tag{14}$$

$$g_u = -\frac{uv}{r} \tag{15}$$

$$g_v = -(\frac{\mu}{r^2} - \frac{u^2}{r}) \tag{16}$$

The control variable is the thrust angle (β), where thrust is assumed to lie along the vehicle x-body axis. Thus, it is related to the flight path angle and the angle of attack by $\beta = \alpha + \gamma$. In this setting the problem of minimizing fuel to orbit is equivalent to a minimum time problem. Thus, the Hamiltonian for this problem is

$$H = \lambda_v \dot{v} + \lambda_u \dot{u} + \lambda_r \dot{r} - 1 \tag{17}$$

Treating g_v, g_u as constant (flat Earth approximation) the remaining first-order necessary conditions give the following relations:

$$\dot{\lambda}_v = -\lambda_r \tag{18}$$

$$\dot{\lambda}_u = 0 \tag{19}$$

$$\dot{\lambda}_r = 0 \tag{20}$$

$$\tan\beta = \frac{\lambda_v}{\lambda_u} \tag{21}$$

Substituting Eq. (21) into Eqs. (8) and (9), we obtained an exact closed-form solution for the equations of motion:

$$v_f = v_o + g_v(\Delta t) - \frac{a_1}{cm_1}\{F(n_1,m_1,\beta_s) - F(n_1,m_1,\beta_o)\} - \frac{a_2}{cm_2}\{F(n_2,m_2,\beta_f) - F(n_2,m_2,\beta_s)\} \tag{22}$$

$$u_f = u_o + g_u(\Delta t) - \frac{a_1}{c\sqrt{n_1^2+m_1^2}}\{G(n_1,m_1,\beta_s) - G(n_1,m_1,\beta_o)\} - \frac{a_2}{c\sqrt{n_2^2+m_2^2}}\{G(n_2,m_2,\beta_f) - G(n_2,m_2,\beta_s)\} \tag{23}$$

$$r_f = r_o + v_o(\Delta t) + \frac{1}{2}g_v(\Delta t)^2 + \frac{a_1}{c^2 m_1}\{(\frac{n_1+m_1\tan\beta_s}{m_1})[F(n_1,m_1,\beta_s) - F(n_1,m_1,\beta_o)] - (\sec\beta_s - \sec\beta_o)\} + \frac{a_2}{c^2 m_2}\{(\frac{n_1+m_1\tan\beta_s}{m_1})[F(n_2,m_2,\beta_f) - F(n_2,m_2,\beta_s)] - (\sec\beta_f - \sec\beta_s)\} \tag{24}$$

where

$$F(n,m,\beta) = \log\frac{(\tan\beta + \sec\beta)(n + m\tan\beta)^p}{(\sqrt{n^2+m^2}\sec\beta + n\tan\beta - m)^p} \tag{25}$$

$$G(n,m,\beta) = \log\left(\frac{\sqrt{n^2+m^2}\sec\beta + n\tan\beta - m}{n + m\tan\beta}\right) \tag{26}$$

$$p = \frac{n}{\sqrt{n^2 + m^2}} \tag{27}$$

$$a_1 = \frac{T_{vac}^{(1)}}{m(t_o)} \quad ; \quad a_2 = \frac{T_{vac}^{(2)}}{m(t_{s+})} \tag{28}$$

$$\alpha_1 = \frac{|\dot{m}^{(1)}|}{m(t_o)} \quad ; \quad \alpha_2 = \frac{|\dot{m}^{(2)}|}{m(t_{s+})} \tag{29}$$

$$n_1 = 1 - \frac{\alpha_1}{c}\tan\beta_o \quad ; \quad n_2 = 1 - \frac{\alpha_2}{c}\tan\beta_s \tag{30}$$

$$m_1 = \frac{\alpha_1}{c} \quad ; \quad m_2 = \frac{\alpha_2}{c} \tag{31}$$

$$\tan\beta_s = \tan\beta_o - c(t_s - t_o) \tag{32}$$

The subscripts 1 and 2 and the superscripts (1) and (2) are used to denote the stage-1 and stage-2 values, and the subscript s denotes the value as the staging time. The resulting optimal control is the familiar linear tangent law

$$\tan\beta = \tan\beta_o - c(t - t_o) \tag{33}$$

where c and β_o (and t_f) are determined from Eqs. (22 – 24) using a Newton method. Note that in a real time application, $t=t_o$ at each update of the solution, and the second term in Eq. (33) would be used only to calculate the control between updates.

A numerical study was performed to investigate the accuracy of the above solution, by comparison to the more exact solution for the spherical Earth case. In addition, the spherical Earth solution was approximated by updating the parameters g_v, g_u periodically along the trajectory.

Three sets of results expressed in equivalent wind frame coordinates are given in Figs. 6 and 7. The flat Earth results were obtained with g_v =-9.81m/s², g_u =0, whereas the spherical Earth results were obtained by numerical optimization using the expressions in Eq. (15) and (16). The spherical Earth (S.E.) approximation uses the analytical results derived above with g_v, g_u terms updated at 15 second intervals during the first stage and 10 second intervals during the second stage. The final time is approximately 352 seconds in all three cases. The only major difference in these results can be seen in the angle of attack profile in Fig. 7. There is can be seen that the S.E. approximate solution is effective in reducing the error due to the flat Earth approximation used in deriving the analytic solution. Fig. 8 shows the corresponding costate histories, which are for the problem J = max $m(t_f)$ with states (m, h, V, γ). The transformations relating the costates of the formulation in Eqs. (8 – 10) to the equivalent formulation in m,h,V,γ variables are given by:

$$\lambda_V = -\dot{m}(t_f)\left(\lambda_v \frac{v}{\sqrt{v^2+u^2}} + \lambda_u \frac{u}{\sqrt{v^2+u^2}}\right) \tag{33}$$

$$\lambda_\gamma = -\dot{m}(t_f)(\lambda_v u - \lambda_u v) \tag{34}$$

$$\lambda_h = -\dot{m}(t_f)\lambda_r \tag{35}$$

$$\lambda_m = \frac{\lambda_V \dot{V} + \lambda_\gamma \dot{\gamma} + \lambda_h \dot{h}}{-\dot{m}} \tag{36}$$

The solutions are presented in this format to allow a direct comparison to the numerical solutions obtained using the finite elements method in future work.

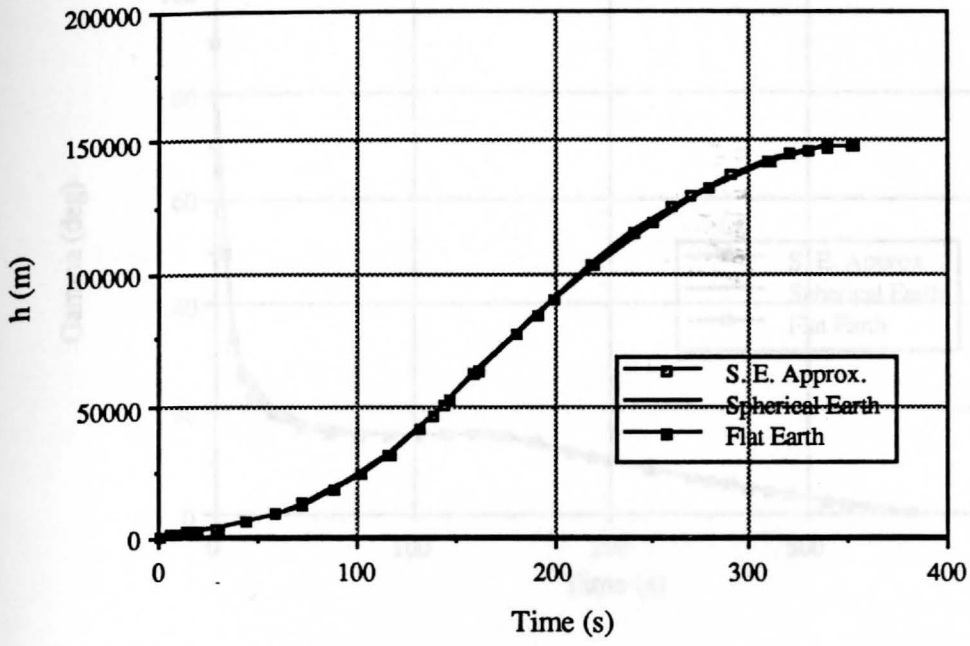

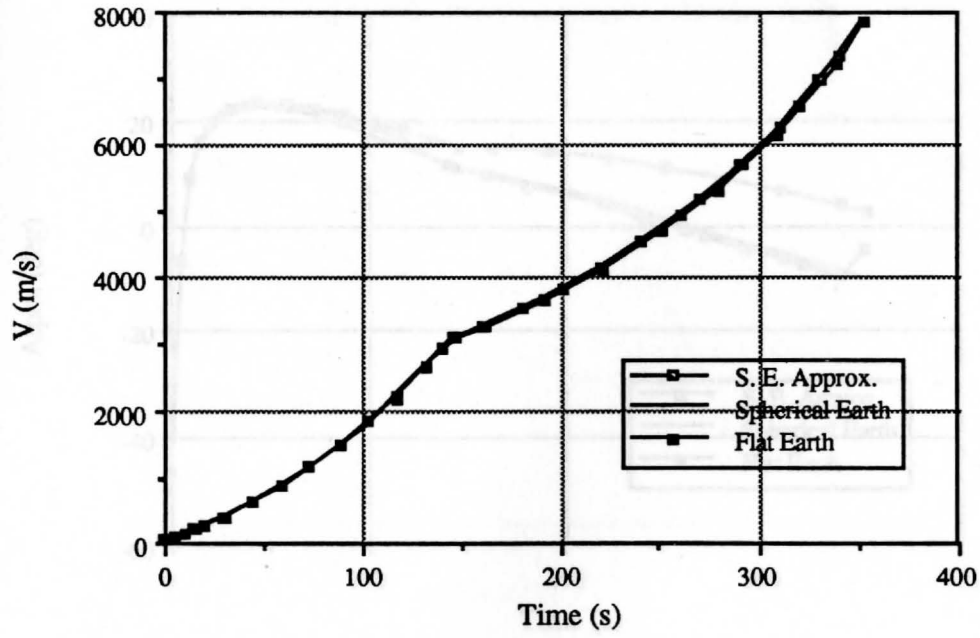

Fig. 6: Comparison of altitude and velocity profiles for the three state model

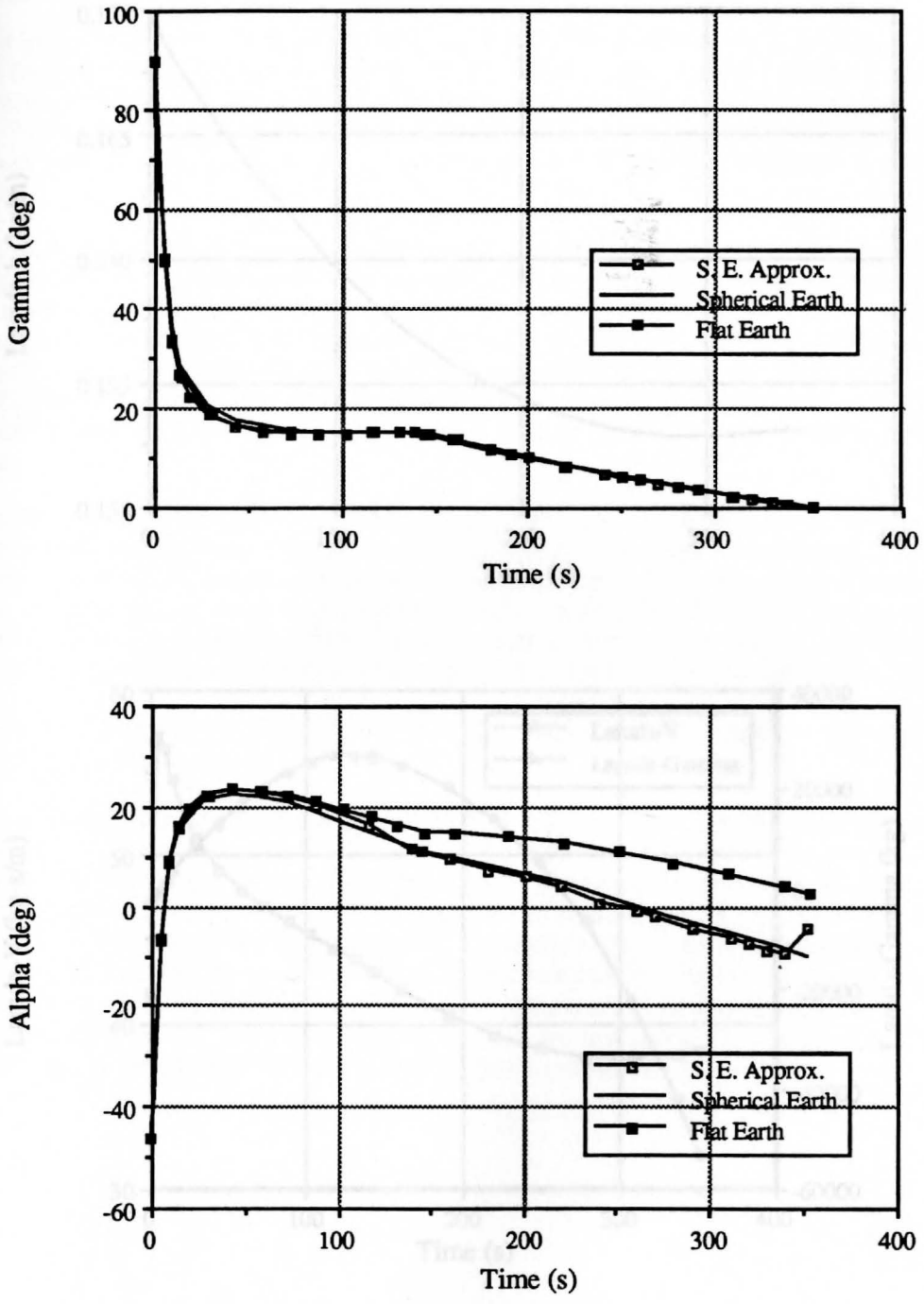

Fig. 7: Comparison of fligth path angle and angle of attack profiles for the three state model

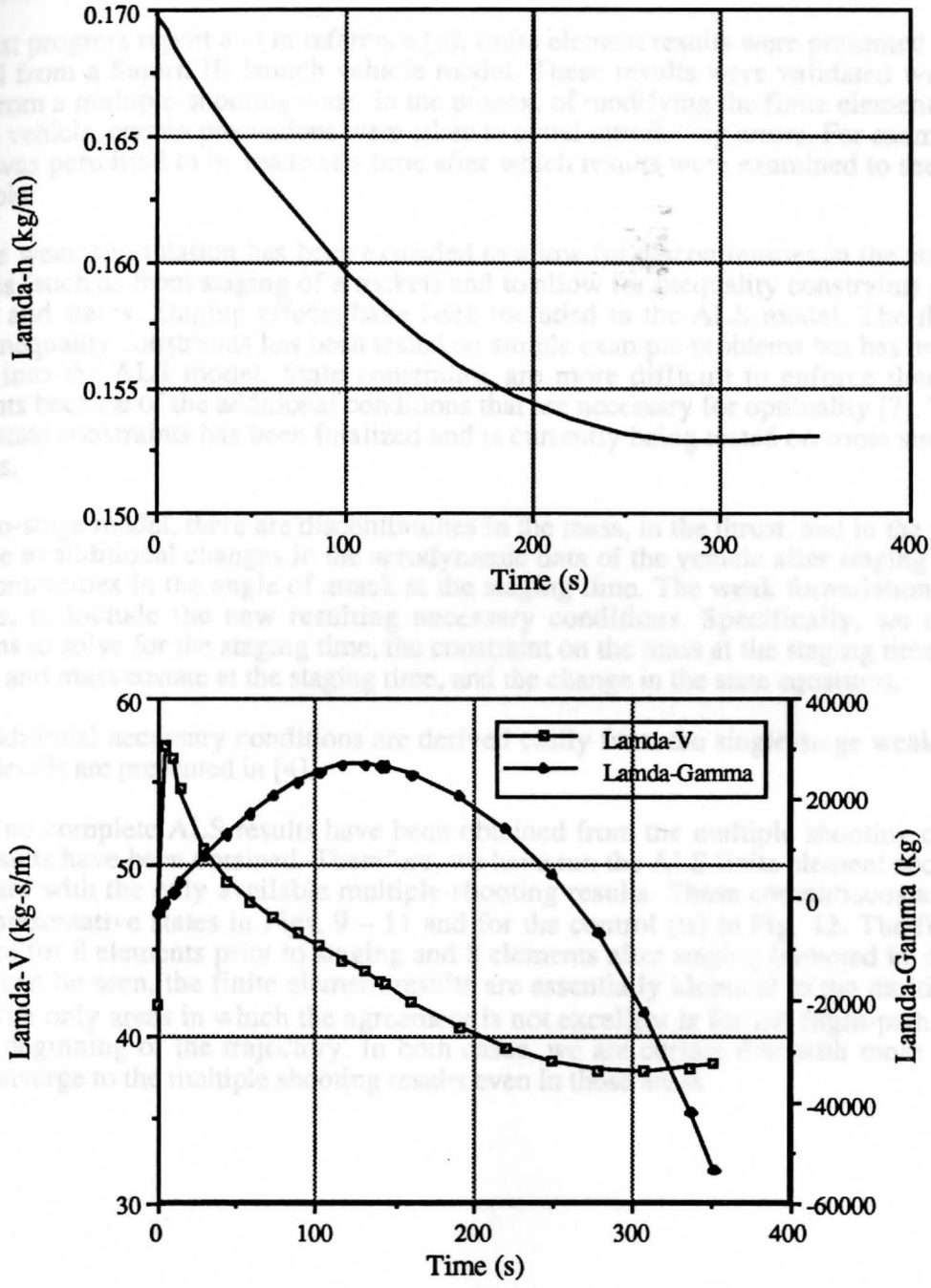

Fig. 8: Costate time histories for the three state spherical Earth model

2.2 Finite Elements in Time

In the last progress report and in reference [3], finite element results were presented that had been obtained from a Saturn IB launch vehicle model. These results were validated with analogous results from a multiple-shooting code. In the process of modifying the finite element code to treat the ALS vehicle, certain precautions were taken to avoid introducing errors. For example, only one change was permitted to be made at a time after which results were examined to see if they were reasonable.

Also, the weak formulation has been extended to allow for discontinuities in the states and state equations (such as from staging of a rocket) and to allow for inequality constraints placed on the controls and states. Staging effects have been included in the ALS model. The theory behind control inequality constraints has been tested on simple example problems but has not been incorporated into the ALS model. State constraints are more difficult to enforce than are control constraints because of the additional conditions that are necessary for optimality [7]. The theory to include state constraints has been finalized and is currently being tested on some simple example problems.

For a two-stage model, there are discontinuities in the mass, in the thrust, and in the mass costate. Also, due to additional changes in the aerodynamic data of the vehicle after staging occurs, there are discontinuities in the angle of attack at the staging time. The weak formulation is modified, therefore, to include the new resulting necessary conditions. Specifically, we must include conditions to solve for the staging time, the constraint on the mass at the staging time, the jump in the mass and mass costate at the staging time, and the change in the state equations.

These additional necessary conditions are derived easily from the single-stage weak formulation and the details are presented in [4].

To date, no complete ALS results have been obtained from the multiple shooting code; only *en vacuo* results have been obtained. Therefore, we have run the ALS finite element code without air to compare with the only available multiple-shooting results. These comparisons are shown for some representative states in Figs. 9 – 11 and for the control (α) in Fig. 12. The finite element results are for 8 elements prior to staging and 8 elements after staging (denoted in the figures by 8:8). As can be seen, the finite element results are essentially identical to the multiple-shooting results. The only areas in which the agreement is not excellent is for the flight-path angle and α near the beginning of the trajectory. In both cases, we are certain that with more elements we would converge to the multiple shooting results even in those areas.

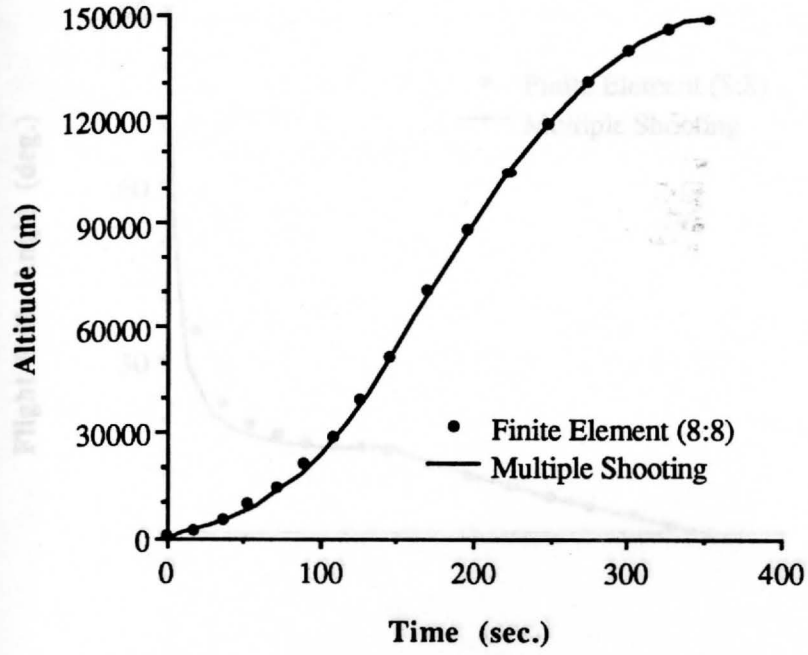

Fig. 9: Altitude vs. Time; Finite Element Method compared with a Multiple Shooting Code (No atmospheric effects)

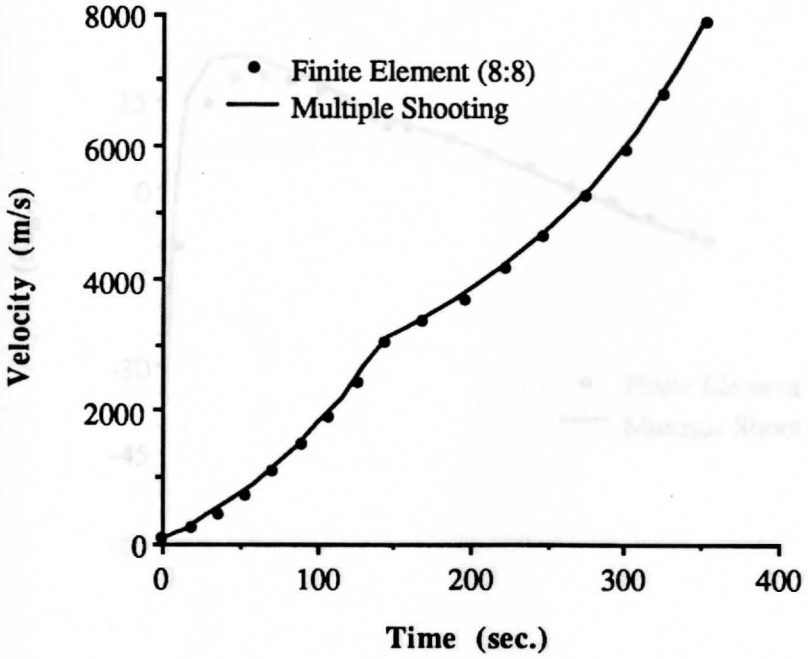

Fig. 10: Velocity vs. Time; Finite Element Method compared with a Multiple Shooting Code (No atmospheric effects)

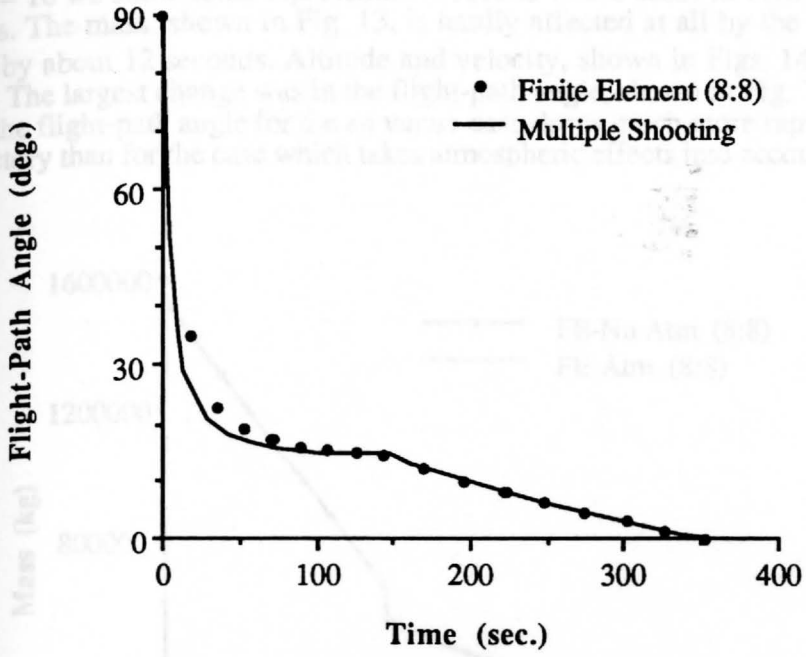

Fig. 11: Flight-Path Angle vs. Time; Finite Element Method compared with a Multiple Shooting Code (No atmospheric effects)

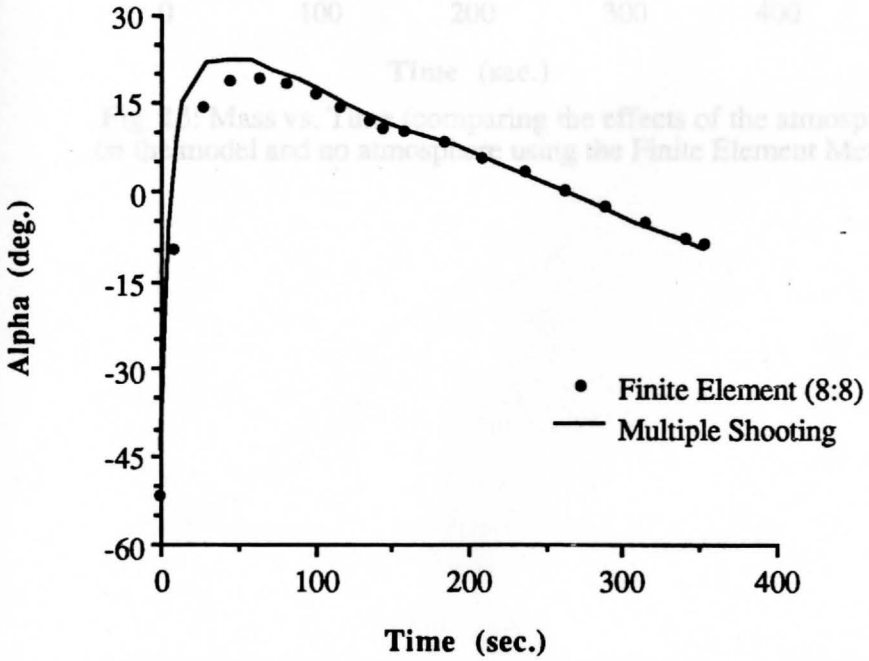

Fig. 12: Angle of Attack vs. Time; Finite Element Method compared with a Multiple Shooting Code (No atmospheric effects)

It was noted in the process of preparing these results that the atmosphere does not seem to have much effect. The vehicle thrust is evidently so large that lift and drag do not have a strong effect. In Figs. 13 – 16 we show some representative results which seem to verify this, at least for most of the states. The mass, shown in Fig. 13, is hardly affected at all by the atmosphere except that t_f changes by about 12 seconds. Altitude and velocity, shown in Figs. 14 and 15, are only slightly affected. The largest change was in the flight-path angle, shown in Fig. 16. Although qualitatively similar, the flight-path angle for the *en vacuo* case drops much more rapidly in the early portion of the trajectory than for the case which takes atmospheric effects into account.

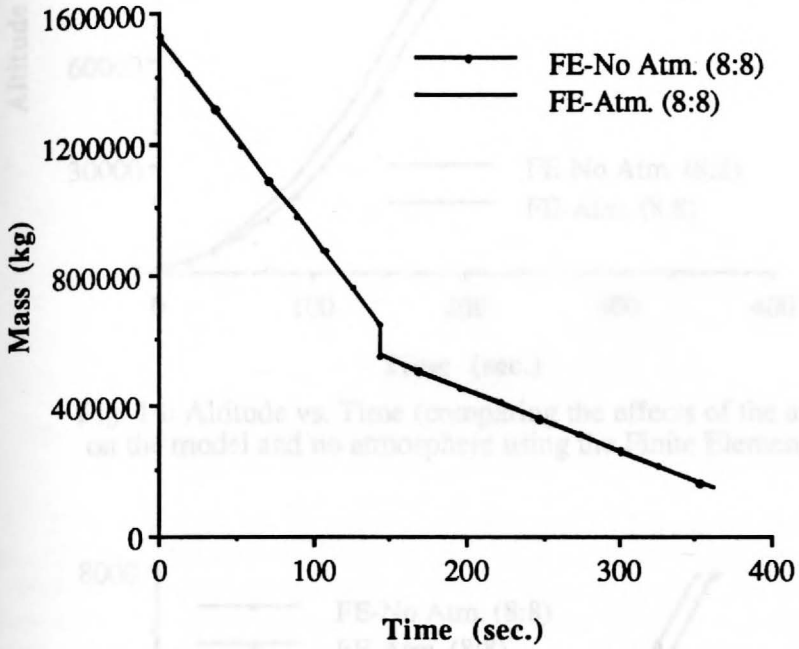

Fig. 13: Mass vs. Time (comparing the effects of the atmosphere on the model and no atmosphere using the Finite Element Method)

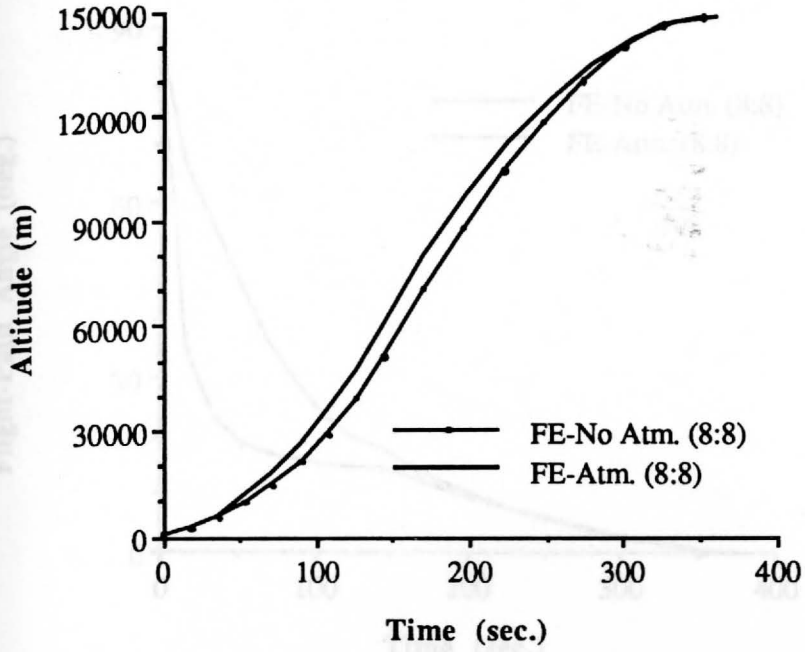

Fig. 14: Altitude vs. Time (comparing the effects of the atmosphere on the model and no atmosphere using the Finite Element Method)

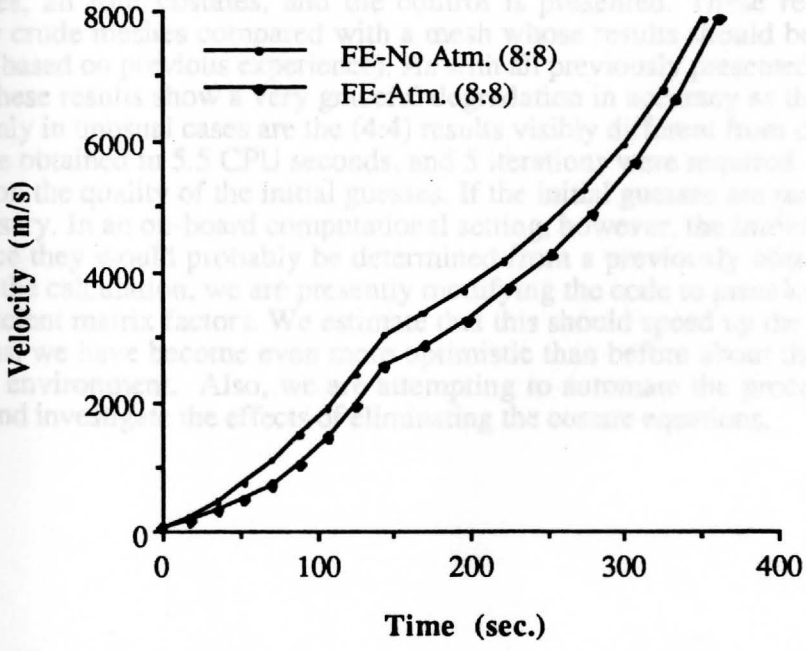

Fig. 15: Velocity vs. Time (comparing the effects of the atmosphere on the model and no atmosphere using the Finite Element Method)

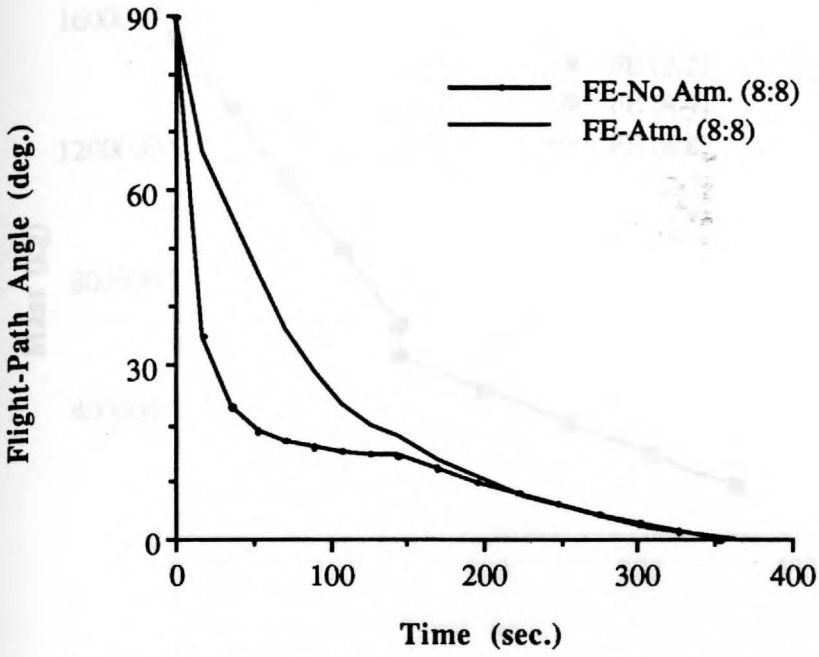

Fig. 16: Flight-Path Angle vs. Time (comparing the effects of the atmosphere on the model and no atmosphere using the Finite Element Method)

In Figs. 17 – 25, a complete set of results, including all ALS parameters and aerodynamics, for all four states, all four costates, and the control is presented. These results are presented with relatively crude meshes compared with a mesh whose results should be fairly close to the exact solution (based on previous experience). As with all previously presented results in our papers and reports, these results show a very graceful degradation in accuracy as the mesh becomes coarser. In fact, only in unusual cases are the (4:4) results visibly different from the (8:8) results. The (4:4) results are obtained in 5.5 CPU seconds, and 5 iterations were required. The number of iterations depends on the quality of the initial guesses. If the initial guesses are reasonably good only a few are necessary. In an on-board computational setting, however, the initial guesses should be pretty good since they would probably be determined from a previously obtained solution. To further speed up the calculation, we are presently modifying the code to precalculate the configuration of the coefficient matrix factors. We estimate that this should speed up the calculation by a factor of four. Thus, we have become even more optimistic than before about the method's potential in a real-time environment. Also, we are attempting to automate the process of determining initial guesses and investigate the effects of eliminating the costate equations.

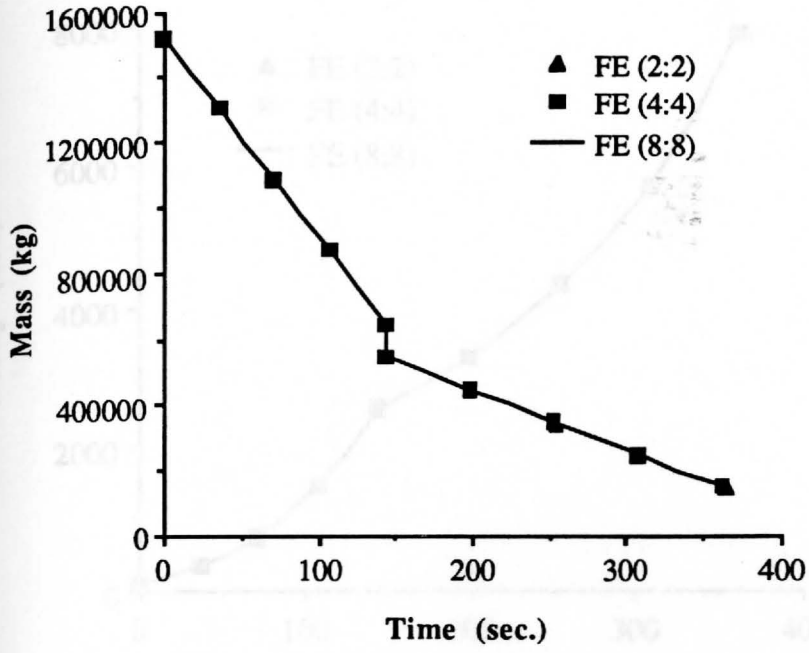

Fig. 17: Mass vs. Time (We are maximizing the final mass)

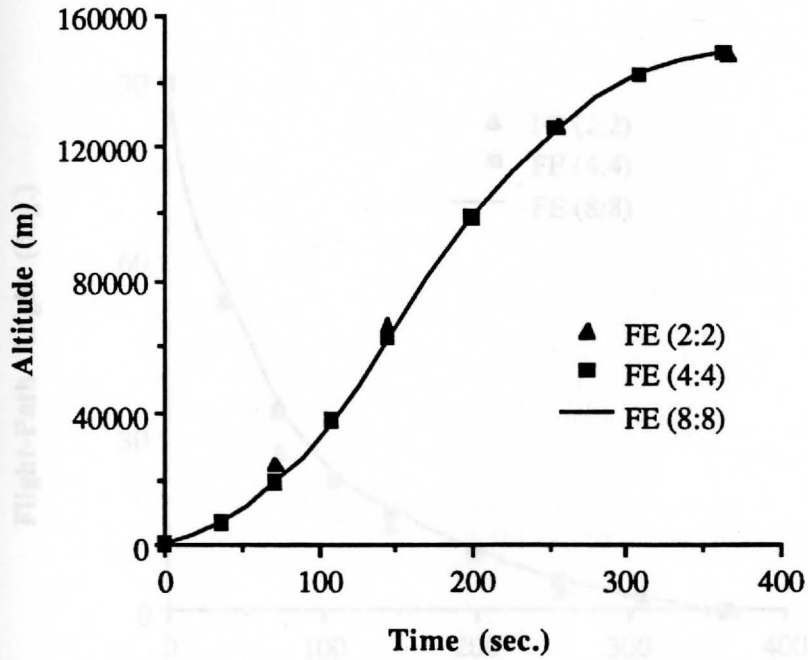

Fig. 18: Altitude vs. Time (The final altitude is constrained to be 148160.0 m)

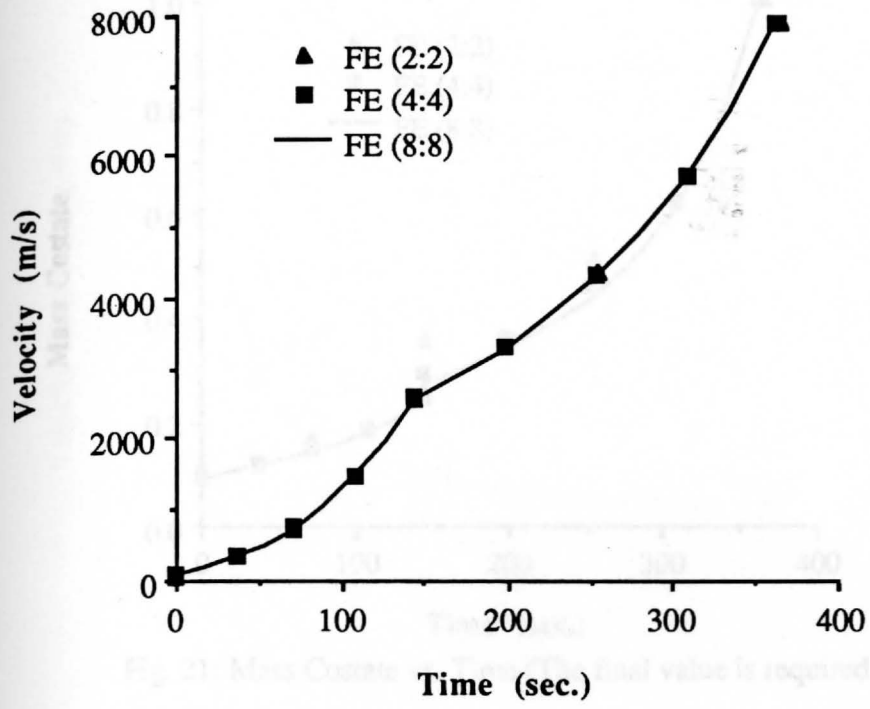

Fig. 19: Velocity vs. Time (The final velocity is constrained to be 7858.1995 m/s)

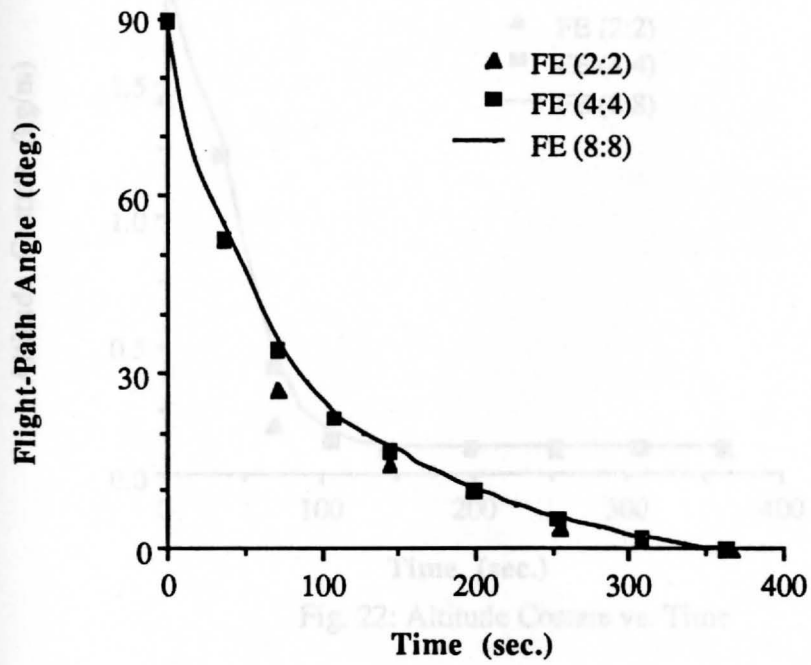

Fig. 20: Flight-Path Angle vs. Time (The final flight-path angle is constrained to be 0°)

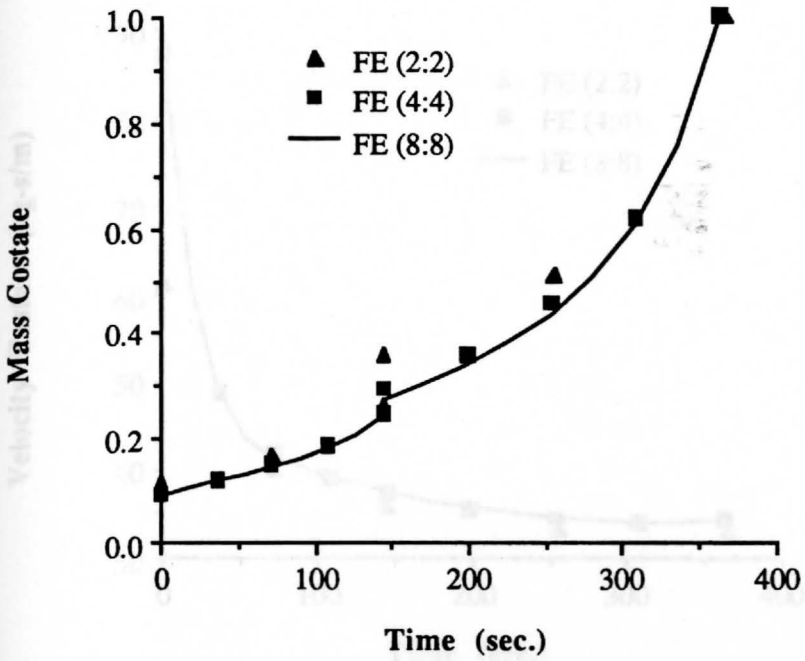

Fig. 21: Mass Costate vs. Time (The final value is required to be 1)

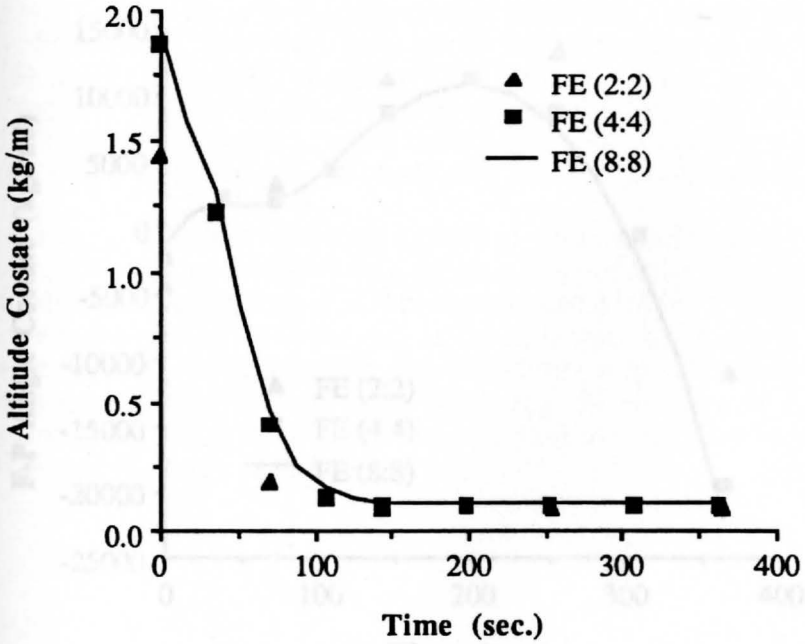

Fig. 22: Altitude Costate vs. Time

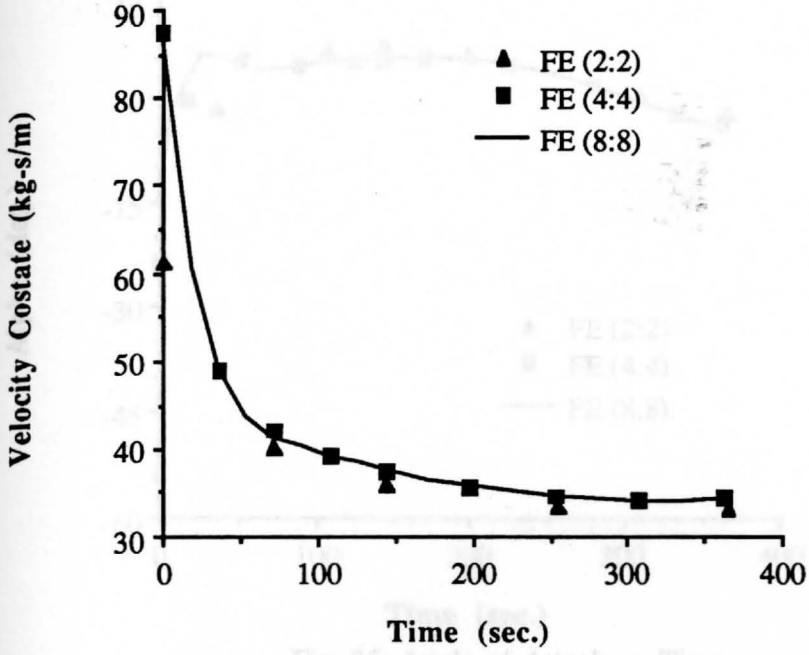

Fig. 23: Velocity Costate vs. Time

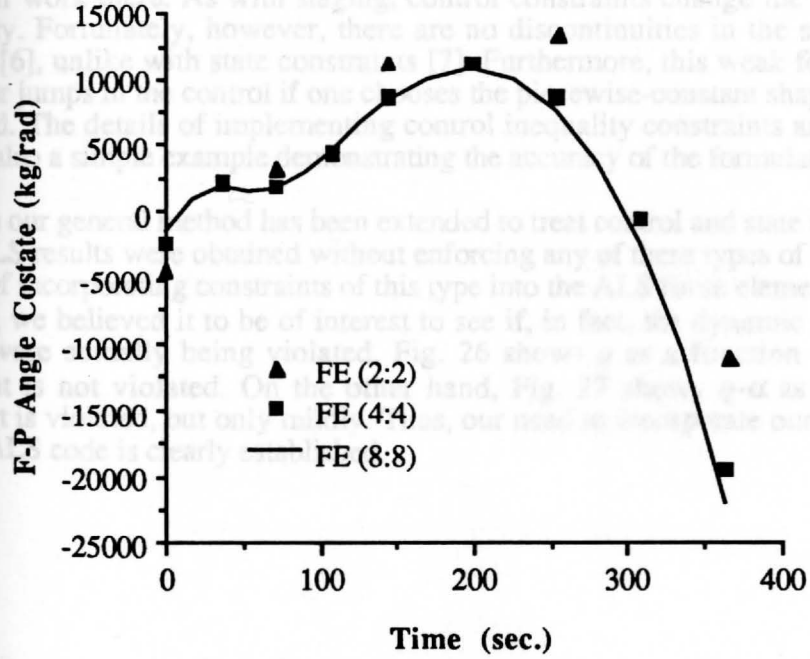

Fig. 24: Flight-Path Angle Costate vs. Time

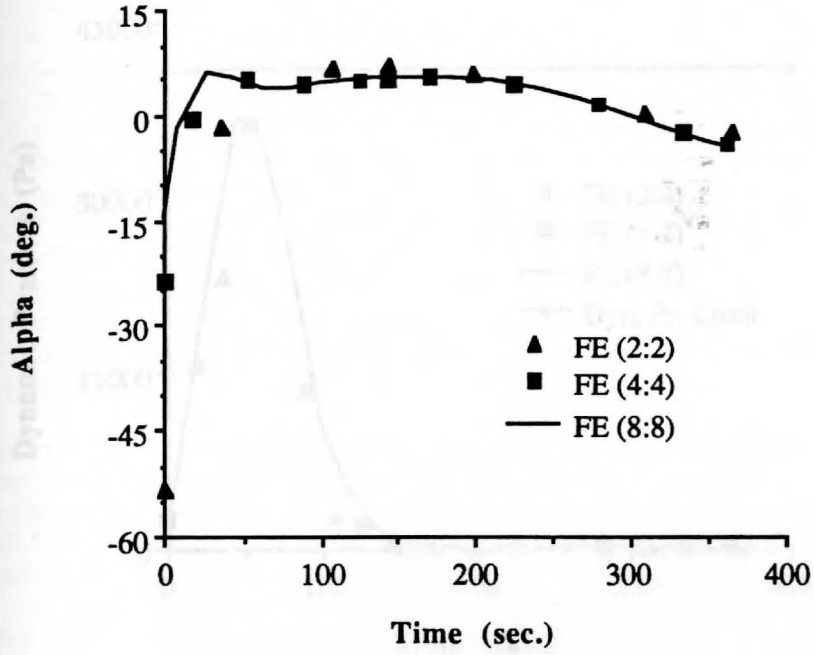

Fig. 25: Angle-of-Attack vs. Time

Some initial work has been done toward extension of the methodology to account for inequality constraints. Since control constraints are much easier to deal with than are state constraints, we began our work there. As with staging, control constraints change the conditions necessary for optimality. Fortunately, however, there are no discontinuities in the states or costates for this problem [6], unlike with state constraints [7]. Furthermore, this weak formulation automatically allows for jumps in the control if one chooses the piecewise-constant shape functions that we have employed. The details of implementing control inequality constraints are found in the appendix. There is also a simple example demonstrating the accuracy of the formulation.

Although our general method has been extended to treat control and state inequality constraints, the above ALS results were obtained without enforcing any of these types of constraints. We are in the process of incorporating constraints of this type into the ALS finite element code. In the meantime, however, we believed it to be of interest to see if, in fact, the dynamic pressure (q) or q-α constraints were actually being violated. Fig. 26 shows q as a function of time. Obviously, this constraint is not violated. On the other hand, Fig. 27 shows q-α as a function of time; this constraint is violated, but only mildly. Thus, our need to incorporate our developed methodology into the ALS code is clearly established.

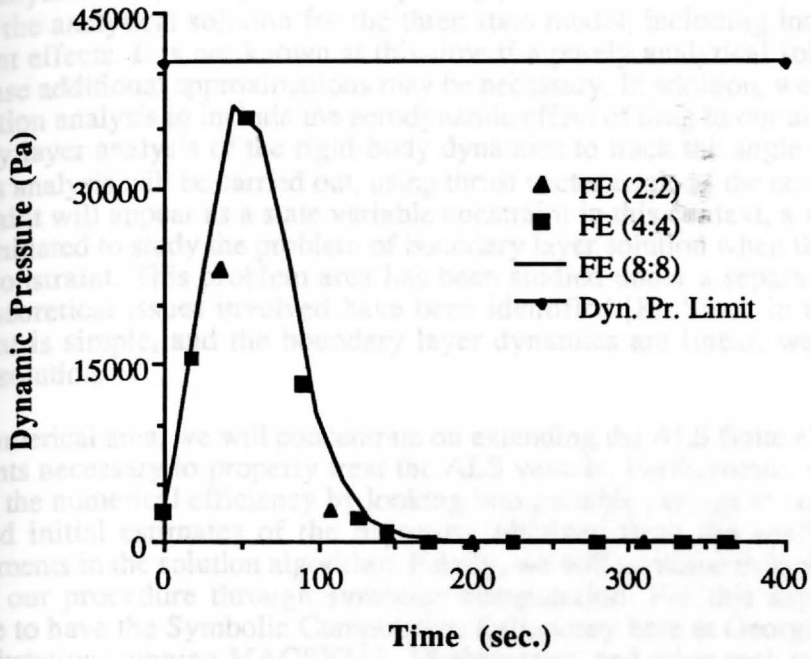

Fig. 26: Dynamic Pressure q vs. Time (Notice that this state constraint is not violated)

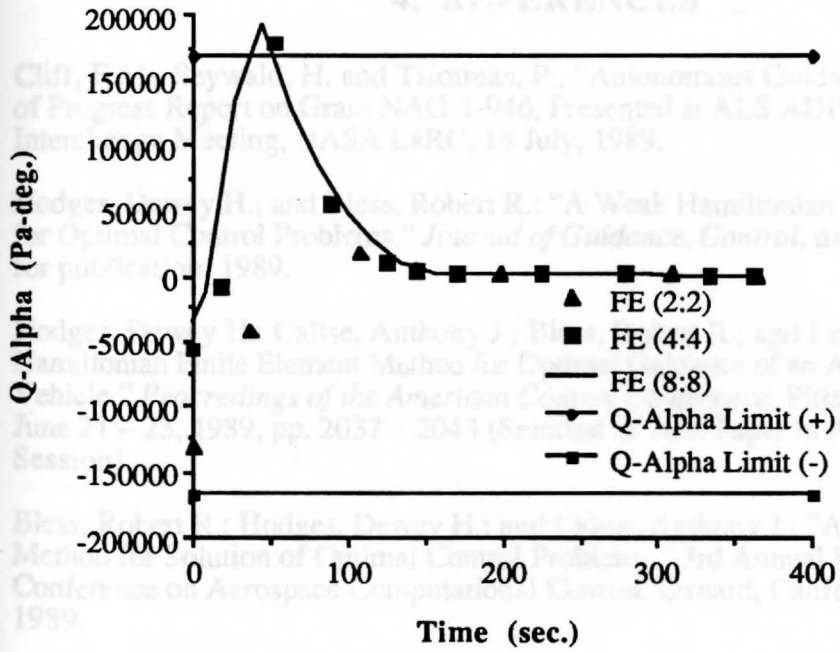

Fig. 27: α-q vs. Time (Notice that this control constraint is violated for a short time)

3. FUTURE RESEARCH

In the analytical area, during the next reporting period we will complete our analysis and development of the analytical solution for the three state model, including incorporating the q and α-q constraint effects. It is not known at this time if a purely analytical solution will be possible, in which case additional approximations may be necessary. In addition, we plan to consider a regular perturbation analysis to include the aerodynamic effect of drag in our analysis. Finally, a separate boundary layer analysis of the rigid-body dynamics to track the angle of attack profile obtained from this analysis will be carried out, using thrust vector angle as the control variable. Since the α-q constraint will appear as a state variable constraint in this context, a separate but parallel effort will be initiated to study the problem of boundary layer solution when the reduced solution lies on a state constraint. This problem area has been studied under a separate study, and some of the major theoretical issues involved have been identified [8]. Since in this case, the form of the constraint is simple, and the boundary layer dynamics are linear, we hope to obtain a purely analytic solution.

In the numerical area, we will concentrate on extending the ALS finite element code to include the constraints necessary to properly treat the ALS vehicle. Furthermore, we will attempt to further improve the numerical efficiency by looking into possible savings in computational time through improved initial estimates of the trajectory obtained from the analytical work and through improvements in the solution algorithm. Finally, we will continue to look into ways of automating parts of our procedure through symbolic computation. For this aspect of the work, we are fortunate to have the Symbolic Computation Laboratory here at Georgia Tech with a network of Sun workstations running MACSYMA, Mathematica, and other such tools. Delays in getting this laboratory set up did not allow us to devote much time to this aspect of the effort during the past reporting period.

4. REFERENCES

1. Cliff, E.M., Seywald, H. and Tsiotreas, P., "Autonomous Guidance Study," Presentation of Progress Report on Grant NAG-1-946, Presented at ALS ADP 2202 Technical Interchange Meeting, NASA LaRC, 18 July, 1989.

2. Hodges, Dewey H.; and Bless, Robert R.: "A Weak Hamiltonian Finite Element Method for Optimal Control Problems," *Journal of Guidance, Control, and Dynamics*, submitted for publication, 1989.

3. Hodges, Dewey H.; Calise, Anthony J.; Bless, Robert R.; and Leung, Martin: "A Weak Hamiltonian Finite Element Method for Optimal Guidance of an Advanced Launch Vehicle." *Proceedings of the American Control Conference*, Pittsburgh, Pennsylvania, June 21 – 23, 1989, pp. 2037 – 2043 (Selected as Best Paper in Aerospace Guidance Session).

4. Bless, Robert R.; Hodges, Dewey H.; and Calise, Anthony J.: "A Finite Element Based Method for Solution of Optimal Control Problems." 3rd Annual NASA, NSF, DoD Conference on Aerospace Computational Control, Oxnard, California, August 28 – 30, 1989.

5. Speyer, J.L., Feeley, T. and Hull, D.G., "Real-Time Approximate Optimal Guidance Laws For The Advanced Launch System," ACC 89, Pittsburgh, July 1989.

6. Bryson, Arthur E. Jr.; and Ho, Yu-Chi: *Applied Optimal Control*, Blaisdell Publishing Company, Waltham, Massachusetts, 1969, Chapters 2 and 3.

7. Jacobson, D. H.; Lele, M. M.; and Speyer, J. L.: "New Necessary Conditions of Optimality for Control Problems with State-Variable Inequality Constraints." *Journal of Mathematical Analysis and Applications*, vol. 35, 1971, pp. 255 – 284.

8. Calise, A.J., Corban, J. E., "Optimal Control of Singularly Perturbed Nonlinear Systems with State-Variable Inequality Constraints," IFAC Workshop on Singular Perturbations and Asymptotic Methods, Boston, Aug. 1989.

APPENDIX: Inequality Constraints

Theoretical Treatment of Inequality Constraints

Consider a system of n states x and m controls u defined by $\dot{x} = f(x,u,t)$. Suppose that there are p inequality constraints on the controls (for all time t) of the form

$$g(u,t) \leq 0 \tag{1}$$

where

$$g = \lfloor g_1 \quad g_2 \quad \cdots \quad g_p \rfloor^T \tag{2}$$

Let us introduce the $p \times p$ diagonal matrix

$$k(t) = \begin{bmatrix} k_1 & 0 & \cdots & 0 \\ 0 & k_2 & \cdots & 0 \\ \vdots & \vdots & \ddots & \vdots \\ 0 & 0 & \cdots & k_p \end{bmatrix} = k^T(t) \tag{3}$$

and the p-dimensional column matrix

$$C = \lfloor 1 \quad 1 \quad \cdots \quad 1 \rfloor^T \tag{4}$$

Then

$$k^2 C = \lfloor k_1^2 \quad k_2^2 \quad \cdots \quad k_p^2 \rfloor^T \tag{5}$$

and the following from Eq. (1) is true if we choose k wisely.

$$[g(u,t) + k^2 C] = 0 \tag{6}$$

We will now adjoin Eq. (6) to our performance index J by using p Lagrange multiplier functions

$$\pi(t) = \lfloor \pi_1^2 \quad \pi_2^2 \quad \cdots \quad \pi_p^2 \rfloor^T \tag{7}$$

where

$$\delta\pi(t) = \lfloor \delta\pi_1^2 \quad \delta\pi_2^2 \quad \cdots \quad \delta\pi_p^2 \rfloor^T \tag{8}$$

The performance index now takes the form:

$$J = \int_{t_0}^{t_f} \left[\lambda^T(\dot{x} - f) + \pi^T(k^2 C + g) - L\right] dt - \phi|_{t_f} - \nu^T \psi|_{t_f} \tag{9}$$

Following the same steps as we have before in developing our weak formulation, we take a straightforward variation, integrate an $\dot{x}$ term by parts, and finally obtain

$$\begin{aligned}
&\int_{t_0}^{t_f} \left\{ \delta\dot{x}^T \lambda - \delta x^T \left[\left(\frac{\partial L}{\partial x}\right)^T + \left(\frac{\partial f}{\partial x}\right)^T \lambda \right] \right. \\
&- \delta\dot{\lambda}^T x - \delta\lambda^T f - \delta u^T \left[\left(\frac{\partial L}{\partial u}\right)^T + \left(\frac{\partial f}{\partial u}\right)^T \lambda + \left(\frac{\partial g}{\partial u}\right)^T \pi \right] \\
&\left. + \delta\pi^T(k^2 C + g) + (\delta k C)^T (2k\pi) \right\} dt - \delta\nu^T \psi \Big|_{t_f} \\
&- \delta t_f \left[L + \lambda^T f + \frac{\partial \phi}{\partial t} + \nu^T \frac{\partial \psi}{\partial t} + \pi^T (g + k^2 C) \right] \Big|_{t_f} \\
&- \delta x^T(t = t_f)\hat{\lambda}_f + \delta x^T(t = t_0)\hat{\lambda}_0 + \delta\lambda^T(t = t_f)\hat{x}_f - \delta\lambda^T(t = t_0)\hat{x}_0 = 0
\end{aligned} \tag{10}$$

This is the governing equation for the weak Hamiltonian method which includes inequality constraints on the controls. The next step is to introduce shape functions for k and π. These will be

$$\begin{aligned}
k &= \bar{k}_i & \pi &= \bar{\pi}_i \\
\delta k &= \delta\bar{k}_i & \delta\pi &= \delta\bar{\pi}_i
\end{aligned} \tag{11}$$

We may now substitute these shape functions into Eq. (10) and carry out the integration to obtain a set of algebraic equations. Note that we have picked up Np unknown $\bar{k}$'s and Np unknown $\bar{\pi}$'s, along with $2Np$ extra equations. Thus, the number of equations and unknowns are still the same.

Example

This example is taken from section 3.8 in [5]. The problem is to minimize

$$J = \frac{1}{2}x(T)^2 + \frac{1}{2}\int_0^T u^2\, dt \tag{12}$$

where $t_0 = 0$, $t_f = T = 10$, x and u are scalars, and the initial condition is $x(t = 0) = -19.945596$. The state equation is

$$\dot{x} = h(t)u \tag{13}$$

with

$$h(t) = 1 + t - \frac{3}{17}t^2 \tag{14}$$

There are two control constraints in this example, and they are

$$\begin{aligned}
u - 1 &\leq 0 \\
-(u + 1) &\leq 0
\end{aligned}$$

Results for the control and multipliers π are shown in Figs. A-1 and A-2. Note that for the 4 element case, the first constrained arc is completely skipped over by the finite element discretization, yet the remainder of the solution is still very accurate. Thus, in a problem with many constrained and unconstrained arcs, a small number of elements could still be used to generate guesses for a higher number of elements.

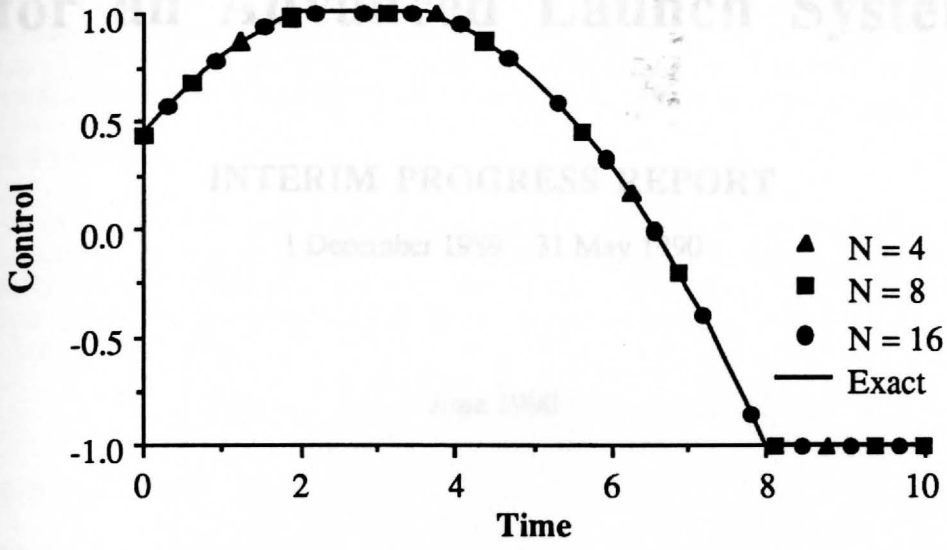

Fig. A-1: Control vs. Time

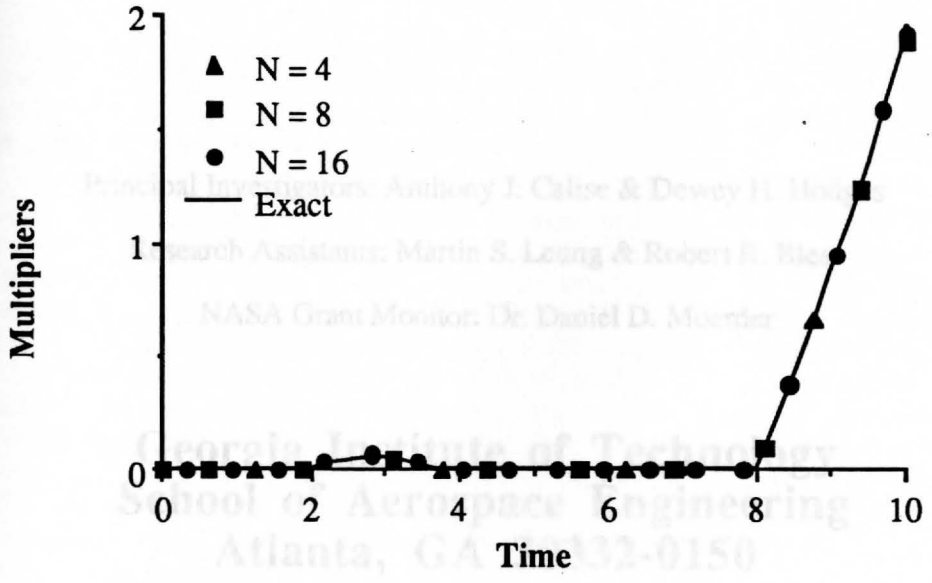

Fig. A-2: Multipliers vs. Time

Optimal Guidance Law Development for an Advanced Launch System

INTERIM PROGRESS REPORT

1 December 1989 – 31 May 1990

June 1990

Research Supported by NASA Langley Research Center

NASA Grant No. NAG-1-939

Principal Investigators: Anthony J. Calise & Dewey H. Hodges

Research Assistants: Martin S. Leung & Robert R. Bless

NASA Grant Monitor: Dr. Daniel D. Moerder

Georgia Institute of Technology
School of Aerospace Engineering
Atlanta, GA 30332-0150

1. SUMMARY

1.1 Three-State Model Analysis

This is the extension of the work we reported in the last Interim Progress Report. A state-transition matrix technique is used to find the correction for the neglected dynamics in the three-state model. We successfully incorporated the first-order correction for the neglected spherical Earth effect and the rocket motor back-pressure effect; see Figs. 1 – 7. These results have been published in [1]. We also found that the technique can be employed without requiring on-board quadrature which represents a significant enhancement for any real time guidance application.

1.2 Finite Elements In Time

We have successfully incorporated the theory for control constraints in the finite element trajectory optimization code [2] and results have been obtained. Results for both the constrained and unconstrained ALV have also been compared with those of a multiple shooting code and incorporated in [3]. Development of the state constraint coding methodology has also been underway, but at a low level.

2. RESEARCH ACCOMPLISHMENTS

2.1 Three-State Model analysis

A Regular Perturbation Method is used to derive the higher-order correction dynamics based on the expansion of the state and costate dynamics, and the optimality condition about the zero-order solution. The zero-order solution corresponds to a flat Earth assumption with no atmosphere and analytic expressions are given in [1] as well as in the last report. With a change of the independent variable, time in our case, we identify a correction term for this open final time problem.

The higher order dynamics are defined by sets of non-homogeneous linear ordinary differential equations. These equations can be solved by computing the state transition matrix, which depends only on the zero-order solution, and a numerical quadrature of the nonlinear forcing functions that depend on all the lower order terms.

However, instead of repeatedly solving the zero-order solution and performing on-line quadrature at every update in a feedback control formulation (using the instantaneous states values as the initial conditions), we found that the zero order solution computed at the initial time can be used for the first order correction all along the solution. This is due to the fact that an analytical expression is available for the state transition matrix. This method requires storing the numerical quadrature as a function of a monotonically increasing variable, such as total velocity. The key is to properly define the initial condition for the first order correction of the state time history to be the difference between the zero order solution and the present vehicle state. That is, regard t_o as any time along the trajectory. The zero order solution is defined for the initial conditions at launch, and evaluated for the current vehicle velocity, $\mathbf{x}_0(V)$. This means that at t_o there will be an error between the current state and $\mathbf{x}_0(V)$, which defines the initial condition for the first order correction term. This is mathematically represented by the following equations:

$$
\begin{aligned}
& \mathbf{x}(t_o) = \mathbf{x}_0(t_o) + \varepsilon \mathbf{x}_1(t_o) + \varepsilon^2 \mathbf{x}_2(t_o) + \ldots . \\
\Rightarrow \quad & \mathbf{x}_0(t_o) = \mathbf{x}_0(V) \\
\Rightarrow \quad & \varepsilon \mathbf{x}_1(t_o) = \mathbf{x}(t_o) - \mathbf{x}_0(V) \\
\Rightarrow \quad & \mathbf{x}_2(t_o) = \mathbf{x}_3(t_o) = \ldots . = \mathbf{0} \qquad (1)
\end{aligned}
$$

This allows us to completely avoid on-line quadrature since the zero order solution is now divorced for the current vehicle state. For completeness we enclose a copy of [1], and an addendum which more fully explains the on-line procedure in Appendix A. This method of first-order correction did not occur to us until after we submitted [1] for conference publication. However, the results were included in the conference presentation, and the addendum was handed out at the session. The feasibility of this approach is demonstrated in Figures 8 – 11 of the addendum by introducing an initial deviation of +100% in each of the state components (v, u, h). These results are preliminary because the first order correction is calculated only once at the beginning of the trajectory, instead of along the whole trajectory. Thus they more or less represent the worst case scenario, and a closed loop simulation should give a much better approximation which we hopefully can demonstrate in the next few months. Note that these solutions accurately track the optimal solution as the final time is approached even without updating the solution along the trajectory.

2.2 Finite Elements In Time

The theory involving control inequality constraints was incorporated into the ALV code. After noting that one of the specified constraints was violated, that constraint was included into the code. A full set of results is given in Appendix B. The results from the finite element code are compared to the results obtained from a multiple shooting code. This provided a means of validating the code.

Some work was also done with state inequality constraints. This work was done at a low level of priority; therefore, no results are ready to be shown at this time. However, the theory is well developed now and is derived in Appendix C.

3. FUTURE RESEARCH

The closed loop simulation using Method 2 for a first-order correction will be performed and analyzed. Also we will incorporate the aerodynamic effects in the neglected dynamics. A general programming code will be developed for the nonlinear forcing function in the higher order dynamics to avoid specific algebraic derivation for each problem. The α-q inequality constraint will be investigated. We will also look at the effect of using some small physical parameter, ε (*e.g.* atmospheric scale height) on the range of convergence of the asymptotic expansion solution, which in our analysis to date is only introduced as a bookkeeping parameter and has a value of unity.

Problems involving state inequality constraints will be researched more thoroughly. Some simple example problems given in [5] will be used to test the theory set forth in Appendix C. The use of homotopy methods will be investigated in order to have the code as self-starting and reliable as possible. Also, a more general code using MACSYMA will be written. This code will evaluate necessary derivatives of the state equations and write FORTRAN code. This will eliminate possible errors and much of the programming work required by the user. Finally, we will always be looking for ways to run the code more quickly. Our goal is to run the Advanced Launch Vehicle code in 1 to 2 seconds.

4. REFERENCES

[1] Leung, S. K., Calise A. J., "An Approach To Optimal Guidance Of An Advanced Launch Vehicle Concept," *Proceedings of the Amercan Control Conference*, San Diego, California, May 23 – 25, 1990 (Invited).

[2] Bless, R. R., and Hodges, D. H., "Finite Element Solution of Optimal Control Problems with Inequality Constraints," *Proceedings of the American Control Conference*, San Diego, California, May 23 – 25, 1990 (Invited; selected as best paper in the session Aerospace Vehicle Guidance and Trajectory Optimization – I).

[3] Hodges, D. H., Bless, R. R., Calise, A. J., and Leung, S. K., "Finite Element Method for Optimal Guidance of an Advanced Launch Vehicle with Inequality Constraints," in preparation for submittal to the *Journal of Guidance, Control, and Dynamics*.

[4] Byson, Arthur E. Jr., and Ho, Yu-Chi, *Applied Optimal Control*, Blaisdell Publishing Company, Waltham, Massachusetts, 1969, Chapters 2 and 3.

[5] Jacobson, D. H., Lele, M. M., and Speyer, J. L., "New Necessary Conditions of Optimality for Control Problems with State-Variable Inequality Constraints," *Journal of Mathematical Analysis and Applications*, Vol. 35, 1971, pp. 255 – 284.

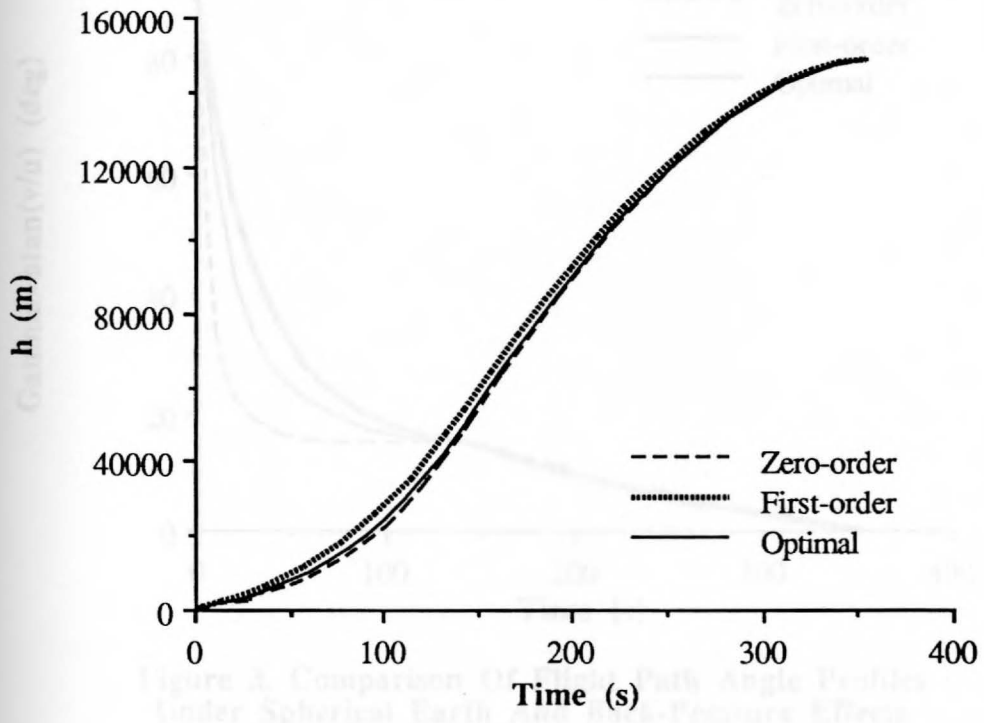

Figure 1. Comparison Of Altitude Profiles Under Spherical Earth And Back-Pressure Effects

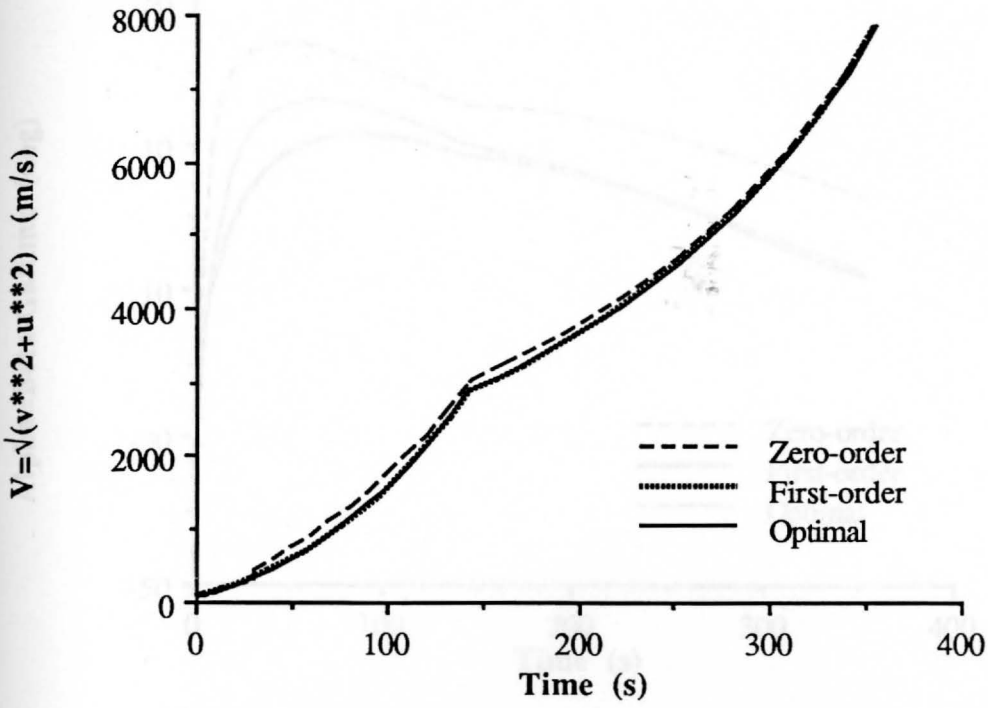

Figure 2. Comparison Of Velocity Profiles Under Spherical Earth And Back-Pressure Effects

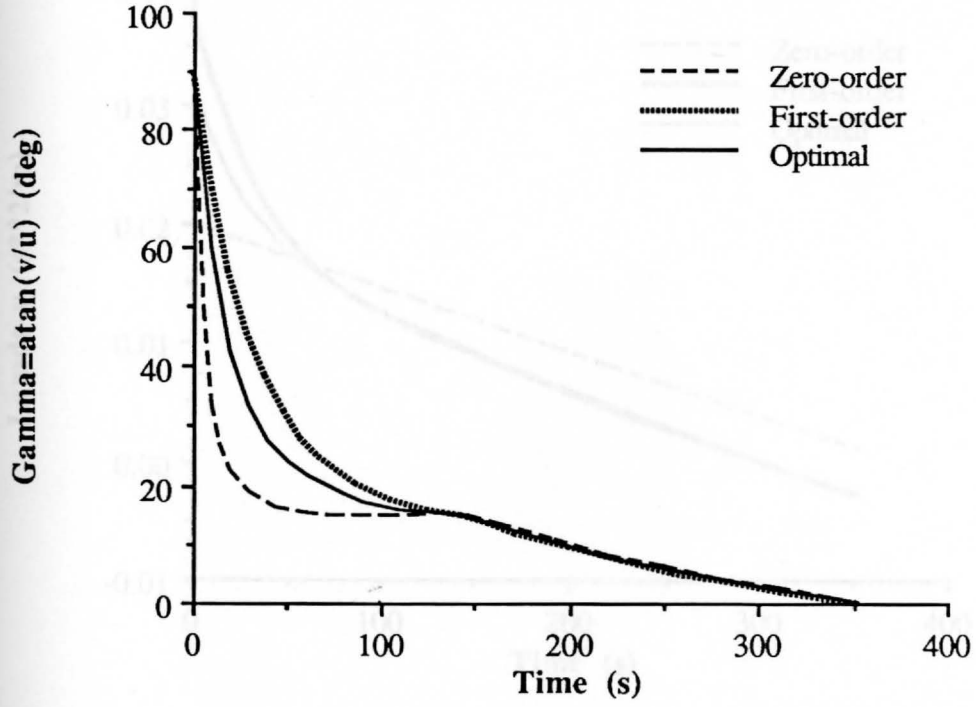

Figure 3. Comparison Of Flight Path Angle Profiles Under Spherical Earth And Back-Pressure Effects

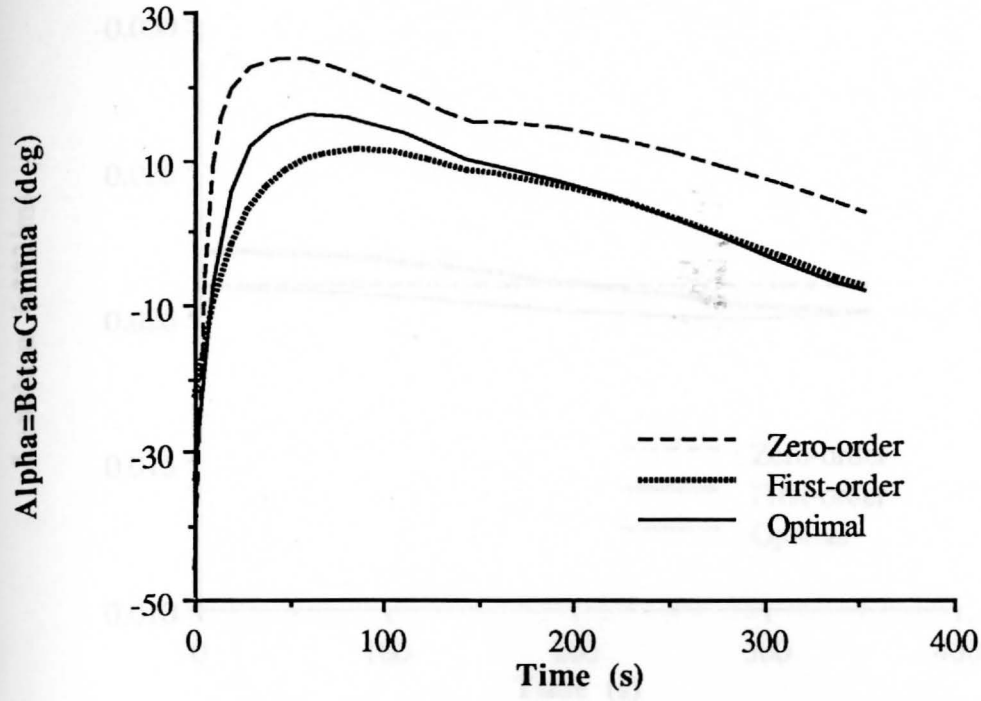

Figure 4. Comparison Of Angle Of Attack Profiles Under Spherical Earth And Back-Pressure Effects

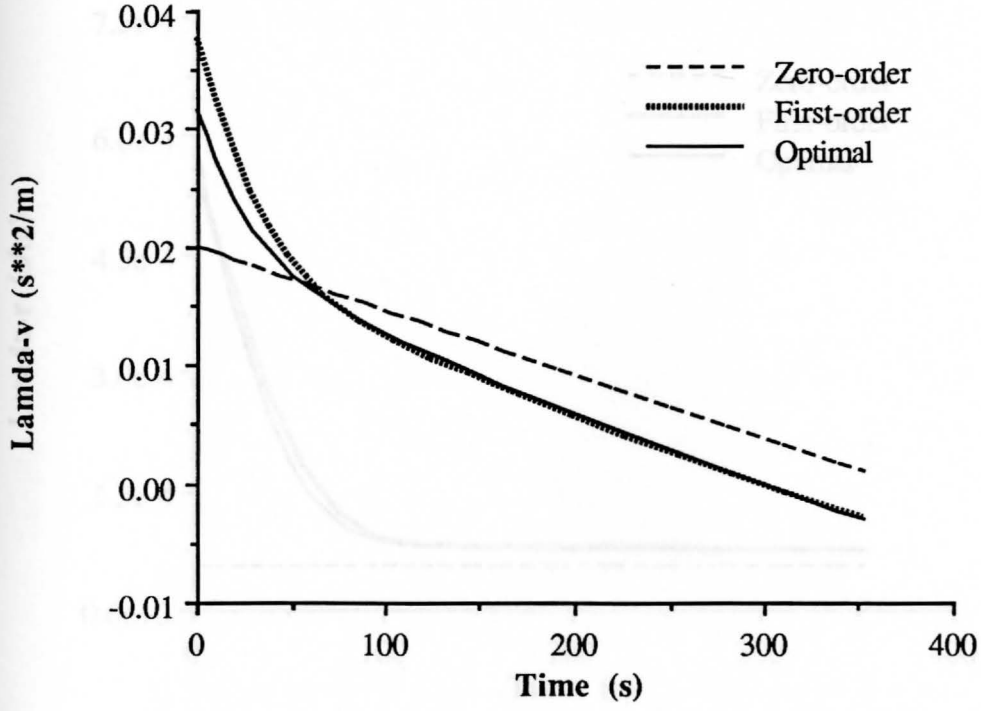

Figure 5. Comparison Of Lambda-v Profile Under Spherical Earth And Back-Pressure Effects

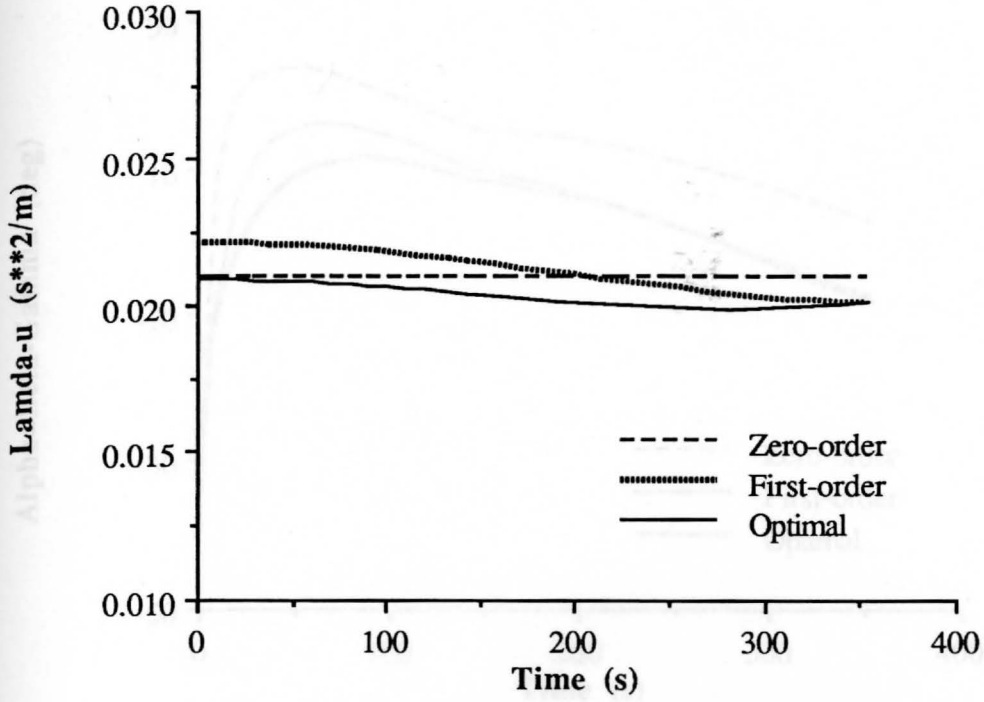

Figure 6. Comparison Of Lambda-u Profile Under Spherical Earth And Back-Pressure Effects

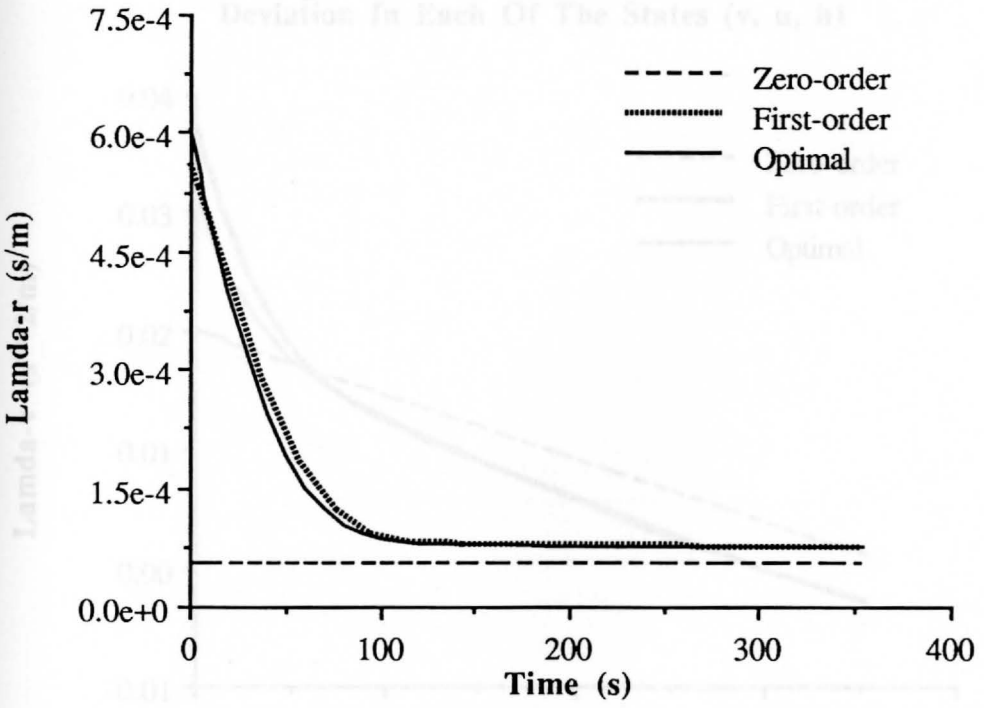

Figure 7. Comparison Of Lambda-r Profiles Under Spherical Earth And Back-Pressure Effects

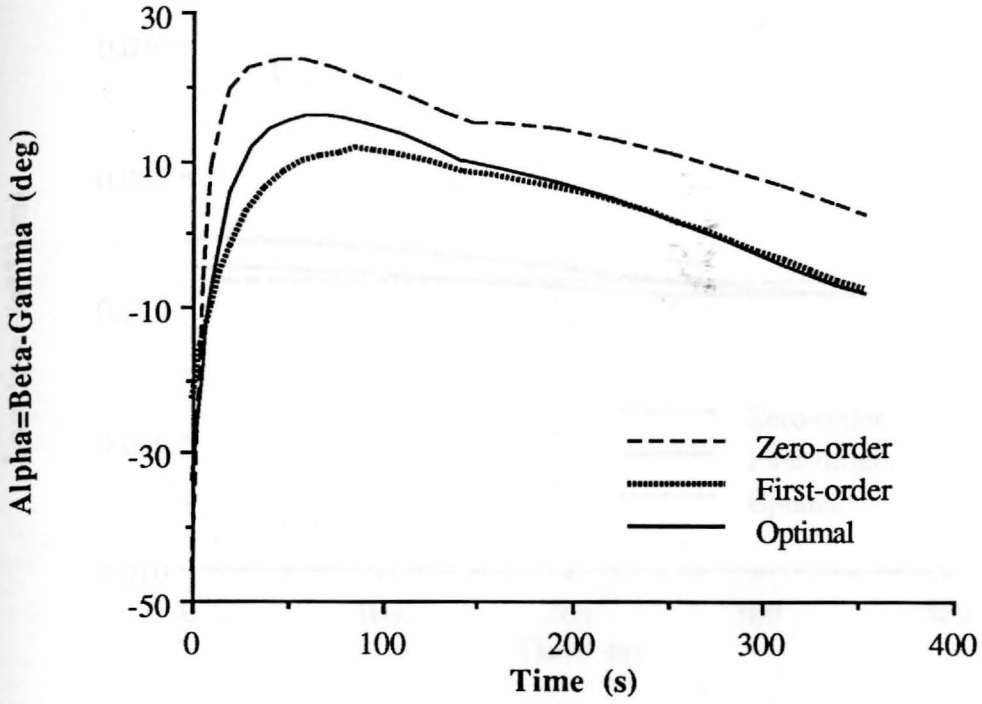

Figure 8. Comparison Of Angle Of Attack Profiles Using Method 2 With An Initial +100% Deviation In Each Of The States (v, u, h)

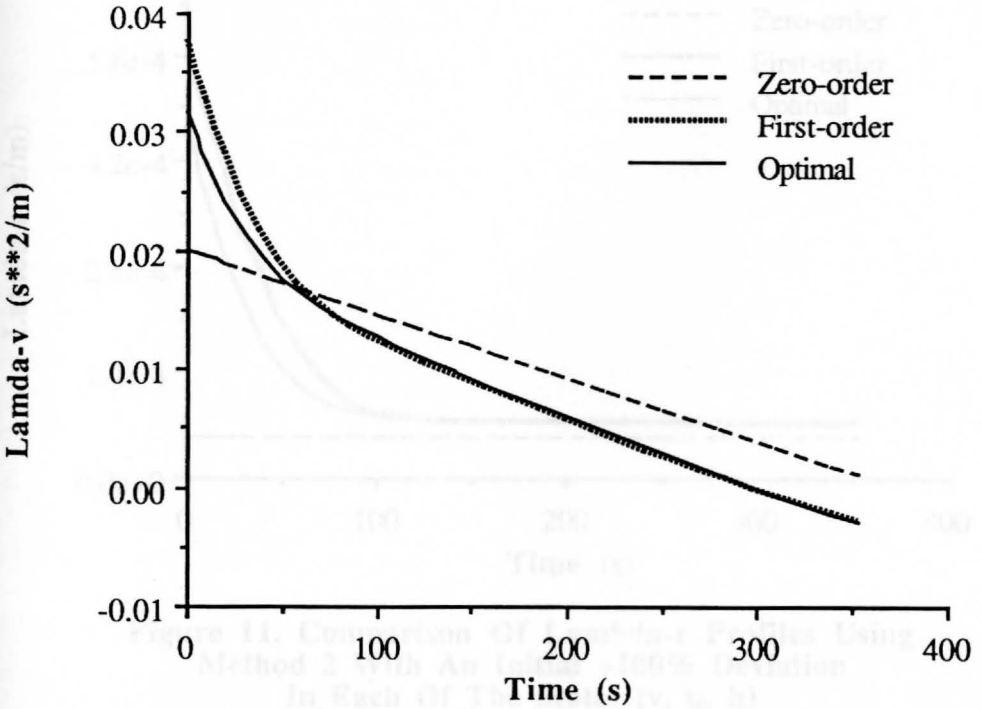

Figure 9. Comparison Of Lambda-v Profiles Using Method 2 With An Initial +100% Deviation In Each Of The States (v, u, h)

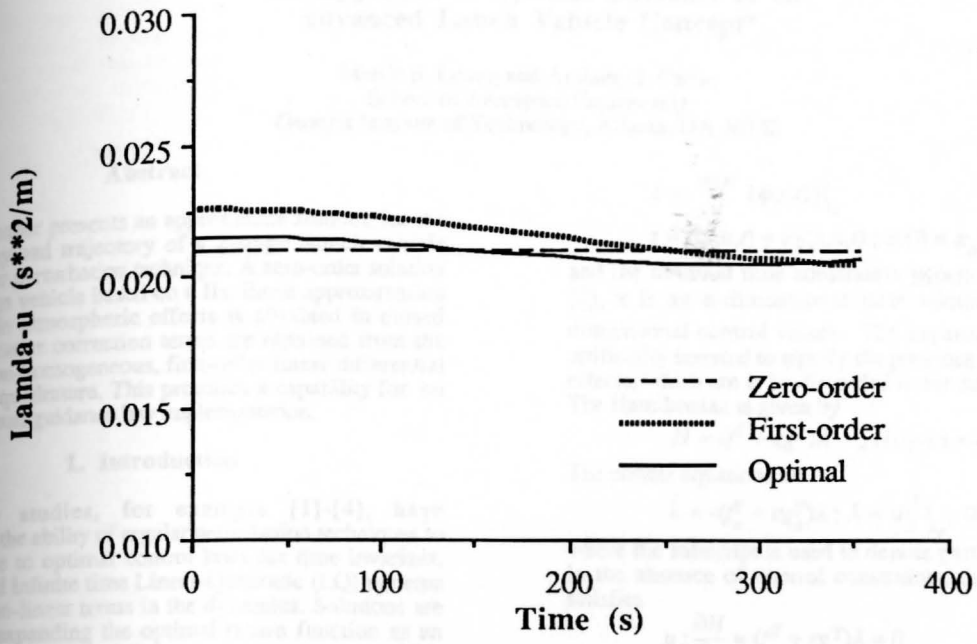

Figure 10. Comparison Of Lambda-u Profiles Using Method 2 With An Initial +100% Deviation In Each Of The States (v, u, h)

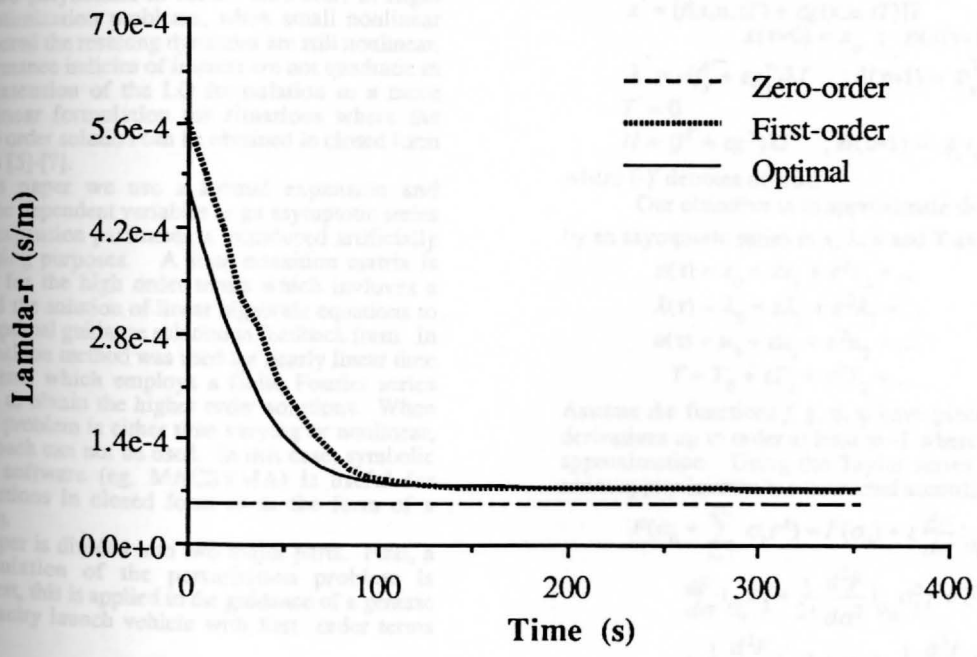

Figure 11. Comparison Of Lambda-r Profiles Using Method 2 With An Initial +100% Deviation In Each Of The States (v, u, h)

Appendix A

1990 ACC

An Approach to Optimal Guidance of an Advanced Lauch Vehicle Concept*

Martin S. Leung and Anthony J. Calise
School of Aerospace Engineering
Georgia Institute of Technology, Atlanta, GA 30332

Abstract

This paper presents an approximate solution for the maximum payload trajectory of a 2-stage launch vehicle using a regular perturbation technique. A zero-order solution for a two stage vehicle based on a flat Earth approximation and negligible atmospheric effects is obtained in closed form. High order correction terms are obtained from the solution of non-homogeneous, first-order linear differential equations by quadrature. This promises a capability for an on-board optimal guidance law implementation.

1. Introduction

Many studies, for example [1]-[4], have demonstrated the ability of regular perturbation techniques to generate close to optimal control laws for time invariant, fixed time and infinite time Linear-Quadratic (LQ) systems with small non-linear terms in the dynamics. Solutions are obtained by expanding the optimal return function as an asymptotic series in terms of a perturbation parameter. This results in an approximate solution to the Hamilton-Jacobi-Bellman partial differential equation. The success of this approach relies on the fact that the zero order solution is known to be quadratic in the state vector, and the higher order terms are polynomial in form. However, in flight mechanics optimization problems, when small nonlinear effects are ignored the resulting dynamics are still nonlinear, and the performance indicies of interest are not quadratic in form. The extension of the LQ formulation to a more general nonlinear formulation for situations where the nonlinear zero order solution can be obtained in closed form is presented in [5]-[7].

In this paper we use a formal expansion and represent all the dependent variables as an asymptotic series in which the expansion parameter is introduced artificially for book-keeping purposes. A state transition matrix is used to solve for the high order terms which invloves a quadrature and the solution of linear algebraic equations to obtain a near optimal guidance solution in feedback form. In [8], a state transition method was used for nearly linear time invariant systems which employs a finite Fourier series representation to obtain the higher order solutions. When the zero order problem is either time varying or nonlinear, then this approach can not be used. In this case, symbolic manipulation software (eg. MACSYMA) is useful for obtaining solutions in closed form or in the form of a truncated series.

The paper is divided into two major parts. First, a general formulation of the perturbation problem is developed. Next, this is applied to the guidance of a generic heavy lift capacity launch vehicle with first order terms included.

2. Regular Perturbation In Optimal Control

The optimal control problem is to maximize a performance index which is a function of the terminal states and time, subject to non-linear dynamic constraints:

$$J = \min_{u} \{\phi(x,t)\}|_{t_f} \tag{1}$$

$$\dot{x} = f(x,u,t) + \varepsilon g(x,u,t)\ ;\ x(0) = x_o\ ;\ t \in [0,t_f] \tag{2}$$

and the terminal time constraints $\psi_i(x_f) = 0$, i=1...p<n. In (2), x is an n-dimensional state vector and u is an m-dimensional control vector. The expansion parameter ε is artificially inserted to signify the presence of small nonlinear effects, which are to be discarded in the zero order solution. The Hamiltonian is given by

$$H = (f^T + \varepsilon g^T)\lambda \quad ;\ H(t_f=1) = -\phi_t|_{t_f} \tag{3}$$

The costate equations are

$$\dot{\lambda} = -(f_x^T + \varepsilon g_x^T)\lambda\ ;\ \lambda = \Phi_x^T|_{t_f}\ ;\ \Phi = \phi + \nu^T\varphi \tag{4}$$

where the subscript is used to denote partial differentiation. In the absence of control constraints, the optimal control satisfies

$$u : \frac{\partial H}{\partial u} = (f_u^T + \varepsilon g_u^T)\lambda = 0 \tag{5}$$

assuming that $H_{uu} < 0$. In the above final time is free, thus we introduce a new independent variable $\tau = t/T$ where $T = t_f$ and rewrite the necessary conditions in (2-4) in the following equivalent form:

$$x' = [f(x,u,\tau T) + \varepsilon g(x,u,\tau T)]T$$
$$x(\tau=0) = x_o\ ;\ \varphi(x(\tau=1)) = 0 \tag{6}$$

$$\lambda' = -(f_x^T + \varepsilon g_x^T)\lambda T \quad ;\ \lambda(\tau=1) = \Phi_x^T|_{\tau=1} \tag{7}$$

$$T' = 0 \tag{8}$$

$$H = (f^T + \varepsilon g^T)\lambda T \quad ;\ H(\tau=1) = -\phi_t|_{\tau=1} \tag{9}$$

where (-)' denotes d(-)/dτ.

Our objective is to approximate the solution to (6-9) by an asymptotic series in x, λ, u and T as follows:

$$x(\tau) = x_0 + \varepsilon x_1 + \varepsilon^2 x_2 + \ldots \tag{10}$$

$$\lambda(\tau) = \lambda_0 + \varepsilon\lambda_1 + \varepsilon^2\lambda_2 + \ldots \tag{11}$$

$$u(\tau) = u_0 + \varepsilon u_1 + \varepsilon^2 u_2 + \ldots. \tag{12}$$

$$T = T_0 + \varepsilon T_1 + \varepsilon^2 T_2 + \ldots. \tag{13}$$

Assume the functions f, g, ϕ, ψ have piecewise continuous derivatives up to order at least m+1 where m is the order of approximation. Using the Taylor series formula, a finite series approximation is constructed according to

$$F(\sigma_0 + \sum_{k=1}^{m} \sigma_k\varepsilon^k) = F(\sigma_0) + \varepsilon\frac{dF}{d\sigma}|_{\sigma_0}\sigma_1 + \varepsilon^2\{$$
$$\frac{dF}{d\sigma}|_{\sigma_0}\sigma_2 + \frac{1}{2!}\frac{d^2F}{d\sigma^2}|_{\sigma_0}\sigma_1^2\} + \varepsilon^3\{\frac{dF}{d\sigma}|_{\sigma_0}\sigma_3$$
$$+ \frac{1}{2!}\frac{d^2F}{d\sigma^2}|_{\sigma_0}2\sigma_1\sigma_1 + \frac{1}{3!}\frac{d^3F}{d\sigma^3}|_{\sigma_0}\sigma_1^3\} + \cdots \tag{14}$$

where $\sigma = \{x,\lambda,\nu,u,T\}$. Substituting these series approximations in (6) and (7) and equating like powers in ε, we obtain the following zero order necessary conditions:

$$x_0' = f^{oT}T_0 \quad ;\ x_0(\tau=o) = x_o\ ;\ \varphi(x_0(\tau=1)) = 0 \tag{15}$$

$$\lambda_0' = -f_x^{oT}\lambda_0 \quad ;\ \lambda_0(\tau=1) = \Phi_x^{oT}|_{t=T_0} \tag{16}$$

where the superscript denotes that the arguments are the leading terms in the series expansions of x, u and T. Transforming back to a zero order approximation of the

* Supported by NASA LaRC under Grant # NAC-1-939.

original independent variable $t^o = \tau T_0$, where it should be noted that the zero order solution for T is used, the zero order necessary conditions are equivalently written (with some abuse of derivative notation) as:

$$\dot{x}_0 = f^o \quad ; x_0(t=0) = x_o \; ; \; \varphi(x_0(t=T_0)) = 0 \tag{17}$$

$$\dot{\lambda}_0 = -f_x^{oT}\lambda_0 \quad ; \lambda_0(t=T_0) = \Phi_x^{oT}\,|_{t=T_0} \tag{18}$$

$$u_0 : 0 = f_u^{oT}\lambda_0 \tag{19}$$

$$H_0 = \lambda_0^T f^o \quad ; H_0(T_0) = -\phi_t^o\,|_{t=T_0} \tag{20}$$

For the application that follows in the next section, it is shown that it is possible to solve this zero order problem in closed form. Equating the first order terms of the expansion results in the following first order necessary conditions:

$$\dot{x}_1 = f_x^o x_1 + f_u^o u_1 + \frac{T_1}{T_0}(f^o + tf_t^o) + g^o$$
$$x_1(0) = 0 \; ; \; \varphi_x^o x_1(T_0) = 0 \tag{21}$$

$$\dot{\lambda}_1 = -(f_x^T\lambda_0)_x^o x_1 - (f_x^T\lambda_0)_u^o u_1 - f_x^{oT}\lambda_1 - \frac{T_1}{T_0}(f_x^{oT}\lambda_0 - g_x^{oT}\lambda_0) \; ; \lambda_0(T_0) = (\Phi_{xx}^{oT}x_1 + \Phi_{xt}^o T_1)|_{T_0} \tag{22}$$

$$u_1 = -[(f_u^T\lambda_0)_u^o]^{-1}[f_u^{oT}\lambda_1 + (f_u^T\lambda_0)_x^o x_1 + t\frac{T_1}{T_0}(f_u^T\lambda_0)_t^o + g_u^{oT}\lambda_0] \tag{23}$$

$$H_1 = (\lambda_0^T f)_x^o x_1 + t\frac{T_1}{T_0}\lambda_0^T f_t^o + \lambda_0^T g^o + f^{oT}\lambda_1 \quad ; H_1(T_0) = -(\phi_{tx}^o x_1 + \phi_{tt}^o T_1)|_{T_0} \tag{24}$$

Note that (21) - (24) explicitly show the effect of the first order corrections to the final time, T. If the solution process is terminated at this point, then a real time sampled data implementation of the control solution would be impelemted as follows. For the original system in (2), the optimal control can be determined as a function of x and λ from the optimality condtion $H_u = 0$, where $H = f + \varepsilon g$. At $t=0$ then a first order approximation is obtained by using $\lambda_0(0) + \varepsilon\lambda_1(0)$ as an approximation for $\lambda(0)$ to compute the control as a function of the present value of the state. This process is repeated at the next control update time by regarding the present value of the state as the new initial state, $\mathbf{x}_o$. However, it is necessary to repeat the zero and first order solutions in updating the estimate of the costate variable.

It can be shown that all the high order terms are given by a set of non-homogeneous linear differential equations which have the form.

$$\dot{x}_j = A_{11}x_j + A_{12}\lambda_j + \frac{T_j}{T_0}C_1 + \Psi_1(x_0, \ldots, x_{j-1}, \lambda_0, \ldots, \lambda_{j-1}, T_0, \ldots, T_{j-1}) \tag{25}$$

$$\dot{\lambda}_j = A_{21}x_j + A_{22}\lambda_j + \frac{T_j}{T_0}C_2 + \Psi_2(x_0, \ldots, x_{j-1}, \lambda_0, \ldots, \lambda_{j-1}, T_0, \ldots, T_{j-1}) \tag{26}$$

where

$$A_{11} = f_x^o - f_u^o[(f_u^T\lambda_0)_u^o]^{-1}(f_u^T\lambda_0)_x^o \qquad A_{12} = -f_u^o[(f_u^T\lambda_0)_u^o]^{-1}f_u^o$$
$$A_{21} = -(f_x^T\lambda_0)_x^o + (f_x^T\lambda_0)_u^o[(f_u^T\lambda_0)_u^o]^{-1}(f_u^T\lambda_0)_x^o$$
$$A_{22} = -f_x^{oT} + (f_x^T\lambda_0)_u^o[(f_u^T\lambda_0)_u^o]^{-1}f_u^{oT} \tag{27}$$

$$C = \begin{bmatrix} f^o + t\{f_t^o - f_u^o[(f_u^T\lambda_0)_u^o]^{-1}(f_u^T\lambda_0)_t\} \\ -f_x^{oT}\lambda_0 - t\{(f_x^T\lambda_0)_t - (f_x^T\lambda_0)_u^o[(f_u^T\lambda_0)_u^o]^{-1}(f_u^T\lambda_0)_t\} \end{bmatrix} \tag{28}$$

and can be solved by the state transition matrix $\Phi_A(t,0)$

$$\begin{bmatrix} x_j(t) \\ \lambda_j(t) \end{bmatrix} = \Phi_A(t,0)\begin{bmatrix} 0 \\ \lambda_j(0) \end{bmatrix} + \frac{T_j}{T_0}\int_0^t \Phi_A(t,\tau)\begin{bmatrix} C_1(\tau) \\ C_2(\tau) \end{bmatrix}d\tau + \int_0^t \Phi_A(t,\tau)\begin{bmatrix} \Psi_1(\tau) \\ \Psi_2(\tau) \end{bmatrix}d\tau \quad \forall\, t \in [0,T_0] \tag{29}$$

Using the above expression at $t=T_0$ and the corresponding expansion terms of ψ, $H_x(T_0)$ and $H_j(T_0)$, we can solve for $\lambda_j(T_0)$, ν and T_j from a set of linear algebraic equations for the terminal boundary conditions involving these higher order correction terms.

3. The Ascent Trajectory Guidance

We now present the solution of an optimal control problem for optimizing the ascent trajectory of a two stage advanced launch vehicle concept. The performace objective is to minimize the fuel consumed, which for a given launch mass is equivalent to maximizing payload to orbit. Our objective here is show that a closed form solution for the zero order problem is possible, and to develop a closed form solution for the state transition matrix needed for the first and higher order corrections to the solutions. A comparison will be given between the zero order solution and an exact solution obtained using a multiple shooting algorithm.

Equations Of Motion

For a point mass vehicle in planar motion over a non-rotating spherical Earth, the equations of motion can be expressed in the following form:

$$\dot{m} = -k_i \quad ; m(0) = \mathbf{m}_o \tag{30}$$

$$\dot{v} = \frac{T_i sin\beta - D_i sin\gamma + L_i cos\gamma}{m} - \frac{\mu_e}{r^2} + \frac{u^2}{r} \; ; v(0) = \mathbf{v}_o \tag{31}$$

$$\dot{u} = \frac{T_i cos\beta - D_i cos\gamma - L_i sin\gamma}{m} - \frac{uv}{r} \quad ; u(0) = \mathbf{u}_o \tag{32}$$

$$\dot{r} = v \quad ; r(0) = \mathbf{r}_o \tag{33}$$

$$\dot{\phi} = \frac{u}{r} \quad ; \phi(0) = \phi_o \tag{34}$$

where

$$T_i = T_{vaci} - A_e p \qquad \alpha = \beta - \gamma$$
$$D_i = qS_f C_D(\alpha, M) \qquad L_i = qS_f C_L(\alpha, M)$$
$$\gamma = tan^{-1}(\frac{v}{u}) \tag{35}$$

Subscript i=1,2 denotes the first and the second stage parameters. The states are mass (m), radial speed (v), transverse speed (u), radial distance (r) and down range angle (ϕ). The control variable is β, the angle between the thrust vector and the local horizon. T_{vaci} is the vacuum thrust where A_e the nozzle exit area, p is the atmospheric pressure respectively, α is the angle of attack, and γ is the flight path anlge. C_{Di} and C_{Li} are the drag and lift coefficients whose dependence on α and the Mach number (M) is given in the form of tabular data. The performance index is $J=\max\{m(t_f)\}$ subject to the terminal constraints $v(t_f)=\mathbf{v}_f$, $u(t_f)=0$, $r(t_f)=\mathbf{r}_f$.

The Optimal Control Formulation

Since $\dot{\phi}$ does not enter into the dynamics and is unspecifed at the final time, its equation can be ignored and be treated separately. We eliminate m from (30) with

$$m(t) = m_i - k_i t \quad ; i=1,2 \tag{36}$$

where

$$m_1 = \mathbf{m}_o \, , \; m_2 = \mathbf{m}_{s+} + k_2 t_s \tag{37}$$

t_s is the staging time and m_{s+} is the mass immediately after staging. This results in a system of equations with a discontinuity at the staging time. Since the staging condition is simply $t-t_s=0$, we have a discontinuity in the Hamiltonian, but the state and costate variables are continuous [9]. In the remaining equations, the perturbation parameter is introduced as follows:

$$\dot{v} = \frac{T_{vaci}\sin\beta}{m_i - k_i t} - g_e + \varepsilon g_1 \tag{38}$$

$$\dot{u} = \frac{T_{vaci}\cos\beta}{m_i - k_i t} + \varepsilon g_2 \tag{39}$$

$$\dot{r} = v \tag{40}$$

$$\dot{\lambda}_v = -\lambda_r + \varepsilon\{-\lambda_v \frac{\partial y_1}{\partial v} - \lambda_u \frac{\partial y_2}{\partial v}\} \tag{41}$$

$$\dot{\lambda}_u = \varepsilon\{-\lambda_v \frac{\partial y_1}{\partial u} - \lambda_u \frac{\partial y_2}{\partial u}\} \tag{42}$$

$$\dot{\lambda}_r = \varepsilon\{-\lambda_v \frac{\partial y_1}{\partial r} - \lambda_u \frac{\partial y_2}{\partial r}\} \tag{43}$$

where

$$g_1 = \{g_e(1 - \frac{R_e^2}{r^2}) + \frac{u^2}{r} + \frac{-A_{ef}p\sin\beta - D_i\sin\gamma + L_i\cos\gamma}{m_i - k_i t}\}$$

$$g_2 = \{\frac{-uv}{r} + \frac{-A_{ef}p\cos\beta - D_i\cos\gamma - L_i\sin\gamma}{m_i - k_i t}\} \tag{44}$$

Clearly, the zero-order dynamics correspond to a flat Earth approximation with no atmospheric effects. The gravitational acceleration is $g_e=\mu_e/R_e$ where R_e is the Earth's radius. The solution to this probem for a constant mass single stage vehicle is discussed in [9]. The extension to a variable mass vehicle is presented in [7]. Below we develop the solution for a variable mass two stage vehicle.

Setting $\varepsilon = 0$, the costate solutions and the optimal control are given as follows:

$$\lambda_{u0} = c_{u0} \qquad \lambda_{v0} = c_{v0} - c_{r0}t \qquad \lambda_{r0} = c_{r0} \tag{45}$$

$$\tan\beta = \frac{\lambda_{v0}}{\lambda_{u0}} \tag{46}$$

where c_{vo}, c_{uo}, c_{ro} are constants to be determined by enforcing the boundary conditions. Substituting (46) into (38-39), the state equations can be integrated in closed form The solution that relates the states at the final time to the states at the current time is presented below for the case where the current time is less than t_s. During the second stage, the terms involving variables with a subscript 1 would simply be deleted.

$$v_f = v_o - g_e t_f + \frac{T_{vac1}}{k_1}\{G(m_1,k_1,t_s) - G(m_1,k_1,0)\} + \frac{T_{vac2}}{k_2}\{G(m_2,k_2,t_f) - G(m_2,k_2,t_s)\} \tag{47}$$

$$u_f = u_o + \frac{T_{vac1}}{k_1}\{F(m_1,k_1,t_s) - F(m_1,k_1,0)\} + \frac{T_{vac2}}{k_2}\{F(m_2,k_2,t_f) - F(m_2,k_2,t_s)\} \tag{48}$$

$$r_f = r_o + v_o t_f - \frac{1}{2}g_e t_f^2 - \frac{T_{vac1}}{k_1}G(m_1,k_1,0)t_f - [\frac{T_{vac2}}{k_2}G(m_2,k_2,t_s) - \frac{T_{vac1}}{k_1}G(m_1,k_1,t_s)](t_f - t_s) + \frac{T_{vac1}}{k_1 q_1}\{K(m_1,k_1,t_s) - K(m_1,k_1,0)\} + \frac{T_{vac2}}{k_2 q_2}\{K(m_2,k_2,t_f) - K(m_2,k_2,t_s)\} \tag{49}$$

where $F(m,k,t) = \frac{-1}{\sqrt{\Delta^2+1}}\sinh^{-1}[\tan(\beta - \eta)]$

$$G(m,k,t) = -\Delta F(m,k,t) - \sinh^{-1}(\tan\beta)$$

$$K(m,k,t) = -\sec\beta - (\tan\beta + \Delta)G(m,k,t)$$

$$\tan\beta = p - qt$$

$$\tan\eta = \frac{1}{\Delta} \qquad \Delta = \frac{mq - pk}{k}$$

$$p = \frac{c_{v0}}{c_{u0}} \qquad q = \frac{c_{r0}}{c_{u0}} \tag{50}$$

The Hamiltonian at the final time satisfies

$$H_0(t_f) = \{(c_{v0} - tc_{v0})(\frac{T_{vac2}}{m_2 - k_2 t}\sin\beta - g_e) + c_{u0}\frac{T_{vac2}}{m_2 - k_2 t}\cos\beta + + c_{r0}v_0\}|_{t_f} = 1 \tag{51}$$

The unknowns are c_{u0}, c_{v0}, c_{r0} and $t_f=T_0$. These can be solved by enforcing the boundary conditions using a Newton method. In particular, we first use (47)-(50) to solve for p, q and t_f. Then the last of (50) and (51) are used to determine c_{u0}, c_{v0} and c_{r0}.

For the first-order solution, the differential equation is given by

$$\frac{d}{dt}\begin{bmatrix} v_1 \\ u_1 \\ r_1 \\ \lambda_{v1} \\ \lambda_{u1} \\ \lambda_{r1} \end{bmatrix} = \begin{bmatrix} 0&0&0&a_{14}&a_{15}&0 \\ 0&0&0&a_{24}&a_{25}&0 \\ 1&0&0&0&0&0 \\ 0&0&0&0&0&-1 \\ 0&0&0&0&0&0 \\ 0&0&0&0&0&0 \end{bmatrix}\begin{bmatrix} v_1 \\ u_1 \\ r_1 \\ \lambda_{v1} \\ \lambda_{u1} \\ \lambda_{r1} \end{bmatrix} + \frac{T_1}{T_0}C + \Psi \tag{52}$$

with $v_1(0) = u_1(0) = r_1(0) = v_1(T_0) = u_1(T_0) = r_1(T_0) = 0$.
where

$$a_{14} = \frac{T_{vaci}}{m_i - k_i t}\left(\frac{\cos^2\beta_0}{\lambda_{v0}\sin\beta_0 + \lambda_{uo}\cos\beta_0}\right)$$

$$a_{15} = \frac{-T_{vaci}}{m_i - k_i t}\left(\frac{\cos\beta_0\sin\beta_0}{\lambda_{v0}\sin\beta_0 + \lambda_{uo}\cos\beta_0}\right)$$

$$a_{24} = a_{15}$$

$$a_{25} = \frac{T_{vaci}}{m_i - k_i t}\left(\frac{\sin^2\beta_0}{\lambda_{v0}\sin\beta_0 + \lambda_{uo}\cos\beta_0}\right) \tag{53}$$

and the non-homogeneous terms are

$$C^T = [c_1, c_2, v_0, -\lambda_{r0}, 0, 0]^T \tag{54}$$

$$\Psi^T = [\varphi_{11}, \varphi_{12}, 0, \varphi_{21}, \varphi_{22}, \varphi_{23}]^T \tag{55}$$

where

$$c_1 = \frac{T_{vaci}}{m_i - k_i t}\sin\beta - g_o + tk_i\frac{T_{vaci}}{(m_i - k_i t)^2}\sin\beta$$

$$c_2 = \frac{T_{vaci}}{m_i - k_i t}\cos\beta + tk_i\frac{T_{vaci}}{(m_i - k_i t)^2}\cos\beta$$

$$\varphi_{11} = g_1 - \frac{T_{vaci}\cos\beta}{(m_i - k_i t)(\lambda_v\sin\beta + \lambda_u\cos\beta)}\{\lambda_v(-A_e p\cos\beta - \frac{\partial D}{\partial\beta}\sin\gamma + \frac{\partial L}{\partial\beta}\cos\gamma) + \lambda_u(A_e p\sin\beta - \frac{\partial D}{\partial\beta}\cos\gamma - \frac{\partial L}{\partial\beta}\sin\gamma)\}$$

$$\varphi_{12} = g_2 + \frac{T_{vaci}\sin\beta}{(m_i - k_i t)(\lambda_v\sin\beta + \lambda_u\cos\beta)}\{\lambda_v(-A_e p\cos\beta - \frac{\partial D}{\partial\beta}\sin\gamma + \frac{\partial L}{\partial\beta}\cos\gamma) + \lambda_u(A_e p\sin\beta - \frac{\partial D}{\partial\beta}\cos\gamma - \frac{\partial L}{\partial\beta}\sin\gamma)\}$$

$$\varphi_{21} = -\lambda_v\frac{\partial g_1}{\partial v} - \lambda_u\frac{\partial g_2}{\partial v} \qquad \varphi_{22} = -\lambda_v\frac{\partial g_1}{\partial u} - \lambda_u\frac{\partial g_2}{\partial u}$$

$$\varphi_{23} = -\lambda_v\frac{\partial g_1}{\partial r} - \lambda_u\frac{\partial g_2}{\partial r} \tag{56}$$

All the variables are evaluated along the zero-order solution.

In this case, the state transistion matrix can be expressed in closed form as

$$\Phi_A(t_2,t_1)=\begin{bmatrix} 1 & 0 & 0 & \phi_{14} & \phi_{15} & \phi_{16} \\ 0 & 1 & 0 & \phi_{24} & \phi_{25} & \phi_{26} \\ t_2-t_1 & 0 & 1 & \phi_{34} & \phi_{35} & \phi_{36} \\ 0 & 0 & 0 & 1 & 0 & t_1-t_2 \\ 0 & 0 & 0 & 0 & 1 & 0 \\ 0 & 0 & 0 & 0 & 0 & 1 \end{bmatrix} \quad (57)$$

where

$$\phi_{14}=\frac{T_{vaci}}{c_{w0}k_i}\{\frac{-sinh^{-1}[tan(\beta-\eta)]}{(\Delta^2+1)^{3/2}}-\frac{\Delta sin\beta+cos\beta}{\Delta^2+1}\}|_{t_1}^{t_2}$$

$$\phi_{15}=\frac{T_{vaci}}{c_{w0}k_i}\{\frac{-\Delta sinh^{-1}[tan(\beta-\eta)]}{(\Delta^2+1)^{3/2}}+\frac{sin\beta-\Delta cos\beta}{\Delta^2+1}\}|_{t_1}^{t_2}$$

$$\phi_{16}=\frac{T_{vaci}}{c_{w0}k_iq}\{\frac{(p+\Delta)sinh^{-1}[tan(\beta-\eta)]}{(\Delta^2+1)^{3/2}}+\frac{(p+\Delta)cos\beta+(p\Delta-1)sin\beta}{\Delta^2+1}\}|_{t_1}^{t_2}$$

$$\phi_{24}=\phi_{15}$$

$$\phi_{25}=\frac{T_{vaci}}{c_{w0}k_i}\{\frac{-\Delta^2 sinh^{-1}[tan(\beta-\eta)]}{(\Delta^2+1)^{3/2}}+\frac{\Delta sin\beta+cos\beta}{\Delta^2+1}\}|_{t_1}^{t_2}$$

$$\phi_{26}=\frac{T_{vaci}}{c_{w0}k_iq}\{\frac{\Delta(p+\Delta)sinh^{-1}[tan(\beta-\eta)]}{(\Delta^2+1)^{3/2}}-\frac{(p+\Delta)sin\beta-(p\Delta-1)cos\beta}{\Delta^2+1}\}|_{t_1}^{t_2}$$

$$\phi_{34}=\frac{T_{vaci}}{c_{w0}k_i}\{\frac{(m_i-k_it)sinh^{-1}[tan(\beta-\eta)]}{k_i(\Delta^2+1)^{3/2}}+\frac{\Delta sec\beta}{q(\Delta^2+1)}\}|_{t_1}^{t_2}$$

$$\phi_{35}=\frac{T_{vaci}}{c_{w0}k_i}\{\frac{\Delta(m_i-k_it)sinh^{-1}[tan(\beta-\eta)]}{k_i(\Delta^2+1)^{3/2}}-\frac{sec\beta}{q(\Delta^2+1)}\}|_{t_1}^{t_2}$$

$$\phi_{36}=\frac{T_{vaci}m_i}{c_{w0}k_i^2}\{\frac{-(m_i-k_it)sinh^{-1}[tan(\beta-\eta)]}{k_i(\Delta^2+1)^{3/2}}-\frac{k_i}{mq^2}\frac{(p\Delta-1)sec\beta}{\Delta^2+1}\}|_{t_1}^{t_2} \quad (58)$$

Now the Hamiltonian at T_0 becomes

$$H_1(T_0)=\{\lambda_{v1}g_1^o+\lambda_{u1}g_2^o+T_1[\frac{T_{vac2}k_2}{(m_2-k_2t)^2}][\lambda_{v0}sin\beta+\lambda_{v0}cos\beta]+\lambda_{v1}(\frac{T_{vac2}sin\beta}{m_2-k_2t}-g_e)+\lambda_{u1}\frac{T_{vac2}cos\beta}{m_2-k_2t}\}|_{T_0}=0 \quad (59)$$

Since the dynamics are discontinuous at $t=t_s$, the state transition expression in (29) becomes

$$\begin{bmatrix} x_1(T_0) \\ \lambda_1(T_0) \end{bmatrix}=\Phi_{A_{i=2}}(T_0,t_s)\{\Phi_{A_{i=1}}(t_s,0)\begin{bmatrix} 0 \\ \lambda_1(0) \end{bmatrix}+\int_0^{t_s}\Phi_{A_{i=1}}(t_s,\tau)[\frac{T_1}{T_0}C_{i=1}(\tau)+\Psi_{i=1}(\tau)]d\tau\}+\int_{t_s}^{T_0}\Phi_{A_{i=2}}(T_0,\tau)[\frac{T_1}{T_0}C_{i=2}(\tau)+\Psi_{i=2}(\tau)]d\tau \quad (60)$$

during the first stage of the trajectory. During the second stage, the i=1 terms are discarded.

Numerical Results

Figures 1-4 show the zero-order and the optimal solutions generated using a multiple shooting code [10]. The boundary conditions are $h(0)$ = 400m, $V(0)$ = 64.5m/s, $\gamma(0)$ = 89.5^0 and $h(t_f)$ =148160m, $V(t_f)$ = 7858.2m/s, $\gamma(t_f)$ = 0^0. Other vehicle parameters are: m_o = 1523450kg, m_{s+} = 546620kg, t_s = 143.47s. The objective is to minimize the final time, which is equivalent to minimizing the fuel consumption for this formulation. The final times for the two solutions are 353.539s and 362.187s.

The zero order solution gives good approxImation to the second stage portion of the trajectory, which is flown under nearly exoatmospheric conditions where the thrust and gravity forces are dominant. Future work will examine the effect of the first order correction terms, and consider the merits or shortcomings of this approach over the approach proposed in [7].

4. Conclusions

A regular perturbation method has been outlined and examined for application to launch vehicle guidance. The approach can be applied for more general optimization problems in flight mechanics when the zero order solution can be obtained in closed form. A zero order solution for a two stage vehicle is presented and used to obtain a closed form solution for the state transition matrix needed in forming the first order correction. The advantages or disadvantages of this approach to an alternative approach that involves expansion of the solution for the Hamilton-Jacobi-Bellman equation have yet to be evaluated.

Acknowledgement

This research was supported by NASA Langley Research Center under Grant No. NAG-1-939.

5. References

1. Garrard, W. L., McClamroch, N. H., Clark, L. G., "An Approach To Sub-optimal Feedback Control Of Nonlinear Systems", International Journal Of Control Vol. 5, 425-435, 1967.
2. Baldwin, J. F., Sims Willams, J. H., "The Use Of Perturbation In The Synthesis Of Closed-loop Optimal Control Laws For Non-linear Systems", Automatica Vol.5, 357-367, 1969.
3. Garrard, W. L., "Suboptimal Feedback Control For Nonlinear System", Automatica Vol. 8, 219-221, 1972.
4. Garrard, W. L., Enns, D. F., Snell, A., "Nonlinear Longitudinal Control Of A Supermaneuverable Aircraft", ACC Proceedings, 142-145,1989.
5. Breakwell, J. V., Shinar, J., Visser, H. G., "Uniformly Valid Feedback Expansions For Optimal Control Of Singularly Perturbed Dynamic Systems", Journal Of Optimization Theory and Appl. Vol. 46, 441-453,1985.
6. Speyer, J. L., Crues, E. Z., "An Approximate Atmospheric Guidance Law For Aeroassisted Plane Change Maneuvers", AIAA GN&C Proceedings, 1989.
7. Speyer, J. L., Feeley, T., Hull, D. G., "Real-time Approximate Optimal Guidance Laws For The Advanced Launch System", ACC Proceedings, 2032-2036,1989.
8. Junkins, J. L., "An Asymptotic Perturbation Method For Nonlinear Optimal Control Problems", Journal Of Guidance Vol. 9, 391-396.

9. Bryson, A. E., Ho, Y. C., *Applied Optimal Control*, Hemisphere Publishing Corp.
10. Burlirsch, R., "The Multiple Shooting Method For Numerical Solution for Nonlinear Boundar Value Problems and Optimal Control Problems", Carl-Cranz-Gesellschaft, Tech. Rpt., Heidelberg, 1971.

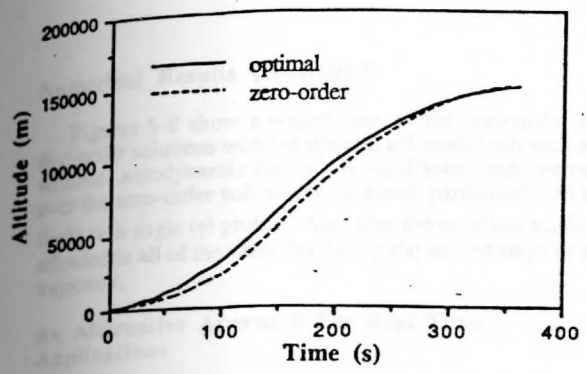

Figure 1. Altitude Profile

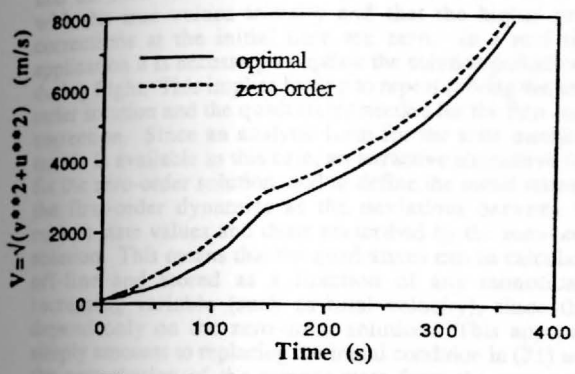

Figure 2. Velocity Profile

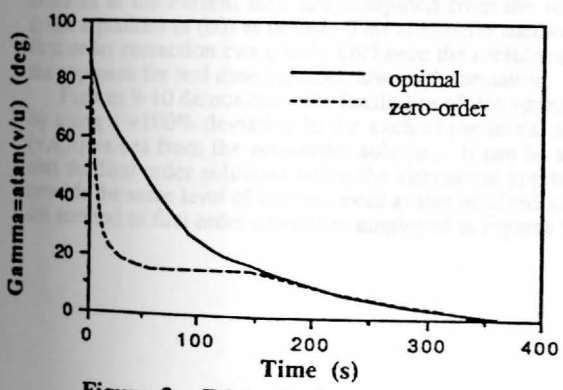

Figure 3. Flight Path Angle Profile

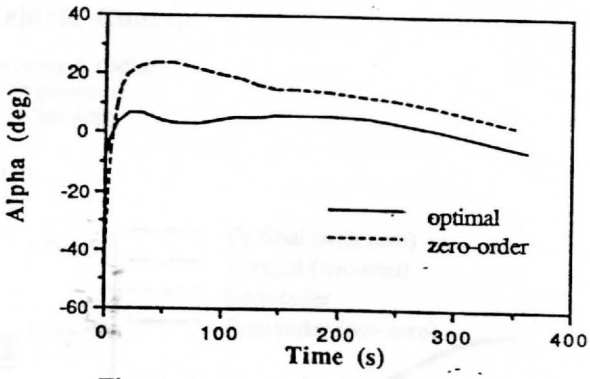

Figure 4. Angle Of Attack Profile

An Approach to Optimal Guidance of an Advanced Launch Vehicle Concept

Martin S. Leung and Anthony J. Calise
School of Aerospace Engineering
Georgia Institute of Technology

Addendum

Numerical Results (continued)

Figures 5-8 show a comparison of the zero-order and first-order solutions with the optimal solutions both with and without aerodynamic forces. A significant improvement over the zero-order solution is obtained, particularly in the flight path angle (γ) profile. Also note the excellent tracking afforded in all of the variables during the second stage of the trajectory.

An Alternative Approach For Real Time Applications

In (60) the costates corrections are evaluated assuming that the state variables in the zero-order solution coincide with the true values initially and that the higher order corrections at the initial time are zero. In a real time application it is necessary to update the solution periodically during flight. This implies having to repeat solving the zero-order solution and the quadratures needed for the first-order correction. Since an analytic form for the state transition matrix is available in this case, an attractive alternative is to fix the zero-order solution, and to define the initial states of the first-order dynamics as the deviations between the current state values and those prescribed by the zero-order solution. This means that the quadratures can be calculated off-line and stored as a function of any monotically increasing variable (such as total velocity), since they depend only on the zero-order solution. This approach simply amounts to replacing the initial condition in (21) with the perturbation of the current state from the zero-order solution. Subsequently, the first-order correction for the costates at the current time are computed from the set of linear equations in (60) as before. This alternative method of first order correction can greatly enchance the usefulness of the approach for real time guidance law implementation.

Figures 9-10 demonstrate the feasibility of this approach by using a +100% deviation in the each of the initial state (v,u,h) values from the zero-order solution. It can be seen that the first order solutions using the alternative approach provide the same level of improvement as that obtained using the method of first order correction employed in Figures 5-8.

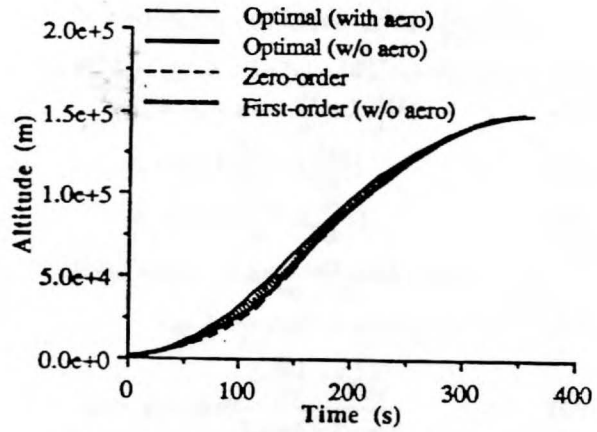

Figure 5 Comparison Of Altitude Profiles.

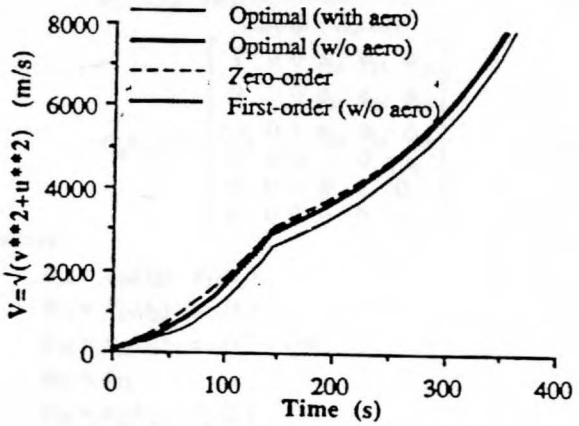

Figure 6 Comparison Of Velocity Profiles.

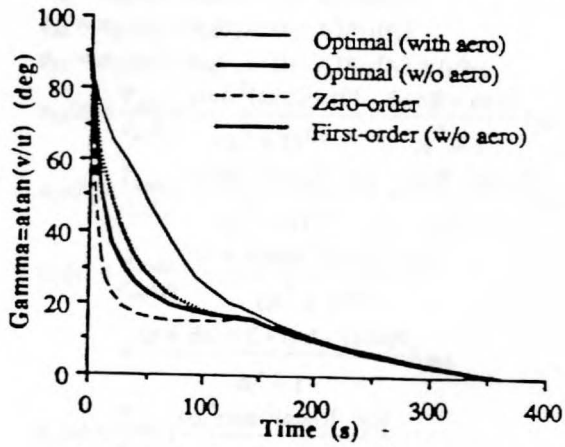

Figure 7 Comparison Of Flight Path Angle Profiles.

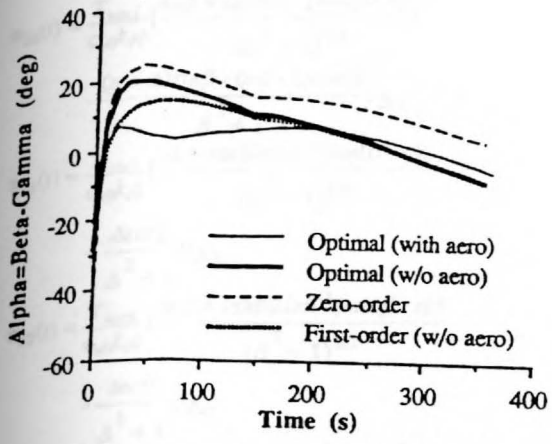

Figure 8 Comparison Of Angle Of Attack Profiles.

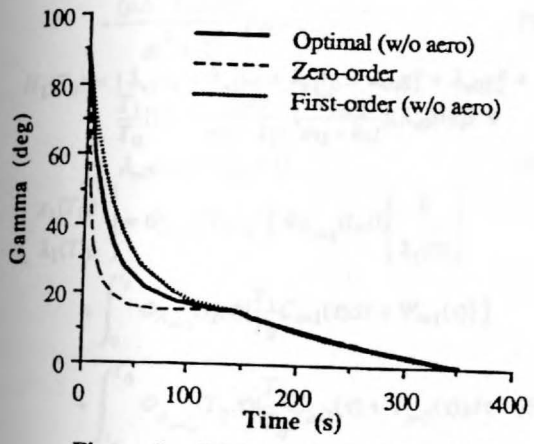

Figure 9 Flight Path Angle Profiles With The Alternative Method Of First-Order Correction.

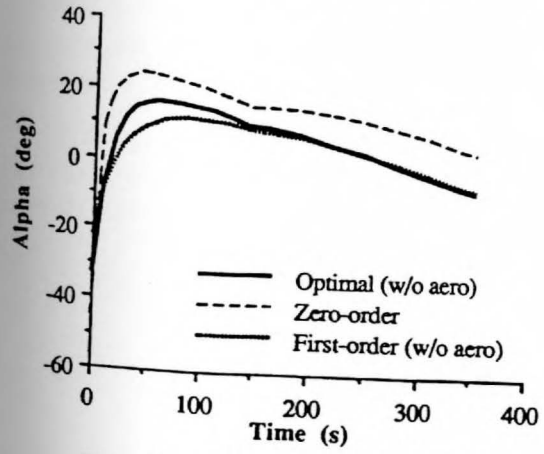

Figure 10 Angle Of Attack Profiles With The Alternative Method Of First-Order Correction.

Errata for Original Text

$$H = (f^T + \varepsilon g^T)\lambda \quad ; H(t_f) = -\phi_t|_{t_f} \tag{3}$$

$$\dot{\lambda} = -(f_x^T + \varepsilon g_x^T)\lambda \; ; \lambda(t_f) = \Phi_x^T|_{t_f} ; \Phi = \phi + \nu^T\varphi \tag{4}$$

$$+ \frac{1}{2!}\frac{d^2F}{d\sigma^2}|_{\sigma 0} 2\sigma_1\sigma_2 + \frac{1}{3!}\frac{d^3F}{d\sigma^3}|_{\sigma 0}\sigma_1^3\} + \cdots \tag{14}$$

$$\dot{\lambda}_1 = -(f_x^T\lambda_0)_x^o x_1 - (f_x^T\lambda_0)_u^o u_1 - f_x^{oT}\lambda_1 - \frac{T_1}{T_0}(f_x^{oT}\lambda_0$$

$$+ tf_{xt}^{oT}\lambda_0) - g_x^T\lambda_0 \; ; \lambda_0(T_0) = (\Phi_{xx}^{oT}x_1 + \Phi_{xt}^{o}T_1)|_{T_0} \tag{22}$$

$$\dot{\lambda}_v = -\lambda_r + \varepsilon\{-\lambda_v\frac{\partial g_1}{\partial v} - \lambda_w\frac{\partial g_2}{\partial v}\} \tag{41}$$

$$\dot{\lambda}_u = \varepsilon\{-\lambda_v\frac{\partial g_1}{\partial u} - \lambda_w\frac{\partial g_2}{\partial u}\} \tag{42}$$

$$\dot{\lambda}_r = \varepsilon\{-\lambda_v\frac{\partial y_1}{\partial r} - \lambda_w\frac{\partial y_2}{\partial r}\} \tag{43}$$

$$H_0(t_f) = \{(c_{r0} - tc_{v0})(\frac{T_{vac2}}{m_2 - k_2 t}sin\beta - g_e) +$$

$$c_{w0}\frac{T_{vac2}}{m_2 - k_2 t}cos\beta + c_{r0}v_0\}|_{t_f} = 1 \tag{51}$$

$$\varphi_{11} = g_1 + cos\beta\frac{\lambda_v\frac{\partial g_1}{\partial v} + \lambda_w\frac{\partial g_2}{\partial v}}{\lambda_v sin\beta + \lambda_w cos\beta} \tag{52}$$

$$\varphi_{12} = g_2 - sin\beta\frac{\lambda_v\frac{\partial g_1}{\partial u} + \lambda_w\frac{\partial g_2}{\partial u}}{\lambda_v sin\beta + \lambda_w cos\beta} \tag{52}$$

$$\Phi_A(t_2,t_1) = \begin{bmatrix} 1 & 0 & 0 & \phi_{14} & \phi_{15} & \phi_{16} \\ 0 & 1 & 0 & \phi_{24} & \phi_{25} & \phi_{26} \\ t_2 - t_1 & 0 & 1 & \phi_{34} & \phi_{35} & \phi_{36} \\ 0 & 0 & 0 & 1 & 0 & t_1 - t_2 \\ 0 & 0 & 0 & 0 & 1 & 0 \\ 0 & 0 & 0 & 0 & 0 & 1 \end{bmatrix} \tag{57}$$

where

$$\phi_{14} = \pi_{14}(t_2) - \pi_{14}(t_1)$$

$$\phi_{15} = \pi_{15}(t_2) - \pi_{15}(t_1)$$

$$\phi_{16} = \pi_{16}(t_2) - \pi_{16}(t_1) + t_1\phi_{14}$$

$$\phi_{24} = \phi_{15}$$

$$\phi_{25} = \pi_{25}(t_2) - \pi_{25}(t_1)$$

$$\phi_{26} = \pi_{26}(t_2) - \pi_{26}(t_1) + t_1\phi_{24}$$

$$\phi_{34} = \pi_{34}(t_2) - \pi_{34}(t_1) - (t_2 - t_1)\pi_{14}(t_1)$$

$$\phi_{35} = \pi_{35}(t_2) - \pi_{35}(t_1) - (t_2 - t_1)\pi_{15}(t_1)$$

$$\phi_{35} = \pi_{36}(t_2) - \pi_{36}(t_1) - (t_2 - t_1)\pi_{16}(t_1) + t_1\phi_{16}$$

$$\pi_{14}(t) = \frac{T_{vaci}}{c_{w0}k_i}\{\frac{-sinh^{-1}[tan(\beta - \eta)]}{(\Delta^2 + 1)^{3/2}} - \frac{\Delta sin\beta + cos\beta}{\Delta^2 + 1}\}|_{\beta(t)}$$

$$\pi_{15}(t) = \frac{T_{vaci}}{c_{w0}k_i}\{\frac{-\Delta sinh^{-1}[tan(\beta - \eta)]}{(\Delta^2 + 1)^{3/2}} + \frac{sin\beta - \Delta cos\beta}{\Delta^2 + 1}\}|_{\beta(t)}$$

$$\pi_{16}(t) = \frac{T_{vaci}}{c_{w0}k_i q}\{\frac{(p + \Delta)sinh^{-1}[tan(\beta - \eta)]}{(\Delta^2 + 1)^{3/2}}$$

$$+ \frac{(p + \Delta)cos\beta + (p\Delta - 1)sin\beta}{\Delta^2 + 1}\}|_{\beta(t)}$$

$$\pi_{25}(t) = \frac{T_{vaci}}{c_{w0}k_i}\{\frac{-\Delta^2 sinh^{-1}[tan(\beta - \eta)]}{(\Delta^2 + 1)^{3/2}}$$

$$+ \frac{\Delta sin\beta + cos\beta}{\Delta^2 + 1}\}|_{\beta(t)}$$

$$\pi_{26}(t) = \frac{T_{vaci}}{c_{a0}k_i q}\{\frac{\Delta(p+\Delta)sinh^{-1}[tan(\beta-\eta)]}{(\Delta^2+1)^{3/2}} - \frac{(p+\Delta)sin\beta - (p\Delta-1)cos\beta}{\Delta^2+1}\}|_{\beta(t)}$$

$$\pi_{34}(t) = \frac{T_{vaci}}{c_{a0}k_i q}\{\frac{(\Delta+tan\beta)sinh^{-1}[tan(\beta-\eta)]}{(\Delta^2+1)^{3/2}} + \frac{\Delta sec\beta}{\Delta^2+1}\}|_{\beta(t)}$$

$$\pi_{35}(t) = \frac{T_{vaci}}{c_{a0}k_i q}\{\frac{\Delta(\Delta+tan\beta)sinh^{-1}[tan(\beta-\eta)]}{(\Delta^2+1)^{3/2}} - \frac{sec\beta}{\Delta^2+1}\}|_{\beta(t)}$$

$$\pi_{36}(t) = \frac{T_{vaci}}{c_{a0}k_i q^2}\{\frac{-(p+\Delta)(\Delta+tan\beta)sinh^{-1}[tan(\beta-\eta)]}{(\Delta^2+1)^{3/2}} - \frac{(p\Delta-1)sec\beta}{\Delta^2+1}\}|_{\beta(t)} \quad (58)$$

$$H_1(T_0) = \{\lambda_{v1}\dot{v}_0 + \lambda_{u1}\dot{u}_0 + \lambda_{r1}\dot{r}_0 + \lambda_{v0}g_1^o + \lambda_{u0}g_2^o + \frac{T_1}{T_0}[H_0 + \frac{T_0 k_2}{m_2 - k_2 t}(\frac{T_{vac2}}{m_2 - k_2 t})(\lambda_{v0}sin\beta + \lambda_{u0}cos\beta)]\}_{T_0} = 0 \quad (59)$$

$$\begin{bmatrix} x_1(T_0) \\ \lambda_1(T_0) \end{bmatrix} = \Phi_{A_{i=2}}(T_0, t_s)\left\{\Phi_{A_{i=1}}(t_s,0)\begin{bmatrix} 0 \\ \lambda_1(0) \end{bmatrix} + \int_0^{t_s}\Phi_{A_{i=1}}(t_s,\tau)[\frac{T_1}{T_0}C_{i=1}(\tau)d\tau + \Psi_{i=1}(\tau)]\right\} + \int_{t_s}^{T_0}\Phi_{A_{i=2}}(T_0,\tau)[\frac{T_1}{T_0}C_{i=2}(\tau) + \Psi_{i=2}(\tau)]d\tau \quad (60)$$

Appendix B: ALV Results

In Figs. 1 – 8, numerical results for the ALV model with no constraints enforced are given for 2, 4, and 8 elements per time interval, where the number of elements is denoted by $(N_1 : N_2)$ on the plots. These results are compared to a multiple-shooting code as a check on the accuracy of the method and of the program. For the unconstrained case, the state histories are shown in Figs. 1 – 4 and the costate histories are shown in Figs. 5 – 8. For all cases, the (8:8) run lies on the essentially exact curve corresponding to the multiple shooting (MS) code. In general, even the (4:4) run yields an excellent approximation to the solution.

The control time history is shown in Fig. 9. We see from this graph that although the (8:8) run is close to the exact curve, it has not converged on the answer. Due to the large slopes and sharp peaks in the control, the finite element method required 24 elements in the first stage to converge on the solution. However, it is important to note that we were still able to run only 8 elements in the second stage. Thus one is able to cluster the elements as required to refine the solution.

Fig. 10 shows a graph of αq. (The dynamic pressure q is not shown because it does not violate the constraint.) It can be seen clearly that only one control constraint is violated. This is the only constraint that was added to the program to generate the next two graphs.

The (4:4) results above were obtained in 5.5 CPU seconds on a SUN 3/260, and five iterations were required with a Newton-Raphson method. Of course, the number of iterations depends on the quality of the initial guesses. In an on-board computational setting, the initial guesses should be pretty good since they would probably be determined from a previously obtained solution.

In Figs. 11 and 12, we have included the control constraint ($\alpha q \leq 2925.0$) in the finite element formulation. For academic purposes, we show the unconstrained case, the realistic constraint, and two unrealistic constraints. Even for the most severe constraint, the time histories for the states, costates, and dynamic pressure and the value of the performance index are virtually unchanged. Also, no significant extra computer time was expended.

Finally, as a feel for the global convergence of the method, we plot the Hamiltonian of the unconstrained system in Fig. 13 for 2, 4, 8, and 16 elements per stage. We see a nice convergence toward the exact answer of zero with an increase in the number of elements.

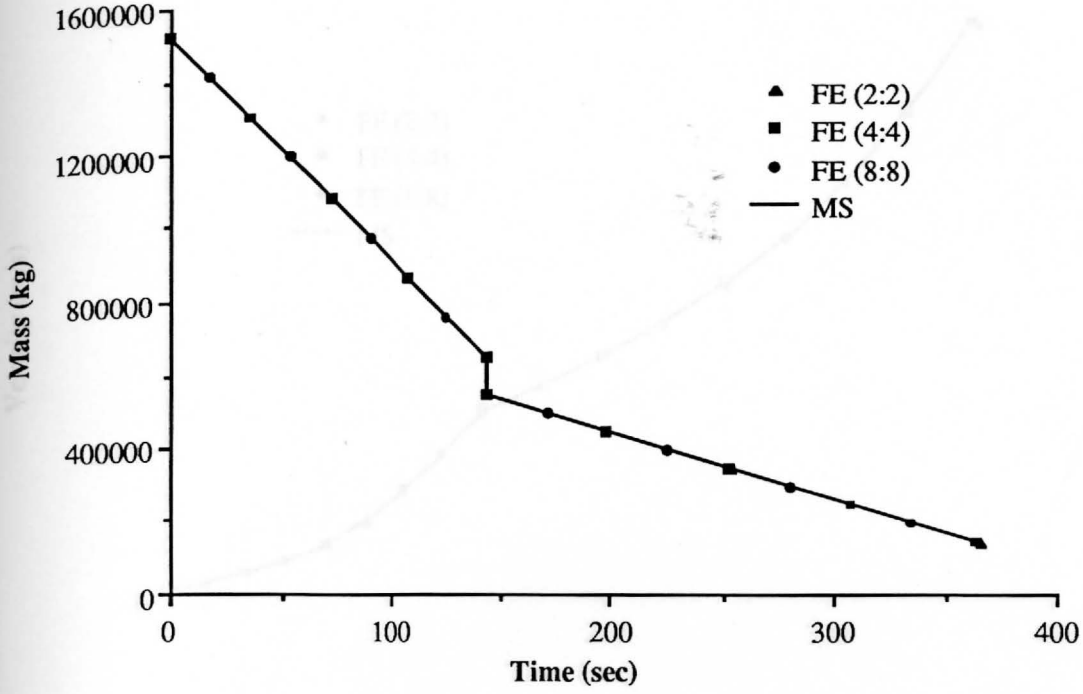

Fig. 1: Mass vs. Time

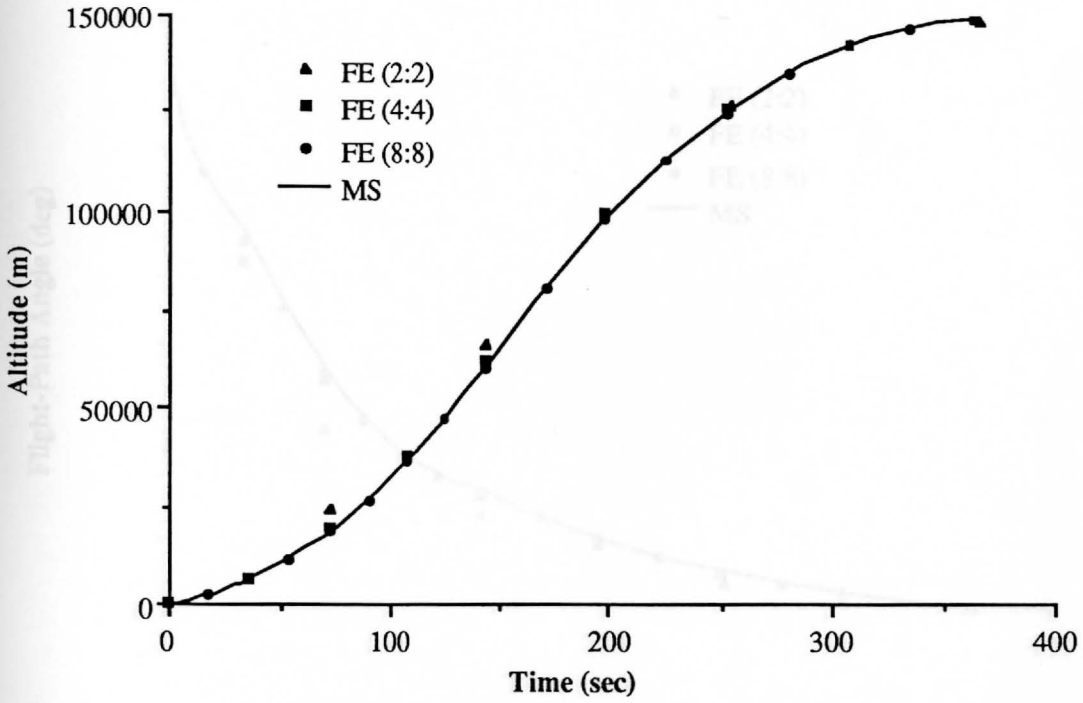

Fig. 2: Altitude vs. Time

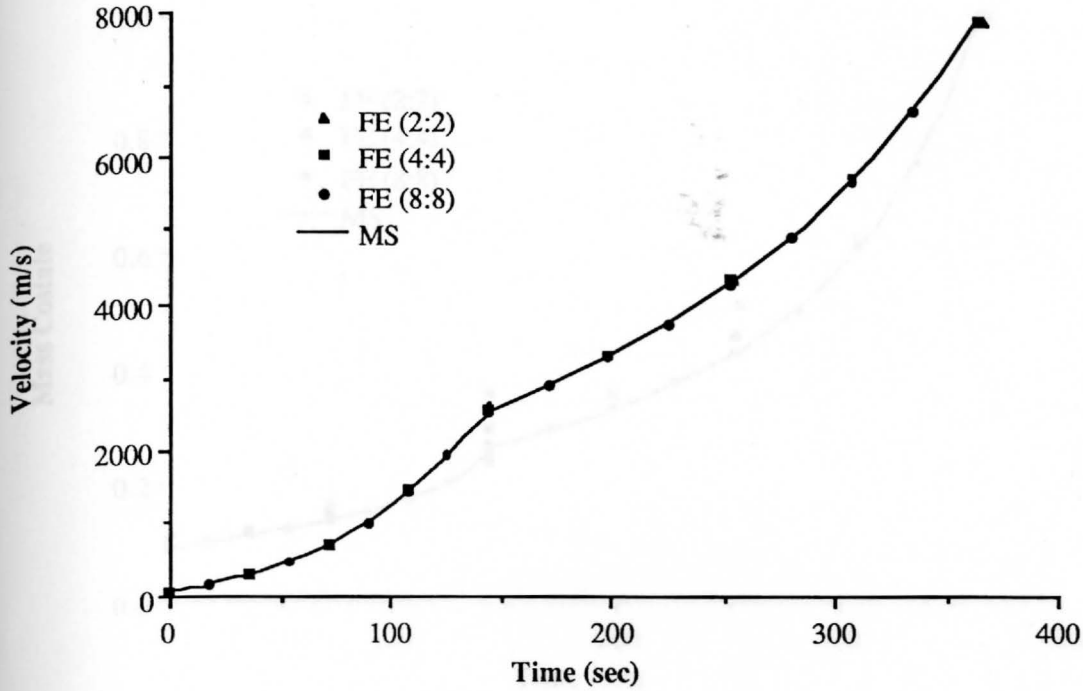

Fig. 3: Velocity vs. Time

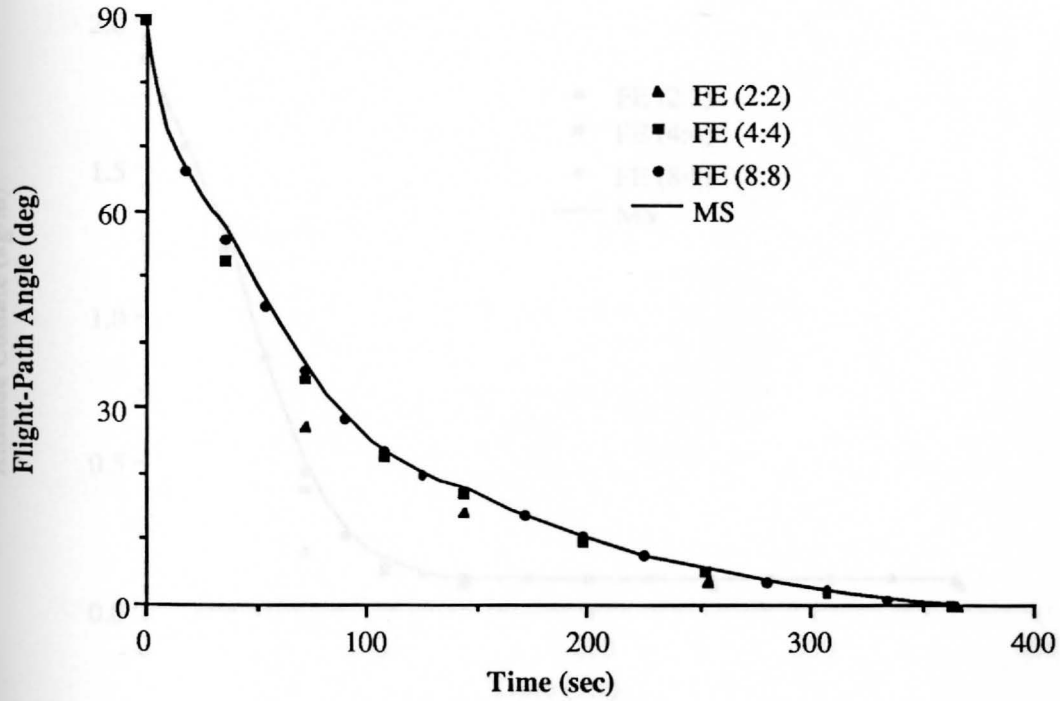

Fig. 4: Flight-Path Angle vs. Time

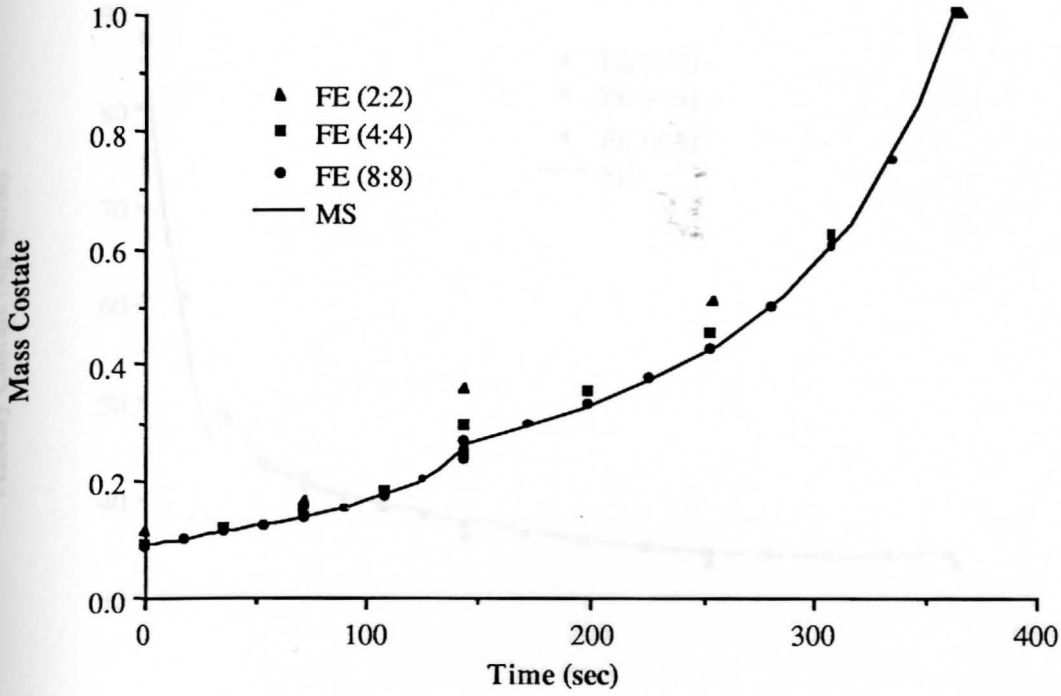

Fig. 5: Mass Costate vs. Time

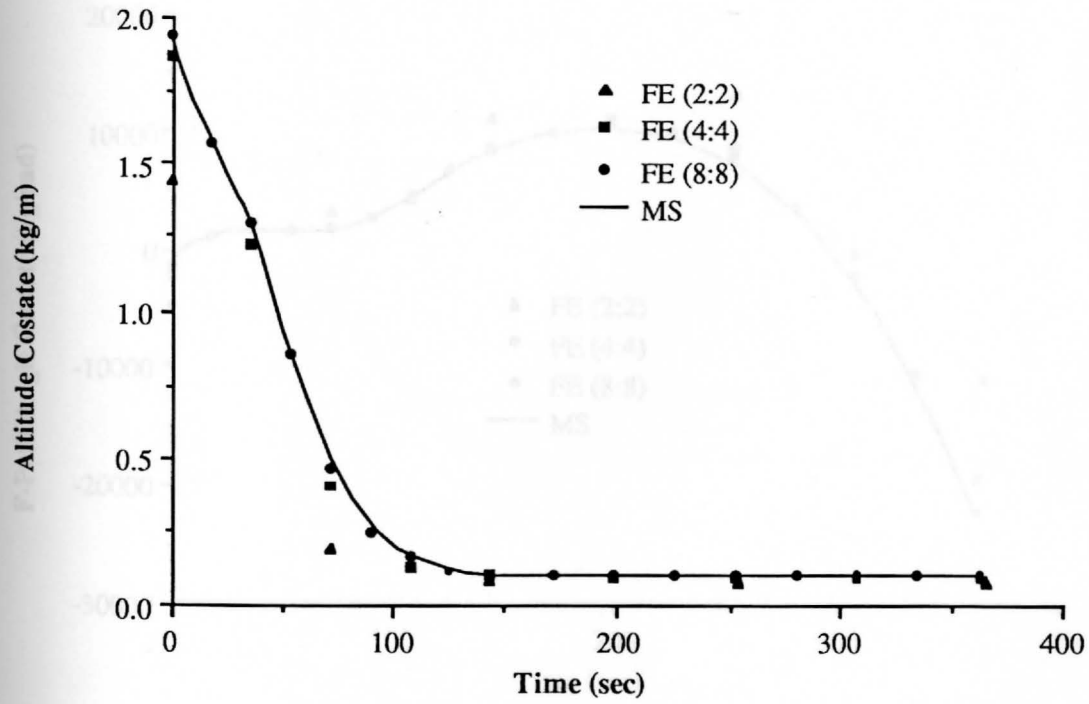

Fig. 6: Altitude Costate vs. Time

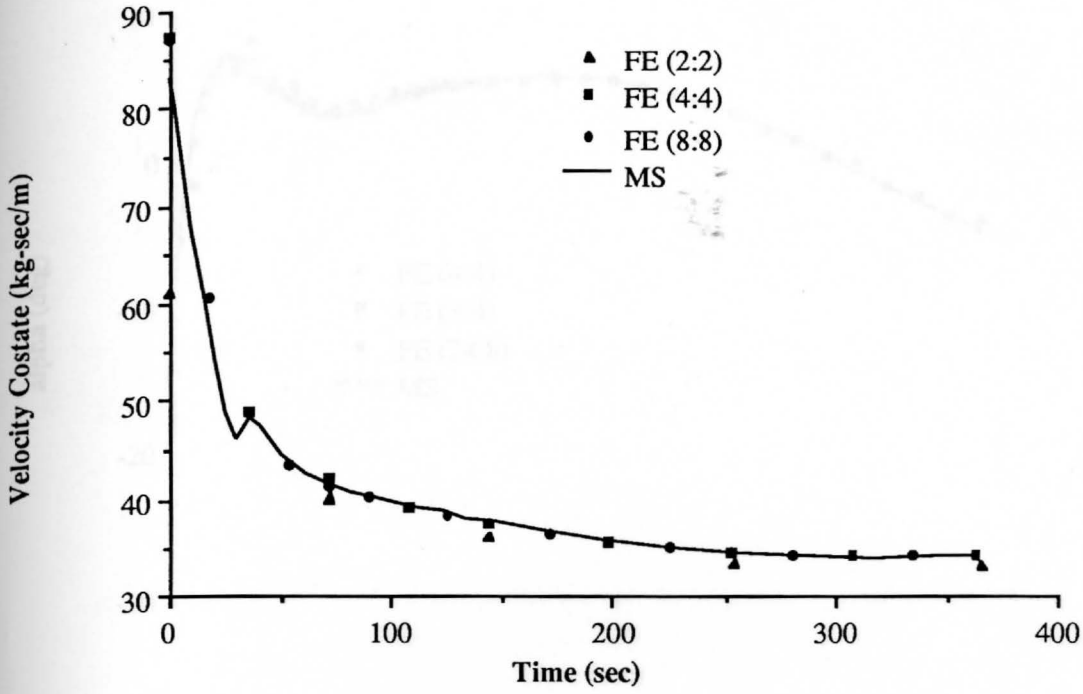

Fig. 7: Velocity Costate vs. Time

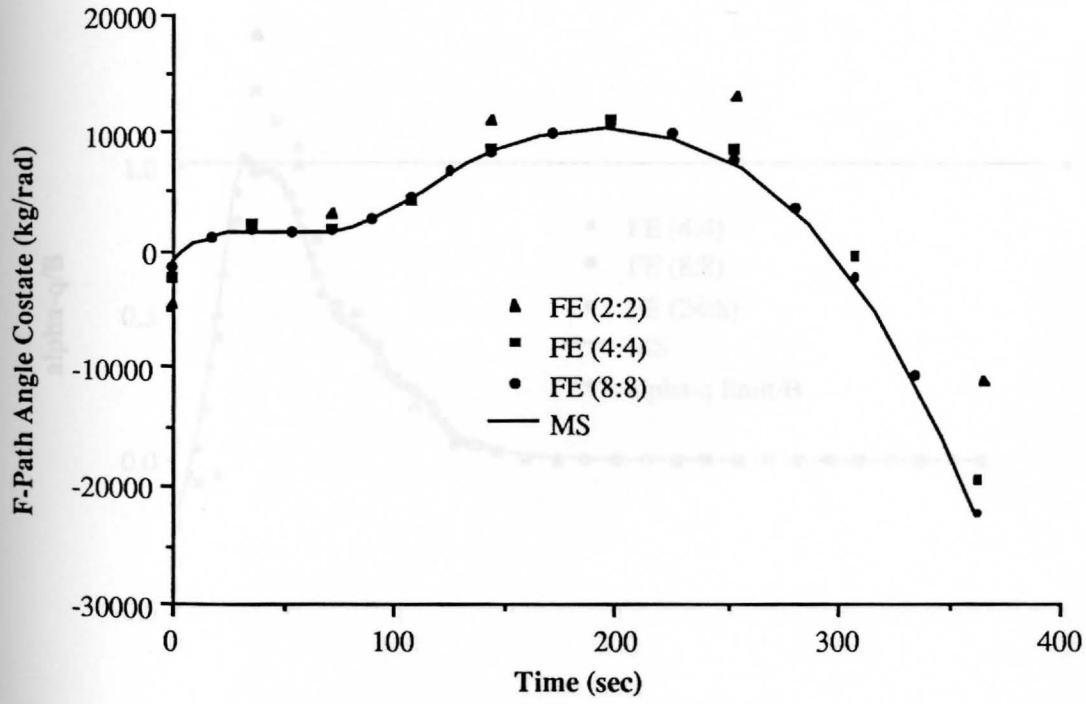

Fig. 8: Flight-Path Angle Costate vs. Time

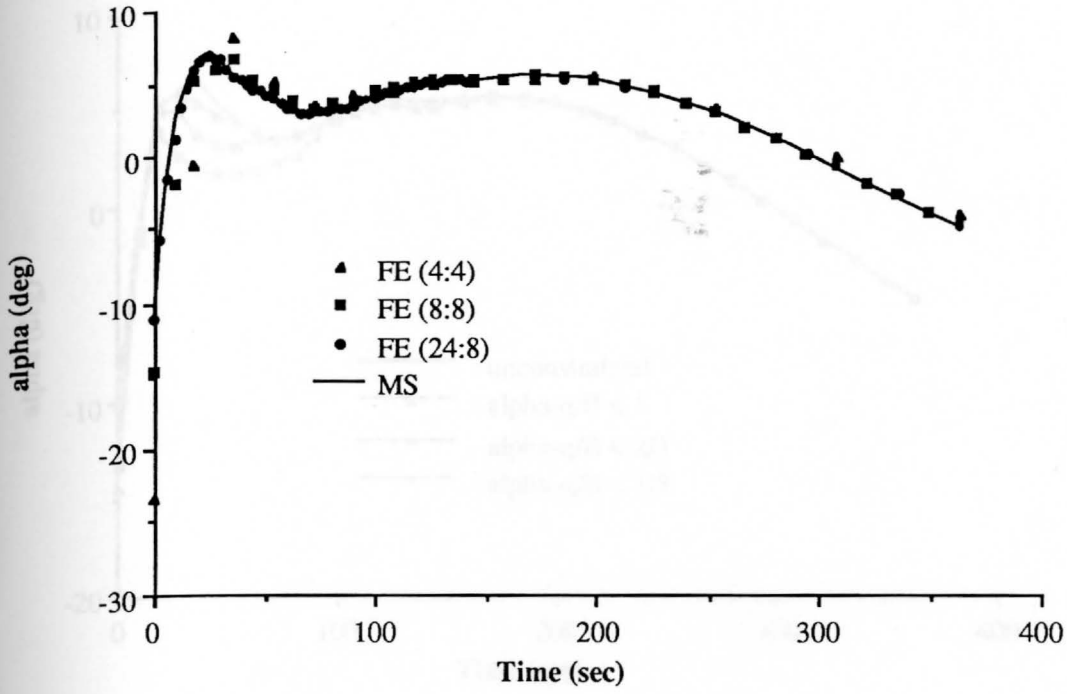

Fig. 9: Angle-of-Attack (α) vs. Time

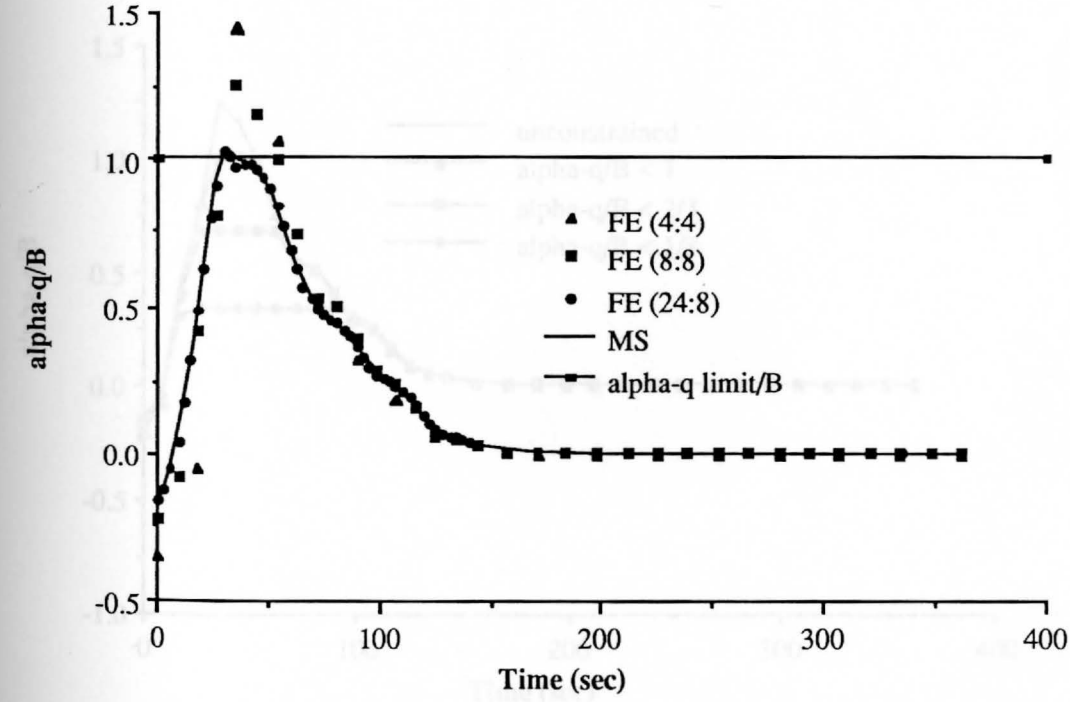

Fig. 10: αq vs. Time

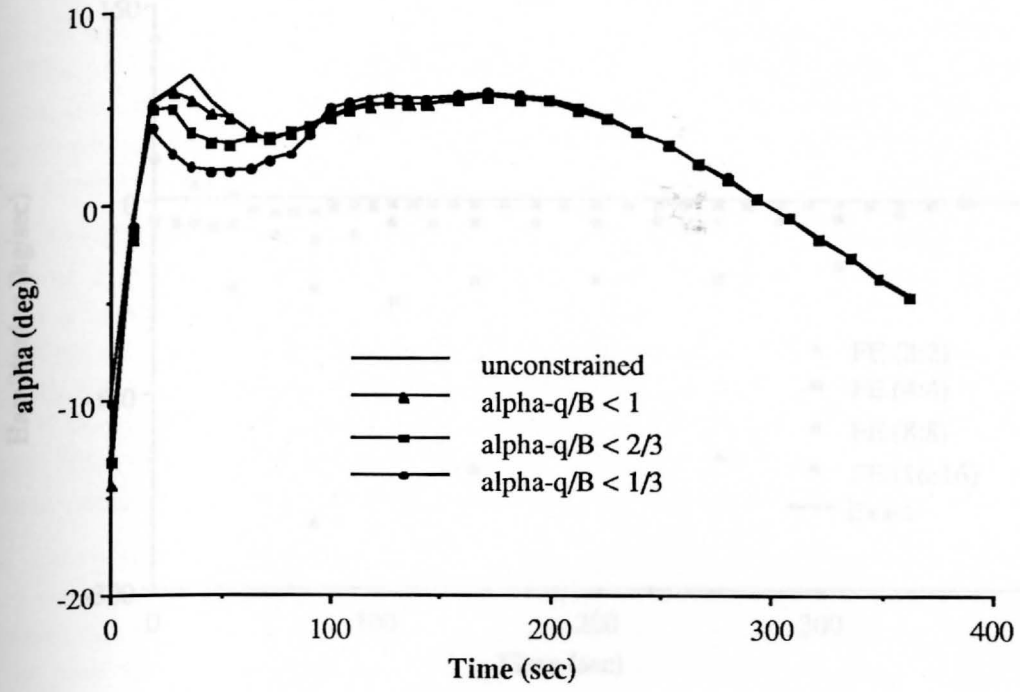

Fig. 11: Angle-of-Attack (α) vs. Time
for various levels of αq constraint

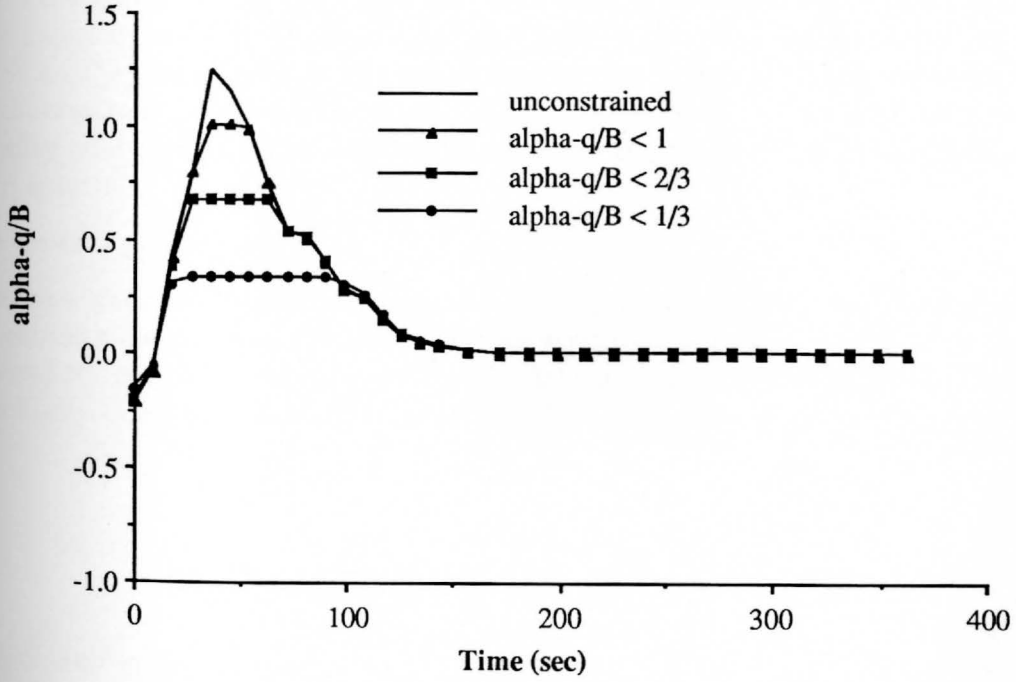

Fig. 12: αq vs. Time
for various levels of αq constraint

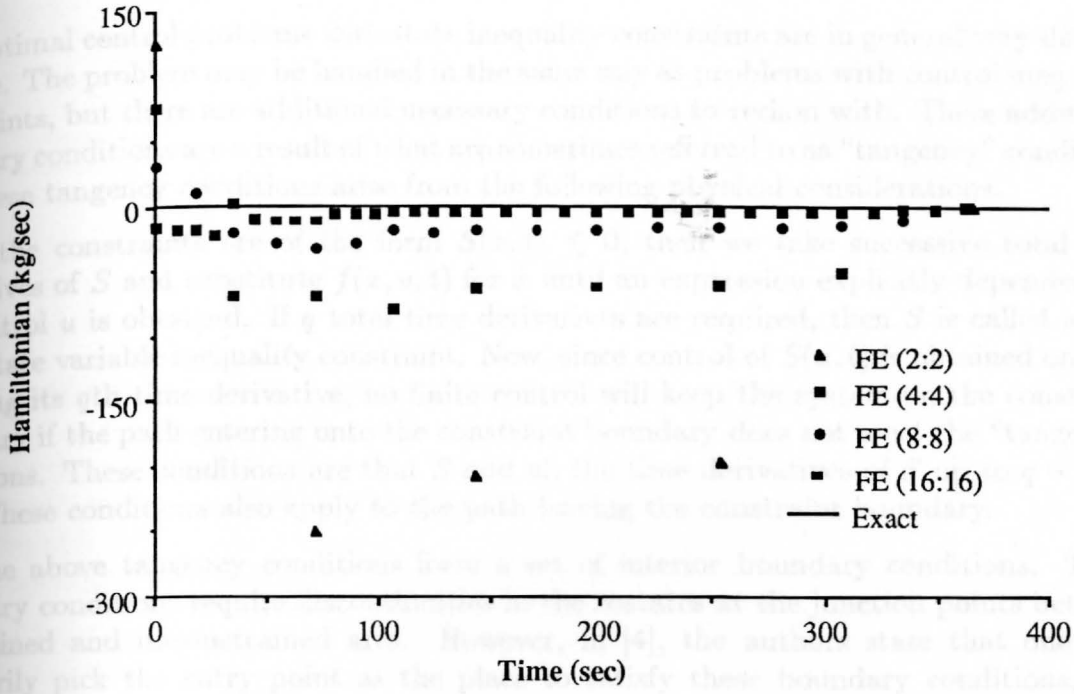

Fig. 13: Hamiltonian vs. Time

Appendix C: State Inequality Constraints

Optimal control problems with state inequality constraints are in general very difficult to solve. The problem may be handled in the same way as problems with control inequality constraints, but there are additional necessary conditions to reckon with. These additional necessary conditions are a result of what are sometimes referred to as "tangency" conditions [4]. These tangency conditions arise from the following physical considerations.

If the constraints are of the form $S(x,t) \leq 0$, then we take successive total time derivatives of S and substitute $f(x,u,t)$ for $\dot{x}$ until an expression explicitly dependent on the control u is obtained. If q total time derivatives are required, then S is called a qth-order state variable inequality constraint. Now, since control of $S(x,t)$ is obtained only by changing its qth time derivative, no finite control will keep the system on the constraint boundary if the path entering onto the constraint boundary does not meet the "tangency" conditions. These conditions are that S and all the time derivatives of S up to $q-1$ are zero. These conditions also apply to the path leaving the constraint boundary.

The above tangency conditions form a set of interior boundary conditions. These boundary conditions require discontinuities in the costates at the junction points between constrained and unconstrained arcs. However, in [4], the authors state that one may arbitrarily pick the entry point as the place to satisfy these boundary conditions, and therefore the costates and Hamiltonian are discontinuous at the entry point and continuous at the exit point.

New necessary conditions for optimal control problems with state inequality constraints were developed in [5]. Therein, the authors tactfully say: "We do not imply that the necessary conditions obtained by previous workers are incorrect, but rather, that, inasmuch as they underspecify the conditions at the junction, there exists the possibility of non-stationary solutions satisfying these conditions ...." The authors generated an admittedley contrived example where the necessary conditions of [4] actually found a non-extremal solution.

New Necessary Conditions

The new necessary conditions derived in [5] greatly simplify problems dealing with state inequality constraints. Rather than take succesive time derivatives of the constraint $S(x,t)$ until the control appears explicitly, the authors adjoin S directly to the Hamiltonian, as is normally done with control inequality constraints. The Hamiltonian now takes the form

$$H = L + \lambda^T f + \eta^2 S(x,t) \tag{1}$$

where η, S, and u are scalars.

As with control inequality constraints, the multiplier is chosen to be a squared term so that η^2 is positive if $S = 0$ and η^2 is zero if $S \leq 0$. At junction points t_i of boundary and interior arcs, the costates may be discontinuous. The boundary conditions are

$$\lambda(t_i^+) = \lambda(t_i^-) - \nu(t_i)\left(\frac{\partial S}{\partial x}\right)_{t_i} ; \qquad \nu(t_i) \geq 0 \tag{2}$$

and in addition (if ϕ and ψ are not explicitly dependent on time)

$$H(t_i^+) = H(t_i^-) \tag{3}$$

An extremely interesting consequence of the new conditions is pointed out in the paper. For an odd-order constraint (*i.e.*, one in which q is odd where q is the number of total time derivatives of S necessary for the control to appear explicitly), the trajectory will, at most, only touch the boundary, if $(u^-)_{q-1} \neq (u^+)_{q-1}$ where $(u^-)_{q-1}$ is the $q-1$th derivative of u evaluated just prior to the junction point. Note that for $q = 1$, $u^- = u^+$, so that boundary arcs *are* permitted for the first-order case.

General Development

Consider a system of n states x and a scalar control u defined by $\dot{x} = f(x, u, t)$. Assume that the final time is fixed for this development. Suppose that there is a state inequality constraint of the form

$$S(x, t) \leq 0 \tag{4}$$

Let us introduce a positive "slack" variable p^2 so that

$$S(x, t) + p^2 = 0 \tag{5}$$

Eq. (5) will now be adjoined to our performance index J by using the Lagrange multiplier function η^2 where the variation is defined as $\delta\eta^2$. The performance index takes the form:

$$J = \int_{t_0}^{t_f} \left[\lambda^T(\dot{x} - f) - \eta^2(p^2 + S) - L\right] dt - \phi|_{t_f} - \nu^T\psi|_{t_f} \tag{6}$$

Following the same steps as before in developing our weak formulation, we take a straightforward variation, integrate the $\dot{x}$ term by parts, put all boundary conditions in weak form, and finally obtain

$$\int_{t_0}^{t_f} \left\{ \delta\dot{x}^T\lambda - \delta\lambda^T f - \delta\dot{\lambda}^T x - \delta x^T \left[\left(\frac{\partial L}{\partial x}\right)^T + \left(\frac{\partial f}{\partial x}\right)^T \lambda + \left(\frac{\partial S}{\partial x}\right)\eta^2 \right] \right.$$
$$\left. - \delta u^T \left[\left(\frac{\partial L}{\partial u}\right)^T + \left(\frac{\partial f}{\partial u}\right)^T \lambda \right] - \delta\eta^2(p^2 + S) - \delta p(2p\eta^2) \right\} dt \qquad (7)$$
$$- \delta\nu^T\psi\Big|_{t_f} - \delta x_f^T\hat{\lambda}_f + \delta x_0^T\hat{\lambda}_0 + \delta\lambda_f^T\hat{x}_f - \delta\lambda_0^T\hat{x}_0 = 0$$

This is the governing equation for the weak Hamiltonian method which includes an inequality constraint on the states. Note that the coefficient of δp requires that either p or η be zero for each element.

The next step is to introduce constant shape functions within each element for p and η^2.

$$\begin{aligned} p &= \bar{p}_i \qquad & \eta^2 &= \bar{\eta}_i^2 \\ \delta p &= \delta\bar{p}_i \qquad & \delta\eta^2 &= \delta\bar{\eta}_i^2 \end{aligned} \qquad (8)$$

As was done with the control inequality constraint problem, these shape functions and the shape functions for x, λ, and u may be substituted into Eq. (7). Carrying out the integration results in a set of algebraic equations.

Optimal Guidance Law Development for an Advanced Launch System

INTERIM PROGRESS REPORT

1 June 1990 – 30 November 1990

December 1990

Research Supported by NASA Langley Research Center

NASA Grant No. NAG-1-939

Principal Investigators: Anthony J. Calise & Dewey H. Hodges

Research Assistants: Martin S. Leung & Robert R. Bless

NASA Grant Monitor: Dr. Daniel D. Moerder

Georgia Institute of Technology
School of Aerospace Engineering
Atlanta, GA 30332-0150

1. Summary

1.1 Regular Perturbation Analysis

During this reporting period research was directed at evaluating the regular perturbation method described in details in [1]. Closed-loop simulations were performed with a first order correction including all of the atmospheric terms. In addition, a method was developed for independently checking the accuracy of the analysis and the rather extensive programming required to implement the complete first order correction with all of the aerodynamic effects included. This amounted to developing an equivalent Hamiltonian for the first order analysis and evaluating it by quadrature. The result was compared to the Hamiltonian computed from the first order analysis. A second order correction was also completed for the neglected spherical Earth and back-pressure effects. Finally, an analysis was begun on a method for dealing with control inequality constraints.

To date, the results on including higher order corrections do show some improvement for this application, however we do not know at this stage if significant improvement will result when the aerodynamic forces are included. If the result is negative, then our recommendation is that the method of Matched Asymptotic Expansions (MAE) be explored as the next major step in this research effort. The results from a parallel research effort on aeroassisted orbit transfer trajectories indicate that the regular perturbation analysis under current investigation actually plays the role of the inner expansion in a MAE analysis. The outer solution in a MAE analysis provides a correction currently not available from a regular expansion. We would like to explore if a similar situation holds for the dynamics associated with launch vehicle trajectories.

1.2 Finite Element Analysis

The weak formulation for solving optimal control problems has now been extended in order to account for state inequality constraints. The formulation has been tested on three example problems and numerical results have been compared to the exact solutions. Development of a general-purpose computational environment for the solution of a large class of optimal control problems is now well underway. An example, along with the necessary input and the output, is given.

2. Research Accomplishments

2.1 Regular Perturbation Analysis

Closed-loop Simulation

Figures 1 and 2 compare the performance of the closed-loop control solutions generated by two different methods, with the open loop optimal solution generated using a multiple shooting method. A first order correction was made in each case for the neglected spherical Earth & engine back-pressure effects. The simulation results are for lift and drag set to zero. In Method 1, the control update interval was 1 second and within each interval the control was held constant. The control was determined by repeatedly calculating a new zero order solution and performing a quadrature at every update. Method 2 was based on a pre-calculated quadrature for a fixed zero order solution corresponding to the conditions near launch. See [1] for details on these two Methods. Nearly continuous control updating was used for Method 2 because the computational effort is trivial. It amounts to solving a set of 4 linear equations to generate the on-line control. A mid-point extrapolation scheme (accuracy equivalent to a Runge-Kutta 7/8) was used in both methods for the simulation. Table 1 gives a comparison of the terminal conditions and the performance index.

Table 1:Terminal Values Comparison

	Method 1	Method 2	Optimal
h_f	148160m	148147m	148160m
V_f	7857.58m/s	7864.99m/s	7858.2m/s
γ_f	0.001deg	0.035deg	0
t_f	355.612s	355.744s	355.591s

The results show a dramatic improvement in comparison to the open loop solutions reported in [1] for these two methods. In [1] the trajectories were obtained from a single calculation at launch, and the trajectories were constructed by simply summing the zero order solution and integrated first order dynamics. For the results shown here, the solutions were obtained by integration of the complete dynamics, with the control computed from the perturbation analysis.

Figures 3 and 4 show the closed loop simulation results for Method 1 including the aerodynamic forces in the first order correction. Since the zero order solution gives an unrealistically high angle-of-attack (approximately –45 deg.) at launch, the simulation was started at an altitude of 10525 meters, so that the zero order solution for alpha was still within the range of the tabulated aerodynamic data. Figure 3 clearly indicates the onset of an instability in alpha at this altitude. The slight increase in alpha near the end is due to a numerical problem that can be removed at a later date.

It was not known at this point if this instability was due to an analysis and/or programming error, or due to the inability of the regular perturbation analysis to account for aerodynamic effects using a first order correction. It could also be that a second-order correction would not significantly improve matters, since at best we are forming an asymptotic series solution to the problem. Thus we decided to develop an independent check on our results before proceeding to a second order analysis, which is described in the next section

Checking the First-order Analysis

Checking was performed by monitoring a Hamiltonian function which corresponds to the first order necessary conditions when viewed as being derived from an equivalent optimization problem. This Hamiltonian is different from the first order expansion of the original Hamiltonian for the full nonlinear dynamics. The first order Taylor's series expansion of the original Hamiltonian does not correspond to the costate equations and the optimality condition of the first-order dynamics [2]. So a new Hamiltonian (H) was derived which has the following form:

$$H = \{\mathbf{f}_{\mathbf{x}}^{\mathrm{To}}\mathbf{x}_1 + \mathbf{f}_{\mathbf{u}}^{\mathrm{To}}\mathbf{u}_1 + \frac{T_1}{T_0}[\mathbf{f}^{\mathrm{o}} + (t - t_o)\mathbf{f}_t^{\mathrm{o}}] + \mathbf{g}^{\mathrm{o}}\}^{\mathrm{T}}\boldsymbol{\lambda}_1$$

$$+\frac{1}{2}[\mathbf{x}_1\ \mathbf{u}_1]\begin{bmatrix} \frac{\partial(\mathbf{f}_{\mathbf{x}}^{\mathrm{T}}\boldsymbol{\lambda})_{|\mathrm{o}}}{\partial \mathbf{x}} & \frac{\partial(\mathbf{f}_{\mathbf{x}}^{\mathrm{T}}\boldsymbol{\lambda})_{|\mathrm{o}}}{\partial \mathbf{u}} \\ \frac{\partial(\mathbf{f}_{\mathbf{x}}^{\mathrm{T}}\boldsymbol{\lambda})_{|\mathrm{To}}}{\partial \mathbf{u}} & \frac{\partial(\mathbf{f}_{\mathbf{u}}^{\mathrm{T}}\boldsymbol{\lambda})_{|\mathrm{o}}}{\partial \mathbf{u}} \end{bmatrix}\begin{bmatrix}\mathbf{x}_1 \\ \mathbf{u}_1\end{bmatrix}$$

$$+\{\frac{T_1}{T_0}[(\mathbf{f}_{\mathbf{x}}^{\mathrm{T}}\boldsymbol{\lambda})^{\mathrm{o}} + (t - t_o)(\mathbf{f}_{\mathbf{x}}^{\mathrm{T}}\boldsymbol{\lambda})_t^{\mathrm{o}}] + (\mathbf{g}_{\mathbf{x}}^{\mathrm{T}}\boldsymbol{\lambda})_t^{\mathrm{o}}\}^{\mathrm{T}}\mathbf{x}_1 + \{\frac{T_1}{T_0}(t - t_o)(\mathbf{f}_{\mathbf{x}}^{\mathrm{T}}\boldsymbol{\lambda})_t^{\mathrm{o}} + (\mathbf{g}_{\mathbf{u}}^{\mathrm{T}}\boldsymbol{\lambda})_t^{\mathrm{o}}\}^{\mathrm{T}}\mathbf{u}_1 \quad (2.1)$$

Since the first order system is time-varying, the Hamiltonian is not constant. The first order analysis is checked by realizing the following two expressions:

$$\frac{dH}{dt} = \frac{\partial H(\mathbf{x}, \boldsymbol{\lambda}, \mathbf{u}^*)}{\partial t} \tag{2.2}$$

$$H = \boldsymbol{\lambda}^T \mathbf{f}(\mathbf{x}, \boldsymbol{\lambda}, \mathbf{u}^*) \tag{2.3}$$

where for the right hand side of (2.2) we mean the partial derivative of the expression in (2.1). The Hamiltonian was computed in two ways. First by numerical integration of (2.2) along the trajectory with an arbitrary initial condition. Second, by direct substitution of the state, costate and control values from the first order solution into (2.3). If the analysis and programming is correct, the *difference* between the two ways of computing H should be stagewise constant. This was verified by the results in Figures 5 and 6. In this setting, both the zero and first-order optimality conditions and their costate equations were verified because H also depends on the zero order solution. The difference in the two calculations is zero to within 4 significant digits.

Second-order Correction

A second order analysis was also carried out to determine if any improvement results in comparison to the first order solution. At this stage, the second order analysis including the aerodynamic forces is not completed. However, a second order correction for the spherical Earth and back-pressure effects was evaluated and the results are depicted in Figures 7-11. These are the open-loop histories obtained by summing the forward integration results for each corrected term. In integrating the second order dynamics, the first order state and costate histories are required. This is done by a forward integration of the first order dynamics using the known initial values for $\mathbf{x}_1(t_o)$ and the calculated initial costate correction $\boldsymbol{\lambda}_1(t_o)$. The histories are stored for a sufficient number of sample points, and retrieved using a piecewise linear interpolation for the integration of the second order dynamics.

In examining the results of Figures 7-11 it should be noted that the pattern throughout is that the first-order correction over-corrects the zeroth-order solution, and that the secord-order correction over- corrects the first-order solution. Unfortunately, the error is not significantly decreased by the second-order correction in most of the results, with the exception of the λ_u profile which shows a dramatic improvement. The estimates for the initial values of the costates and the final time (performance index) are compared in Table 2.

Table 2. Performance Comparison Of The Open-loop Results

	$\lambda_v(0)/s^2m^{-1}$	$\lambda_u(0)/s^2m^{-1}$	$\lambda_r(0)/sm^{-1}$	t_f/s
Zeroth-order	0.20156e-1	0.19334e-1	0.54560e-4	360.047
First-order	0.39188e-1	0.22036e-1	0.56468e-3	354.335
Second-order	0.35344e-1	0.20899e-1	0.57143e-3	355.254
Optimal	0.37352e-1	0.20868e-1	0.60304e-3	355.606

Control Inequality Constraint

Preliminary work on addressing control inequality constraints ($C(\mathbf{x},\mathbf{u}) \leq 0$) is under investigation. This approach makes use of a slack variable (σ) to transform to a strict equality constraint [3]. The necessary conditions are as follows:

$$\dot{x} = f + \varepsilon g ; \qquad t \in [t_0, t_f] \tag{2.4}$$

$$\dot{\lambda} = -f_x^T\lambda - C_x\mu - \varepsilon g_x^T\lambda \tag{2.5}$$

$$0 = f_u^T\lambda + C_u\mu + \varepsilon g_u^T\lambda \tag{2.6}$$

$$0 = \alpha\mu \tag{2.7}$$

$$0 = C + \frac{1}{2}\alpha^2 \tag{2.8}$$

Equations (2.4-2.6) are derived from the necessary conditions on the augmented Hamiltonian,

$$H = f^T\lambda + \varepsilon g^T\lambda + (C + \frac{1}{2}\alpha^2)\mu \tag{2.9}$$

When the trajectory is on the constraint, $\alpha = 0$. When it is off the constraint, $\mu = 0$. Note that the product is zero at every instant. Alternatively, (2.7) can be derived if we realize that the slack variable can be treated as a control variable and then use the optimality condition $H_\alpha = 0$. Equations (2.7) and (2.8) provides the additional information needed to determine α and μ.

To obtain the zeroth- and higher-order formulations, we simply need to carry out the expansions including:

$$\mu = \mu_0 + \varepsilon\mu_1 + \varepsilon^2\mu_2 + ... \tag{2.10}$$

$$\alpha = \alpha_0 + \varepsilon\alpha_1 + \varepsilon^2\alpha_2 + ... \tag{2.11}$$

Substituting these expansions and equating like powers in ε, the algebraic equations (2.6-2.8) can be grouped as (note that for simplicity, we consider a scalar u case):

$$\begin{bmatrix} (f_u^T\lambda)_u^o + C_{uu}^o\mu_0 & C_u^o & 0 \\ 0 & \alpha_0 & \mu_0 \\ C_u^o & 0 & \alpha_0 \end{bmatrix} \begin{bmatrix} u_j \\ \mu_j \\ \alpha_j \end{bmatrix} = -\begin{bmatrix} (f_u^T\lambda)_x^o + C_{ux}^o\mu_0 \\ 0 \\ C_x^o \end{bmatrix} x_j - \begin{bmatrix} f_u^{oT} \\ 0 \\ 0 \end{bmatrix} \lambda_j$$

$$- \begin{bmatrix} \Omega(x_0,..,x_{j-1},u_0,..,u_{j-1},\lambda_0,..,\lambda_{j-1}) \\ 0 \\ 0 \end{bmatrix} \tag{2.12}$$

where j = 1, 2, ...

Solving the control constraint problem requires a guess of the switching structure. This is true of all indirect methods. In this case, it is the switching structure on the zero order solution that matters. The method requires that the zero order solution captures the true switching structure because it affects the matrix on the left-hand-side of (2.12). It is this matrix which subsequently produces the control correction that leads to a better approximation. If the matrix is singular the method and the expansion technique will fail. On case that does lead to a singular matrix is the touch-point switching structure, where

$$\alpha_0 = \mu_0 = 0$$

$$\det\left(\begin{bmatrix} (\mathbf{f}_u^T\lambda)_u^o + C_{uu}^o\mu_0 & C_u^o & 0 \\ 0 & \alpha_0 & \mu_0 \\ C_u^o & 0 & \alpha_0 \end{bmatrix}\right) = (\mathbf{f}_u^T\lambda)_u^o\alpha_0^2 + C_u^{o2}\mu_0 = 0 \qquad (2.13)$$

For some simple cases, it may be possible to incorporate the control constraint in the zero order problem, thus capturing the true switching structure. However, for the launch vehicle problem, where the dynamics are nonlinear and time varying, and incorporation of any form of control constraint will make the derivation of an analytic solution difficult. Further analysis is required to see whether any simplification is possible.

2.2 Finite Element Analysis

2.2.1 Extension of the Analysis. The method based on the weak Hamiltonian formulation derived in [4] and [5] has now been extended to handle problems with state inequality constraints. An outline of the derivation and a simple example problem are given in Appendix A. (Even more details of the derivation can be found in [6], a copy of which will be sent to the Technical Monitor as soon as it is complete.)

The derivation proceeds in the following manner. It is desired to develop a solution strategy for optimal control problems with state inequality constraints based on finite elements in time. In an attempt to make the solution scheme as general as possible, all strong boundary conditions are transformed into natural boundary conditions. This is done so that the shape functions can be chosen from a less restrictive class of functions, which enables one to choose the same shape functions for every optimal control problem.

The idea of transforming the strong boundary conditions to natural boundary conditions [7] revolves around adjoining a constraint equation to the performance index with an unknown Lagrange multiplier. The variation of the performance index is then taken in a straightforward manner. Through appropriate integration by parts, it is possible to show that the Euler-Lagrange equations are identical to those derived in classical textbooks [8] and that the boundary conditions are the same, only stated weakly instead of strongly.

2.2.2 Development of a General Code. The weak formulation is capable of solving optimal control problems that have continuous states, costates, and controls, and problems with discontinuities arising from staging (i.e., discontinuities in the system equations), control inequality constraints and state inequality constraints. The algebraic equations which come from the weak formulation may be derived prior to specifying the problem to be solved. It is this feature in particular that allows for a general problem-solving environment to be created.

The main goal of the general code is to reliably solve a large class of optimal control problems with a *minimum* of user interaction. Specifically, it is desired to create an environment where the user does not have to write subroutines. To this end, the general code is being developed on a SUN 3/260 workstation and requires a FORTRAN 77 compiler, MACSYMA [9], and the Harwell subroutine library [10]. The general procedure can be broken into three parts that must interface together. The first part is the FORTRAN code. This code contains all the subroutines necessary to solve any of the optimal control problems described above. However, if certain problems require table look-up routines (such as aerodynamic data for a rocket model), then these subroutines must be given by the user and interfaced to the rest of the general code. Thus, there may be a need for some user programming for certain problems. The second part of the general procedure is the use of MACSYMA. The user must supply an input file specifying the problem. This input file is in symbolic form and will be loaded into MACSYMA. MACSYMA will then evaluate all the necessary expressions and automatically generate the FORTRAN code. This code is spliced into a

template file and becomes one of the subroutines. The third and final part of the general procedure will consists of subroutines to generate initial guesses that will reliably converge. Homotopy methods are the prime candidates for this. A very simple type of homotopy method described in [11] is being used. This method converts the algebraic equations to initial-value ordinary differential equations. A second-order Runge-Kutta method is used to integrate the equations and obtain initial guesses for a Newton-Raphson method. This method has worked on all the problems tested to date.

The general code is still being developed at this time. Currently, the code can handle problems with continuous states, costates, and controls, problems with control inequality constraints, and problems with state inequality constraints that only touch the constraint boundary. The general code is now functional (but not complete) for a large class of optimal control problems. An example problem demonstrating the use of the code is given in Appendix B.

3. Future Research

In the perturbation analysis area we plan to complete the second order analysis, and to perform both open loop and closed loop comparisons to the first order results and to the optimal solution. However, we are skeptical at this point that second order correction will remove the instability observed in the first order results when aerodynamic forces are included. Along this line we plan to spend some time investigating the potential that Matched Asymptotic Expansions has for improving the solutions that we have obtained to date. We will also continue investigating the control inequality constraint formulation. Results will first be developed for several simpler problems to evaluate its potential for application to launch vehicle guidance problems.

In the finite element analysis area we plan to complete the development of the general code so as to make it applicable to all types of optimal control problems encountered so far (i.e., up through state inequality constraints). We further plan to document the methodology through the completion of one paper (which we are now revising in response to reviewers) on the application of the method to launch vehicle trajectory analysis, two technical notes on control and state inequality constraints, one paper on the general code, and a user's manual for the code. We have received several calls from parties interested in application of the methodology in industry and, although there is nothing concrete established as yet, hope to somehow transfer the technology to an industry application in the future.

4. References

[1]. Leung, S. K., Calise A. J., "An Approach To Real-time Guidance Law For An Advanced Launch System," ACC 1990 Proc., San Diego.

[2]. Lietmann, G., *Optimization Techniques*, Academic Press, 1962.

[3]. Bensoussan A., *Perturbation Methods In Optimal Control*, John Wiley & Sons, 1982

[4]. Hodges, Dewey. H., and Bless, Robert R., "Weak Hamiltonian Finite Element Method for Optimal Control Problems," *Journal of Guidance, Control, and Dynamics*, Vol. 14, No. 1, January-February, 1991, to appear.

[5]. Hodges, Dewey H., Bless, Robert R., Calise, Anthony J., and Leung, Martin, "Finite Element Method for Optimal Guidance of an Advanced Launch Vehicle with Inequality Constraints," *Journal of Guidance, Control, and Dynamics*, submitted for publication, 1990.

[6]. Bless, Robert R., and Hodges, Dewey H., "Finite Element Solution of Optimal Control Problems with State Inequality Constraints," in preparation.

[7]. Wu, J. J., and Simkins, T. E., "A Numerical Comparison Between Two Unconstrained Variational Formulations," *Journal of Sound and Vibration*, Vol. 72, 1980, pp. 491 – 505.

[8]. Bryson, Arthur E. Jr., and Ho, Yu-Chi, *Applied Optimal Control*, Blaisdell Publishing Company, Waltham, Massachusetts, 1969, Chapter 2.

[9]. MACSYMA Reference Manual, Symbolics, Inc., Burlington, Massachusetts, 1988.

[10]. Duff, I. S., Harwell Subroutine Library, Computer Science and Systems Division, Harwell Laboratory, Oxfordshire, England, February 1988, Chapt. M.

[11]. Kane, Thomas R., and Levinson, David A., *Dynamics: Theory and Applications*, McGraw-Hill Book Company, New York, 1985, Chapter 7.

[12]. Jacobson, D. H., Lele, M. M., and Speyer, J. L., "New Necessary Conditions of Optimality for Control Problems with State-Variable Inequality Constraints," *Journal of Mathematical Analysis and Applications*, Vol. 35, 1971, pp. 255 – 284.

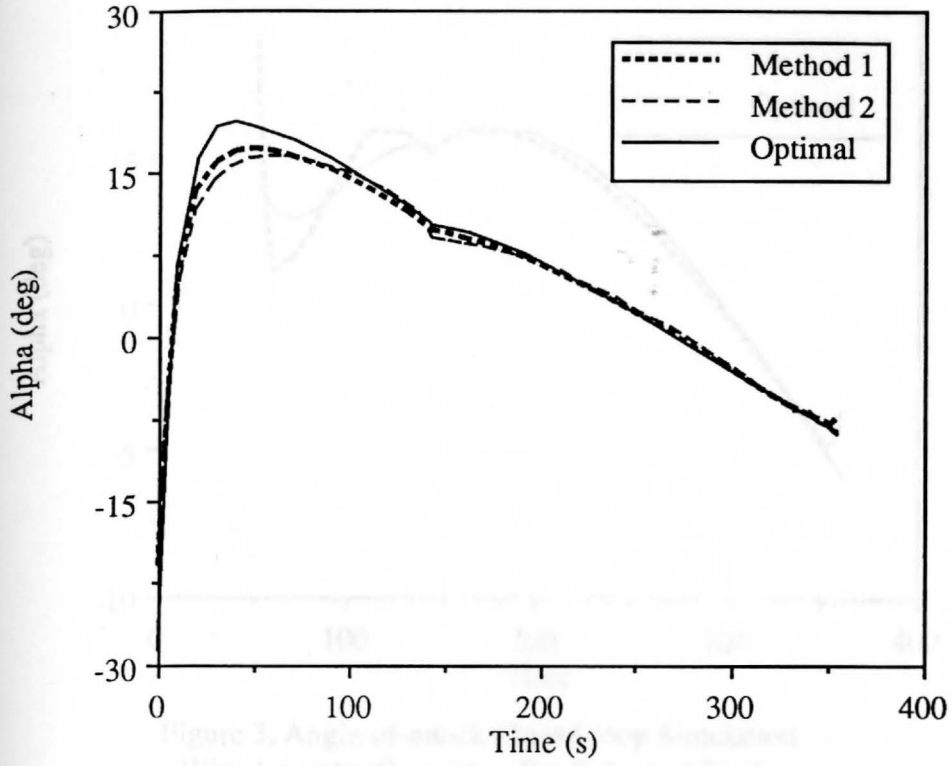

Figure 1:Angle-of-attack Closed-loop Simulation With 1st-order Correction For Spherical Earth & Back-pressure Effects.

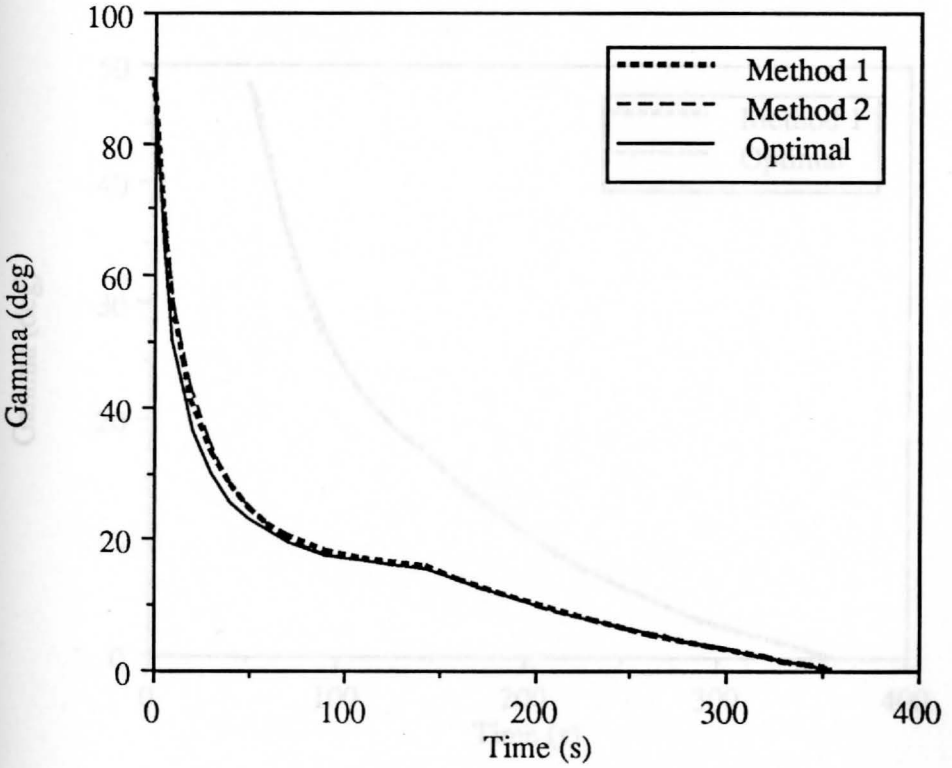

Figure 2:Flight Path Angle Closed-loop Simulation With 1st-order Correction For Spherical Earth & Back-pressure Effects.

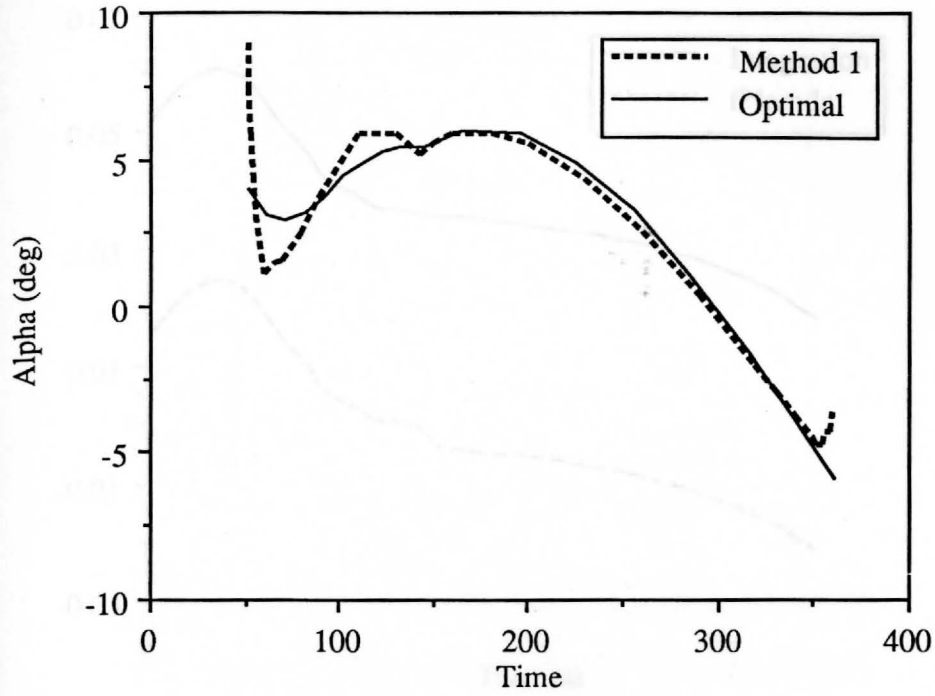

Figure 3. Angle-of-attack Closed-loop Simulation
With 1st-order Correction For Spherical Earth,
Back-pressure & Aerodynamic Effects

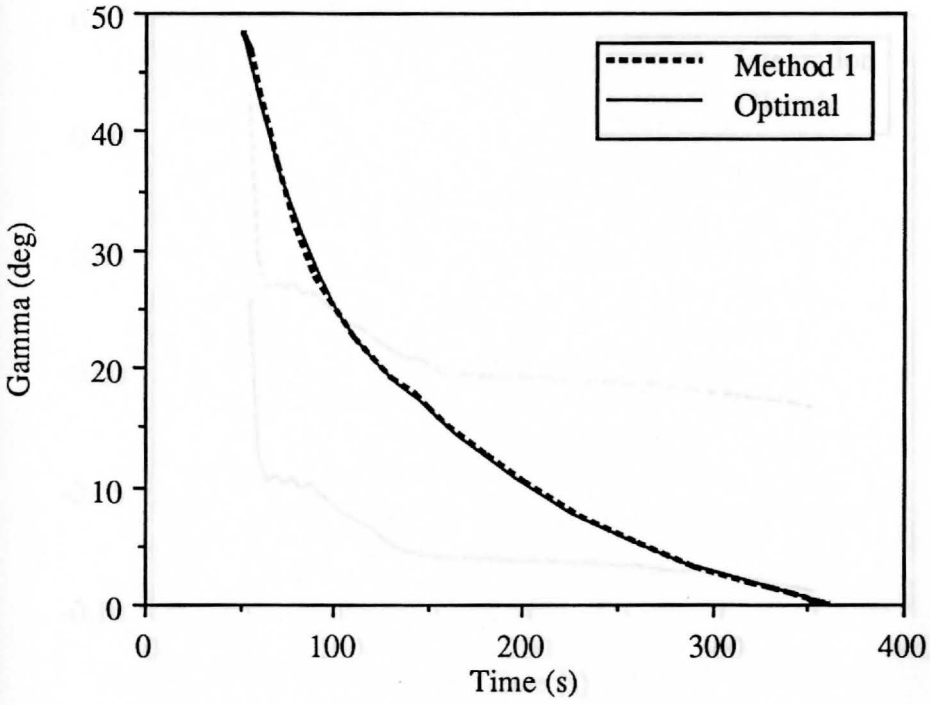

Figure 4. Flight Path Angle Closed-loop Simulation Result

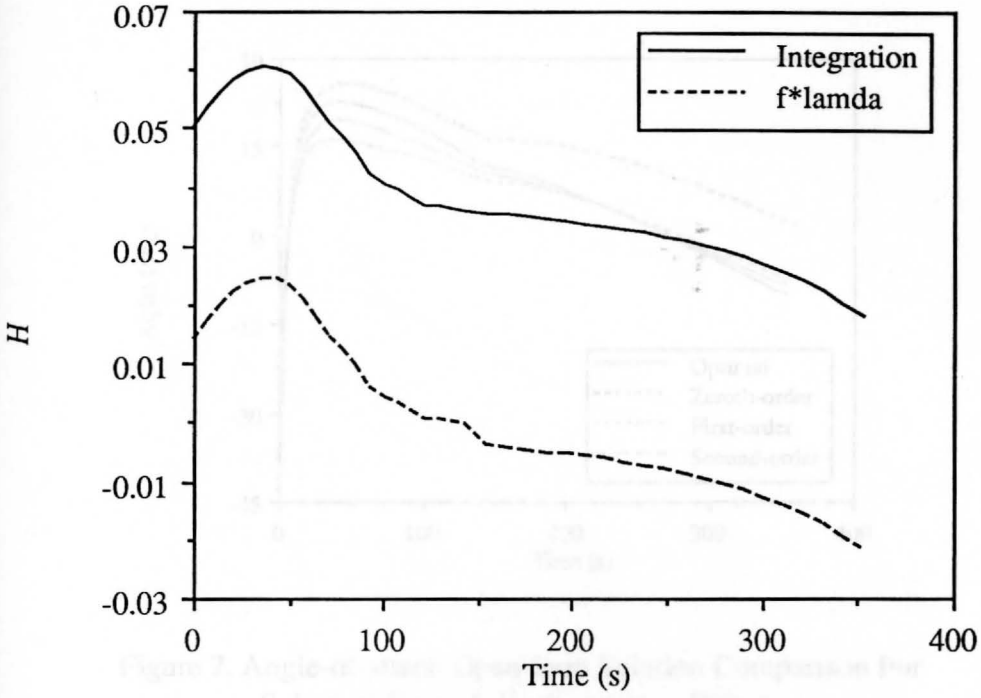

Figure 5. 1st-order Formulation (Spherical Earth & Back-pressure) Checking Using The Hamiltonian H

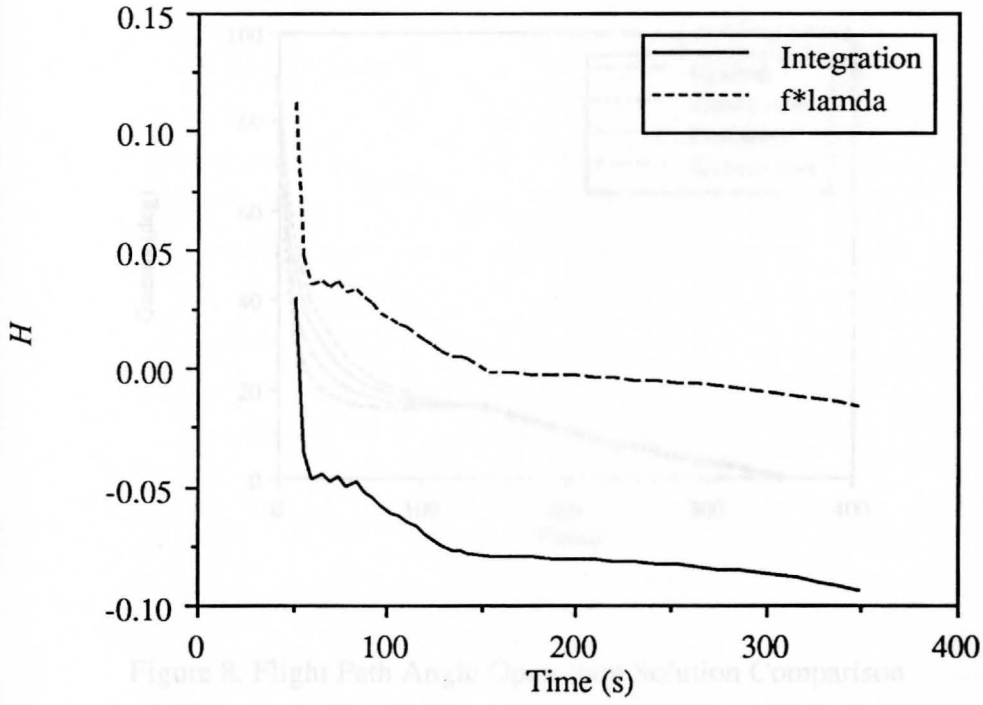

Figure 6. 1st-order Formulation (Spherical Earth, Back-pressure & Aerodynamic Effects) Checking Using H

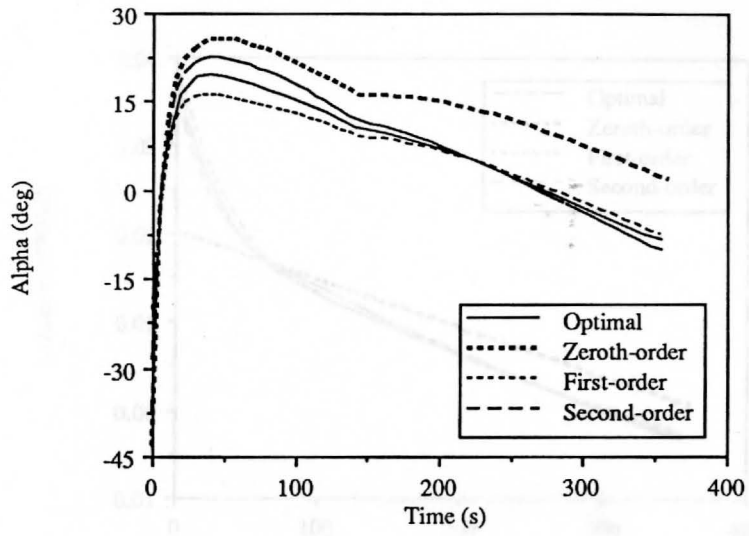

Figure 7. Angle-of-attack Open-loop Solution Comparison For Spherical Earth & Back-pressure Effects

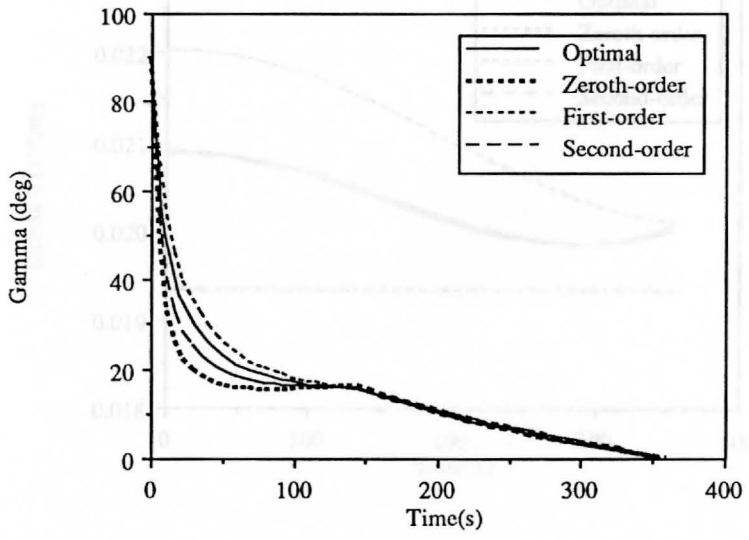

Figure 8. Flight Path Angle Open-loop Solution Comparison

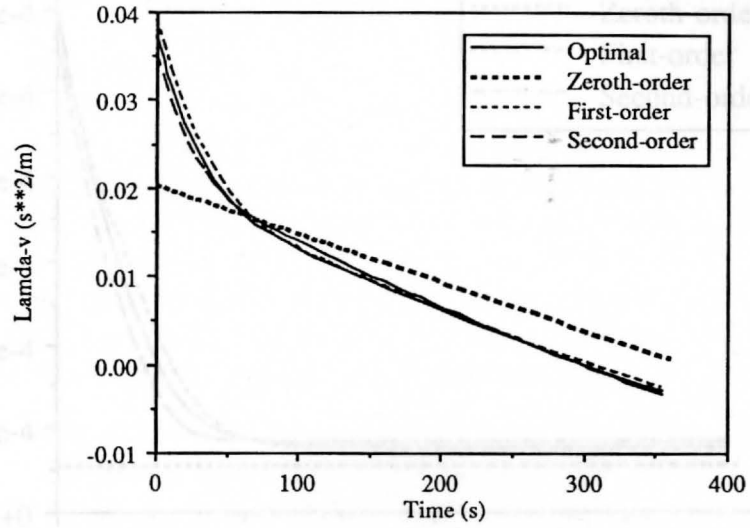

Figure 9. Lamda-v Open-loop Solution Comparison

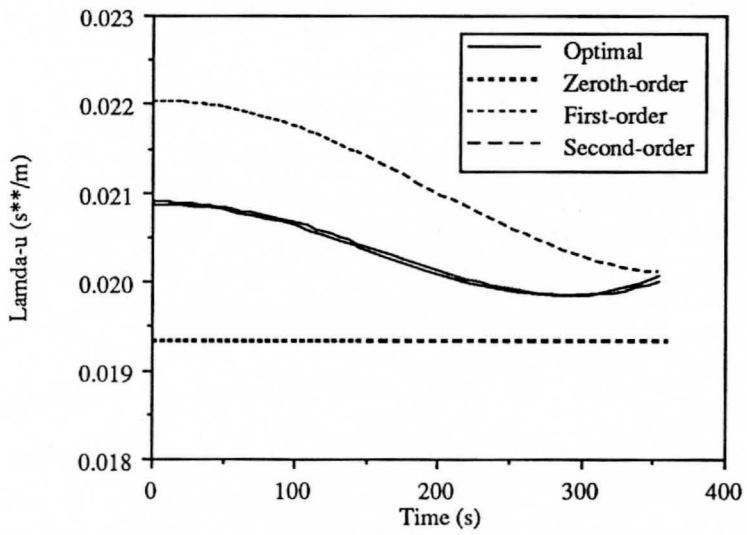

Figure 10. Lamda-u Open-loop Solution Comparison

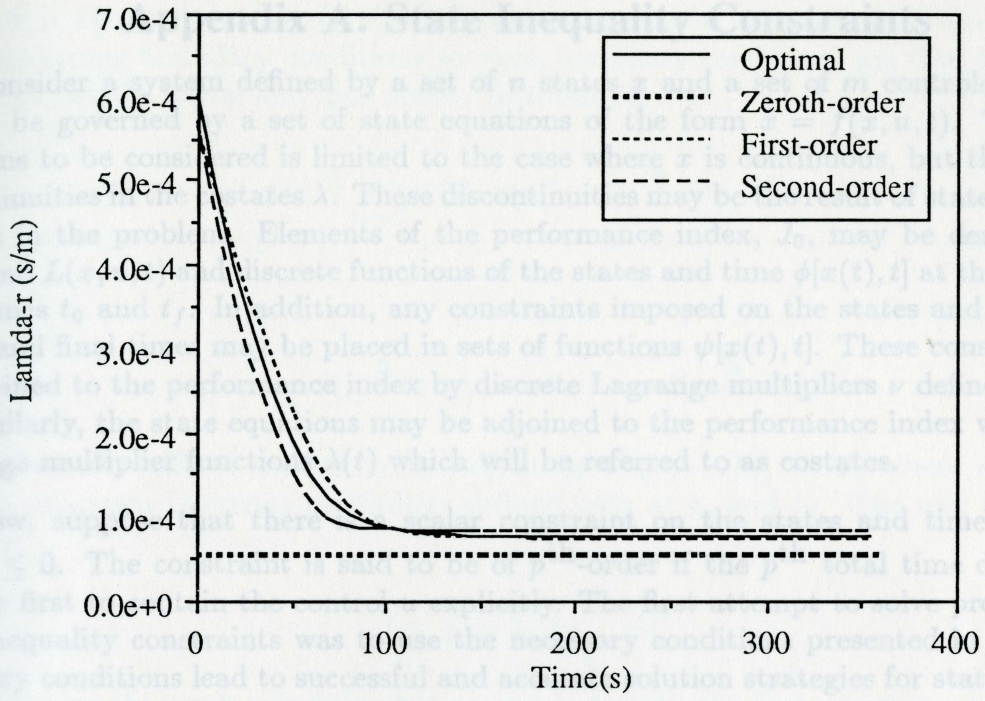

Figure 11. Lamda-r Open-loop solution Comparison

Appendix A: State Inequality Constraints

Consider a system defined by a set of n states x and a set of m controls u. Let the system be governed by a set of state equations of the form $\dot{x} = f(x, u, t)$. The class of problems to be considered is limited to the case where x is continuous, but there may be discontinuities in the costates λ. These discontinuities may be the result of state constraints present in the problem. Elements of the performance index, J_0, may be denoted by an integrand $L(x, u, t)$ and discrete functions of the states and time $\phi[x(t), t]$ at the initial and final times t_0 and t_f. In addition, any constraints imposed on the states and time at the initial and final times may be placed in sets of functions $\psi[x(t), t]$. These constraints may be adjoined to the performance index by discrete Lagrange multipliers ν defined at t_0 and t_f. Similarly, the state equations may be adjoined to the performance index with a set of Lagrange multiplier functions $\lambda(t)$ which will be referred to as costates.

Now, suppose that there is a scalar constraint on the states and time defined by $S(x, t) \leq 0$. The constraint is said to be of p^{th}-order if the p^{th} total time derivative of S is the first to contain the control u explicitly. The first attempt to solve problems with state inequality constraints was to use the necessary conditions presented in [12]. These necessary conditions lead to successful and accurate solution strategies for states that only touch (*i.e.*, do not ride) the constraint boundary. As is derived in [12], for constraints of odd order greater than one, the solution can at most only touch the constraint boundary. However, for cases where the states ride the constraint boundaries for a nonzero length of time, the algebraic equations developed by the weak form are singular. Private discussions with Jason Speyer and Dan Moerder indicate that the cause is related to a reduced-dimensional manifold; however, we have not been able to develop a nonsingular weak form as of now.

Fortunately, the necessary conditions presented in [8] are accurate for first and second order constraints where the solution often rides the constraint boundary. Thus a weak formulation is also developed using these necessary conditions for constraints where $p = 1$ or $p = 2$. Therefore, below are presented two very similar weak formulations which are accurate for up to a third order constraint and odd-ordered constraints beyond that. Most practical applications will be third-order or less.

General Development

The weak formulation is now derived for touch-point cases. Without loss of generality, assume that there is only one touch-point over the time interval of interest. In this case, the state constraint is nothing more than an interior boundary point which creates a jump in the costate.

The performance index J_0 now takes the form:

$$J_0 = \int_{t_0}^{t_1} \left[L(x,u,t) + \lambda^T(f - \dot{x})\right]\, dt + \int_{t_2}^{t_f} \left[L(x,u,t) + \lambda^T(f - \dot{x})\right]\, dt + \nu_1 S|_{t_1} + \Phi|_{t_0}^{t_f} \quad (1)$$

where $\Phi = \phi[x(t),t] + \nu^T\psi[x(t),t]$. The constraints to be adjoined to J_0 above to transform the strong boundary conditions to weak boundary conditions are that the states be continuous at the initial and final times. Introducing

$$x|_{t_0} \triangleq \lim_{t\to t_0^+} x(t) \quad \text{and} \quad x|_{t_f} \triangleq \lim_{t\to t_f^-} x(t) \tag{2}$$

and

$$\hat{x}_0 = \hat{x}|_{t_0} \triangleq x(t_0) \quad \text{and} \quad \hat{x}_f = \hat{x}|_{t_f} \triangleq x(t_f) \tag{3}$$

one can weakly enforce continuity by adjoining $\alpha^T(x-\hat{x})|_{t_0}^{t_f}$ to J_0 where α is a set of discrete unknown Lagrange multipliers defined only at t_0 and t_f. The new performance index is

$$J = J_0 + \alpha^T(x-\hat{x})|_{t_0}^{t_f} \tag{4}$$

To derive the weak principle, it is necessary to take the first variation of J and set it equal to zero. For notational convenience, the following variables are introduced.

$$\hat{\lambda}_0 = \left.\frac{\partial\Phi}{\partial x}\right|_{t_0} \quad \text{and} \quad \hat{\lambda}_f = \left.\frac{\partial\Phi}{\partial x}\right|_{t_f} \tag{5}$$

Also, as is shown in [4], the Lagrange multiplier α can be chosen so that $\delta\alpha = \delta\lambda$. The final form of the weak principle is obtained after integrating by parts so that no derivatives of the states or costates appear. After defining the Hamiltonian $H = L + \lambda^T f$ and denoting the variations of the variables at the initial, touch-point, and final times with subscripts 0, 1, and f respectively, then the resulting equation is

$$\begin{aligned}
&\int_{t_0}^{t_1}\left\{-\delta\dot{x}^T\lambda + \delta\lambda^T f + \delta\dot{\lambda}^T x + \delta x^T\left[\left(\frac{\partial L}{\partial x}\right)^T + \left(\frac{\partial f}{\partial x}\right)^T\lambda\right]\right.\\
&\left.+\,\delta u^T\left[\left(\frac{\partial L}{\partial u}\right)^T + \left(\frac{\partial f}{\partial u}\right)^T\lambda\right]\right\}dt + \int_{t_1}^{t_f}\left\{-\delta\dot{x}^T\lambda + \delta\lambda^T f + \delta\dot{\lambda}^T x\right.\\
&\left.+\,\delta x^T\left[\left(\frac{\partial L}{\partial x}\right)^T + \left(\frac{\partial f}{\partial x}\right)^T\lambda\right] + \delta u^T\left[\left(\frac{\partial L}{\partial u}\right)^T + \left(\frac{\partial f}{\partial u}\right)^T\lambda\right]\right\}dt\\
&+\,\delta\nu_1^T S|_{t_1} + \delta\nu^T\psi|_{t_f} + \delta x_1^T\left(\frac{\partial S}{\partial x}\right)^T\nu_1 + \delta x_f^T\hat{\lambda}_f - \delta x_0^T\hat{\lambda}_0 - \delta\lambda_f^T\hat{x}_f + \delta\lambda_0^T\hat{x}_0\\
&+\,\delta t_1\left[H(t_1^-) - H(t_1^+) + \nu_1\frac{\partial S}{\partial t}\right] + \delta t_f H(t_f) = 0
\end{aligned} \tag{6}$$

This is the governing equation for the weak Hamiltonian method for problems with touch-point state inequality constraints. It is easily shown by integrating the $\delta\dot{x}$ and $\delta\dot{\lambda}$ terms by parts in Eq. (6) that all the Euler-Lagrange equations are the same as in [12] and that all boundary conditions are now of the natural type.

One simplification may be made to Eq. (6). If the control is continuous across t_1 (as is often the case), then it is possible to simplify the δt_1 equation since then $f(t_1^-) = f(t_1^+) = f(t_1)$ and $L(t_1^-) = L(t_1^+) = L(t_1)$. From the necessary conditions that are found in [12] or from the ones that could be found from Eq. (6), it is seen that

$$\lambda^T(t_1^-) - \lambda^T(t_1^+) = \nu_1 \frac{\partial S}{\partial x} \tag{7}$$

Now, rewriting the coefficient of δt_1 as

$$\begin{aligned} H(t_1^-) - H(t_1^+) + \nu_1 \frac{\partial S}{\partial t} &= \left[\lambda^T(t_1^-) - \lambda^T(t_1^+)\right] f(t_1) + \nu_1 \frac{\partial S}{\partial t} \\ &= \nu_1 \frac{\partial S}{\partial x}\dot{x} + \nu_1 \frac{\partial S}{\partial t} = \nu_1 \frac{dS}{dt} \end{aligned} \tag{8}$$

we see that the condition for continuity of the Hamiltonian reduces to the condition that the first total time derivative of the constraint be zero at t_1 if the control is continuous.

For cases where there is a boundary arc (*i.e.*, the solution rides the constraint boundary for a nonzero length of time), then the weak formulation must be modified. For simplicity and without loss of generality, consider the case where the solution has an unconstrained arc followed by a constrained arc and then another unconstrained arc. Introducing a new Lagrange multiplier function η to adjoin the p^{th} derivative of the constraint S to the performance index, then J_0 becomes

$$\begin{aligned} J_0 = &\int_{t_0}^{t_1} \left[L(x,u,t) + \lambda^T(f - \dot{x})\right] dt + \int_{t_1}^{t_2} \left[L(x,u,t) + \lambda^T(f - \dot{x}) + \eta \frac{d^p S}{dt^p}\right] dt \\ &+ \int_{t_2}^{t_f} \left[L(x,u,t) + \lambda^T(f - \dot{x})\right] dt + \nu_1 N|_{t_1} + \Phi|_{t_0}^{t_f} \end{aligned} \tag{9}$$

where N is a column matrix defined as

$$N^T = \left[\, S \quad \tfrac{dS}{dt} \quad \cdots \quad \tfrac{d^{p-1}S}{dt^{p-1}} \,\right] \tag{10}$$

Again, we define

$$J = J_0 + \alpha^T(x - \hat{x})|_{t_0}^{t_f} \tag{11}$$

Analogous steps to those described above lead to a weak formulation for state constraint problems which ride the constraint boundary. These details are presented in [6].

Example

This example is taken from section 3.11 of [8]. The problem is to minimize

$$J = \frac{1}{2}\int_0^1 u^2\, dt \tag{12}$$

The state equations are

$$\begin{aligned} \dot{x}_1 &= u \\ \dot{x}_2 &= x_1 \end{aligned} \tag{13}$$

The state inequality constraint $S(x,t) = x_2 - \theta \leq 0$ is to be imposed. For certain values of θ, the solution only touches the boundary, whereas for other values of θ the solution rides the boundary.

The algebraic equations were solved using a Newton-Raphson method and a FORTRAN code written on a SUN 3/260. The sparse, linearized equations are solved using subroutine MA28 from the Harwell subroutine library [10]. This subroutine takes advantage of sparsity which leads to great computational savings.

The state x_2 is shown in Fig. 12 for the single touch-point case. Results for 2, 4, and 8 elements on either side of the touch-point (denoted by 2:2, etc.) are compared to the exact solution. Note that even the 2:2 element case lies essentially on the exact solution. In Fig. 13, the state x_2 is shown for an example case where the state rides the boundary. Here, there are three time intervals and the number of elements in each interval is denoted by 2:2:2 etc. Again we see that the 2:2:2 case has essentially converged on the exact solution. One drawback of the weak formulation is that two separate codes had to be written to solve this problem. Also, one must determine in advance if the solution will ride or just touch the constraint. However, with the general code described in Appendix B, these are simple and quick things to do.

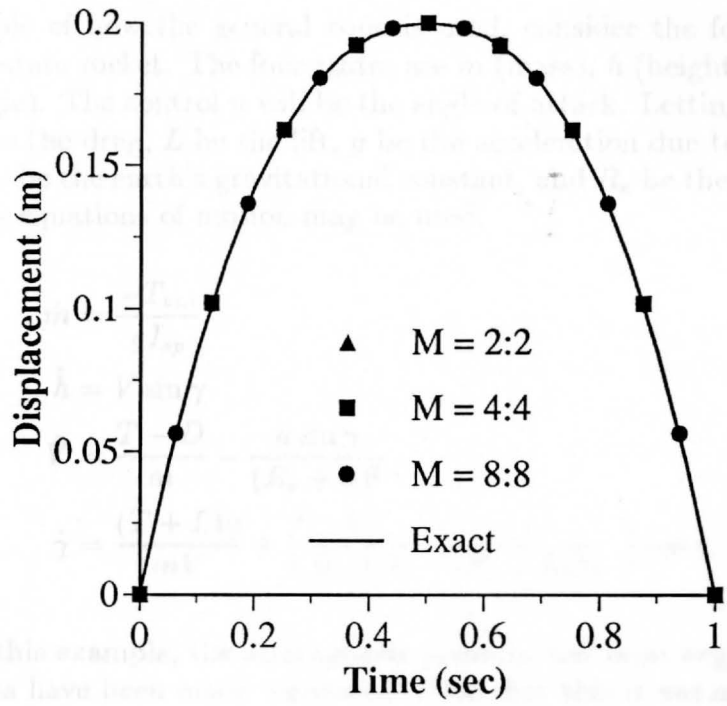

Figure 12: Displacement vs. Time for a touch-point case of θ=0.2

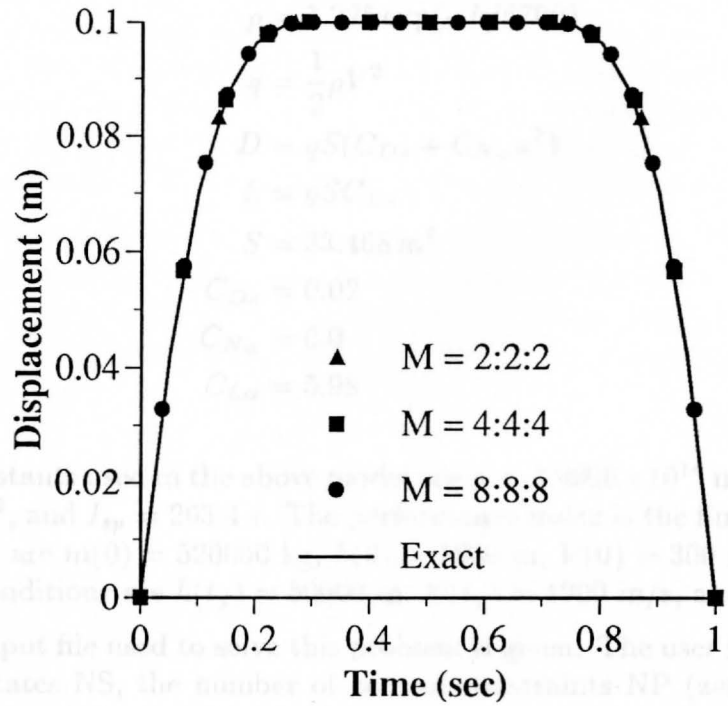

Figure 13: Displacement vs. Time for a boundary arc case of θ=0.1

Appendix B: General Code Usage

As an example of how the general code is used, consider the following model of a single-stage, four-state rocket. The four states are m (mass), h (height), V (velocity), and γ (flight-path angle). The control u will be the angle-of-attack. Letting T_{vac} be the thrust in a vacuum, D be the drag, L be the lift, g be the acceleration due to gravity, I_{sp} be the specific impulse, μ be the earth's gravitational constant, and R_e be the radius of the earth, then the following equations of motion may be used.

$$\begin{aligned}
\dot{m} &= \frac{-T_{vac}}{gI_{sp}} \\
\dot{h} &= V\sin\gamma \\
\dot{V} &= \frac{T-D}{m} - \frac{\mu\sin\gamma}{(R_e+h)^2} \\
\dot{\gamma} &= \frac{(T+L)u}{mV} + \left(\frac{V}{R_e+h} - \frac{\mu}{(R_e+h)^2V}\right)\cos\gamma
\end{aligned} \tag{14}$$

For simplicity in this example, the atmospheric pressure has been neglected and the drag and lift coefficients have been made constants. Note that this is *not* necessary in general. Thus,

$$\begin{aligned}
T &= T_{vac} = 8155800\,\mathrm{N} \\
\rho &= 1.225\exp(-h/6700) \\
q &= \frac{1}{2}\rho V^2 \\
D &= qS(C_{Do} + C_{N\alpha}u^2) \\
L &= qSC_{L\alpha} \\
S &= 33.468\,\mathrm{m}^2 \\
C_{Do} &= 0.02 \\
C_{N\alpha} &= 6.0 \\
C_{L\alpha} &= 5.98
\end{aligned} \tag{15}$$

The physical constants used in the above model are $\mu = 3.9906\times10^{14}$ m^{3}s^{-2}, $R_e = 6378000$ m, $g = 9.81$ ms^{-2}, and $I_{sp} = 263.4$ s. The performance index is the final mass. The known initial conditions are $m(0) = 520000$ kg, $h(0) = 1800$ m, $V(0) = 300$ m/s, and $\gamma(0) = 1.5$ rad. The final conditions are $h(t_f) = 50000$ m, $V(t_f) = 4000$ m/s, and $\gamma(t_f) = 0.0$ rad.

Below the input file used to solve this problem is given. The user is required to supply the number of states NS, the number of control constraints NP (zero in this example), the number of controls M, and the number of constraints on the states at the final time Q. The next series of lines from TVAC to F[4] define the system equations as given in Eqs. (14) and (15) above. (The lines from TVAC to DRAG are not required but are used

to simplify the actual expressions for F[1] thru F[4].) After the equations are formed, the user supplies the performance index L and PHI. Then the Q constraints are given in PSI and the initial conditions are given in IC. Next the user supplies the final time TF and a guess at the value of the final time TFGUES. Since the final time is unknown, TF is set to zero and the user gives a guess at the final time. Also, guesses for the states at the midpoint of the trajectory and the final point are given in XGUES. These guesses may be *very* crude and can even be zero for many problems. Since the final value of three of the states were known for this problem, crude guesses were easily and obviously obtained. Finally, the number of elements to be run is given in NE.

Regardless of the value of NE, the code automatically starts with the two element case and uses the continuation method of [11] and the Newton-Raphson method to solve the problem. The code then interpolates the solution to this case and runs a four element case using only the Newton-Raphson method. The code continues in this manner until NE is met. If the Newton-Raphson fails to converge for the four or higher element case (which is rare) then the program will start that case over and try the continuation method to solve the four element case.

The output of the example is given after the input file and consists of the solutions for the states, costates, controls, and Hamiltonian for 2, 4, and 8 elements. At the top of each page is the total elapsed computer time from the start of the program. On the two element case sheets is 15.74 secs. This is the time the code took to run the continuation method and the Newton-Raphson method for this case. This is a rather small number given the complexity of the problem and the fact that an accurate second-order Runge-Kutta method was used to solve the problem. The time at the top of the four element case is 18.84 which tells us that only 18.84 – 15.74 = 3.1 seconds was required to run the four-element case given the solution to the two element case. Finally, the desired eight element case solution was obtained in a total of 23.46 secs and only 4.62 secs from the four element case. Note that this time includes the extraction of nodal values and the production of the data files. This is a nonnegligible part of the total time.

In summary, a complicated rocket trajectory optimization problem which originally took several weeks to program and solve is now solved in about 10 or 15 minutes. The simple input file is typed in a few minutes and a few minutes are required by MACSYMA to create the FORTRAN subroutines. After that, the program runs in a matter of seconds.

```
NS:4;
NP:0;
M:1;
Q:3;
TVAC:8155800.0;
ISP:263.4;
GRAV:9.81;
MU:3.9906E14;
RE:6378000.0;
H(X):= RE+X(2);
RHOSEA:1.225;
S:33.468;
CNA:6.0;
CAT:0.02;
CLA:5.98;
RHO(X):=RHOSEA*EXP(-X(2)/6700.0);
DP(X):=0.5*RHO(X)*X(3)^2;
LIFT(X):=DP(X)*S*CLA;
DRAG(X,U):=DP(X)*S*(CAT+CNA*U(1)^2);
F[1]:-TVAC/(GRAV*ISP);
F[2]:X(3)*SIN(X(4));
F[3]:(TVAC-DRAG(X,U))/X(1) - MU*SIN(X(4))/H(X)^2;
F[4]:(TVAC+LIFT(X))*U(1)/(X(1)*X(3)) + (X(3)/H(X)-MU/(X(3)*H(X)**2))*COS(X(4));
L:0.0;
PHI:X(1);
PSI[1]:X(2) - 50000.0;
PSI[2]:X(3)-4000.0;
PSI[3]:X(4);
IC[1]:520000.0;
IC[2]:1800.0;
IC[3]:300.0;
IC[4]:1.5;
TF:0.0;
TFGUES:100.0;
XGUES[1,1]:260000.0;
XGUES[1,2]:1000.0;
XGUES[2,1]:25000.0;
XGUES[2,2]:50000.0;
XGUES[3,1]:2000.0;
XGUES[3,2]:4000.0;
XGUES[4,1]:0.5;
XGUES[4,2]:.0;
NE:8;
```

NODAL VALUES FOR THE STATES

NUMBER OF ELEMENTS = 2 TOTAL ELAPSED TIME = 15.74

X1	X2	X3	X4	TIME
0.52000E+06	0.18000E+04	0.30000E+03	0.15000E+01	0.00000E+00
0.30215E+06	0.37957E+05	0.11357E+04	0.13600E+00	0.69021E+02
0.84297E+05	0.50000E+05	0.40000E+04	-.27756E-16	0.13804E+03

NODAL VALUES FOR THE STATES

NUMBER OF ELEMENTS = 4 TOTAL ELAPSED TIME = 18.84

X1	X2	X3	X4	TIME
0.52000E+06	0.18000E+04	0.30000E+03	0.15000E+01	0.00000E+00
0.41393E+06	0.14334E+05	0.57867E+03	0.52797E+00	0.33606E+02
0.30786E+06	0.26293E+05	0.12035E+04	0.29367E+00	0.67212E+02
0.20179E+06	0.40027E+05	0.21967E+04	0.19185E+00	0.10082E+03
0.95716E+05	0.50000E+05	0.40000E+04	-.83267E-16	0.13442E+03

NODAL VALUES FOR THE STATES

NUMBER OF ELEMENTS = 8 TOTAL ELAPSED TIME = 23.46

X1	X2	X3	X4	TIME
0.52000E+06	0.18000E+04	0.30000E+03	0.15000E+01	0.00000E+00
0.46737E+06	0.71167E+04	0.39732E+03	0.80861E+00	0.16674E+02
0.41474E+06	0.12224E+05	0.60461E+03	0.50716E+00	0.33349E+02
0.36211E+06	0.17557E+05	0.88158E+03	0.38264E+00	0.50023E+02
0.30948E+06	0.23577E+05	0.12259E+04	0.31682E+00	0.66697E+02
0.25685E+06	0.30505E+05	0.16554E+04	0.26830E+00	0.83371E+02
0.20422E+06	0.38270E+05	0.22047E+04	0.21910E+00	0.10005E+03
0.15159E+06	0.45939E+05	0.29391E+04	0.14049E+00	0.11672E+03
0.98964E+05	0.50000E+05	0.40000E+04	-.24980E-15	0.13339E+03

ALL VALUES FOR CONTROL AND HAMILTONIAN

NUMBER OF ELEMENTS = 2 TOTAL ELAPSED TIME = 15.74

U1	U2	U3	HAMIL	TIME
-.92485E+00	0.00000E+00	0.00000E+00	-.46274E+03	0.00000E+00
-.27303E+00	0.00000E+00	0.00000E+00	-.82633E+03	0.34510E+02
0.42760E+00	0.00000E+00	0.00000E+00	-.71640E+03	0.69021E+02
0.74199E-01	0.00000E+00	0.00000E+00	-.98340E+03	0.10353E+03
0.33028E-01	0.00000E+00	0.00000E+00	-.10640E-08	0.13804E+03

ALL VALUES FOR CONTROL AND HAMILTONIAN

NUMBER OF ELEMENTS = 4 TOTAL ELAPSED TIME = 18.84

U1	U2	U3	HAMIL	TIME
-.61026E+00	0.00000E+00	0.00000E+00	-.17105E+03	0.00000E+00
-.23120E+00	0.00000E+00	0.00000E+00	-.28890E+03	0.16803E+02
-.12248E-01	0.00000E+00	0.00000E+00	-.23618E+03	0.33606E+02
0.73313E-01	0.00000E+00	0.00000E+00	-.24606E+03	0.50409E+02
0.14683E+00	0.00000E+00	0.00000E+00	-.23657E+03	0.67212E+02
0.91624E-01	0.00000E+00	0.00000E+00	-.26451E+03	0.84015E+02
0.56181E-01	0.00000E+00	0.00000E+00	-.21651E+03	0.10082E+03
-.14828E+00	0.00000E+00	0.00000E+00	-.38816E+03	0.11762E+03
-.32205E+00	0.00000E+00	0.00000E+00	0.24727E-11	0.13442E+03

ALL VALUES FOR CONTROL AND HAMILTONIAN

NUMBER OF ELEMENTS = 8 TOTAL ELAPSED TIME = 23.46

U1	U2	U3	HAMIL	TIME
-.55186E+00	0.00000E+00	0.00000E+00	-.51935E+02	0.00000E+00
-.32779E+00	0.00000E+00	0.00000E+00	-.95367E+02	0.83371E+01
-.16595E+00	0.00000E+00	0.00000E+00	-.62856E+02	0.16674E+02
-.38584E-01	0.00000E+00	0.00000E+00	-.76463E+02	0.25011E+02
0.44739E-01	0.00000E+00	0.00000E+00	-.69769E+02	0.33349E+02
0.79906E-01	0.00000E+00	0.00000E+00	-.71521E+02	0.41686E+02
0.10973E+00	0.00000E+00	0.00000E+00	-.70243E+02	0.50023E+02
0.11215E+00	0.00000E+00	0.00000E+00	-.72219E+02	0.58360E+02
0.12021E+00	0.00000E+00	0.00000E+00	-.69462E+02	0.66697E+02
0.10770E+00	0.00000E+00	0.00000E+00	-.74437E+02	0.75034E+02
0.10186E+00	0.00000E+00	0.00000E+00	-.67925E+02	0.83371E+02
0.67127E-01	0.00000E+00	0.00000E+00	-.79036E+02	0.91709E+02
0.29691E-01	0.00000E+00	0.00000E+00	-.64306E+02	0.10005E+03
-.66484E-01	0.00000E+00	0.00000E+00	-.92023E+02	0.10838E+03
-.18969E+00	0.00000E+00	0.00000E+00	-.52356E+02	0.11672E+03
-.28902E+00	0.00000E+00	0.00000E+00	-.14072E+03	0.12506E+03
-.37039E+00	0.00000E+00	0.00000E+00	0.16485E-10	0.13339E+03

NODAL VALUES FOR THE COSTATES

NUMBER OF ELEMENTS = 2 TOTAL ELAPSED TIME = 15.74

L1	L2	L3	L4	TIME
0.38777E+00	0.23895E+00	0.33772E+02	-.95589E+04	0.00000E+00
0.50266E+00	0.13755E+00	0.33298E+02	0.20419E+04	0.69021E+02
0.10000E+01	0.12191E+00	0.32653E+02	0.10502E+04	0.13804E+03

NODAL VALUES FOR THE COSTATES

NUMBER OF ELEMENTS = 4 TOTAL ELAPSED TIME = 18.84

L1	L2	L3	L4	TIME
0.24671E+00	0.31034E+00	0.41713E+02	-.77904E+04	0.00000E+00
0.30216E+00	0.28438E+00	0.42814E+02	-.22655E+03	0.33606E+02
0.38809E+00	0.26974E+00	0.38756E+02	0.41327E+04	0.67212E+02
0.54729E+00	0.25414E+00	0.36560E+02	0.14102E+04	0.10082E+03
0.10000E+01	0.22100E+00	0.36298E+02	-.11383E+05	0.13442E+03

NODAL VALUES FOR THE COSTATES

NUMBER OF ELEMENTS = 8 TOTAL ELAPSED TIME = 23.46

L1	L2	L3	L4	TIME
0.19901E+00	0.34293E+00	0.42300E+02	-.71441E+04	0.00000E+00
0.22653E+00	0.32947E+00	0.47525E+02	-.28336E+04	0.16674E+02
0.25878E+00	0.32159E+00	0.44891E+02	0.11449E+04	0.33349E+02
0.29819E+00	0.31294E+00	0.42327E+02	0.37755E+04	0.50023E+02
0.34844E+00	0.30244E+00	0.40402E+02	0.47900E+04	0.66697E+02
0.41599E+00	0.29121E+00	0.38903E+02	0.39834E+04	0.83371E+02
0.51405E+00	0.28441E+00	0.37713E+02	0.96373E+03	0.10005E+03
0.67453E+00	0.27907E+00	0.36970E+02	-.49726E+04	0.11672E+03
0.10000E+01	0.22278E+00	0.37315E+02	-.13459E+05	0.13339E+03

Optimal Guidance Law Development for an Advanced Launch System

Interim Progress Report
1 December 1990 - 15 June 1991

June 1991

Research Supported by NASA Langley Research Center
NASA Grant No. NAG-1-939

Principal Investigators: Anthony J. Calise & Dewey H. Hodges
Research Assistant: Martin S. Leung & Robert R. Bless
NASA Grant Monitor: Daniel D. Moerder

Georgia Institute of Technology
School of Aerospace Engineering
Atlanta, GA 30332-0150

Summary

Following the previous report, the proposed investigation on a Matched Asymptotic Expansion (MAE) method was carried out. It was concluded that the method of MAE is not applicable to launch vehicle ascent trajectory optimization due to a lack of a suitable stretched variable. More work was done on the earlier regular perturbation approach using a piecewise analytic zeroth order solution to generate a more accurate approximation. In the meantime, a singular perturbation approach using manifold theory is also under current investigated

Work on a general computational environment based on the use of MACSYMA and the weak Hamiltonian finite element method continued during this period. This methodology is capable of the solution of a large class of optimal control problems. This part of the work continued until the departure of Dr. Robert R. Bless, who was supported under the grant as a Graduate Research Assistant at Georgia Tech. The first version of his computer code is now complete. A NASA contractor report (CR), based on Dr. Bless' Ph.D. Dissertation [1] is presently in press. It contains the details of the general code as well as sample input and output. These details are not repeated herein. Work has continued since his departure to more fully understand the accuracy and limitations of the method and to adapt Dr. Bless' code to use Mathematica which is available on a wider variety of computers than MACSYMA.

Table of Contents

1. Research Accomplishments

1.1 Matched Asymptotic Expansion (MAE) Investigation

The MAE approach was first investigated to handle the launch vehicle atmospheric flight phase where the earlier regular perturbation approach did not produce satisfactory results. The essence of the MAE approach is outlined below.

We first evaluate the outer solution which corresponds to a propulsion dominant phase of flight. This part of the solution is just our zeroth order solution in the earlier regular perturbation approach [12]. Next, we formulate the inner solution which corresponds to an aerodynamic force dominant phase. This part of the solution has been developed in [9] where the analytic solutions involve elliptical integrals of the first and second kind. Finally, a composite solution is formed by joining the outer and inner parts with the extraction of the common part using the matching conditions (see [10] and [11] for details).

First of all, we non-dimensionalize and rewrite the dynamics as:

$$\frac{d\hat{V}}{d\hat{t}} = \frac{\hat{T}_{vac}}{\hat{m}}\cos\alpha - \frac{\hat{p}_i e^{-\hat{h}/\varepsilon}}{\hat{m}}\cos\alpha - \frac{\hat{\rho}_i \hat{V}^2 (k_0 + k_1\alpha + k_2\alpha^2 + \delta K)e^{-\hat{h}/\varepsilon}}{\varepsilon 2\hat{m}} - \sin\gamma + \delta\left\{1 - \frac{1}{(1+\hat{h})^2}\right\}\sin\gamma \qquad 1)$$

$$\hat{V}\frac{d\gamma}{d\hat{t}} = \frac{\hat{T}_{vac}}{\hat{m}}\sin\alpha - \frac{\hat{p}_i e^{-\hat{h}/\varepsilon}}{\hat{m}}\sin\alpha + \frac{\hat{\rho}_i \hat{V}^2 (\eta_0 + \eta_1\alpha + \delta N)e^{-\hat{h}/\varepsilon}}{\varepsilon 2\hat{m}} - \cos\gamma + \delta\left\{(1 - \frac{1}{(1+\hat{h})^2})\cos\gamma + \frac{\hat{V}^2\cos\gamma}{1+\hat{h}}\right\} \qquad 2)$$

$$\frac{d\hat{h}}{d\hat{t}} = \hat{V}\sin\gamma \qquad 3)$$

$$\frac{d\hat{m}}{d\hat{t}} = -\hat{c} \qquad 4)$$

where

$$\varepsilon = \frac{1}{\beta r_i} \qquad \hat{c} = \frac{c}{m_i\sqrt{g_i / r_i}} \qquad \hat{p}_i = \frac{p_i A_e}{m_i g_i}$$

$$\hat{h} = \frac{h}{r_i} \qquad \hat{T}_{vac} = \frac{T_{vac}}{m_i g_i} \qquad \hat{m} = \frac{m}{m_i}$$

$$\hat{V} = \frac{V}{\sqrt{r_i g_i}} \qquad \hat{\rho}_i = \frac{\rho_i S}{\beta m_i} \qquad \hat{t} = \frac{t}{\sqrt{r_i / g_i}}$$

$$h = r - r_i \qquad \rho = \rho_i e^{-\beta(h-h_i)} \qquad p = \frac{\rho_i g_i}{\beta} e^{-\beta h}$$

$$C_D(\alpha,M) = k_0 + k_1\alpha + k_2\alpha^2 + \delta K(\alpha,M) \qquad C_L(\alpha,M) = \eta_0 + \eta_1\alpha + \delta N(\alpha,M)$$

The notation of the variables are self-explanatory. The hatted variables are non-dimensional and the subscript i stands for initial value of the variables. Here ε is a small physical parameter whereas δ is a bookkeeping perturbation parameter with a nominal value of one. We are actually using a combination of singular and regular perturbation expansions. Setting ε to zero, we retrieve the zeroth order outer dynamics (no aerodynamic forces). On the other hand, introducing the stretched variables $t = \hat{t}/\varepsilon$, $h = \hat{h}/\varepsilon$ and setting ε to zero we obtain the zeroth order inner dynamics (no thrust terms). The atmospheric pressure and the Mach number dependency of the aerodynamics data will be introduced in the first order correction which will subsequently involve solving a set of non-homogeneous linear O. D. E's. The advantage of this approach over our earlier perturbation approach lies in the fact that we are now able to introduce aerodynamic forces in our zeroth order formulation.

Our first attempt was to evaluate the composite zeroth order solution using the existent results in [9,12] by solving a set of 21 nonlinear algebraic equations. However, we were not able to find a solution The problem is not due to numerical difficulties but lies in the flaws of our MAE arguments. From the optimal solution using BNDSCO we determined that magnitude of the aerodynamic forces is less than 15% of the thrust over the whole trajectory, which means there is never a flight phase where the aerodynamic forces dominate over the propulsive force. However, the magnitude of the aerodynamics forces is largely determined by the dynamic pressure profile. The aerodynamic forces increases as dynamic pressure initially builds up due to gain in velocity. As the launch vehicle rises in altitude, the drop in air density outweighs the gain in velocity and the dynamic pressure decreases. This phenomenon indicates that we need two different regions (2 pairs of outer and inner solutions) to formulate our whole trajectory (see figure 1). We also need a new independent variable such that if it is set to the right and left hand side limits, the two respective outer solutions are obtained. Clearly, altitude is not the suitable candidate because we can only retrieve the right hand side of our solution as $h \to \infty$.

In a nutshell, we conclude that the traditional (using altitude as the stretched variable) MAE approach which has found success in aero-assisted orbital transfer application is not applicable in a straight forward manner to the ascent trajectory launch vehicle problem. Further research is needed to identify a more suitable independent variable. Rather than pursue this line of investigation, we decided to return to our earlier regular perturbation study, and to investigate a singular perturbation approach based on a slow manifold concept.

1.2 A Modified Regular Perturbation Approach

An idea to extend the earlier regular perturbation method into the atmospheric flight phase is through a finite element approach. Since we cannot find a complete analytic zeroth order solution that incorporates the aerodynamic effects, our approach is to improve accuracy with minimal increase in computational complexity. Using several pieces of simple solutions instead one complete and complicated solution, we are able to improve the zeroth order solution so that it accounts for the aerodynamic effects.

From our earlier study, the state dynamics can be fairly represented by those of a flat Earth no atmosphere approximation. However, this is not true of the costate dynamics. If we use the previous approximation, we will end up with (in a rectangular coordinate system):

$$\dot{v} = \frac{T_{vac}\sin\beta}{m_i - ct} - g_e + \varepsilon\left\{\frac{-A_e p\sin\beta - D\sin\gamma + L\cos\gamma}{m_i - ct} + (g_e - \frac{\mu_e}{r^2})\right\} \quad 5)$$

$$\dot{u} = \frac{T_{vac}\cos\beta}{m_i - ct} + \varepsilon\left\{\frac{-A_e p\cos\beta - D\cos\gamma - L\sin\gamma}{m_i - ct} - \frac{uv}{r}\right\} \quad 6)$$

$$\dot{r} = v \quad 7)$$

$$\dot{\lambda}_v = -\lambda_r - \varepsilon(\lambda_v \frac{\partial\dot{v}}{\partial v} + \lambda_u \frac{\partial\dot{u}}{\partial v}) \quad 8)$$

$$\dot{\lambda}_u = -\varepsilon(\lambda_v \frac{\partial\dot{v}}{\partial u} + \lambda_u \frac{\partial\dot{u}}{\partial u}) \quad 9)$$

$$\dot{\lambda}_r = -\varepsilon(\lambda_v \frac{\partial\dot{v}}{\partial r} + \lambda_u \frac{\partial\dot{u}}{\partial r}) \quad 10)$$

The approximate set of zeroth order dynamics are especially poor in λ_u and λ_r because both derivatives become zero to zeroth order in ε. Consequently, they produce large forcing function

terms (in L_2-norm sense) in the first order correction dynamics which may cause divergence of our corrected results. The easy way to decrease these large error magnitudes is to represent the λ_u and λ_r with linear function such that

$$\dot{\lambda}_u = p_u - \varepsilon(\lambda_v \frac{\partial \dot{v}}{\partial u} + \lambda_u \frac{\partial \dot{u}}{\partial u} + p_u) \qquad 11)$$

$$\dot{\lambda}_r = p_r - \varepsilon(\lambda_v \frac{\partial \dot{v}}{\partial u} + \lambda_u \frac{\partial \dot{u}}{\partial u} + p_r) \qquad 12)$$

and p_u, p_r are constants to be determined by other means. The optimal control of the zeroth order problem is now governed by a bilinear tangent law.

The constants p_u and p_r are evaluated using collocation method [13]. We approximate the solution with pre-specified functions, in this case first order polynomials. Constraining the solution such that it is continuous at the node and satisfies the original dynamics at the mid point of each segment determines the unknown coefficients of the polynomials. Mathematically, these constraints are formulated as follows:

$$p_u = \frac{\lambda_{u2} - \lambda_{u1}}{t_2 - t_1} = \left\{ -\lambda_v \frac{\partial \dot{v}}{\partial u} - \lambda_u \frac{\partial \dot{u}}{\partial u} \right\}\Bigg|_{t=\frac{t_1+t_2}{2};\ v=\frac{v_1+v_2}{2};\ \ldots;\ \lambda_r=\frac{\lambda_{r1}+\lambda_{r2}}{2}} \qquad 13)$$

$$p_r = \frac{\lambda_{r2} - \lambda_{r1}}{t_2 - t_1} = \left\{ -\lambda_v \frac{\partial \dot{v}}{\partial r} - \lambda_u \frac{\partial \dot{u}}{\partial r} \right\}\Bigg|_{t=\frac{t_1+t_2}{2};\ v=\frac{v_1+v_2}{2};\ \ldots;\ \lambda_r=\frac{\lambda_{r1}+\lambda_{r2}}{2}} \qquad 14)$$

The unknowns to be solved are the nodal values (subscript 1, 2) of the interpolated variables. However, for this linear function case, we simply equate the unknowns p_u and p_r with the averages, ie.

$$p_u = \frac{\lambda_{u2} - \lambda_{u1}}{t_2 - t_1} = -\frac{1}{2}\left\{ (\lambda_v \frac{\partial \dot{v}}{\partial u} + \lambda_u \frac{\partial \dot{u}}{\partial u})\Big|_{t_1;\ v_1;\ldots;\ \lambda_{r1}} + (\lambda_v \frac{\partial \dot{v}}{\partial u} + \lambda_u \frac{\partial \dot{u}}{\partial u})\Big|_{t_2;\ v_2;\ldots;\ \lambda_{r2}} \right\} \qquad 15)$$

$$p_r = \frac{\lambda_{r2} - \lambda_{r1}}{t_2 - t_1} = -\frac{1}{2}\left\{ (\lambda_v \frac{\partial \dot{v}}{\partial r} + \lambda_u \frac{\partial \dot{u}}{\partial r})\Big|_{t_1;\ v_1;\ldots;\ \lambda_{r1}} + (\lambda_v \frac{\partial \dot{v}}{\partial r} + \lambda_u \frac{\partial \dot{u}}{\partial r})\Big|_{t_2;\ v_2;\ldots;\ \lambda_{r2}} \right\} \qquad 16)$$

Figures 2 - 8 show an open loop 4-piece zeroth order solution segmented at 30s, 60s, 90s. In our present formulation, we also treat λ_v as a linear function with the unknown p_v. The first 3 segments are computed using collocation method described above, and the last segment uses a flat Earth approximation ($p_u = p_r = 0$). As a comparison, the costate profiles (figures 6 - 8) of the

earlier 1-piece zeroth order solution and the optimal solution (see Errata) are also plotted. We can clearly observe the significant improvements of this modification.

The new analytic expressions of v, u, h are given below:

$$v(t) = \frac{T_{vac}D}{c}\left\{\frac{\varsigma+\Delta}{\sqrt{1+\Delta^2}}\sinh^{-1}[\tan(\theta+\omega)] - \sinh^{-1}(\tan\theta)\right\}\Bigg|_{\theta(t_i)}^{\theta(t)} - g_e(t-t_i) + v_i \qquad 17)$$

$$u(t) = \frac{T_{vac}E}{c}\left\{\frac{1+\Delta\xi}{\sqrt{1+\Delta^2}}\sinh^{-1}[\tan(\theta+\omega)] - \xi\sinh^{-1}(\tan\theta)\right\}\Bigg|_{\theta(t_i)}^{\theta(t)} + u_i \qquad 18)$$

$$h(t) = -\frac{T_{vac}DC}{cA}\left\{(\Delta-\tan\theta)[\frac{\varsigma+\Delta}{\sqrt{1+\Delta^2}}\sinh^{-1}[\tan(\theta+\omega)] - \sinh^{-1}(\tan\theta)\right\}\Bigg|_{\theta(t_i)}^{\theta(t)}$$
$$-(t-t_i)\frac{T_{vac}D}{c}\left\{\frac{\varsigma+\Delta}{\sqrt{1+\Delta^2}}\sinh^{-1}[\tan(\theta+\omega)] - \sinh^{-1}(\tan\theta)\right\}\Bigg|_{\theta(t_i)}$$
$$-\frac{1}{2}g_e(t-t_i)^2 + v_i(t-t_i) + h_i \qquad 19)$$

where

$$A = \sqrt{p_v^2 + p_u^2} \qquad B = \frac{c_v p_v + c_u p_u}{A} \qquad C = \sqrt{c_v^2 + c_u^2 - B^2}$$

$$D = \frac{p_v}{A} \qquad \Delta = \frac{m_i A + cB}{cC} \qquad \varsigma = \frac{c_v A - p_v B}{p_v C}$$

$$\tan\theta = \frac{At+B}{C} \qquad \xi = \frac{p_u C}{c_u A - p_u B} \qquad E = \frac{c_u A - p_u B}{AC}$$

$$\omega = \begin{cases} \tan^{-1}(1/\Delta) & ;\ \Delta \geq 0 \\ \pi + \tan^{-1}(1/\Delta) & ;\ \Delta < 0 \end{cases}$$

The state transition matrix can be found by differentiating the above analytic expressions with respect to the initial values (c_v, c_u, c_r are the initial costate values). First order correction using the zeroth order solution above and the state transition matrix will be obtained in next progress report.

1.3 Singular Perturbation Approach Using Manifold Theory

In [15], we showed that a singular perturbation, using a 2-state model with mass and energy as slow variables, failed because the flight path angle dynamics are highly coupled with the slow variables at high flight path angle. However, if we use a more accurate 3-state model (mass,

energy and altitude), a chattering solution of flight path angle will be encountered. Our proposed research for the next reporting period is to attempt to use the Manifold condition [14]:

$$g = \varepsilon\left(\frac{\partial \phi}{\partial x} f + \frac{\partial \phi}{\partial t}\right) \qquad 20)$$

where

$$\frac{dx}{dt} = f(x,z,t) \qquad \varepsilon\frac{dz}{dt} = g(x,z,t) \qquad z = \phi(\varepsilon,x,t)$$

to generate another zeroth order outer solution (slow manifold). Since we now include ε in our slow manifold (ϕ) formulation, the chattering effect is eliminated. Our first step is to demonstrate that we can compute an off-line slow manifold solution and perform an on-line boundary layer (inner solution) correction for the flight path angle dynamics. This will result in a nonlinear feedback control solution for the angle of attack (see below).

$$H = \hat{\lambda}_{Eo}\dot{E}(\hat{E}_o,\hat{h}_o,\hat{m}_o,\alpha) + \hat{\lambda}_{ho}\hat{V}_o \sin\gamma - \hat{\lambda}_{mo}k + \lambda_\gamma\dot{\gamma}(\hat{E}_o,\hat{h}_o,\hat{m}_o,\alpha) = 0 \qquad (21)$$

$$H_\alpha = 0 \qquad (22)$$

These two equations are used to determine α and λ_γ. The subscript 'o' stands for the initial value.

1.4 Finite Element Analysis

The main accomplishment during this reporting period involved the development of the general code. The main purpose of the general code is to reliably solve a large class of optimal control problems with a minimum of user-written subroutines. To this end, the general code runs on a SUN 3 and later workstations. It and requires a FORTRAN 77 compiler, MACSYMA [2], and the Harwell subroutine library [3]. The general procedure can be broken into three parts that must interface together. The first part is the FORTRAN code. This code contains all the subroutines necessary to solve any of the optimal control problems described above. However, if certain problems require table look-up routines (such as aerodynamic data for a rocket model), then these subroutines must be given by the user and interfaced to the rest of the general code. Thus, there may be a need for some user programming for certain problems. The second part of the general procedure is the use of MACSYMA. The user must supply an input file specifying the problem. This input file is in symbolic form and will be loaded into MACSYMA. MACSYMA will then evaluate all the necessary expressions and automatically generate the FORTRAN code. This code is spliced into a template file and becomes one of the subroutines. The third and final part of the general procedure will consists of subroutines to generate initial guesses that will reliably converge. A continuation method is being used which converts the algebraic equations to

initial-value ordinary differential equations. A second-order Runge-Kutta method is then used to integrate the equations and obtain initial guesses for a Newton-Raphson method. We also continued to further document the methodology through the publication of one paper [4] and the completion of three others. The first of these three is a technical note [5] which covers the extension of the method to state-control inequality constraints. The second deals with the application of the method to the ALS problem, per se [6]. Both of these are now accepted for publication. The third deals with the general code and will be presented at the upcoming ACC meeting [7].

2. Errata

An error in our previous 2-stage ALS optimal solution was found. The optimality condition was incorrectly formulated due to a missing conversion factor from degree to radian. The correct results are now shown in Figures 9 - 15. There are 3 jumps in the control profile (Figure 9). The first two jumps are due to the fact that the Hamiltonian is a non-convex function of the control. These jumps occur at about Mach 1.4 and 2.0 respectively. The last small jump is due to staging. However, the costates are all continuous. Though the control profile changes substantially, the performance index (final time) differs by less than 0.1s. Figures 16, 17 are the optimal solution under αq-constraint. The final time in this case is 362.103s which is 0.007s more than the unconstrained case.

3. Future Research

3.1 Analytical Investigation

We will follow two different directions. One will be the continuation of the modification of the regular perturbation technique. A first order closed loop simulation will be done. We will investigate the effect of number of segments and the segment intervals on the computational performance. At present a first order correction can be done in 0.5 to 7.0 CPUsec, depending on the current vehicle altitude on a MacIIci (a 32-bit 25MHz PC). At low altitude, the complicated aerodynamic effects require a more dense integration steps to complete the quadratures, however, the computational time can be significantly shortened if we perform parallel processing. The other line of research direction is to investigate the slow manifold approach to singular perturbation to a launch vehicle trajectory. Further approximation and analysis are expected.

3.2 Finite Elements Work

In the finite element analysis area we plan to continue to port the general code and complete a user's manual for it. We further plan to document the methodology through the completion of one paper (which we are now revising in response to reviewers) on the application of the method to launch vehicle trajectory analysis, two technical notes on control and state inequality constraints, one paper on the general code, and a user's manual for the code. We continue to receive calls from parties interested in application of the methodology in industry, and still hope to transfer the technology to an industry application in the future.

In a future phase of the work we hope to extend the work to higher-order finite element shape functions – the so-called p-version of the finite element method. This approach has been shown to be of value in linear time-domain problems [8] but has not yet been investigated for the nonlinear case.

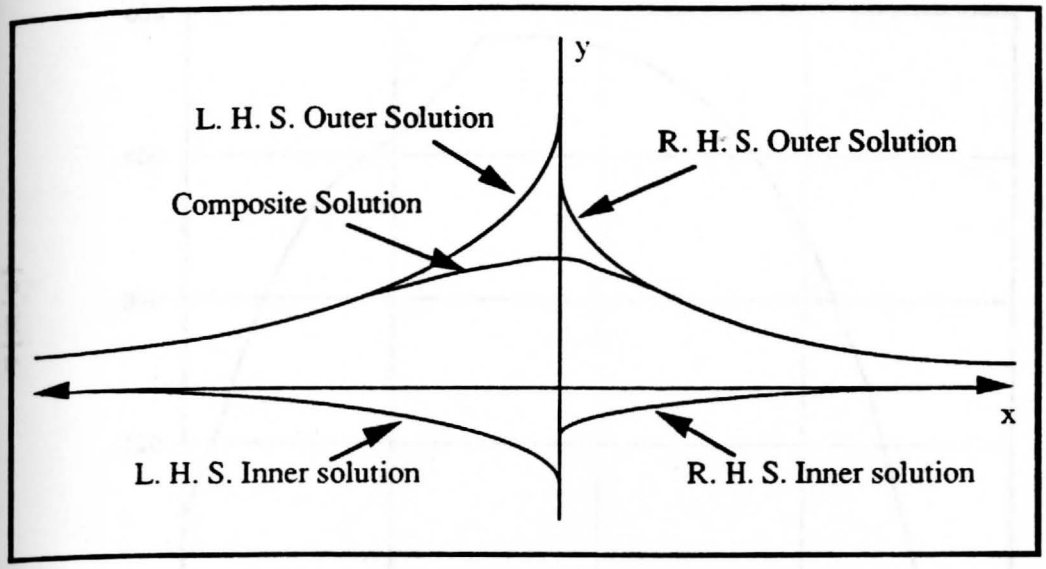

Figure 1. Illustration of Using MAE on the Launch Vehicle Problem

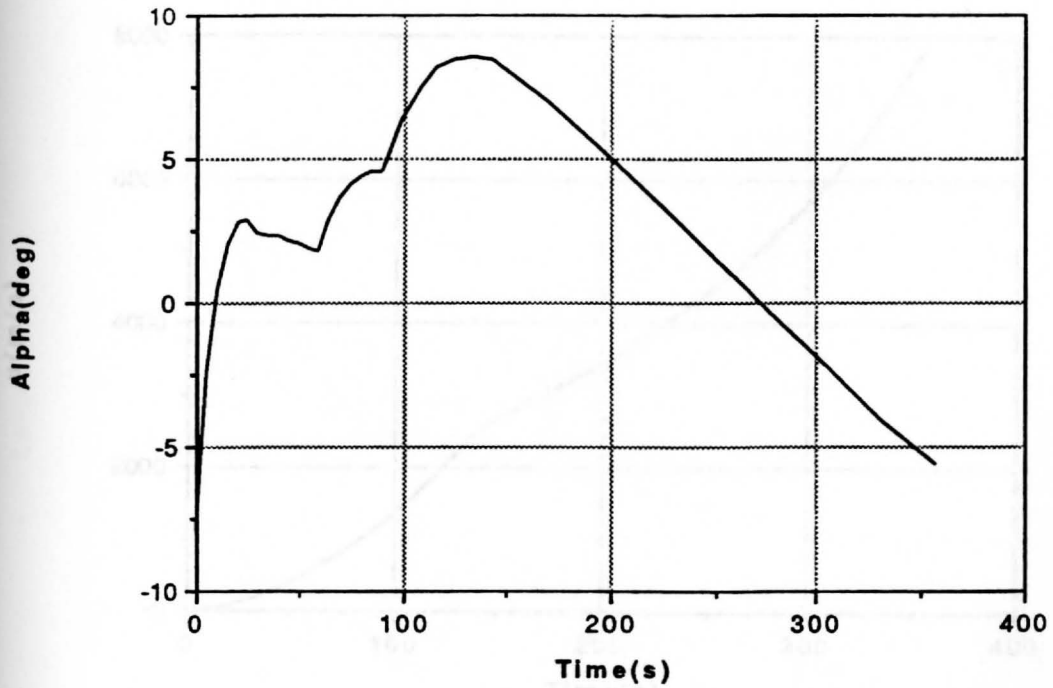

Figure 2. Angle of Attack Profile (4-pc. Zeroth Order Solution)

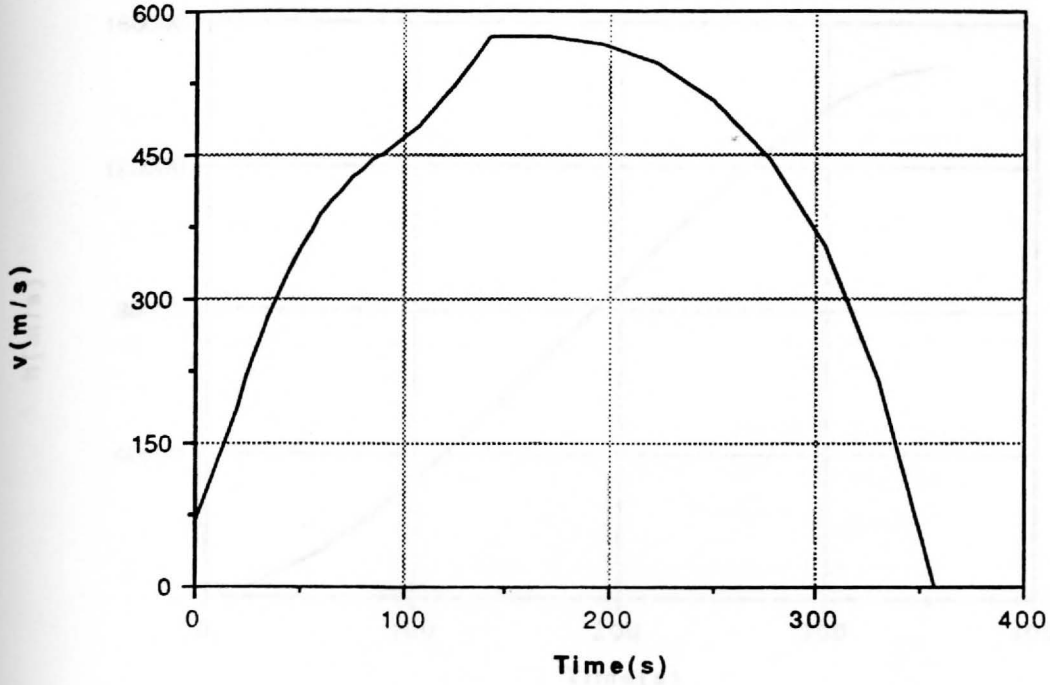

Figure 3. Vertical Velocity Component Profile

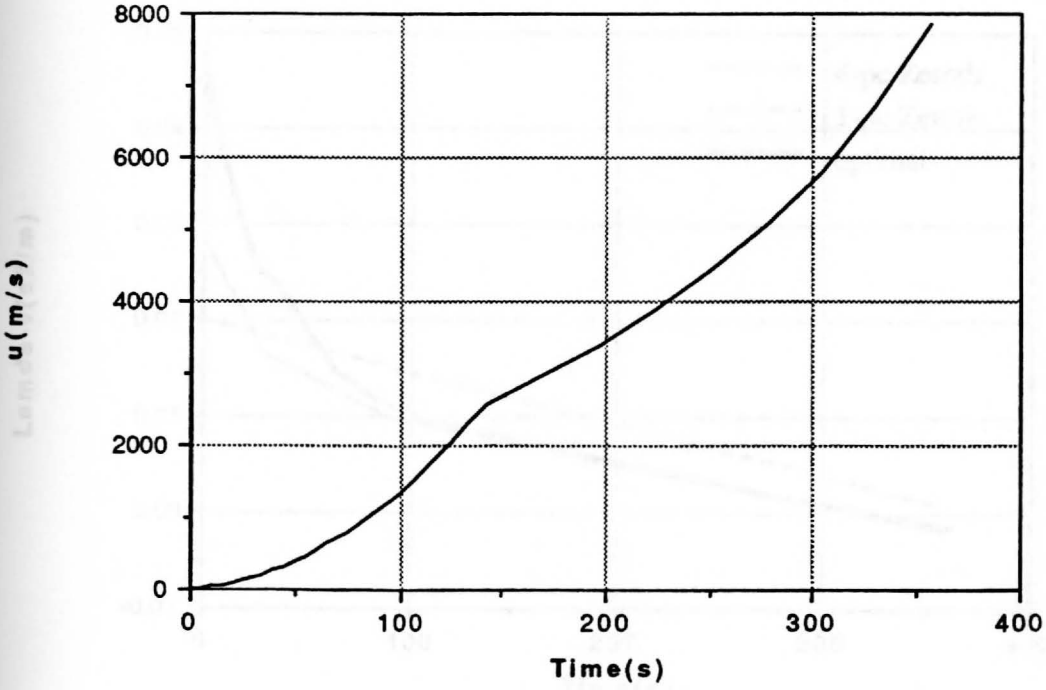

Figure 4. Horizontal Velocity Component Profile

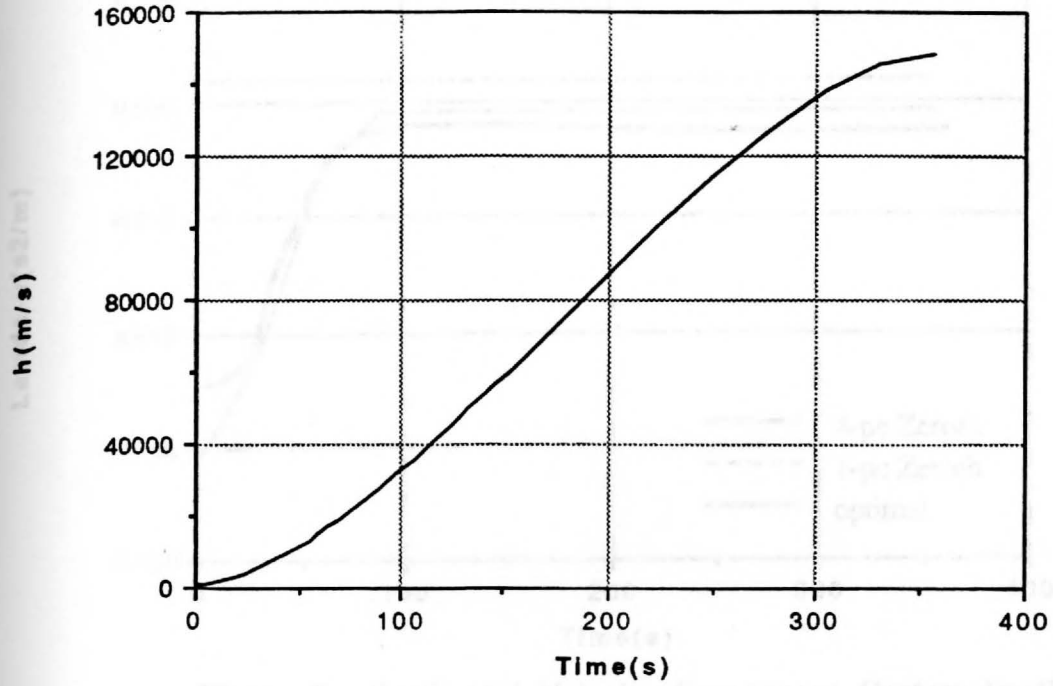

Figure 5. Altitude Profile

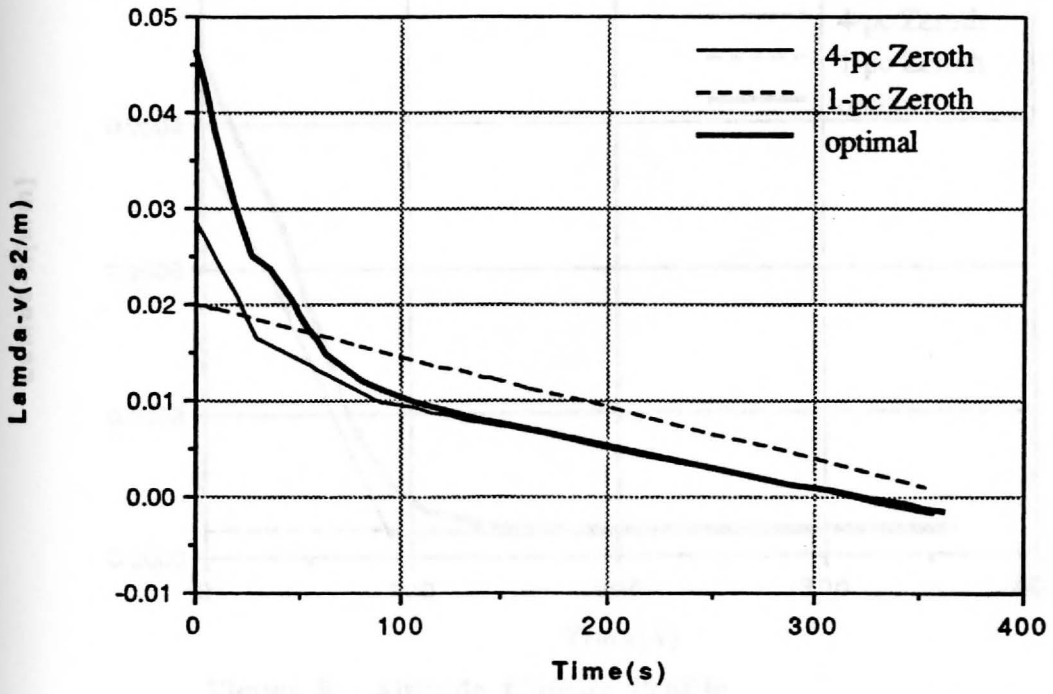

Figure 6. Vertical Velocity Component Costate Profile

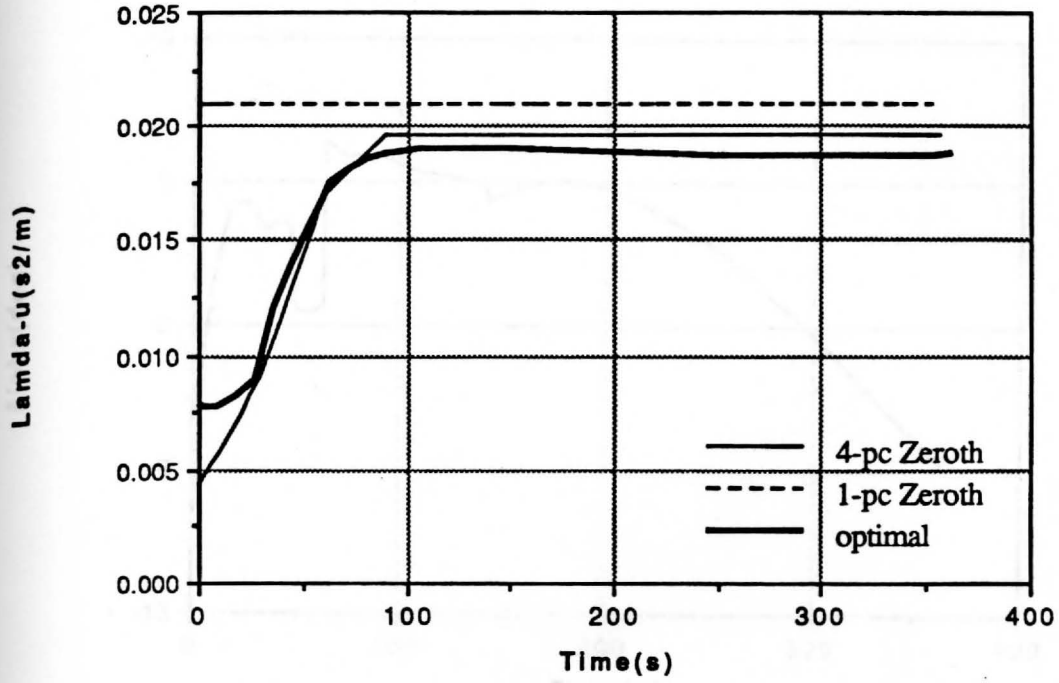

Figure 7. Horizontal Velocity Component Costate Profile

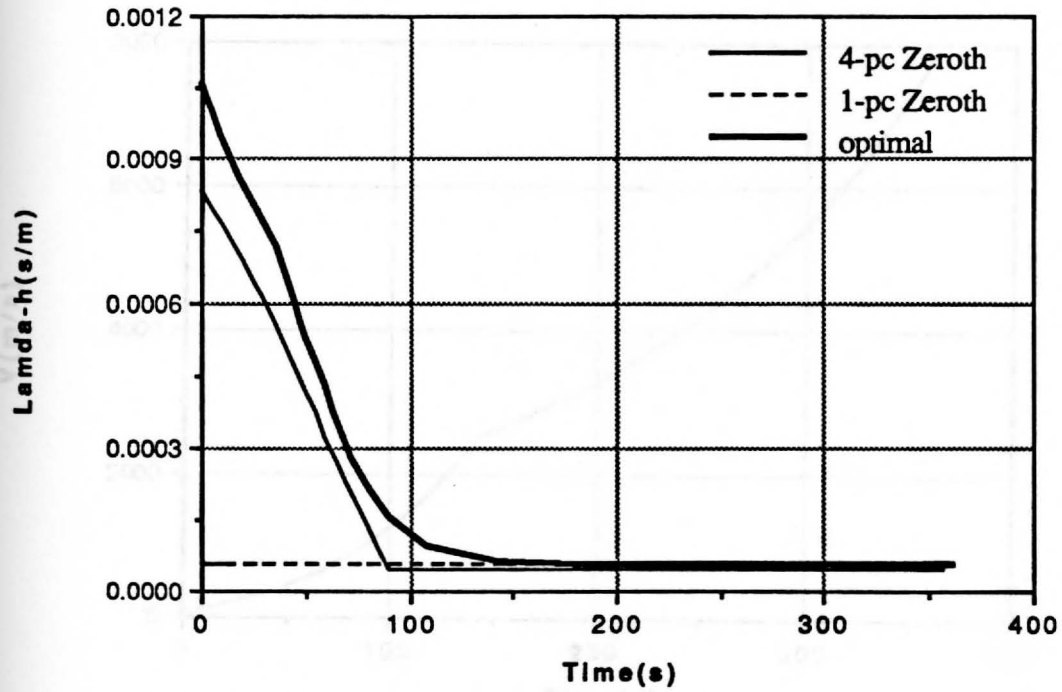

Figure 8. Altitude Costate Profile

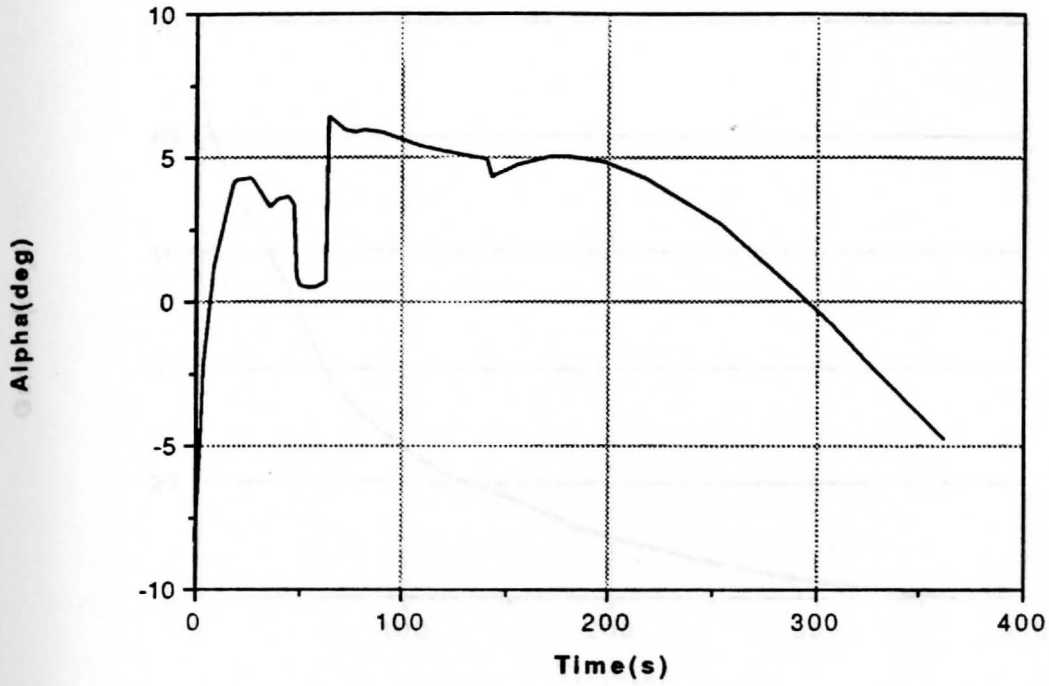

Figure 9. Optimal Angle of Attack Profile (Unconstrained Case)

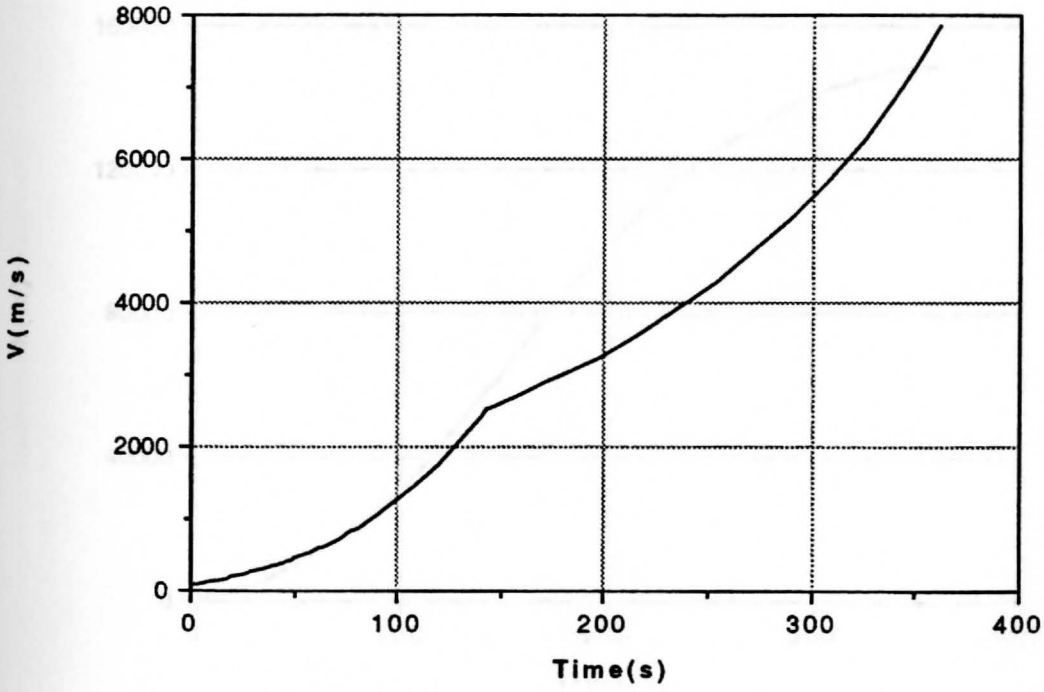

Figure 10. Velocity Profile

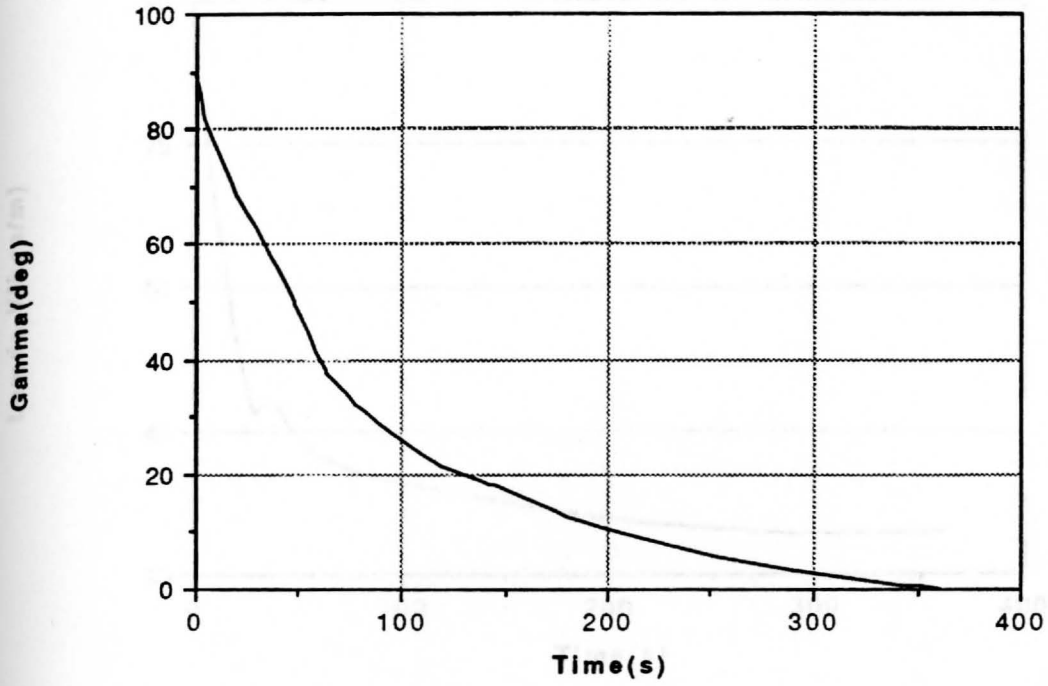

Figure 11. Flight Path Angle Profile

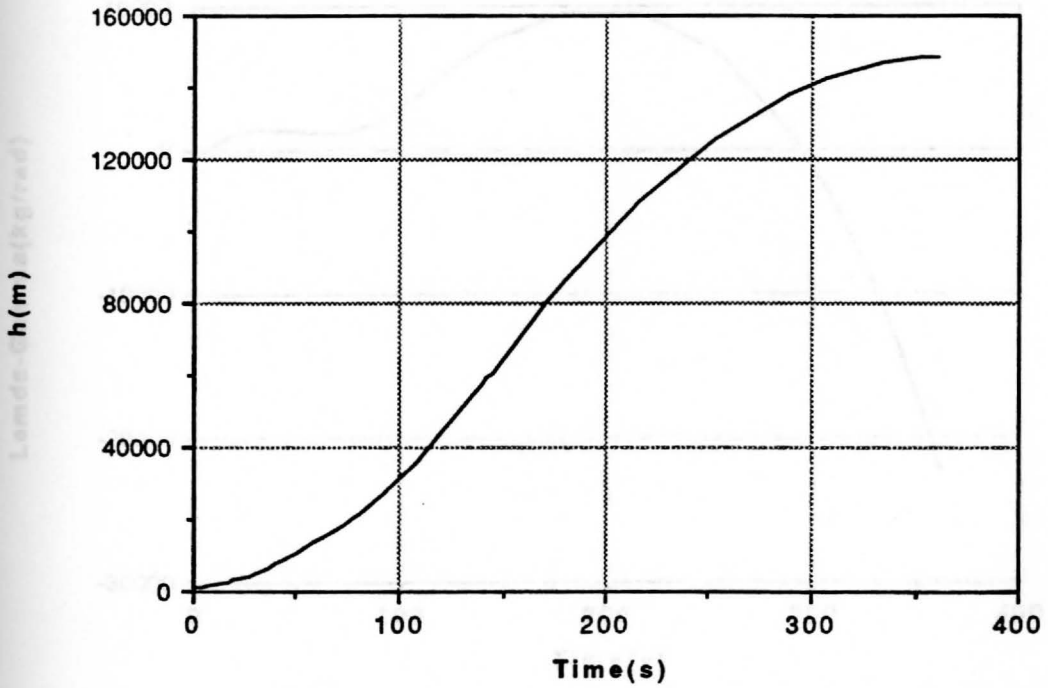

Figure 12. Altitude Profile

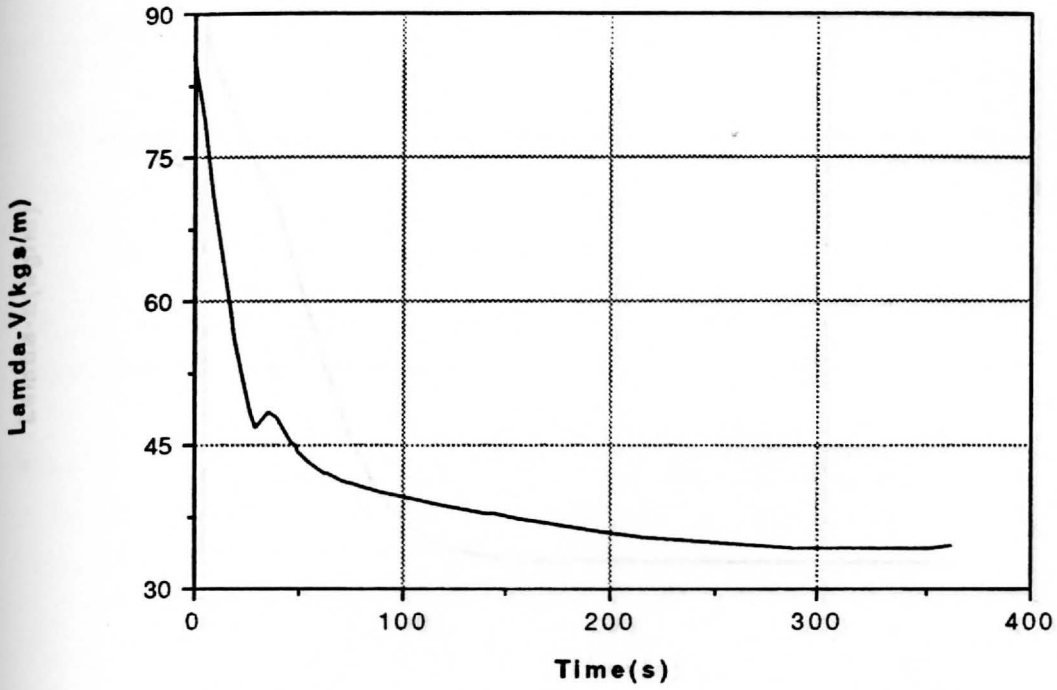

Figure 13. Velocity Costate Profile

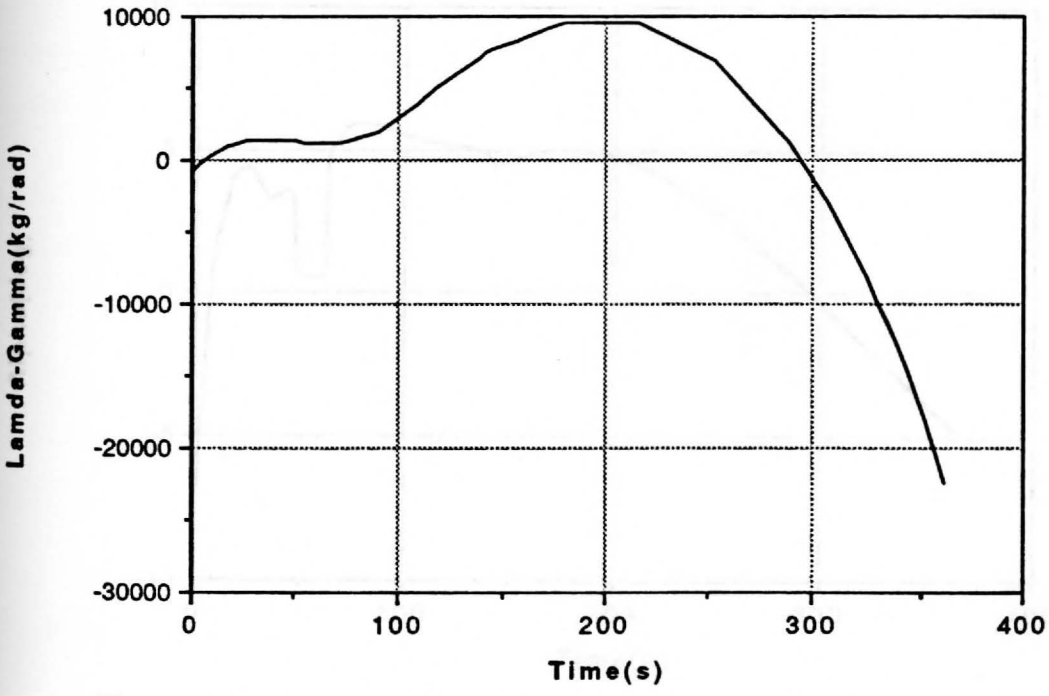

Figure 14. Flight Path Angle Costate Profile

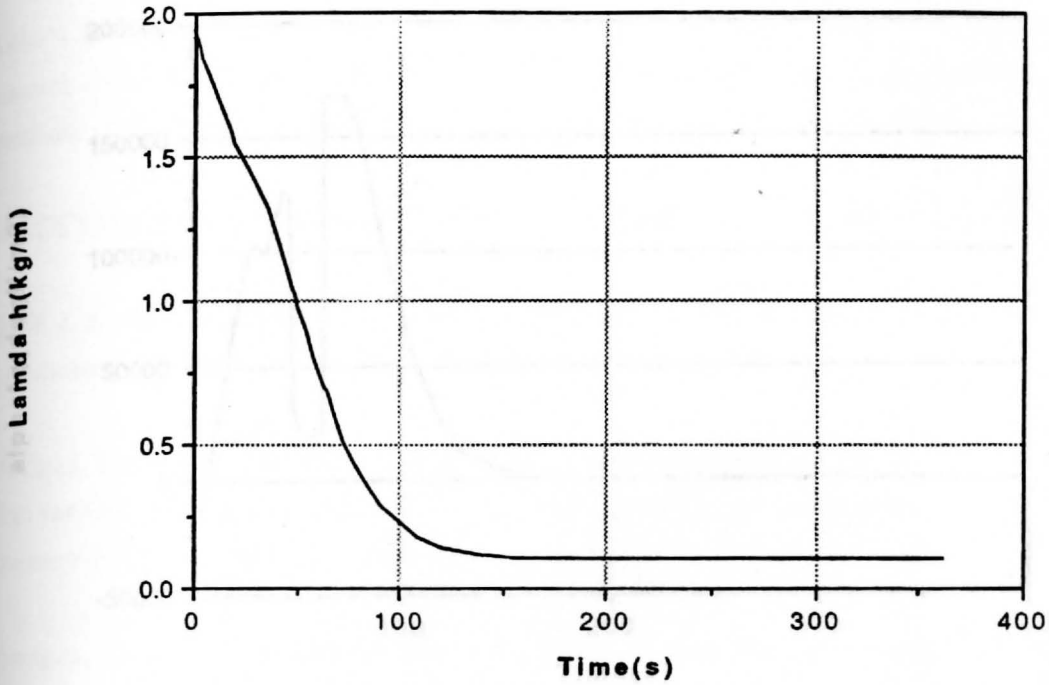

Figure 15. Altitude Costate Profile

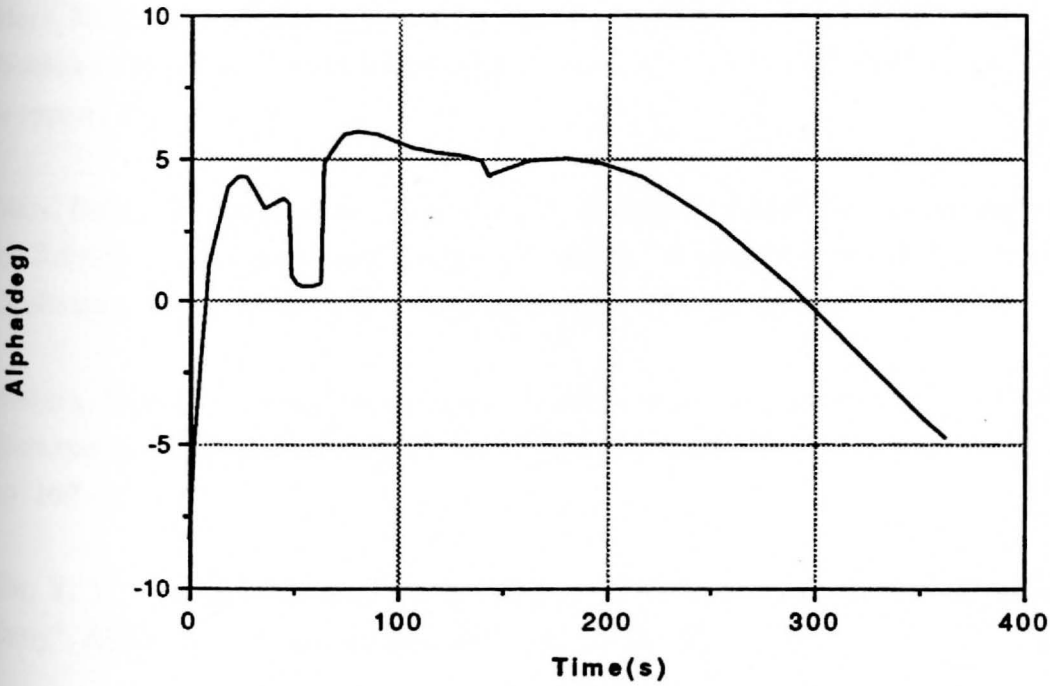

Figure 16. Optimal Angle of Attack Profile with αq-constraint

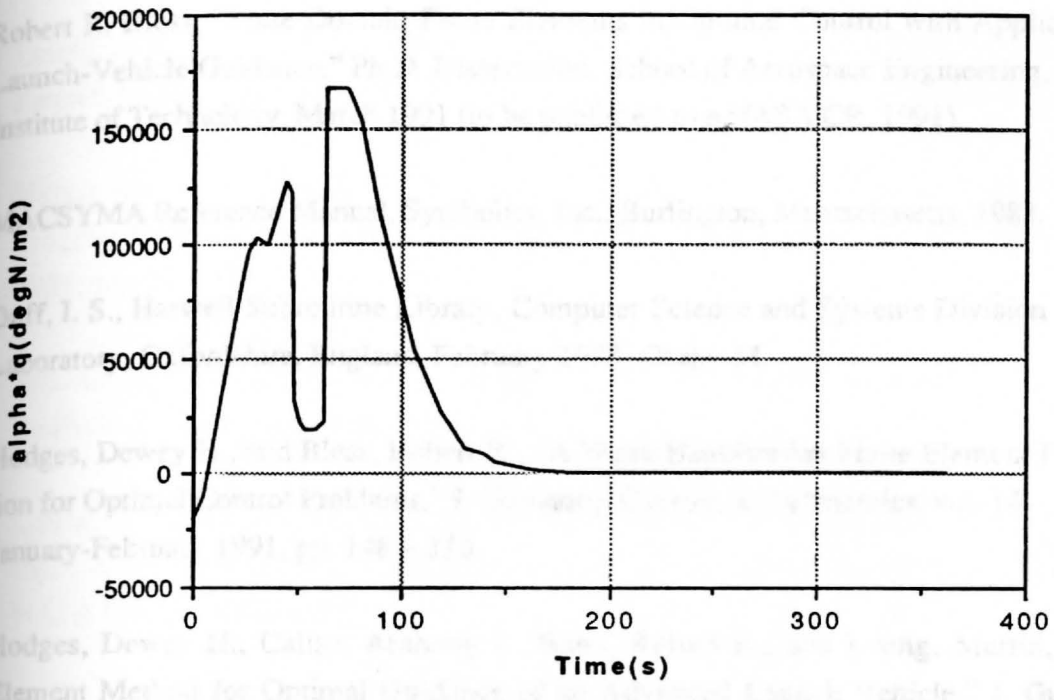

Figure 17. αq Profile of the Constrained Case

References

[1] Robert R. Bless, "Time-Domain Finite Elements in Optimal Control with Application to Launch-Vehicle Guidance," Ph.D. Dissertation, School of Aerospace Engineering, Georgia Institute of Technology, March 1991 (to be published as a NASA CR, 1991).

[2] MACSYMA Reference Manual, Symbolics, Inc., Burlington, Massachusetts, 1988.

[3] Duff, I. S., Harwell Subroutine Library, Computer Science and Systems Division Harwell Laboratory, Oxfordshire, England, February 1988, Chapt. M.

[4] Hodges, Dewey H., and Bless, Robert R., "A Weak Hamiltonian Finite Element Formulation for Optimal Control Problems," J. Guidance, Control, and Dynamics, vol. 14, no. 1, January-February 1991, pp. 148 – 156.

[5] Hodges, Dewey H., Calise, Anthony J., Bless, Robert R., and Leung, Martin, "Finite Element Method for Optimal Guidance of an Advanced Launch Vehicle," J. Guidance, Control, and Dynamics, to appear, 1991.

[6] Bless, Robert R., and Hodges, Dewey H., "Finite Element Solution of Optimal Control Problems with State-Control Inequality Constraints," J. Guidance, Control, and Dynamics, to appear, 1991.

[7] Bless, Robert R, and Hodges, Dewey H., "A Hybrid Symbolic/Finite-Element Algorithm for Solving Nonlinear Optimal Control Problems," Proceedings of the American Control Conference, Boston, Massachusetts, June 26 – 28, 1991, to appear.

[8] Hodges, Dewey H., and Hou, Lin Jun, "Shape Functions for Mixed p-Version Finite Elements in the Time Domain," J. Sound and Vibration, vol. 145, no. 2, March 8, 1991, pp. 169 – 178.

[9] Shi, Y. Y., "Matched Asymptotic Solutions For Optimum Lift Controlled Atmospheric Entry", AIAA Journal, Vol. 9, Nov. 1971, pp. 2229 - 2238.

[10] Ardema, M. D., "Singular Perturbations In Flight Mechanics", NASA TM X-62, 380, 1977.

[11] Calise, A. J., Melamed, N., "Analytical Guidance Law Development For Aerocapture at Mars", Progress Report, Dec. 90 - Apr. 91, NASA Grant # NAG-1-1139.

[12] Leung, S. K., Calise, A. J., "An Approach To Real-time Guidance Law For An Advanced Launch System", American Control Conference Proceedings, June 1990, San Diego,

[13] Hargraves, C. R., Paris, S. W., "Direct Trajectory Optimization Using Nonlinear Programming and Collocation", J. Guidance, Control and Dynamics, Vol. 10, July - Aug. 1987, pp. 338-342.

[14] Kokotovic, P. V., Khalil, H. K., O'Reilly, J., *Singular Perturbation Methods In Control: Analysis & Design*, Academic press, 1986.

[15] Calise, A. J., Hodges, D. H., Leung, S. K., Bless, R. R., "Optimal Guidance Law Development for an Advanced Launch System", Interim Progress Report, Dec. 90 - Jun. 91., NASA Grant # NAG-1-939.

NASA Contractor Report

Optimal Guidance Law Development for an Advanced Launch System

Anthony J. Calise and Martin S. K. Leung
Georgia Institute of Technology
School of Aerospace Engineering
Atlanta, Georgia 30332

May, 1992

Prepared for
NASA Langley Research Center
under Grant NSG-1-939

TABLE OF CONTENTS

Table of Contents (cont.)

LIST OF ILLUSTRATIONS

List of Illustrations (cont.)

Figure

List of Illustrations (cont.)

LIST OF TABLES

OPTIMAL GUIDANCE LAW DEVELOPMENT FOR AN ADVANCED LAUNCH SYSTEM

Anthony J. Calise* and Martin S. K. Leung**
Georgia Institute of Technology, GA 30332

SUMMARY

The objective of this research effort was to develop a real-time guidance approach for launch vehicles ascent to orbit injection. Various analytical approaches combined with a variety of model order and model complexity reduction have been investigated. Singular perturbation methods were first attempted, and found to be unsatisfactory. The second approach based on regular perturbation analysis was subsequently investigated. It also fails because the aerodynamic effects (ignored in the zero order solution) are too large to be treated as perturbations. Therefore, the study demonstrates that perturbation methods alone (both regular and singular perturbations) are inadequate for use in developing a guidance algorithm for the atmospheric flight phase of a launch vehicle.

During a second phase of the research effort, a hybrid analytic/numerical approach was developed and evaluated. The approach combines the numerical method of collocation and the analytical method of regular perturbations. The concept of choosing intelligent interpolating functions is also introduced. Regular perturbation analysis allows the use of a crude representation for the collocation solution, and intelligent interpolating functions further reduce the number of elements without sacrificing the approximation accuracy. As a result, the combined method forms a powerful tool for solving real-time optimal control problems. Details of the approach are illustrated in a fourth order nonlinear example. The hybrid approach is then applied to the launch vehicle problem. The collocation solution is derived from a bilinear tangent steering law, and results in a guidance solution for the entire flight regime, that includes both atmospheric and exoatmospheric flight phases. Assessment of performance and reliability are demonstrated through closed loop simulations. The hybrid guidance approach delivers over 99.9% of optimal performance and orbit injection accuracy while the control computation is completed in tenths of a second on a SPARCstation 1. Wind shear effects and a control constraint are also addressed.

---

* Professor, School of Aerospace Engineering.
** Graduate Research Assistant.

A second effort that paralleled this work under the same grant number was lead by Dr. Dewey Hodges, of the School of Aerospace Engineering at Georgia Tech. This work has been documented under a separate contractor report.

SECTION I

INTRODUCTION

The objective of the Advanced Launch System (ALS) program is to develop an unmanned, all-weather launch system for placing large payloads (100,000lb - 150,000lb) into a low Earth orbit at a fraction of present cost. Part of the guidance requirement is to realize an efficient algorithm for solving the launch vehicle ascent trajectory problem.

1.1 Background

To date, first stage guidance has been realized in open loop form. The vehicle is typically guided by using a pre-stored steering program. The steering program is calculated as a part of pre-launched preparation to account for structural loads from aerodynamic forces and from atmospheric disturbances such as wind shear. Typically it involves flying with nearly zero angle of attack, and performing a gravity turn [1]. Near zero angle of attack is employed to avoid creating excessive aerodynamic bending moments, which is proportional to the product of angle of attack and dynamic pressure. Guidance for the second stage and any subsequent stages is closed loop, employing various approaches. The Saturn V vehicle uses an Iterative Guidance Mode (IGM) [2], and the Space Shuttle employs Powered Explicit Guidance (PEG) [3]. These are retargeting schemes because the guidance commands are recalculated at each update cycle using the current vehicle's position and velocity vectors as the initial conditions for the optimization process.

Traditional Guidance Solution Methods

Traditional launch vehicle guidance may involve either two or three different phases [1 - 3]. The first is an open loop guidance phase for the atmospheric portion of flight which typically flies with a non-optimal piecewise linear attitude program. The second is a closed loop guidance phase for the exoatmospheric portion of flight. This has an analytic solution under certain assumptions. Then a third closed loop phase is possibly required when the vehicle is approaching orbital conditions for final precision orbit injection.

Numerical approaches to optimal guidance typically employ either nonlinear programming [4 - 9] or multiple shooting [10]. In a direct method formulation such as nonlinear programming, the optimization problem is transformed into a parametric optimization problem. The unknown control profile is parameterized with undetermined coefficients of typically piecewise linear polynomials. The states are considered as functions of the control through the differential equations of dynamics. Constraints, if any, are enforced discretely along the trajectory, typically at a finite number of nodal points of the parameterized control. So the original infinite dimensional problem is approximated by

a finite dimensional problem in the reduced space of the control parameters, and gradient techniques are used to search for a solution that optimizes the performance index. In [8], Hargraves and Paris have combined the nonlinear programming method with collocation by approximating all the state and control histories with piecewise smooth functions, thus avoiding any integration process. Similar to the collocation method, Pamadi [9] has used splines as function of velocity to approximate the altitude profile and applied an optimization algorithm to determine the unknown coefficients of the splines. To be useful as a feedback guidance solution, it is essential that these approaches converge quickly and reliably at each instant the solution is updated during the flight.

On the other hand, multiple shooting is a technique used in indirect methods. Instead of evaluating the performance index directly, optimization is achieved by satisfying a set of necessary conditions which are expressed in the form of a Two-Point Boundary Value Problem (TPBVP). For a constrained case, this may lead to a Multi-Point Boundary Value Problem (MPBVP), for which a guess of the switching structure is required. To reduce the sensitivity to an initial guess of the solution, piecewise integration or multiple shooting is used. Instead of integrating for the complete trajectory starting from one set of initial conditions, the trajectory is divided into intervals and integration is performed separately from different sets of initial conditions for each interval. Then the boundary conditions and continuity conditions (or jump conditions in the case of state constraints or discontinuous dynamics) between intervals are enforced. A relaxed Newton's method [11] is typically used to iterate for a solution. Though the indirect method produces extremely accurate results, it involves complicated programming in formulating the costates differential equations and the control structure. The process is also complicated by the requirement to provide an initial guess for both costate and state variables. On the contrary, nonlinear programming is relatively simple to formulate. The method does not require the use of costate variables or a knowledge of switching structure. In practice, it is favored over indirect methods for solving optimization problems in general purpose programs.

Due to the intensive computation requirements, direct and indirect methods are used only to generate off-line solutions for analysis purposes or to provide a first stage open loop guidance program. To compensate for using an open loop approach during the first stage flight, a feedback guidance scheme is introduced for the subsequent exoatmospheric stages of flight where a more simplified dynamic model permits a more analytic solution.

Using Simplified Models

In [2], Chandler and Smith have developed an IGM for the Saturn V vehicle. It is based on a flat Earth no-atmosphere model, and is further simplified with linear angle steering guidance. The guidance solution requires solving only a set of linear equations.

Ten years later, the Boeing Aerospace Company [3] adopted the linear tangent steering guidance as the baseline program for the Space Shuttle's PEG. Using an approximate gravity model, the program is extended to handle the spherical Earth case, and the solution is solved by an iterative algorithm.

Perturbation Methods of Analysis

Perturbation methods of analysis have been shown to be powerful approaches to spacecraft guidance design. Breakwell and Rauch [12] have used regular perturbation to solve a low thrust space flight problem. It is a neighboring extremal technique. A linear feedback control is formulated by linearizing about the reference trajectory and the solution is solved with a numerically determined state transition matrix. In [13], Jacobson and Powers have developed an explicit guidance scheme also for low thrust space flight. It is basically a retargeting procedure and uses an analytic solution for the inertially fixed and constant acceleration flight. Recently, Feeley and Speyer [14] have used regular perturbations on the expansion of the Hamilton-Jacobi-Bellman (HJB) equation, and have applied it to the launch vehicle guidance problem for exoatmospheric flight. The approach requires an analytic zero order solution and quadrature evaluation. The analytic solution is again based on a flat Earth, no-atmosphere approximation, and the neglected dynamics are introduced as perturbations. Solution is obtained by expanding the HJB equation. In this method, higher order state histories are not required and higher order corrections for the costates are obtained by partial differentiation of the power series solution to the HJB equation. An alternative approach based on regular expansion of state and costates was also developed by Leung and Calise [15]. This approach has the advantage that on-line quadrature can be avoided. However, both the solution approaches of [14, 15] were later found to be inadequate when aerodynamic effects are included.

1.2 Research Contributions

The major contributions of this research are: (1) an exhaustive study and simulation effort which demonstrates conclusively that perturbation methods alone (both regular and/or singular perturbations) are inadequate for use in developing a guidance algorithm for the atmospheric phase of a launch vehicle trajectory, and (2) the development of a hybrid approach, that combines the numerical method of collocation and the analytic method of regular perturbation to make it suitable for real-time guidance, and superior to either method alone. The hybrid approach retains the desirable and complimentary features of the individual methods. The collocation method is further improved by providing more intelligent choices of the interpolation functions, which are derived from the analytically tractable portion of the necessary conditions for optimality. When applied to the launch

vehicle guidance problem, the main result is a bilinear tangent steering law for the thrust vector angle that can be employed for all flight phases, including the atmospheric phase of the trajectory. The progress reports and papers that are related to this research effort can be found in [15 - 25].

A second effort that paralleled this work under the same grant number was lead by Dr. Dewey Hodges, of the School of Aerospace Engineering at Georgia Tech. This work has been documented under a separate contractor report [26].

1.3 Report Organization

Sec. 2 presents the formulation of the launch vehicle trajectory optimization problem, which includes the equations of motion and the vehicle aerodynamic and propulsion models that are based on a generic model of the ALS. The results for two purely analytical approaches are documented in Sec. 3. The first is a singular perturbation approach using an energy state approximation and a 2-state model. The second is a regular perturbation approach based on the zero order solution for a flat Earth no-atmosphere assumption. Sec. 4 details the development of a hybrid approach that employs both regular perturbation analysis and the method of collocation. A fourth order nonlinear system is treated in depth to demonstrate its application, and to compare it to solutions obtained by both regular perturbation analysis and purely numerical collocation methods. In Sec. 5, the launch vehicle guidance problem is presented using the hybrid approach. It includes the zero and the first order correction formulations and their solutions, and compares the resulting guided solution with the optimal solution obtained by the method of multiple shooting. Sec. 6 is the conclusions of this research and the recommendations for future research .

SYMBOLS AND ABBREVIATIONS

Symbol

V	- airspeed
W_{ijk}	- wind speed components in the Cijk frame
χ	- heading angle
γ	- flight-path angle
m	- vehicle mass
t_s	- staging time (158.5s for the ALS vehicle)
r	- magnitude of radius vector measured from the Earth's center
r_e	- Earth mean radius (6.378×10^6m)
μ_e	- Earth gravitational constant ($3.9906 \times 10^{14}m^3s^{-2}$)
ω_e	- Earth's rotational rate ($7.27 \times 10^{-5}rads^{-1}$)
h	- altitude, $h = r - r_e$
η	- thrust throttle
α	- angle of attack, control variable in the wind frame
β	- sideslip angle, control variable in the wind frame
M	- Mach number
c	- sound speed
c_e	- reference sound speed on Earth's surface ($340.3ms^{-1}$)
C_D	- aerodynamic drag coefficient $C_D = C_D(\alpha, M, \beta)$
C_L	- aerodynamic lift coefficient $C_L = C_L(\alpha, M, \beta)$
ρ	- atmospheric density
ρ_e	- reference atmospheric density on Earth's surface ($1.225kgm^{-3}$)
p	- atmospheric pressure
p_e	- reference atmospheric pressure on Earth's surface ($101330Nm^{-2}$)
q	- dynamic pressure
T_{vac}	- vacuum thrust
A_e	- engine exit nozzle area
S	- aerodynamic reference area
Ω_A	- state transition matrix for the linear system A
v	- local vertical velocity component
u	- local horizontal velocity component
θ	- thrust-vector angle relative to local horizon, the control variable
g_e	- gravitational acceleration on Earth's surface ($g_e = \mu_e/r_e^2$)

Symbols and Abbreviations (cont.)

Symbol

g_i	- small nonlinear terms (i = 1, 2)
p_x	- interpolated state dynamics in the collocation formulation
q_x	- interpolated costate dynamics in the collocation formulation

Abreviations

ALS	- Advanced Launch System
HJB	- Hamilton-Jacobi-Bellman
IGM	- Iterative Guidance Mode
KSC	- Kennedy Space Center
LEO	- Low Earth Orbit
PEG	- Powered Explicit Guidance
TPBVP	- Two-Point Boundary Value Problems
MPBVP	- Multi-Point Boundary Value Problems

SECTION II

PROBLEM FORMULATION

In this section, we first formulate the optimal launch vehicle guidance problem, which includes the equations of motion for a point mass model of a launch vehicle that the subsequent analyses are applied to. The reference aerodynamic, atmospheric and propulsion models are also included.

2.1 Equations of Motion

Referring to Fig. 2.1, the point mass equations of motion for a multi-stage launch vehicle over a spherical, rotating Earth inside a non-stationary atmosphere are:

$$\dot{V} = \frac{T^{(i)}\cos\alpha\cos\beta - D^{(i)}}{m} - \frac{\mu_e}{r^2}\sin\gamma + r\omega_e^2(\sin\gamma\cos^2\lambda - \cos\gamma\sin\lambda\cos\lambda\cos\chi)$$
$$-\dot{W}_i\cos\gamma\sin\chi - \dot{W}_j\cos\gamma\cos\chi - \dot{W}_k\sin\gamma + 2\omega_e[W_i(\sin\gamma\cos\lambda -$$
$$\cos\gamma\sin\lambda\cos\chi) + \cos\gamma(W_j\sin\lambda - W_k\cos\lambda)\sin\chi] \qquad ; V(t_o) = V_o$$

$$\dot{\chi} = \{-\frac{T^{(i)}\cos\alpha\sin\beta + Y^{(i)}}{m} + \frac{V^2}{r}\cos^2\gamma\tan\lambda\sin\chi + r\omega_e^2\sin\lambda\cos\lambda\sin\chi$$
$$+2\omega_e V(\cos\gamma\sin\lambda - \sin\gamma\cos\lambda\cos\chi) - \dot{W}_i\cos\chi + \dot{W}_j\sin\chi +$$
$$2\omega_e[W_i\sin\lambda\sin\chi + (W_j\sin\lambda - W_k\cos\lambda)\cos\chi]\} / (V\cos\gamma) \; ; \chi(t_o) = \chi_o$$

$$\dot{\gamma} = \{\frac{T^{(i)}\sin\alpha + L^{(i)}}{m} - (\frac{\mu_e}{r^2} - \frac{V^2}{r})\cos\gamma + r\omega_e^2(\cos^2\lambda\cos\gamma + \sin\lambda\cos\lambda\sin\gamma\cos\chi)$$
$$+2\omega_e V\sin\chi\cos\lambda + \dot{W}_i\sin\gamma\sin\chi + \dot{W}_j\sin\gamma\cos\chi - \dot{W}_k\cos\gamma$$
$$+2\omega_e[W_i(\cos\gamma\cos\lambda + \sin\gamma\sin\lambda\cos\chi) - \sin\gamma(W_j\sin\lambda -$$
$$W_k\cos\lambda)\sin\chi]\} / V \qquad ; \gamma(t_o) = \gamma_o$$

$$\dot{\phi} = \frac{V\cos\gamma\sin\chi + W_i}{r\cos\lambda} \qquad ; \phi(t_o) = \phi_o$$

$$\dot{\lambda} = \frac{V\cos\gamma\cos\chi + W_j}{r} \qquad ; \lambda(t_o) = \lambda_o$$

$$\dot{r} = V\sin\gamma + W_k \qquad ; r(t_o) = r_o$$

$$\dot{m} = f(\eta, r, t) \qquad ; m(t_o) = m_o \qquad ; m(t_{s+}^{(i)}) = m_s^{(i)} \qquad (2.1)$$

where

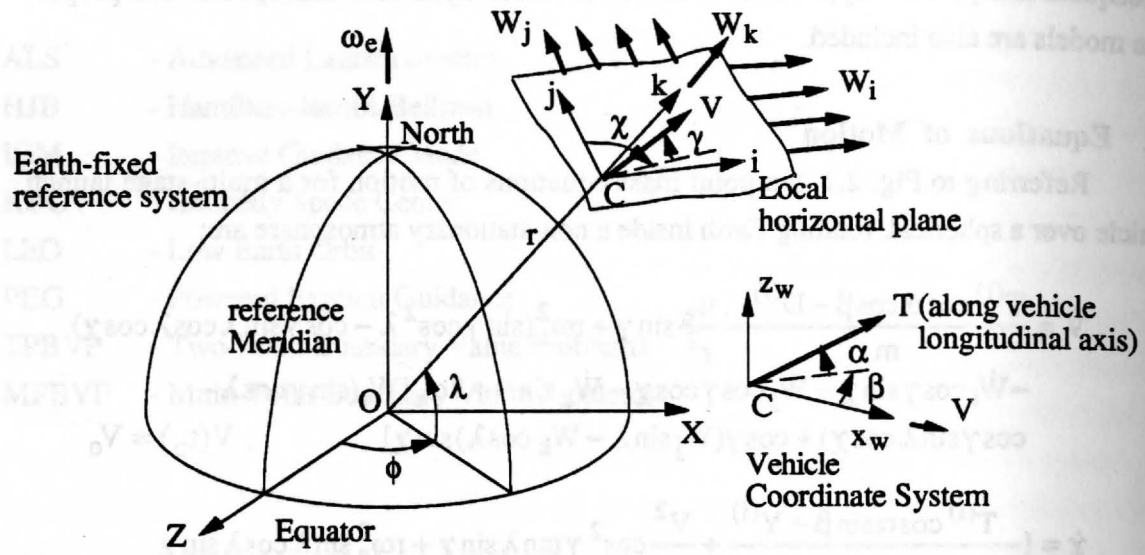

Figure 2.1. Coordinate Systems: Earth-fixed Frame OXYZ, Local Horizontal Cijk, and Wind Frame*.

* Here y_w and z_w are defined in the opposite from their usual convention.

$$\dot{W}_x = \frac{\partial W_x}{\partial \phi}\dot{\phi} + \frac{\partial W_x}{\partial \lambda}\dot{\lambda} + \frac{\partial W_x}{\partial h}\dot{h} \qquad ; x = \{i, j, k\}$$

$$D^{(i)} = qS^{(i)}C_D^{(i)} \quad ; Y^{(i)} = qS^{(i)}C_Y^{(i)} \quad ; L^{(i)} = qS^{(i)}C_L^{(i)}$$

$$q = \rho V^2 / 2 \quad ; T^{(i)} = \eta T_{max}^{(i)} \quad ; \eta \in [0, 1] \qquad (2.2)$$

Here, an inverse-square gravitational field is assumed and μ_e is the Earth's gravitational constant ($3.9906 \times 10^{14} m^3 s^{-2}$). A higher order harmonic model to account for the Earth's oblateness can be used by replacing μ_e/r^2 with the harmonic expression. The superscript (i) = {1, 2, ... , n} indicates different stage values. The above complex model provides sufficient details for most trajectory analysis purposes.

The state variables in this model are airspeed V, heading angle χ, flight-path angle γ, longitude ϕ, latitude λ, radius vector from the Earth's center r, and vehicle mass m. The variables V, γ, χ are relative to the moving air. The wind velocity components W_i, W_j, W_k are assumed to be given as functions of $\{\phi, \lambda, h\}$, where $h = r - r_e$ is the altitude and r_e is the mean Earth radius ($6.378 \times 10^6 m$). The control variables are throttle η , angle of attack α and sideslip angle β. The coefficients of drag C_D, side force C_Y and lift C_L are functions of α, β and Mach number M = V/c. The fuel rate f is a function of throttle setting, altitude and time. The after-jettison stage mass $m(t_{s+})$, staging time t_s, are vehicle parameters, and are both assumed fixed here. Standard atmospheric properties such as density ρ, pressure p, and sound speed c are given functions of h. The coefficients and properties are given in tabular forms which are interpolated as smooth functions of the independent variables.

2.2 Assumptions and Simplifications

To simplify the analysis, the following assumptions are exercised:

Analytic thrust expression - As mentioned in the previous section, a typical launch vehicle employs maximum throttle $\eta = 1.0$ during the ascent phase. For most trajectory analysis purposes, thrust can be adequately modeled as

$$T_{max}^{(i)} = T_{vac}^{(i)} - A_e^{(i)} p \qquad (2.3)$$

where T_{vac} is the vacuum thrust value and A_e is the engine nozzle exit area. The term $A_e p$ represents the back-pressure effect that causes a drop of thrust level as the engine is operated inside the atmosphere.

Constant fuel rate - For a purely rocket propulsion system the rate of fuel consumption is proportional to the vacuum thrust

$$\dot{m} = -T_{vac}^{(i)} / (g_e I_{sp}^{(i)}) \tag{2.4}$$

where $g_e = \mu_e / r_e^2$, and I_{sp} is the specific impulse, a measure of the fuel efficiency. Modern rocket engines have values ranging from 300s to 450s*.

Non-rotating Earth - The Earth's rotation, ω_e is small ($7.27 \times 10^{-5} rads^{-1}$) and the term $r\omega_e^2$ which represents the transport acceleration, was neglected. The term $2\omega_e V$ which represents the Coriolis acceleration may reach $0.1 g_e$ at orbital speed. Here g_e is the gravitational acceleration at the Earth's surface. However, the vehicle reaches orbital speed sharply near the end of its flight phase. Therefore, the dominant effect of this term is only apparent for a short period of time, and setting $\omega_e = 0$ does not produce any significant error.

Planar motion - In actual flight, the lateral maneuver is short. This magnitude is dependent on the launch site which is selected as close to the equator as possible so that a wide range of orbit inclination can be achieved. A large amount of lateral maneuver is typically not required and the desired flight azimuth can be achieved very early in the flight. Hence for simplicity, it is assumed that there is no out-of-plane motion by setting $\beta = W_j = 0$ and considering $C_Y(\beta = 0) = 0$. These assumptions allow us to decouple the dynamics of airspeed, flight-path angle and altitude from those of heading angle, longitude and latitude, and the dynamics are reduced to those associated with motion in the vertical plane. For convenience, the vehicle is assumed to be launched due east on the equator, i.e. $\chi_o = 90^o$ and $\lambda_o = 0$, and ϕ_o is arbitrarily set to zero. The resultant system is a 4-state model:

$$\dot{V} = \frac{T^{(i)}\cos\alpha - D^{(i)}}{m(t)} - \frac{\mu_e}{r^2}\sin\gamma - \dot{W}_i\cos\gamma - \dot{W}_k\sin\gamma \qquad ; V(t_o) = V_o$$

$$\dot{\gamma} = \{\frac{T^{(i)}\sin\alpha + L^{(i)}}{m(t)} - (\frac{\mu_e}{r^2} - \frac{V^2}{r})\cos\gamma + \dot{W}_i\sin\gamma - \dot{W}_k\cos\gamma\}\frac{1}{V} \; ; \gamma(t_o) = \gamma_o$$

$$\dot{\phi} = \frac{V\cos\gamma + W_i}{r} \qquad ; \phi(t_o) = 0$$

$$\dot{r} = V\sin\gamma + W_k \qquad ; r(t_o) = h_o + r_e \tag{2.5}$$

where

---

* For comparison, specific impulse of tubojet engine is over 5000s.

$$m(t) = \begin{cases} m_0 - k^{(1)}(t - t_0) & ; t_0 \le t \le t_s^{(1)} \\ m_s^{(j)} - k^{(j)}(t - t_s^{(j)}) & ; t_s^{(j)} \le t \le t_s^{(j+1)} \end{cases} ; t_s^{(n)} = t_f ; j = 1, \ldots, n-1$$

$$k^{(i)} = T_{vac}^{(i)} / (g_e I_{sp}^{(i)}) \qquad (2.6)$$

The initial conditions chosen for this problem represent the vehicle states following a vertical launch and clearing of the launch tower. The terminal constraints represent direct injection at the perigee of an 80nm x 150nm elliptical transfer orbit.

$$V_0 = 64.49 m/s \quad ; \gamma_0 = 89.5^o \quad ; h_0 = 400m \quad ; t_0 = 15s$$

$$V_f = 7858.2 m/s \quad ; \gamma_f = 0^o \quad ; h_f = 148160m \qquad (2.7)$$

The objective is to minimize the final time, which is equivalent to minimizing the fuel consumption for this formulation. Since there is no constraint on ϕ_f, the ϕ dynamics in Eq. 2.5 are ignorable and can be deleted from the analysis. Also, the optimization must be performed subject to the constraints $q \le q_{max}$ and $|\alpha q| \le (\alpha q)_{max}$.

2.3 Aerodynamic Model and Launch Vehicle Configuration

The aerodynamic model (cf. Figs. 2.3 - 2.8) is obtained from [27]. It corresponds to a generic model of a heavy-lift capacity 2-stage launch vehicle based on a CFD analysis. The vehicle has an asymmetric configuration as shown in Fig. 2.2 with the booster mounted atop the main body. The booster produces a shadowing effect above supersonic speeds during the first stage flight. This shadow effect reduces the C_D at positive angle of attack and the C_D exhibits a nonconvex behavior (cf. Fig. 2.6) in α above Mach 1.3. Other than this behavior, $C_D(\alpha)$ and $C_L(\alpha)$ are nearly parabolic and linear respectively at all Mach numbers.

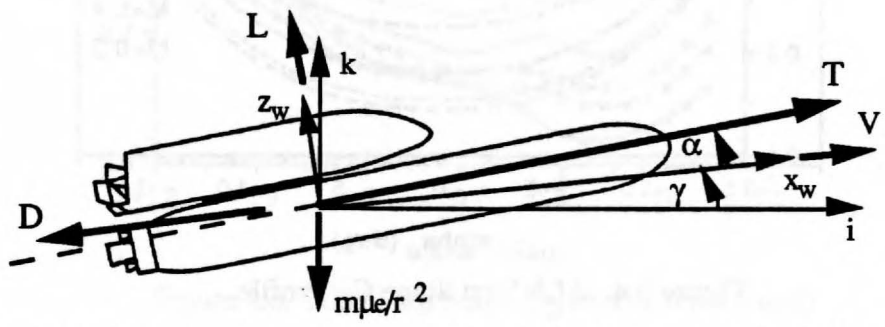

Figure 2.2. Generic Advanced Launch System (ALS) Model in the Cik Plane.

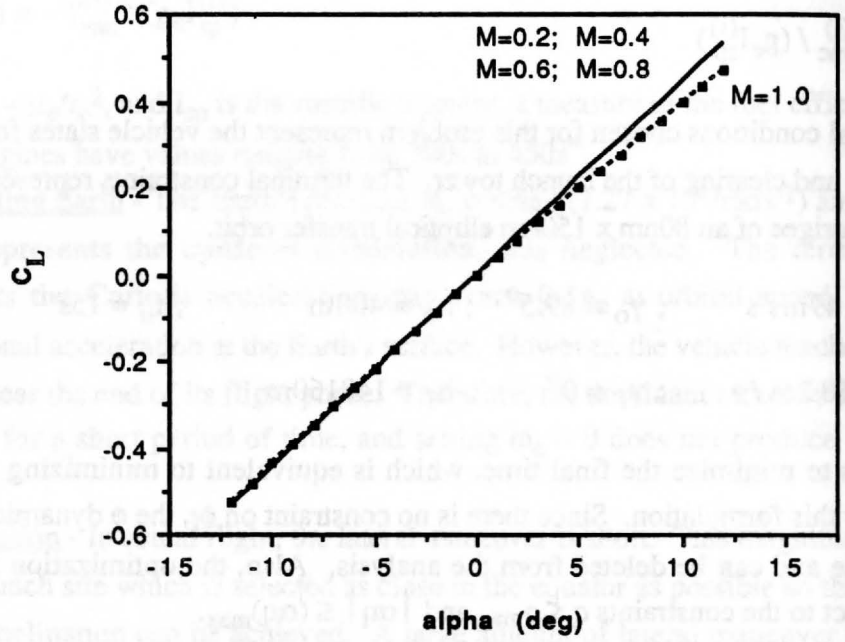

Figure 2.3. ALS First Stage C_L Profile.

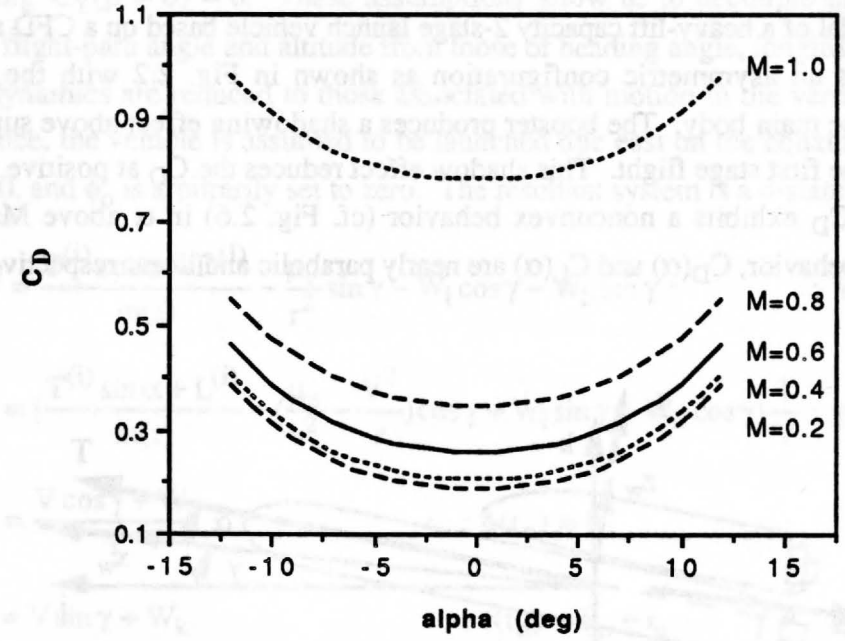

Figure 2.4. ALS First Stage C_D Profile.

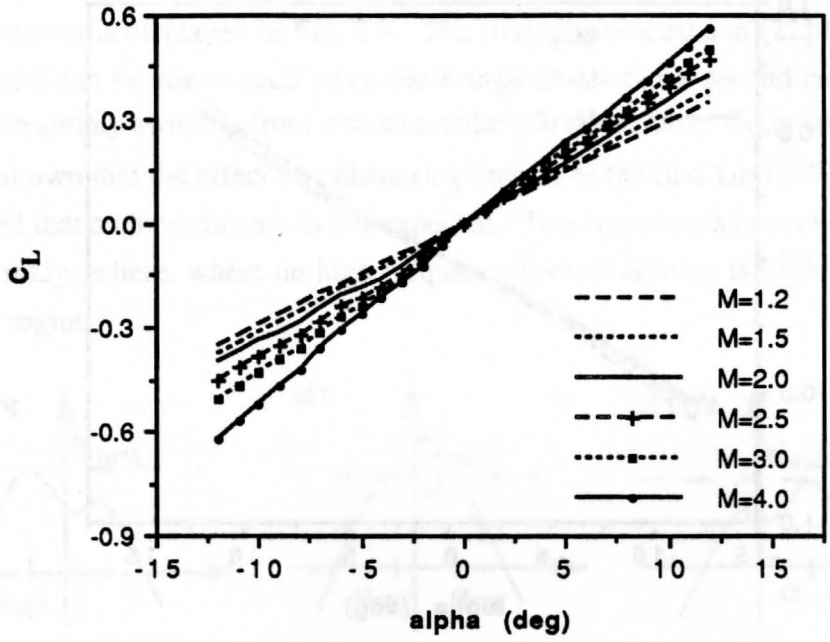

Figure 2.5. ALS First Stage C_L Profile (continued).

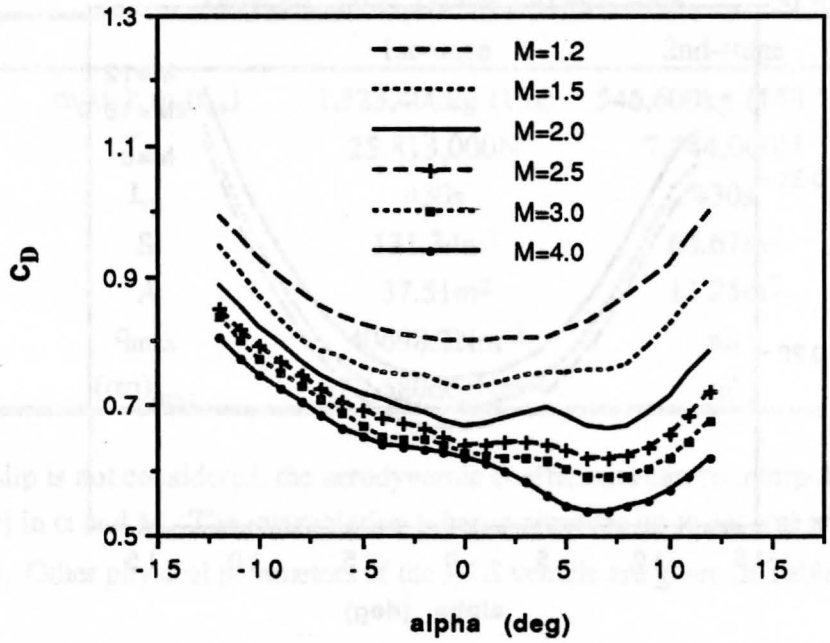

Figure 2.6. ALS First Stage C_D Profile (continued).

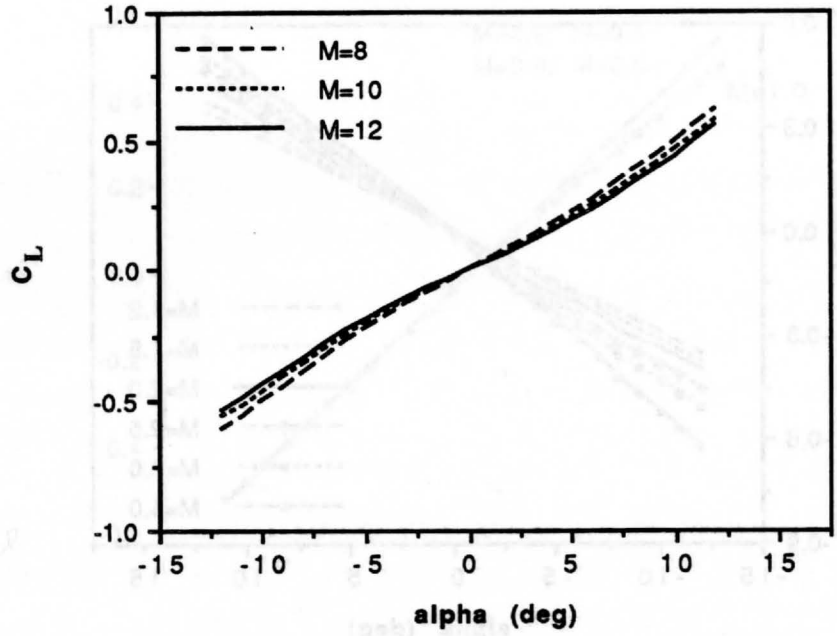

Figure 2.7. ALS Second Stage C_L Profile.

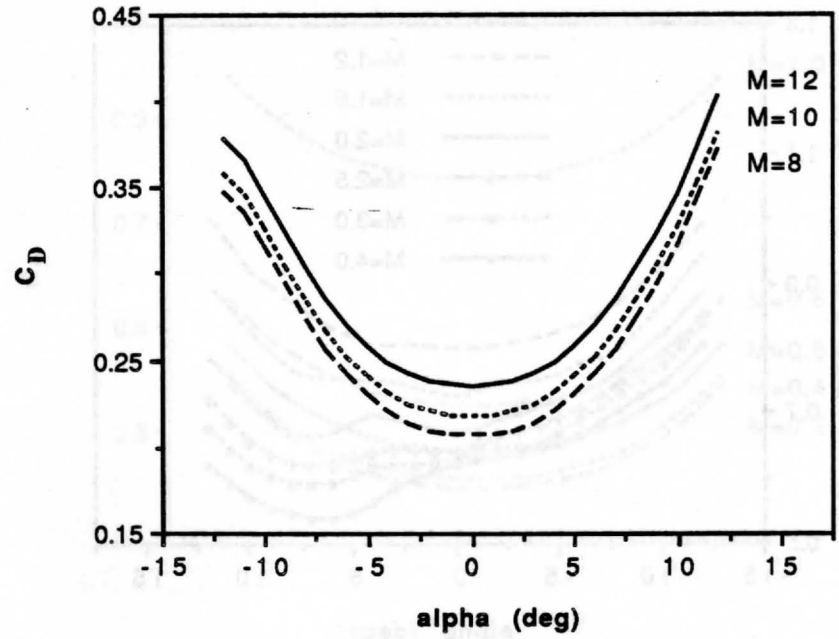

Figure 2.8. ALS Second Stage C_D Profile.

Due to the nonconvexity in C_D, the Hamiltonian also becomes nonconvex. The control is expected to jump as α switches from a lower value to higher value when the two peaks (using Maximum Principle) of the Hamiltonian become equal as time progresses. The phenomenon is displayed in Fig. 2.9. The study documented in [22] has shown that the hodograph can be convexized when bank angle is used as a second control variable, and the angle simply switches from 0 to π to make use of the lower C_D at small positive α. It has also shown that the effect of a chattering control of the first kind [28], if exists, will be small and that a chattering arc is not expected. This hypothesis is consolidated by the numerical analysis here, where no high frequency control activity is observed within the nonconvex region.

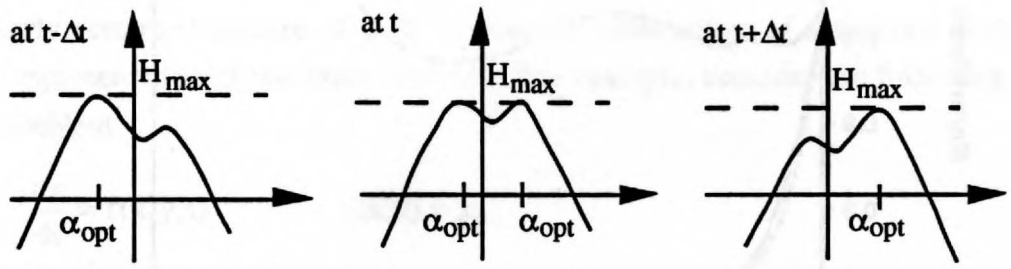

Figure 2.9. Jump in Control due to Nonconvex Hamiltonian.

Table 2.1. ALS Vehicle Physical Data

	1st-stage	2nd-stage
$m_o(t_o)$; $m_s(t_{s+})$	1,523,400kg (15s)	546,600kg (158.5s)
T_{vac}	25,813,000N	7,744,000N
I_{sp}	430s	430s
S	131.34m^2	65.67m^2
A	37.51m^2	11.25m^2
q_{max}	40698.2Nm^{-2}	nil
$(\alpha q)_{max}$	167,580degNm^{-2}	nil

Since sideslip is not considered, the aerodynamic coefficients can be interpolated as bicubic splines [29] in α and M. The interpolation scheme provides up to second order continuous derivatives. Other physical parameters of the ALS vehicle are given in Table 2.1.

2.4 Atmospheric Model

The atmospheric model is based on the 1975 U. S. Standard Atmosphere [30]. Profiles of normalized density, pressure and sound speed with respect to their reference values at the Earth's surface (ρ_e = 1.225kgm^{-3}, p_e = 101330Nm^{-2}, c_e = 340.3ms^{-1}) are

given in Fig. 2.10. To investigate the effect of wind shear, a mean winter wind profile over Kennedy Space Center (KSC) is used to model the non-stationary atmosphere. The profile is shown in Fig. 2.11. It indicates a head-on wind for vehicle launched due east, and the vertical and horizontal (north) wind speed components are assumed to be zero.

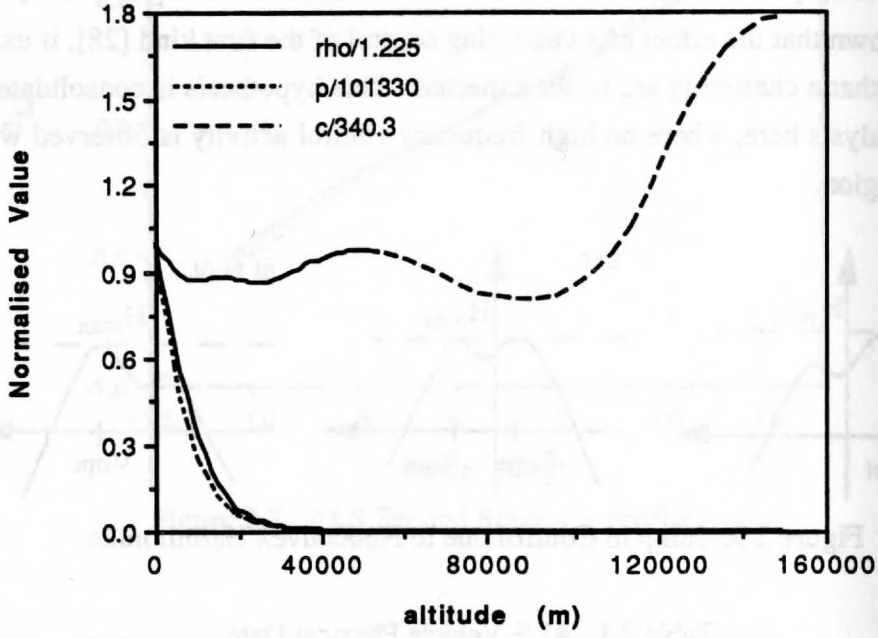

Figure 2.10. Standard Atmospheric Model.

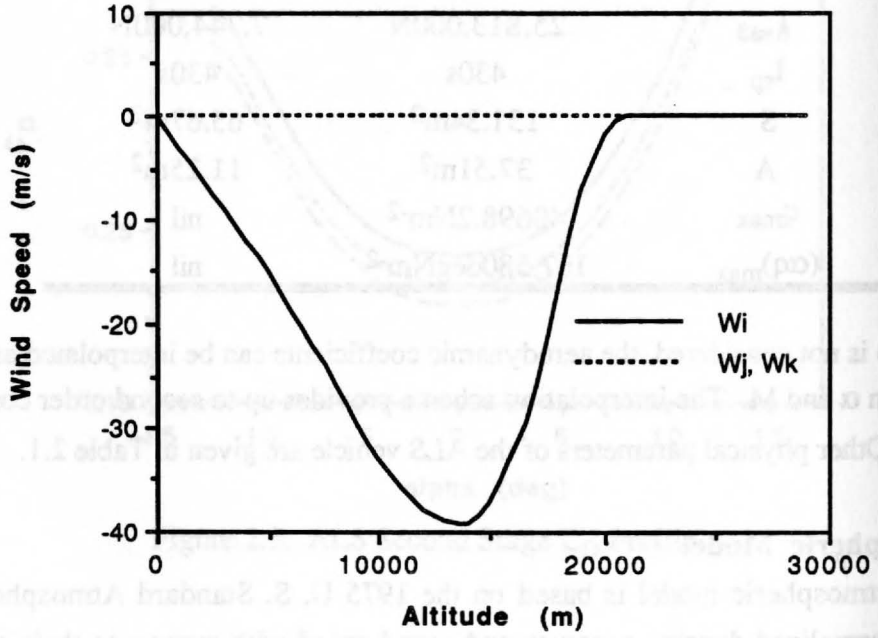

Figure 2.11. KSC Mean Wind Profile.

SECTION III

ANALYTICAL APPROACHES

Two analytical approaches are presented with the objective of simplifying the optimal guidance problem described in Sec. 2. The analytical and numerical results are summarized in this chapter. The analysis results are for: (1) a singular perturbation formulation, and (2) a regular perturbation formulation.

3.1 Singular Perturbations

Singular Perturbation theory is related to the study of a reduced solution of singularly perturbed systems of O. D. E's and the construction of a matched asymptotic series representation of the exact solution. For example, consider the following initial value problem

$$\frac{dx}{dt} = f(x,y,t) \qquad ; x(\varepsilon,0) = x_o$$

$$\varepsilon\frac{dy}{dt} = g(x,y,t) \qquad ; y(\varepsilon,0) = y_o \tag{3.1}$$

where x and y are scalar functions and $\varepsilon > 0$ is a scalar parameter. Setting ε to zero, we have the reduced system. Generally the reduced solution will not satisfy initial conditions on y, and the initial behavior of the reduced solution will be quite different from that of the exact one. This loss of boundary conditions on y (meaning that the reduced solution does not provide a uniformly valid approximation for y) is a characteristic of singular perturbation problem formulations. Basically, the system is separated into the slow variables of x and the fast variables of y. The reduction of higher order problems into lower order ones and the separation of numerically stiff parts by using different time scales are the main advantages of the method. Applications of the method are detailed in [31, 32].

a) Energy state approximation

The energy state approximation is the most widely used approximation in aircraft performance optimization, and sometimes referred to as energy management. It has been applied to minimum time-to-climb, minimum fuel-to-climb and minimum time intercept problems. First we replace the velocity with the mass specific energy

* A third analytical attempt using matched asymptotic methods is documented in [25].

$$E = V^2/2 - \mu_e/r \tag{3.2}$$

as the state variable. Differentiating Eq. 3.2 and using Eqs. 2.5, 2.6 leads to the system

$$\dot{E} = \frac{T^{(i)}\cos\alpha - D^{(i)}}{m(t)}V$$

$$\dot{r} = V\sin\gamma$$

$$\dot{\gamma} = \{\frac{T^{(i)}\sin\alpha + L^{(i)}}{m(t)} - (\frac{\mu_e}{r^2} - \frac{V^2}{r})\cos\gamma\}/V \tag{3.3}$$

where $V = \sqrt{2(E + \mu_e/r)}$. At the moment, the wind shear effects are not considered. In earlier studies on supersonic aircraft [31, 32], specific energy and mass are regarded as slow variables and altitude and flight-path angle are treated as fast variables. So to put Eq. 3.3 into the singular perturbation form, we artificially introduce a bookkeeping parameter ε into Eq. 3.4 as follows:

$$\dot{E} = \frac{T^{(i)}\cos\alpha - D^{(i)}}{m(t)}V$$

$$\varepsilon\dot{r} = V\sin\gamma$$

$$\varepsilon\dot{\gamma} = \{\frac{T^{(i)}\sin\alpha + L^{(i)}}{m(t)} - (\frac{\mu_e}{r^2} - \frac{V^2}{r})\cos\gamma\}/V \tag{3.4}$$

The performance objective is to minimize t_f.

The necessary conditions are formulated by first moving ε to the right hand side of the differential equations, and define the Hamiltonian as

$$H = \tilde{\lambda}_E\frac{T^{(i)}\cos\alpha - D^{(i)}}{m(t)}V + \frac{\tilde{\lambda}_r}{\varepsilon}V\sin\gamma + \frac{\tilde{\lambda}_\gamma}{\varepsilon}\{\frac{T^{(i)}\sin\alpha + L^{(i)}}{m(t)} - (\frac{\mu_e}{r^2} - \frac{V^2}{r})\cos\gamma\}/V + \text{constraints} \tag{3.5}$$

The costate dynamics satisfy:

$$\dot{\tilde{\lambda}}_E = -\frac{\partial H}{\partial E} \quad ; \dot{\tilde{\lambda}}_r = -\frac{\partial H}{\partial r} \quad ; \dot{\tilde{\lambda}}_\gamma = -\frac{\partial H}{\partial \gamma} \tag{3.6}$$

Now introduce the transformations $\lambda_E = \tilde{\lambda}_E$, $\varepsilon\lambda_r = \tilde{\lambda}_r$, $\varepsilon\lambda_\gamma = \tilde{\lambda}_\gamma$ which results in

$$\dot{\lambda}_E = -\frac{\partial H}{\partial E} \quad ; \varepsilon\dot{\lambda}_r = -\frac{\partial H}{\partial r} \quad ; \varepsilon\dot{\lambda}_\gamma = -\frac{\partial H}{\partial \gamma} \tag{3.7}$$

Note that λ_E is a slow variable and that λ_r , λ_γ are fast variables. The optimality condition is given by

$$\partial H / \partial \alpha = 0 \tag{3.8}$$

In the reduced problem ($\varepsilon = 0$) r and γ are treated as control-like variables, which is a consequence of setting $\varepsilon = 0$ in Eq. 3.7. The transformed costates λ_r, λ_γ (when substituted in Eq. 3.6) can be interpreted as Lagrange's multipliers used to enforce the constraints that result from setting $\varepsilon = 0$ in Eq. 3.5.

Reduced (outer) solution

The reduced or outer solution corresponds to the solution of Eqs. 3.4, 3.7 and 3.8 when ε is set to zero. The condition $\partial H/\partial r = 0$ (which results from setting $\varepsilon = 0$ in Eq. 3.7) is a first order necessary condition for a minimum of the Hamiltonian in Eq. 3.5 (we are minimizing the final time). Since the costate λ_E may be interpreted as $\partial t_f/\partial E(t_o)$, it follows that in the reduced problem, $\lambda_E < 0$. Hence a stronger statement for this optimality condition may be written as

$$r^* = \max_r \left\{ \frac{T^{(i)}\cos\alpha - D^{(i)}}{m(t)} V \right\} \Bigg|_{E,m} \tag{3.9}$$

subject to the conditions:

$$\gamma = 0$$

$$0 = \frac{T^{(i)}\sin\alpha + L^{(i)}}{m(t)} - \left(\frac{\mu_e}{r^2} - \frac{V^2}{r}\right)\cos\gamma$$

$$q \le 40698.2 \mathrm{Nm}^{-2}$$

$$|\alpha q| \le 2924.82 \mathrm{radNm}^{-2} \tag{3.10}$$

The last two conditions are the dynamic pressure and aerodynamic load constraints. Starting at an initial energy level and initial mass, a one-dimensional search in altitude is performed. The energy level is then increased and the corresponding change in mass is

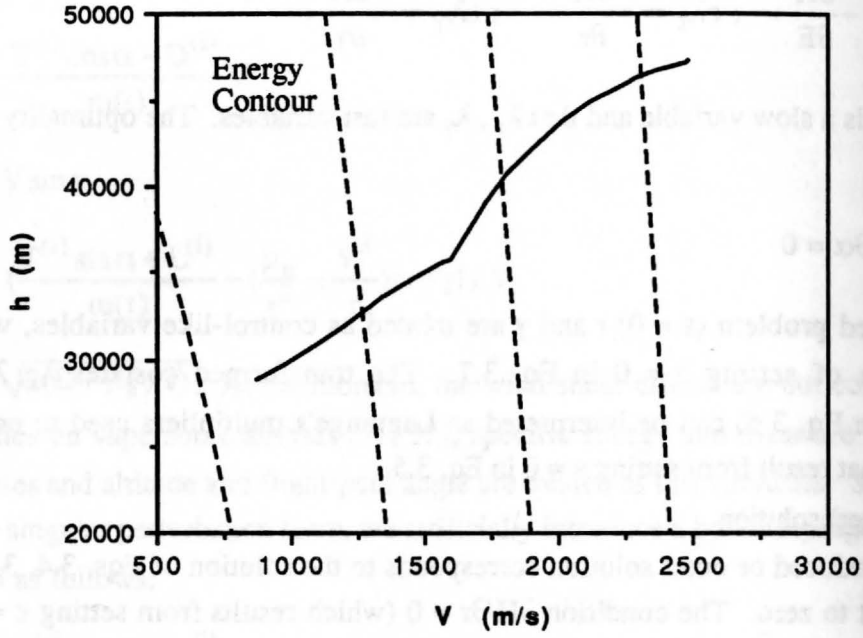

Figure 3.1. Reduced Solution with $\gamma = 0$.

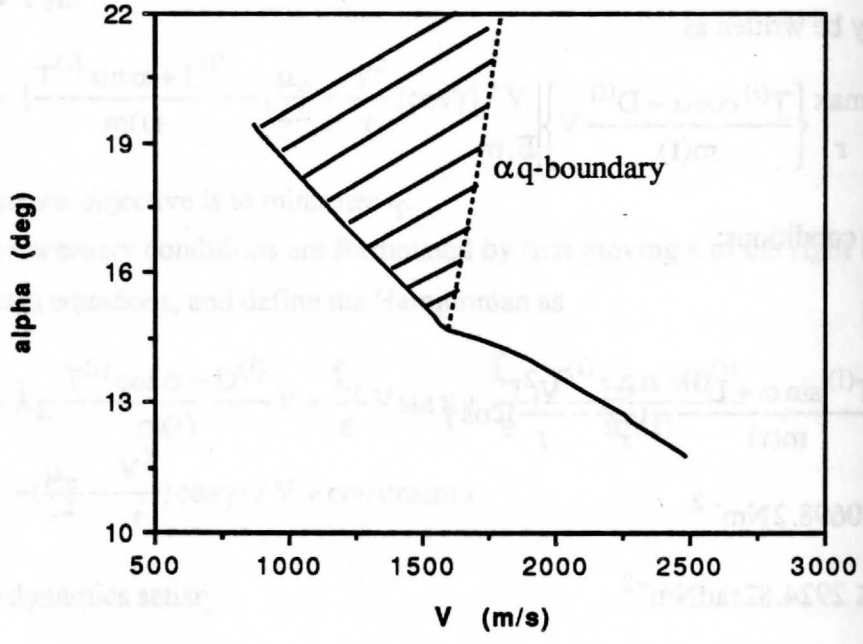

Figure 3.2. Angle of Attack Profile along the Reduced Solution.

Since the optimal solution also exhibits a large value of flight-path angle (inconsistent with the reduced solution approximation), another calculation scheme is used to estimated as

$$\Delta m = -k^{(i)}(\Delta E / \dot{E}^*) \tag{3.11}$$

where the superscript '*' denotes evaluation on the reduced solution. Hence by sweeping through all the energy levels of interest, a reduced feedback guidance law that defines the best altitude profile is obtained. Figs. 3.1 and 3.2 show the results for the reduced problem when the optimization in Eq. 3.9 is carried out for the first-stage flight. The initial conditions in E and m are chosen along a reference optimal trajectory. The solutions at low energy levels result in very large values of angle of attack (> 20^o) that are well beyond the given aerodynamic model range and therefore should not be considered feasible. The reduced solution is unrealistic in that the vehicle stays on the αq constraint up to an energy level of $-6.09 \times 10^7 Jkg^{-1}$.

Since the optimal solution also exhibits a large value of flight-path angle (inconsistent with the reduced solution approximation), another calculation scheme is used to estimate a non-zero flight-path angle and to include the effect of a non-zero flight-path angle in the reduced solution. Assuming the vehicle is already on the reduced solution and is to follow the trajectory, the change in altitude along the reduced solution gives an estimate of the flight-path angle according to

$$\sin\gamma_e = \left\{\frac{\Delta h}{(\Delta E / \dot{E})V}\right\}^* \tag{3.12}$$

By perturbing the energy level from E to E + ΔE, we have

$$\Delta h^* = h^*(E + \Delta E) - h^*(E) \tag{3.13}$$

and a central difference scheme is used to estimate γ. Then the solution of Eqs. 3.9 and 3.10 is recalculated with $\gamma = 0$ replaced with $\gamma = \gamma_e$. The results are given in Figs. 3.3 and 3.4. The inclusion of γ_e gives a slightly lower value of α, and both angle profiles behave reasonably. However, this calculation scheme becomes numerically unstable once the vehicle left the αq constraint boundary.

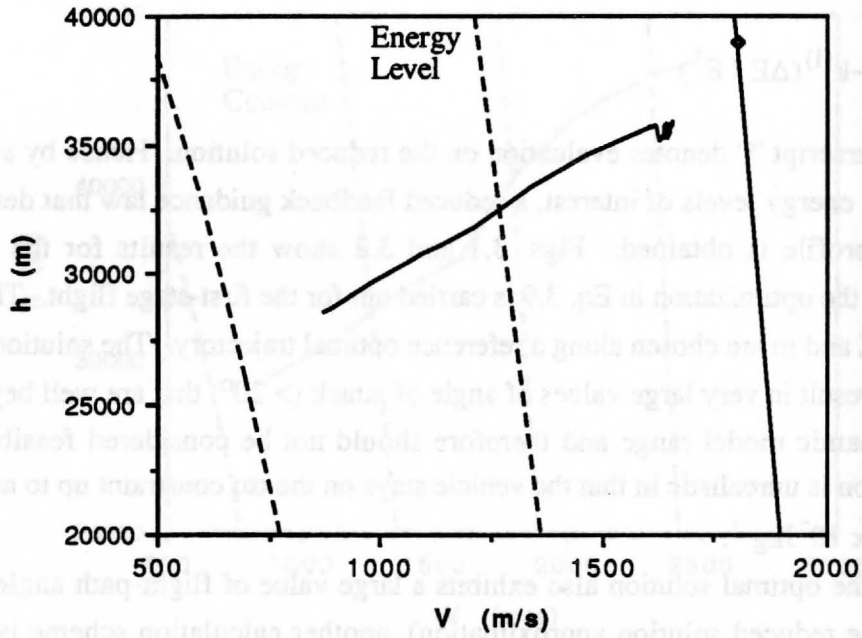

Figure 3.3. Reduced Solution Using Estimated Flight-path Angle.

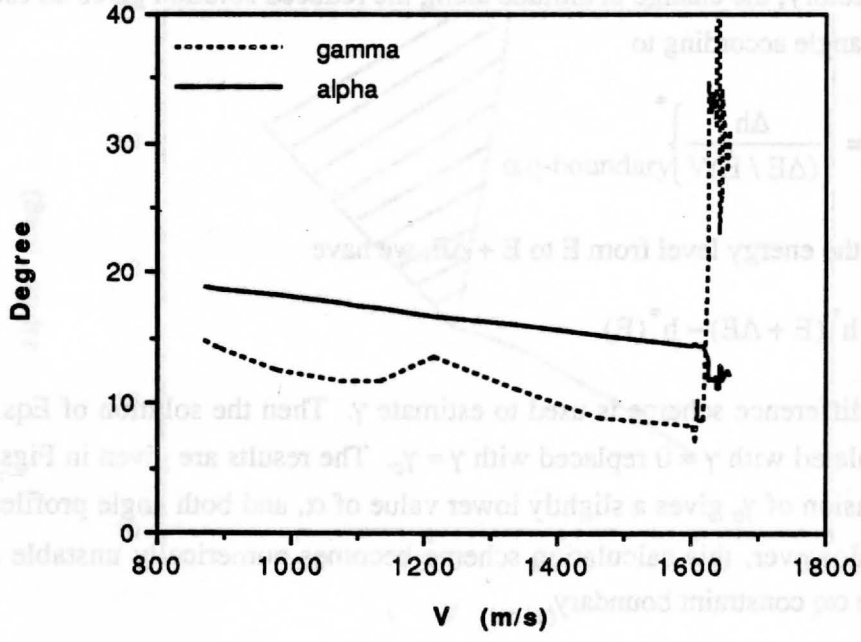

Figure 3.4. Alpha and Gamma Estimate Profiles.

b) Two-state model

Since the energy state approximation does not produce a solution that resembles a reasonable flight trajectory, a more accurate model is employed. The new reduced-order model corresponds to a 2-state approximation:

$$\dot{E} = \frac{T^{(i)} - D^{(i)}}{m(t)} V$$

$$\dot{r} = V \sin\gamma$$

$$\varepsilon\dot{\gamma} = \{\frac{T^{(i)}\alpha + K_L^{(i)}\alpha}{m(t)} - (\frac{\mu_e}{r^2} - \frac{V^2}{r})\cos\gamma\} / V \qquad (3.14)$$

where only the flight-path angle is assumed fast. To make Eq. 2.5 analytically tractable, we adopt the assumptions that the induced drag due to α is negligible and lift is linearly proportional to α ($L^{(i)} = K_L{}^{(i)}\alpha$). The necessary conditions for optimality of flight-path angle and angle of attack on the reduced solution are:

$$\frac{\partial H}{\partial \gamma} = \lambda_r V \sin\gamma \Rightarrow \quad \gamma = \begin{cases} \pi/2 & ; \lambda_r < 0 \\ \text{singular} & ; \lambda_r = 0 \\ -\pi/2 & ; \lambda_r > 0 \end{cases}$$

$$\alpha = \frac{m(t)}{T^{(i)} + K_L^{(i)}} (\frac{\mu_e}{r^2} - \frac{V^2}{r})\cos\gamma \qquad (3.15)$$

In [23] it is shown that the velocity hodograph for the 3-state reduced model (including mass) is nonconvex, and that at $\lambda_r = 0$ the optimal solution chatters between $\gamma = \pm\pi/2$. The interpretation here is that when the altitude reaches its optimum value (for the current energy and mass), then a chattering solution is able to maintain the optimum altitude rate while maximizing the ratio of the mass rate to energy rate. Therefore this formulation is totally inappropriate for the analysis of energy climb in that it produces a reduced solution made up of vertical climbs and dives, connected by chattering arcs.

c) Manifold solution and eigenvalue analysis

The fundamental problem inherent in treating launch vehicle dynamics by energy state approximation relates to the constraints on the γ and h dynamics. They are fast in comparison to energy and mass dynamics and without taking into account the dependency on the singular perturbation parameter ε. For instance, the constraint on altitude dynamics implies $\gamma \equiv 0$ along the reduced solution, which is an extremely crude approximation for the

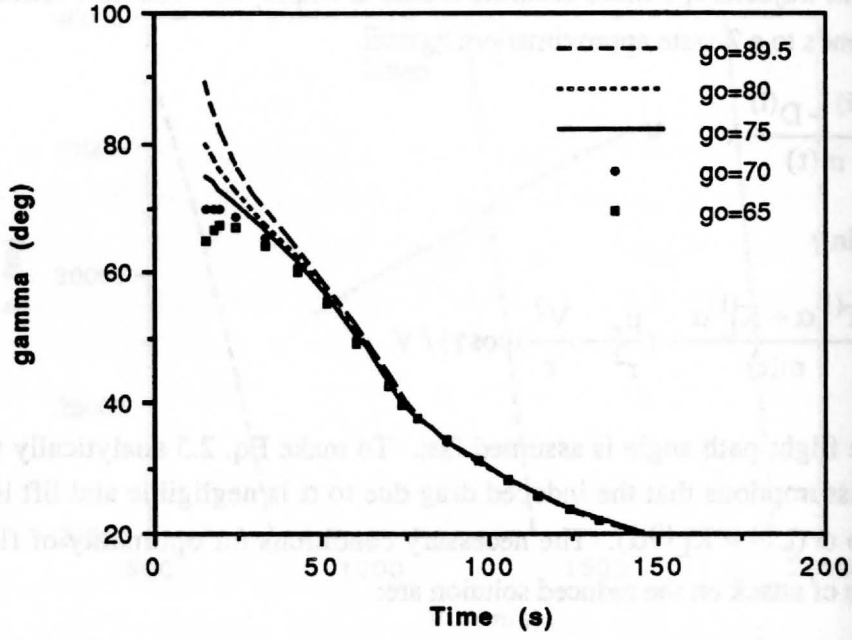

Figure 3.5. Flight-path Angle Profile for Various Reference Trajectories.

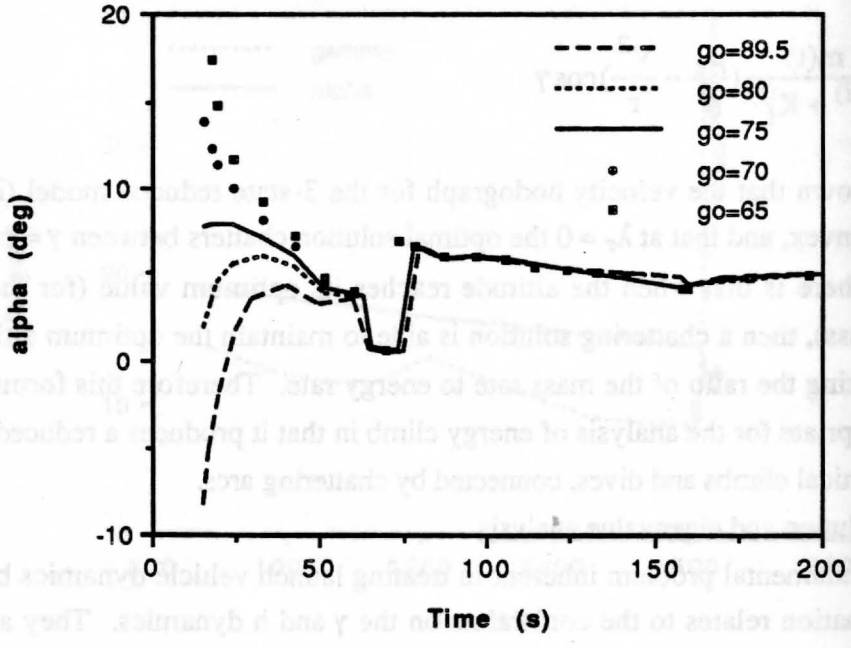

Figure 3.6. Angle of Attack Profile for Various Reference Trajectories.

launch vehicle case. This problem can be alleviated by using a slow manifold solution [33] in place of the reduced solution, which amounts to solving the exact problem with the initial flight-path angle chosen to suppress any fast motion that may be present in the solution. A separate boundary layer analysis could then perform to take into account the actual initial condition on γ (cf. Fig. 3.7). This approach has also been carried out, however it is found that the assumptions regarding the separation of dynamics worsen above supersonic speed, and the reduced-order model approximation deteriorates. This hypothesis is consolidated by the eigenvalues investigation described below.

Computation of the equilibrium manifold corresponds to determining the initial condition on γ so that rapid transients in γ and λ_γ are absent in the exact solution. First a sweep of the initial condition in γ about a nominal value of $\gamma_0 = 89.5^o$ is performed, and the exact dynamics of the states and costates (with the control eliminated using the optimality condition) are numerically integrated. This allows us to identify the equilibrium manifold by visual inspection for the absence of fast transients in γ and λ_γ. The closer the actual initial condition for the fast variable lies to the manifold, the more accurate the subsequent boundary layer correction in γ becomes. Figs 3.5 and 3.6 demonstrate that the manifold is estimated to be at $\gamma_0 = 75^o$, where it can be seen that there is no apparent boundary-layer-like behavior in the fast variable γ and the control α.

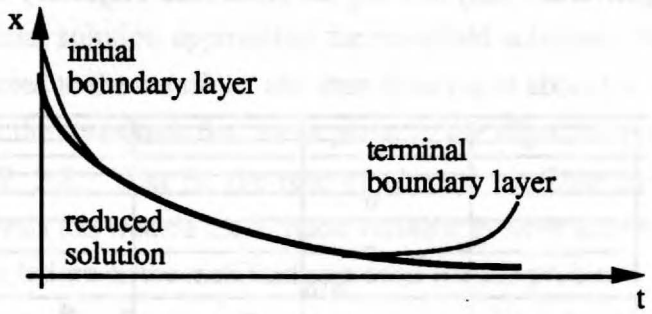

Figure 3.7. Typical Boundary Layer Characteristics.

To shed insight on the separation phenomenon of the fast and slow dynamics of the launch vehicle problem, an eigenvalue test is carried out. By linearizing the dynamics of E, r, γ, λ_E, λ_r, λ_γ about the equilibrium manifold, the eigenvalues of the linearized system are obtained, and the relative magnitudes of the real part of the eigenvalues provide information about the separation possibility of the dynamics. A Hamiltonian matrix appears in the linearized system whose eigenvalues characterize the full order system of dynamics (states and costates) in the vicinity of the equilibrium manifold.

Eigenvalues calculated at discrete points along the trajectory are shown in Figs. 3.8 and 3.9 (only those in the right half s-plane are shown). At the beginning part of the trajec-

tory ($t < 50s$), the results clearly show a separation configuration of 2 slow and 1 fast state (and costate) variables. All the eigenvalues are real. The relative magnitude is separated by a factor of up to 4 in this interval (cf. Fig. 3.9). As the energy level increases, two of the

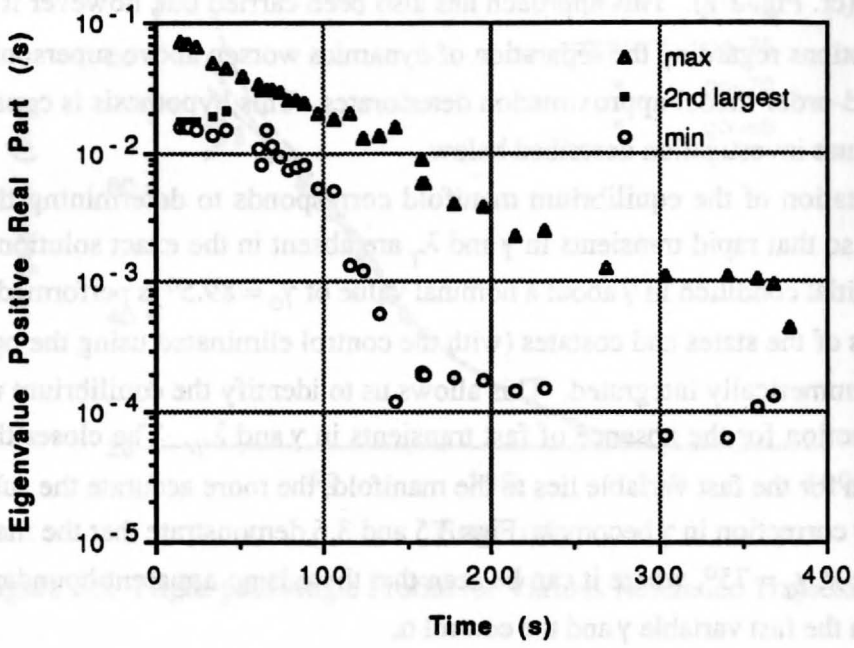

Figure 3.8. Eigenvalue Analysis along the Reference Trajectory of $\gamma_0 = 75^0$.

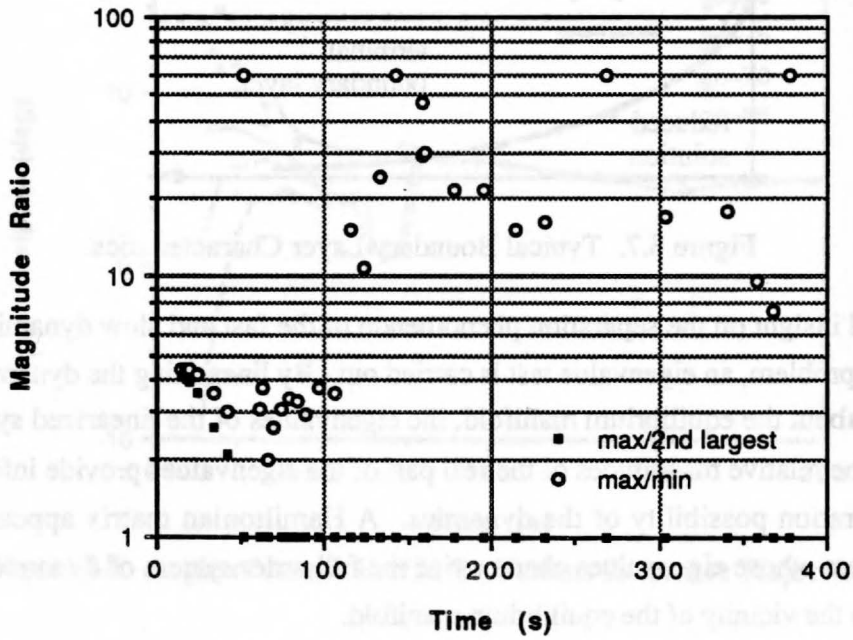

Figure 3.9. Eigenvalue Separation by Relative Magnitude.

eigenvalues join to form a complex conjugate pair, the real part of which is an order of magnitude larger than the third (real) root. This suggests a decomposition of 1 slow and 2 fast state variables. An eigenvector analysis indicates that the fast state variable at low energy levels indeed corresponds to the flight-path angle, whereas at high energy levels specific energy is the only slow state variable. Altitude, which was a slow variable at low energy levels, rapidly transitions to being a fast variable at approximately t = 50s as shown in Figs 3.8 and 3.9.

A nonlinear feedback control solution for angle of attack, based on a boundary layer correction for the flight-path angle dynamics, can be formulated as follows:

$$H = -\lambda_{mo}k^{(i)} + \lambda_{Eo}\dot{E}(E_o, h_o, m_o, \alpha) + \lambda_{ro}V_o \sin\gamma + \lambda_\gamma \dot{\gamma}(E_o, h_o, m_o, \alpha) = 0$$

$$H_\alpha = 0 \qquad (3.16)$$

where m_o, E_o, h_o, λ_{mo}, λ_{Eo}, λ_{ro} are treated as slow variables* in the manifold solution, and are constant in the boundary layer analysis. The manifold solution is stored as a function of energy, and the boundary layer problem defined in Eq. 3.16 is solved at each control update to form a guided solution. Note that there are two equations for the two unknowns in α and λ_γ. The guided solution using the pre-computed slow manifold (chosen for $\gamma_o = 75^o$ in Fig. 3.6) with an on-line boundary layer correction is plotted in Fig. 3.10. The optimal solution approaches the manifold solution. However the guided solution is first attracted to the manifold, and then diverges at about t = 25s. This correlates almost exactly with the transition that takes place in the eigenvalue associated with the altitude state in Fig. 3.8. That is, the role of altitude variable has changed, but the boundary layer analysis has treated the altitude variable as slow (constant to zero-order in ε). This explains the failure of the manifold approach for this problem.

Recalling the previous energy state approximation formulation, even though eigenvalues analysis clearly indicates the existence of a two-time scale behavior, the poor performance of the zero order reduced solution is attributed to the large value of longitudinal load factor inherent in the launch vehicle problem. The value of this non-dimensional variable along the reduced solution is plotted in Fig. 3.10. In comparison with a subsonic transport aircraft with a load factor of 0.1, the launch vehicle averages above 3 in this case and therefore a zero or even a first order solution is not expected to provide any reasonable approximation.

---

* Here we treat m as a state variable, and it is not eliminated by Eq. 2.6.

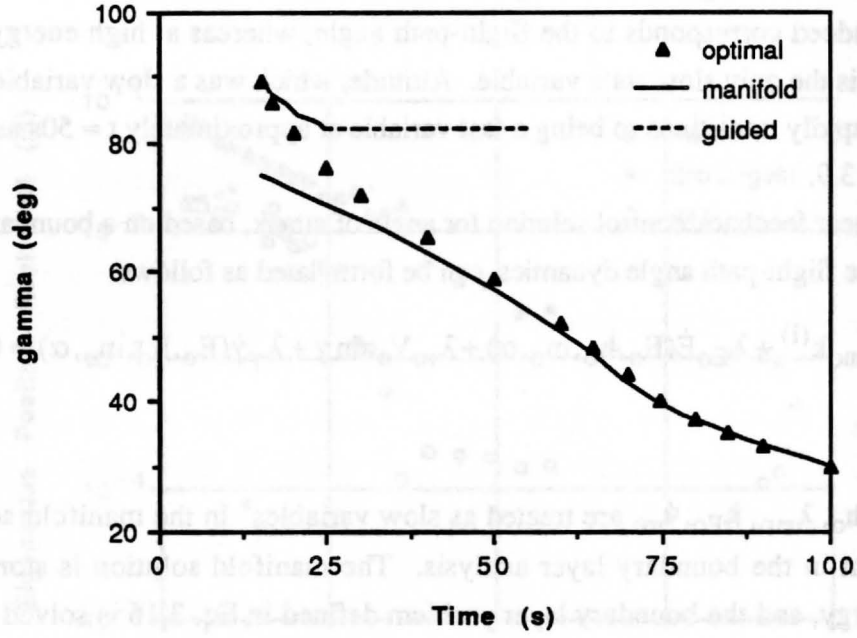

Figure 3.10. Flight-path Angle Profile of the Guided Solution.

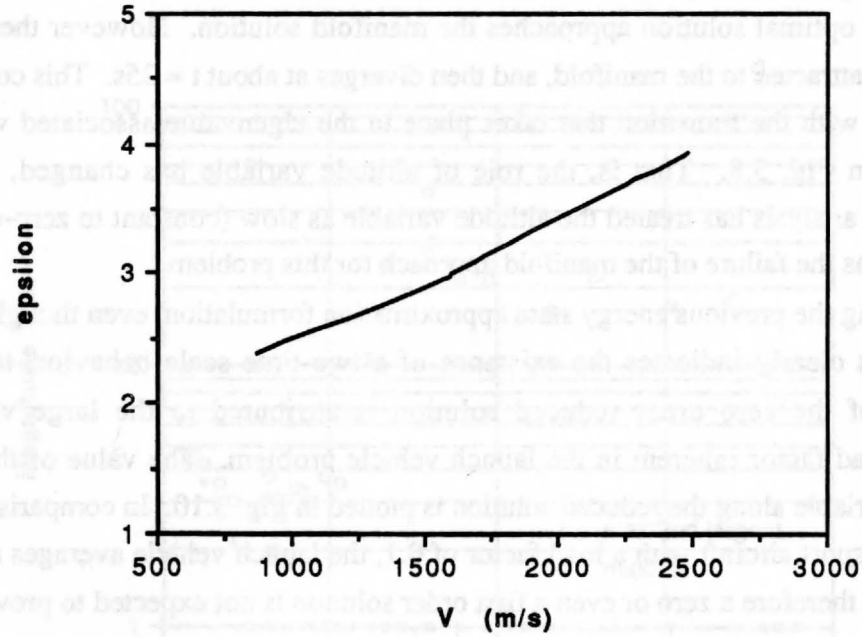

Figure 3.11. Evaluation of the Singular Perturbation Parameter ε(E) for the ALS Vehicle.

3.2 Regular Perturbations

The unsuccessful attempt by singular perturbation analysis led to consideration of another analytic approach that has been used repeatedly on low thrust spaceflight problems, the regular perturbation analysis. In this section, the general regular perturbation formulation for optimal control problems is discussed. An extension over earlier formulations is that higher order corrections for the free final time are made explicitly in the formulation developed here. Then an analytic zero order solution based on the maximum horizontal speed transfer problem in a constant gravity field and in vacuum [34] is extended to a mass-varying multi-stage rocket. This is then followed by an attempt to compute a first order correction to account for a central gravitational field, spherical Earth and all the atmospheric effects.

a) Regular perturbations in optimal control

The optimal control problem formulation consider here is to maximize a performance index which is a function of the terminal states and time, subject to dynamic constraints:

$$J = \max_{u} \{\phi(x,t)\}\Big|_{t_f} \tag{3.17}$$

$$\dot{x} = f(x,u,t) + \varepsilon g(x,u,t) \qquad ; x(t_o) = x_o \; ; \; t \in [t_o, t_f] \tag{3.18}$$

and the terminal time constraints $\psi_i(x(t_f)) = 0$, $i = 1, \ldots, p \leq n$. In Eq. 3.18, x is an n-dimensional state vector and u is an m-dimensional control vector. In applications, the expansion parameter ε is sometimes artificially inserted to signify the presence of small nonlinear effects, and used as a bookkeeping parameter for the regular expansion analysis. The Hamiltonian and transversality condition are given by:

$$H = \lambda^T\{f + \varepsilon g\} \qquad ; H(t_f) = -\Phi_t\Big|_{t_f} \; ; \; \Phi = \phi + \nu^T\psi \tag{3.19}$$

The costate equations and associated boundary conditions are:

$$\dot{\lambda} = -H_x \qquad ; \lambda(t_f) = \Phi_x\Big|_{t_f} \tag{3.20}$$

where the subscript is used to denote partial differentiation. In the absence of control constraints, the optimal control satisfies

$$H_u = \lambda^T\{f_u + \varepsilon g_u\} = 0 \tag{3.21}$$

assuming that $H_{uu} > 0$.

In the above final time is free. Thus, we introduce a new independent variable $\tau = (t - t_o)/T$ where $T = t_f - t_o$ and rewrite the necessary conditions of Eqs. 3.18 - 3.20 in the following equivalent form:

$$x' = H_\lambda T \qquad ; x(\tau = 0) = x_o \; ; \; \psi(x(\tau = 1)) = 0 \tag{3.22}$$

$$\lambda' = -H_x T \qquad ; \lambda(\tau = 1) = \Phi_x\Big|_{\tau = 1} \tag{3.23}$$

$$T' = 0 \tag{3.24}$$

$$H = \lambda^T \{f(x, u, \tau T + t_o) + \varepsilon g(x, u, \tau T + t_o)\} \; ; \; H(\tau = 1) = -\Phi_t\Big|_{\tau = 1} \tag{3.25}$$

where (-)' denotes $d(-)/d\tau$. In a regular perturbation analysis, the objective is to approximate the solution to Eqs. 3.22 - 3.25 by an asymptotic series in x, λ, u and T as follows:

$$\begin{aligned} x &= x_0 + \varepsilon x_1 + \varepsilon^2 x_2 + \ldots \\ \lambda &= x_0 + \varepsilon \lambda_1 + \varepsilon^2 \lambda_2 + \ldots \\ u &= u_0 + \varepsilon u_1 + \varepsilon^2 u_2 + \ldots \\ T &= T_0 + \varepsilon T_1 + \varepsilon^2 T_2 + \ldots \end{aligned} \tag{3.26}$$

Assume the functions f, g, ϕ, ψ have piecewise continuous derivatives up to order at least K+1 where K is the order of approximation. Using the Taylor series formula, a finite series approximation is constructed according to

$$F(\sigma_0 + \sum_{k=1}^{K} \sigma_k \varepsilon^k) = F(\sigma_0) + \varepsilon \frac{dF}{d\sigma}\Big|_{\sigma_0} \sigma_1 + \varepsilon^2 \{\frac{dF}{d\sigma}\Big|_{\sigma_0} \sigma_2 + \frac{1}{2!} \frac{d^2F}{d\sigma^2}\Big|_{\sigma_0} \sigma_1^2\} + \ldots \tag{3.27}$$

where $\sigma = \{x, \lambda, \nu, u, T\}$. Substituting the series representation for each of the variables in Eqs. 3.22 - 3.25 and equating like powers in ε, we obtain the zero order and higher order necessary conditions. To zero order we have:

$$\partial x_0 / \partial \hat{t} = \partial H_0 / \partial \lambda_0 \quad ; x_0(t_o) = x_o \; ; \; \psi(x_0(t_o + T_0)) = 0$$

$$\partial \lambda_0 / \partial \hat{t} = -\partial H_0 / \partial x_0 \; ; \; \lambda_0(\hat{t} = t_o + T_0) = \Phi(x_0, \hat{t}) / \partial x_0\Big|_{\hat{t} = t_o + T_0}$$

$$\partial H_0 / \partial u_0 = 0$$

$$H_0 = \lambda^T f(x_0, u_0, \hat{t}) \quad ; H_0(\hat{t} = t_o + T_0) = -\Phi(x_0, \hat{t}) / \partial \hat{t} \Big|_{\hat{t} = t_o + T_0} \tag{3.28}$$

In Eq. 3.28, the new independent variable $\hat{t} = \tau T_0$ has been introduced, where it should be noted that in the zero order problem $T = T_0$.

For the higher order problems, they are governed by a set of nonhomogeneous linear O. D. E's. with the form of

$$\frac{d}{d\hat{t}}\begin{bmatrix} x_k \\ \lambda_k \end{bmatrix} = \begin{bmatrix} A_{11}(x_0,\lambda_0,T_0) & A_{12}(x_0,\lambda_0,T_0) \\ A_{21}(x_0,\lambda_0,T_0) & A_{22}(x_0,\lambda_0,T_0) \end{bmatrix}\begin{bmatrix} x_k \\ \lambda_k \end{bmatrix} + \frac{T_k}{T_0}\begin{bmatrix} C_1(x_0,\lambda_0,T_0) \\ C_2(x_0,\lambda_0,T_0) \end{bmatrix}$$

$$+\begin{bmatrix} P_{1k}(x_0,\lambda_0,T_0, \ldots, x_{k-1},\lambda_{k-1},T_{k-1}) \\ P_{2k}(x_0,\lambda_0,T_0, \ldots, x_{k-1},\lambda_{k-1},T_{k-1}) \end{bmatrix} \tag{3.29}$$

where

$$A_{11} = f_x - f_u[(f_u^T\lambda)_u]^{-1}(f_u^T\lambda)_x$$

$$A_{12} = -f_u[(f_u^T\lambda)_u]^{-1}f_u^T$$

$$A_{21} = -(f_x^T\lambda)_x + (f_x^T\lambda)_u[(f_u^T\lambda)_u]^{-1}(f_u^T\lambda)_x$$

$$A_{22} = -f_x^T + (f_x^T\lambda)_u[(f_u^T\lambda)_u]^{-1}f_u^T$$

$$C_1 = f + (\hat{t} - t_o)\left\{f_{\hat{t}} - f_u[(f_u^T\lambda)_u]^{-1}(f_u^T\lambda)_{\hat{t}}\right\}$$

$$C_2 = -f_x^T\lambda - (\hat{t} - t_o)\left\{(f_x^T\lambda)_{\hat{t}} - (f_x^T\lambda)_u[(f_u^T\lambda)_u]^{-1}(f_u^T\lambda)_{\hat{t}}\right\} \tag{3.30}$$

and for $k = 1$:

$$P_{11} = g - f_u[(f_u^T\lambda)_u]^{-1}g_u^T\lambda$$

$$P_{21} = -g_x^T\lambda + (f_x^T\lambda)_u[(f_u^T\lambda)_u]^{-1}g_u^T\lambda \tag{3.31}$$

All the matrices in Eq. 3.30 are evaluated at the zero order solution values. To complete the necessary conditions, it is also required to expand the boundary conditions and the transversality condition in Eq. 3.28. Note that Eq. 3.29 explicitly shows the effect of higher order corrections to the final time, T. If the solution process is terminated at say,

$k = 1$, then a real-time sampled data implementation of the control solution would be constructed as follows. For the original system in Eq. 3.18, an expression for the optimal control is obtained as function of x and λ from the optimality condition in Eq. 3.21. Then, treating the present state as the initial state, a first order approximation is obtained by using $\lambda_0(t_o) + \varepsilon\lambda_1(t_o)$ as an approximation for $\lambda(t_o)$ to compute the control, where $\lambda_0(t_o)$ and $\lambda_1(t_o)$ are obtained from the solutions of the zero and the first order necessary conditions. This process is repeated at the next control update time by regarding the value of the state as the new initial state. Therefore, it is necessary to repeat the zero and first order solutions in updating the estimate of the costate variable.

The non-homogeneous linear ordinary differential equations in Eqs. 3.29 - 3.31 may be expressed in terms of a convolution by first obtaining a state transition matrix. The state transition matrix $\Omega_A(\hat{t}, t_o)$ is merely the partial derivative of the zero order solution at $\hat{t}$ with respect to the initial conditions $x_0(t_o)$ and $\lambda_0(t_o)$, hence it is easily computed given an analytic zero order solution. In Appendix A it is shown that the result can be expressed in the following form

$$\begin{bmatrix} x_k(\hat{t}) \\ \lambda_k(\hat{t}) \end{bmatrix} = \Omega_A(\hat{t}, t_o)\begin{bmatrix} x_k(t_o) \\ \lambda_k(t_o) \end{bmatrix} + \int_{t_o}^{\hat{t}} \Omega_A(\hat{t}, \tau)\left\{\frac{T_k}{T_0}\begin{bmatrix} C_1(\tau) \\ C_2(\tau) \end{bmatrix} + \begin{bmatrix} P_{1k}(\tau) \\ P_{2k}(\tau) \end{bmatrix}\right\} d\tau$$

$$= \Omega_A(\hat{t}, t_o)\begin{bmatrix} x_k(t_o) \\ \lambda_k(t_o) \end{bmatrix} + T_k \frac{\hat{t} - t_o}{T_0}\begin{bmatrix} \dot{x}_0(\hat{t}) \\ \dot{\lambda}_0(\hat{t}) \end{bmatrix} + \int_{t_o}^{\hat{t}} \Omega_A(\hat{t}, \tau)\begin{bmatrix} P_{1k}(\tau) \\ P_{2k}(\tau) \end{bmatrix} d\tau \quad (3.32)$$

Using the above expression at $\hat{t} = T_0$ along with the expansions of the boundary conditions, we can solve for $\lambda_k(t_o)$, ν_k and T_k from a set of linear algebraic equations. Thus the major part of the computation for the first order term lies in the quadrature that must be performed in Eq. 3.32. In a discrete time implementation, if the current state is regarded as the initial state then $x_k(t_o) = 0$ in Eq. 3.32 since $x_0(t_o)$ satisfies the initial condition on the state variable. Since zero order solution changes at each update of the initial state, it is necessary to repeat the quadrature at each update for the higher order corrections. Alternatively, we can fix the zero order solution and treat $x_k(t_o)$ as the deviation between the current state and the zero order solution computed for the original epoch time, but evaluated at the present time. In this form it would be possible to pre-compute the quadrature and store it as a function of a monotonic variable along the trajectory. Thus the real-time process of solving the zero order problem and the quadrature can be avoided.

The case of discontinuous dynamics, such as might arise in a multi-stage launch vehicle, can be handled by a simple modification of Eq. 3.32. For example, in a two-stage representation we would have

$$\begin{bmatrix} x_k(\hat{t}) \\ \lambda_k(\hat{t}) \end{bmatrix} = \Omega_A^{(2)}(\hat{t}, t_s)\Big\{ \Omega_A^{(1)}(t_s, t_o)\begin{bmatrix} x_k(t_o) \\ \lambda_k(t_o) \end{bmatrix} + T_k \frac{t_s - t_o}{T_0}\begin{bmatrix} \dot{x}_0^{(1)}(t_s) \\ \dot{\lambda}_0^{(1)}(t_s) \end{bmatrix} +$$

$$\int_{t_o}^{t_s} \Omega_A^{(1)}(\hat{t}, \tau)\begin{bmatrix} P_{1k}^{(1)}(\tau) \\ P_{1k}^{(2)}(\tau) \end{bmatrix} d\tau \Big\} + T_k \frac{\hat{t} - t_s}{T_0}\begin{bmatrix} \dot{x}_0^{(2)}(\hat{t}) \\ \dot{\lambda}_0^{(2)}(\hat{t}) \end{bmatrix} +$$

$$\int_{t_s}^{\hat{t}} \Omega_A^{(2)}(\hat{t}, \tau)\begin{bmatrix} P_{1k}^{(2)}(\tau) \\ P_{2k}^{(2)}(\tau) \end{bmatrix} d\tau \quad ; \hat{t} > t_s \tag{3.33}$$

The superscripts (1), (2) denote the expressions for different sets of dynamics and t_s is the interior point where discontinuity occurs.

b) Launch vehicle application

The performance objective is to maximize $-t_f$ (ie. minimize final time) subject to the terminal conditions $V(t_f) = 7858.2 ms^{-1}$, $\gamma(t_f) = 0$, $h(t_f) = 148160m$, open $\phi(t_f)$. These conditions correspond to direct injection at the perigee of an 80nm x 150nm elliptical transfer orbit. First, it is necessary to derive a closed form, zero order solution which should be simple, but accurate enough such that the neglected dynamics can be corrected in a first order term.

Assuming that the dominant forces on the launch vehicle are thrust and gravity, an attempt is made to treat the atmospheric effects as a perturbation effect. To further simplify the problem, spherical Earth effects are also considered as perturbations (these effects are only apparent when the vehicle reaches orbital speed near the end of the flight). The result is similar to the maximum horizontal speed transfer problem in [34] for a flat Earth no-atmosphere situation. The differences here are that the mass of the vehicle is varying, the dynamics are discontinuous and the terminal boundary conditions are specified at an unknown final time. We now recast the dynamics of Eq. 2.5 in a regular perturbation format as in Eq. 3.18, in accordance with the above desired approximations:

$$\dot{v} = \frac{T_{vac}^{(i)} \sin\theta}{m^{(i)} - k^{(i)}t} - g_e + \varepsilon\left(\frac{-pA_e^{(i)} \sin\theta - D^{(i)} \sin\gamma + L^{(i)} \cos\gamma}{m^{(i)} - k^{(i)}t} \right.$$

$$\left. + g_e - \frac{\mu_e}{r^2} + \frac{u^2}{r} \right) \qquad ; v(t_o) = v_o \; ; \; i = 1, \; 2$$

$$\dot{u} = \frac{T_{vac}^{(i)} \cos\theta}{m^{(i)} - k^{(i)}t} + \varepsilon\left(\frac{-pA_e^{(i)} \cos\theta - D^{(i)} \cos\gamma - L^{(i)} \sin\gamma}{m^{(i)} - k^{(i)}t} - \frac{uv}{r} \right) ; \; u(t_o) = u_o$$

$$\dot{r} = v \qquad ; r(t_o) = r_o \tag{3.34}$$

where

$$m^{(1)} = m_o + k^{(1)}t_o \quad ; m^{(2)} = m_s + k^{(2)}t_s$$

$$v = V\sin\gamma \quad ; u = V\cos\gamma \quad ; \theta = \alpha + \gamma \tag{3.35}$$

Here ε has been artificially introduced as an arbitrary bookkeeping parameter. The dynamics are expressed in a rectangular coordinate system to facilitate the closed form derivation of the zero order solution. The state variables v and u are the local vertical and horizontal velocity components. The control variable is θ, the thrust-vector angle measured from the local horizon.

The necessary conditions of optimality for the above formulation are:

$$\dot{\lambda}_v = -\lambda_r + \varepsilon\left(-\lambda_v\frac{\partial g_1}{\partial v} - \lambda_u\frac{\partial g_2}{\partial v}\right)$$

$$\dot{\lambda}_u = \varepsilon\left(-\lambda_v\frac{\partial g_1}{\partial u} - \lambda_u\frac{\partial g_2}{\partial u}\right)$$

$$\dot{\lambda}_r = \varepsilon\left(-\lambda_v\frac{\partial g_1}{\partial r} - \lambda_u\frac{\partial g_2}{\partial r}\right)$$

$$0 = (\lambda_v\cos\theta - \lambda_u\sin\theta)\frac{T_{vac}^{(i)}}{m^{(i)} - k^{(i)}t} + \varepsilon\left(\lambda_v\frac{\partial g_1}{\partial\theta} + \lambda_u\frac{\partial g_2}{\partial\theta}\right)$$

$$0 = \left\{\lambda_v\dot{v} + \lambda_u\dot{u} + \lambda_r\dot{r}\right\}\Big|_{t_f} - 1 \tag{3.36}$$

where the last two are the optimality and the transversality conditions respectively, and

$$g_1 = \frac{-pA_e^{(i)}\sin\theta - D^{(i)}\sin\gamma + L^{(i)}\cos\gamma}{m^{(i)} - k^{(i)}t} + g_e - \frac{\mu_e}{r^2} + \frac{u^2}{r}$$

$$g_2 = \frac{-pA_e^{(i)}\cos\theta - D^{(i)}\cos\gamma - L^{(i)}\sin\gamma}{m^{(i)} - k^{(i)}t} - \frac{uv}{r} \tag{3.37}$$

Zero order solution

Setting $\varepsilon = 0$, the costate solutions and the optimal control are given as follows (with some license taken with the zero order time notation):

$$\lambda_{v0}(t) = c_{v0} - c_{r0}t \quad ; \lambda_{u0}(t) = c_{u0} \quad ; \lambda_{r0}(t) = c_{r0}$$

$$\tan(\theta_0(t)) = p = qt \quad ; p = c_{v0} / c_{u0} \quad ; q = c_{r0} / c_{u0} \tag{3.38}$$

The control satisfies a linear tangent law. Substituting Eq. 3.38 into Eq. 3.36, the state equations can be integrated in closed form. The solution that relates the states at $t \geq t_s$ to the initial conditions is presented below and for $t < t_s$, the terms involving variables with superscript (1) would simply be deleted.

$$v_0(t) = v_o - g_e(t-t_o) + \frac{T_{vac}^{(1)}}{k^{(1)}} G(m^{(1)},k^{(1)},\tau)\Big|_{\tau=t_o}^{\tau=t_s} + \frac{T_{vac}^{(2)}}{k^{(2)}} G(m^{(2)},k^{(2)},\tau)\Big|_{\tau=t_s}^{\tau=t}$$

$$u_0(t) = u_o + \frac{T_{vac}^{(1)}}{k^{(1)}} F(m^{(1)},k^{(1)},\tau)\Big|_{\tau=t_o}^{\tau=t_s} + \frac{T_{vac}^{(2)}}{k^{(2)}} F(m^{(2)},k^{(2)},\tau)\Big|_{\tau=t_s}^{\tau=t}$$

$$r_0(t) = r_o + v_o(t-t_o) - \frac{1}{2} g_e(t-t_o)^2 - (t-t_o)\frac{T_{vac}^{(1)}}{k^{(1)}} G(m^{(1)},k^{(1)},t_o) -$$
$$(t-t_s)\left\{\frac{T_{vac}^{(2)}}{k^{(2)}} G(m^{(2)},k^{(2)},t_s) - \frac{T_{vac}^{(1)}}{k^{(1)}} G(m^{(1)},k^{(1)},t_s)\right\} +$$
$$\frac{T_{vac}^{(1)}}{qk^{(1)}} K(m^{(1)},k^{(1)},\tau)\Big|_{\tau=t_o}^{\tau=t_s} + \frac{T_{vac}^{(2)}}{qk^{(2)}} K(m^{(2)},k^{(2)},\tau)\Big|_{\tau=t_s}^{\tau=t} \quad ; t \geq t_s \tag{3.39}$$

where

$$F(m^{(i)},k^{(i)},\tau) = \frac{-\sinh^{-1}[\tan(\theta_0(\tau)-\eta)]}{\sqrt{1+\Delta^2}} \quad ; \tan\eta = \frac{1}{\Delta} \quad ; \Delta = \frac{qm^{(i)} - pk^{(i)}}{k^{(i)}}$$

$$G(m^{(i)},k^{(i)},\tau) = -\Delta F(m^{(i)},k^{(i)},\tau) - \sinh^{-1}[\tan(\theta_0(\tau))]$$

$$K(m^{(i)},k^{(i)},\tau) = -\sec(\theta_0(\tau)) - [\tan(\theta_0(\tau)) + \Delta] G(m^{(i)},k^{(i)},\tau) \tag{3.40}$$

To solve for the solution, Eqs. 3.38 - 3.40 are evaluated at the zero order final time $t_{f0} = t_o + t_s + T_0$ where T_0 represents the zero order, second stage, open flight time, and used to enforce the zero order expansion of the terminal boundary conditions and the transversality condition given below:

$$v(t_{f0}) = v_f \quad ; u(t_{f0}) = u_f \quad ; r(t_{f0}) = h_f + r_e$$

$$\left\{\lambda_{v0}\left(\frac{T_{vac}^{(2)} \sin\theta}{m^{(2)} - k^{(2)}t} - g_e\right) + \lambda_{u0} \frac{T_{vac}^{(2)} \cos\theta}{m^{(2)} - k^{(2)}t} + \lambda_{r0} v_0\right\}\Big|_{t_{f0}} = 1 \tag{3.41}$$

There is a total of four unknowns c_{v0}, c_{u0}, c_{r0}, T_0 to be evaluated by the four conditions in Eq. 3.41.

First order solution

Using Eqs. 3.29 to 3.31, the first order correction dynamics for the launch vehicle problem become

$$\frac{d}{dt}\begin{bmatrix} v_1 \\ u_1 \\ r_1 \\ \lambda_{v1} \\ \lambda_{u1} \\ \lambda_{r1} \end{bmatrix} = \begin{bmatrix} 0 & 0 & 0 & a_{14}^{(i)} & a_{15}^{(i)} & 0 \\ 0 & 0 & 0 & a_{24}^{(i)} & a_{25}^{(i)} & 0 \\ 1 & 0 & 0 & 0 & 0 & 0 \\ 0 & 0 & 0 & 0 & 0 & -1 \\ 0 & 0 & 0 & 0 & 0 & 0 \\ 0 & 0 & 0 & 0 & 0 & 0 \end{bmatrix} \begin{bmatrix} v_1 \\ u_1 \\ r_1 \\ \lambda_{v1} \\ \lambda_{u1} \\ \lambda_{r1} \end{bmatrix} + \frac{T_1}{T_0} \begin{bmatrix} c_1^{(i)}(t) \\ c_2^{(i)}(t) \\ v_0(t) \\ -\lambda_{r0} \\ 0 \\ 0 \end{bmatrix} + \begin{bmatrix} p_1^{(i)}(t) \\ p_2^{(i)}(t) \\ 0 \\ p_4^{(i)}(t) \\ p_5^{(i)}(t) \\ p_6^{(i)}(t) \end{bmatrix} \tag{3.42}$$

with $v_1(t_o) = u_1(t_o) = r_1(t_o) = v_1(t_{f0}) = u_1(t_{f0}) = r_1(t_{f0}) = 0$, where

$$a_{14} = \frac{T_{vac}^{(i)}}{m^{(i)} - k^{(i)}t}\left(\frac{\cos^2\theta}{\lambda_{v0}\sin\theta_0 + \lambda_{u0}\cos\theta_0}\right)$$

$$a_{15} = \frac{T_{vac}^{(i)}}{m^{(i)} - k^{(i)}t}\left(\frac{-\cos\theta_0\sin\theta_0}{\lambda_{v0}\sin\theta_0 + \lambda_{u0}\cos\theta_0}\right)$$

$$a_{24} = a_{15} \quad ; a_{25} = \frac{T_{vac}^{(i)}}{m^{(i)} - k^{(i)}t}\left(\frac{\sin^2\theta}{\lambda_{v0}\sin\theta_0 + \lambda_{u0}\cos\theta_0}\right)$$

$$c_1 = \frac{T_{vac}^{(2)}\sin\theta_0}{m^{(2)} - k^{(2)}t}\left[1 + \frac{k^{(2)}(t - t_s)}{m^{(2)} - k^{(2)}t}\right] - g_e \; ; \; c_2 = \frac{T_{vac}^{(2)}\cos\theta_0}{m^{(2)} - k^{(2)}t}\left[1 + \frac{k^{(2)}(t - t_s)}{m^{(2)} - k^{(2)}t}\right]$$

$$p_1 = g_1 - \frac{T_{vac}^{(i)}\cos\theta}{(m^{(i)} - k^{(i)}t)(\lambda_v\sin\theta + \lambda_u\cos\theta)}\left\{\lambda_v\frac{\partial g_1}{\partial\theta} + \lambda_u\frac{\partial g_2}{\partial\theta}\right\}$$

$$p_2 = g_2 + \frac{T_{vac}^{(i)}\sin\theta}{(m^{(i)} - k^{(i)}t)(\lambda_v\sin\theta + \lambda_u\cos\theta)}\left\{\lambda_v\frac{\partial g_1}{\partial\theta} + \lambda_u\frac{\partial g_2}{\partial\theta}\right\}$$

$$p_4 = -\lambda_v\frac{\partial g_1}{\partial v} - \lambda_u\frac{\partial g_2}{\partial v} \qquad ; p_5 = -\lambda_v\frac{\partial g_1}{\partial u} - \lambda_u\frac{\partial g_2}{\partial u}$$

$$p_6 = -\lambda_v\frac{\partial g_1}{\partial r} - \lambda_u\frac{\partial g_2}{\partial r} \tag{3.43}$$

All the variables are evaluated along the zero order solution. Since the first stage flight time is assumed to be fixed, $T = t_f - t_s$. Consequently, $T_1 = 0$ for the dynamics describing $t < t_s$, and the second term in Eq. 3.42 is discarded for the correction dynamics corresponding to this time interval. In this example, the state transition matrix has a structure of

$$\Omega_A^{(i)}(t_2,t_1) = \begin{bmatrix} 1 & 0 & 0 & \omega_{14}^{(i)} & \omega_{15}^{(i)} & \omega_{16}^{(i)} \\ 0 & 1 & 0 & \omega_{24}^{(i)} & \omega_{25}^{(i)} & \omega_{26}^{(i)} \\ t_2 - t_1 & 0 & 1 & \omega_{34}^{(i)} & \omega_{35}^{(i)} & \omega_{36}^{(i)} \\ 0 & 0 & 0 & 1 & 0 & t_1 - t_2 \\ 0 & 0 & 0 & 0 & 1 & 0 \\ 0 & 0 & 0 & 0 & 0 & 1 \end{bmatrix} \tag{3.44}$$

Complete expression of the ω's are given in Appendix B, and the expansion of the transversality condition for the first order case is

$$0 = \left\{ \lambda_{v1}\left(\frac{T_{vac}^{(2)}\sin\theta_0}{m^{(2)} - k^{(2)}t} - g_e + g_{10}\right) + \lambda_{u1}\left(\frac{T_{vac}^{(2)}\cos\theta_0}{m^{(2)} - k^{(2)}t} + g_{20}\right) + T_1 \frac{T_{vac}^{(2)} k^{(2)}}{(m^{(2)} - k^{(2)}t)^2}(\lambda_{v0}\sin\theta_0 + \lambda_{u0}\cos\theta_0) \right\} \Bigg|_{t = t_{f0}} \tag{3.45}$$

From Eq. 3.33, the first order variables at t_{f0} are related to their initial values at t_o by

$$\begin{bmatrix} x_1(t_{f0}) \\ \lambda_1(t_{f0}) \end{bmatrix} = \Omega_A^{(2)}(t_{f0},t_s)\left\{ \Omega_A^{(1)}(t_{f0},t_s)\begin{bmatrix} x_1(t_o) \\ \lambda_1(t_o) \end{bmatrix} + \int_{t_o}^{t_s} \Omega_A^{(1)}(t_s,\tau)\begin{bmatrix} P_{11}^{(1)} \\ P_{21}^{(1)} \end{bmatrix} d\tau \right\} + T_1 \begin{bmatrix} \dot{x}_1^{(2)}(t_{f0}) \\ \dot{\lambda}_1^{(2)}(t_{f0}) \end{bmatrix} + \int_{t_s}^{t_{f0}} \Omega_A^{(2)}(t_{f0},\tau)\begin{bmatrix} P_{11}^{(2)} \\ P_{21}^{(2)} \end{bmatrix} d\tau \tag{3.46}$$

where $x_1 = \{v_1, u_1, r_1\}$, $\lambda_1 = \{\lambda_{v1}, \lambda_{u1}, \lambda_{r1}\}$, $P_{11} = \{p_1, p_2, 0\}$ and $P_{21} = \{p_4, p_5, p_6\}$. Substituting Eq. 3.46 into Eq. 3.45 and using the boundary conditions defined in Eq. 3.42, the unknown costate and final time corrections $\lambda_{v1}(t_o)$, $\lambda_{u1}(t_o)$, $\lambda_{r1}(t_o)$, T_1 can be found from a set of linear algebraic equations.

Figures 3.12 to 3.18 give the zero and first order results for a no-aerodynamic force case (obtained by setting the reference area S = 0). The optimal solution obtained from a multiple shooting code [10] is also included for comparison. As far as spherical Earth and back-pressure effects are concerned, the regular perturbation approach produces very accurate results, especially in the state histories. Next the aerodynamic effect is included,

the resulting angle of attack profile is shown in Fig. 3.19. No reasonable first order solution is found at low altitudes in the region of high dynamic pressure and aerodynamic forces. The first order solution over-corrects the zero order result and gives a very large value of angle of attack that is not considered feasible. The conclusion that is drawn from these results has been that the aerodynamic forces are simply too large to be ignored in the zero order solution. Figure 3.20 show the ratios of the aerodynamic forces to the thrust components along the optimal solution. The magnitude of lift to thrust ratio reaches almost 40% over some time interval during the first stage flight and indicates that a significant amount of aerodynamics effects exist in the ALS vehicle.

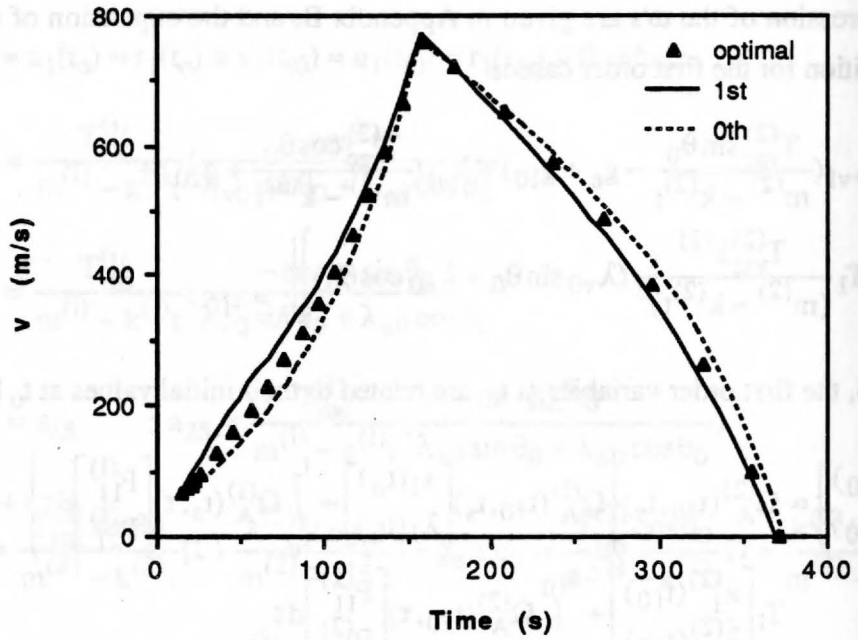

Figure 3.12. Regular Perturbation Results in v with Spherical Earth and Back-pressure Effects.

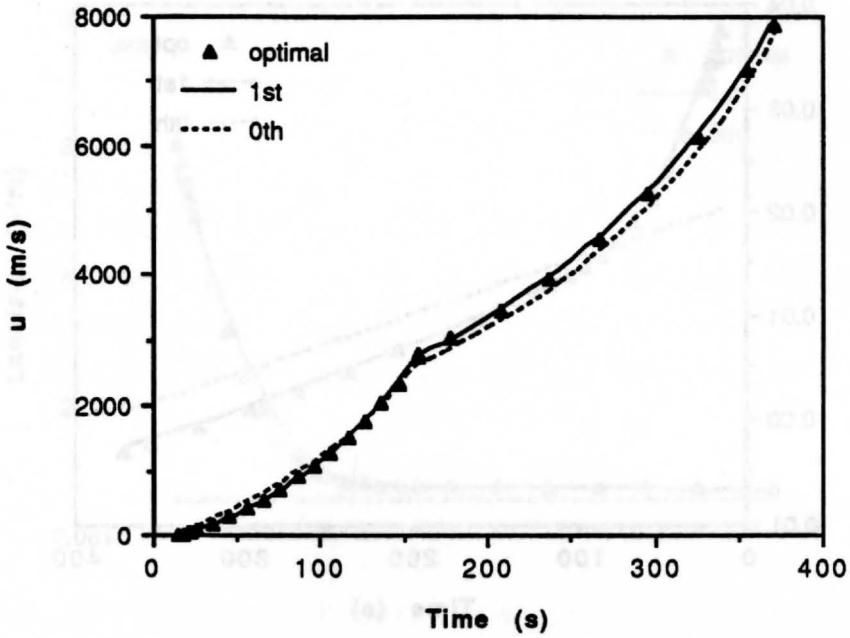

Figure 3.13. Regular Perturbation Results in u with Spherical Earth and Back-pressure Effects.

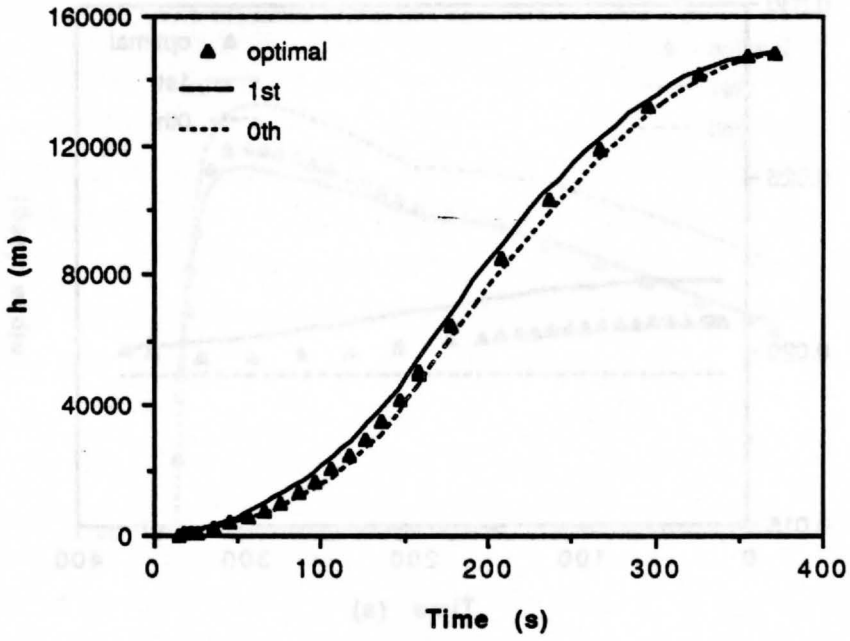

Figure 3.14. Regular Perturbation Results in h with Spherical Earth and Back-pressure Effects.

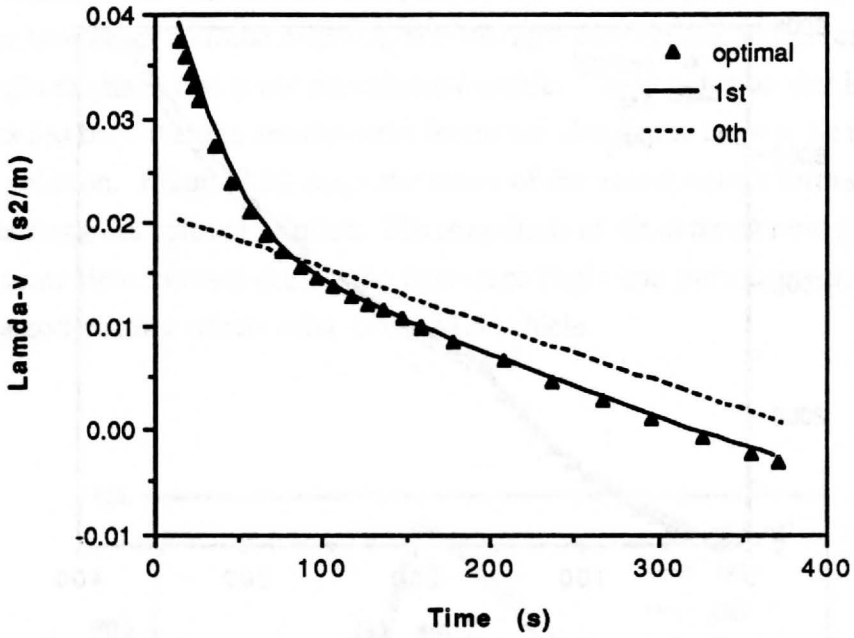

Figure 3.15. Regular Perturbation Results in λ_v with Spherical Earth and Back-pressure Effects.

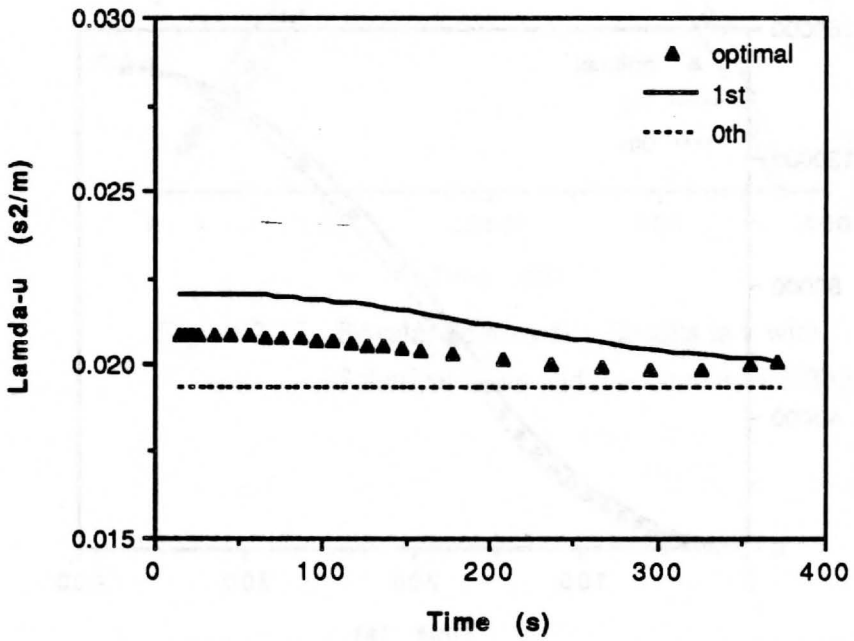

Figure 3.16. Regular Perturbation Results in λ_u with Spherical Earth and Back-pressure Effects.

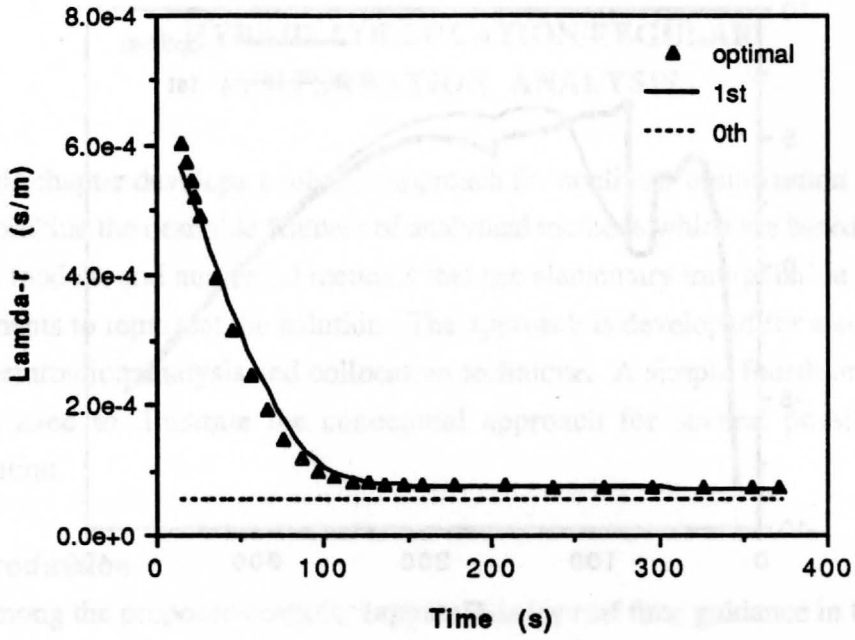

Figure 3.17. Regular Perturbation Results in λ_r with Spherical Earth and Back-pressure Effects.

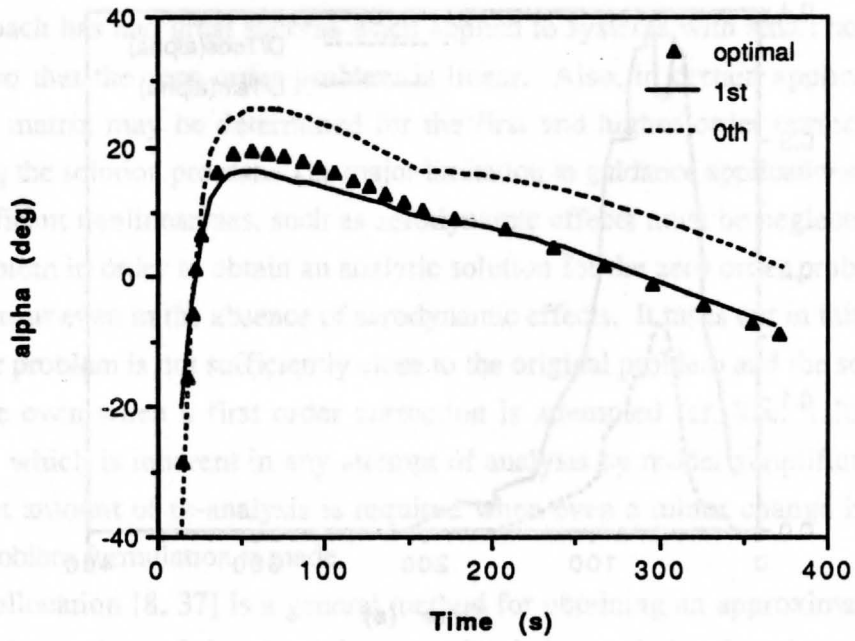

Figure 3.18. Regular Perturbation Results in α with Spherical Earth and Back-pressure Effects.

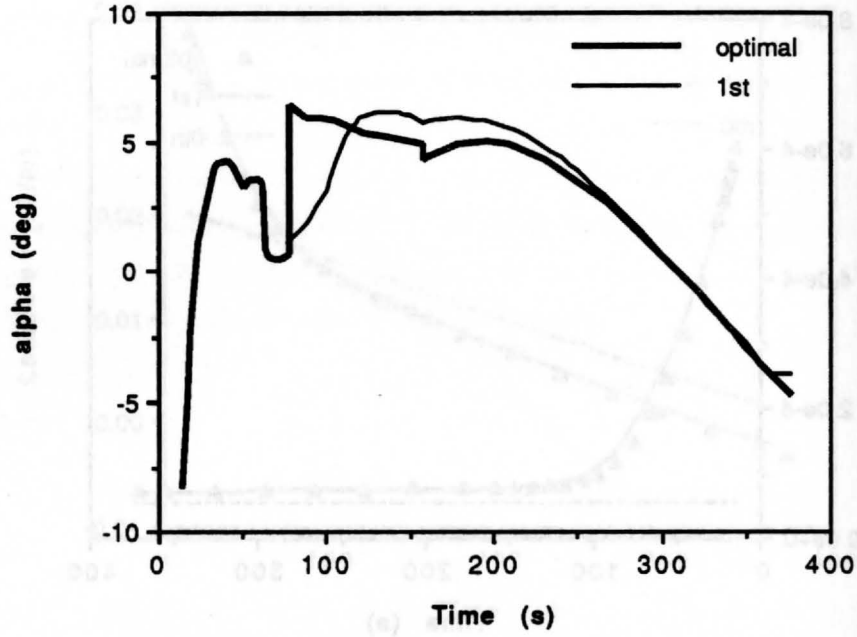

Figure 3.19. Regular Perturbation Results in α Including Aerodynamic Effects.

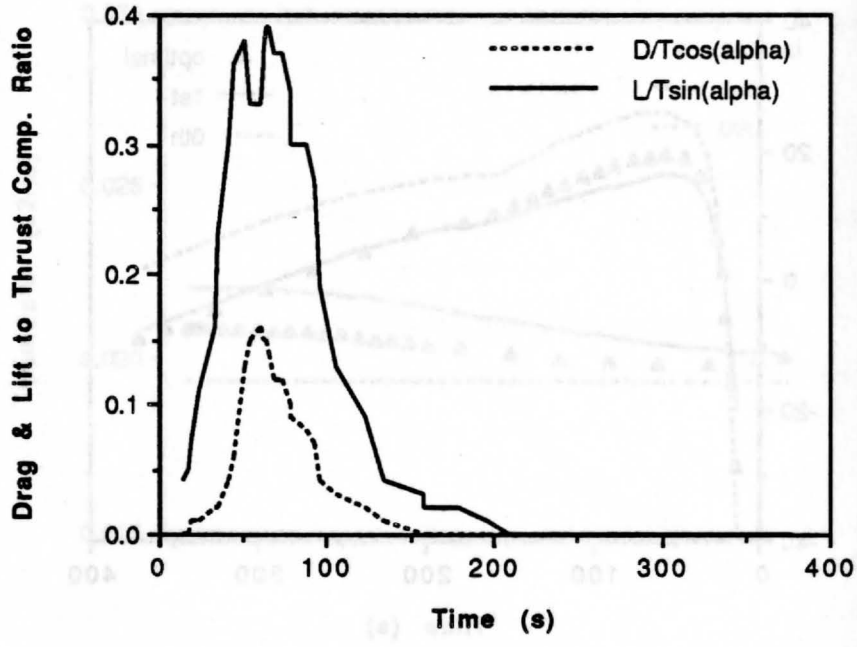

Figure 3.20. Aerodynamic to Propulsive Force Ratios Along the Optimal Trajectory.

SECTION IV

A HYBRID COLLOCATION/REGULAR PERTURBATION ANALYSIS

This chapter develops a solution approach for nonlinear optimization problems that seeks to combine the desirable features of analytical methods which are based on the use of simplified models, and numerical methods that use elementary interpolation functions and finite elements to represent the solution. The approach is developed for a combination of regular perturbation analysis and collocation technique. A simple fourth order nonlinear system is used to illustrate the conceptual approach for several possible levels of approximation.

4.1 Introduction

Among the proposed analytical approaches for real time guidance in Chapter 3, the analysis by regular perturbation expansion of the solution is most appealing. However, crucial to the success of the method is that the optimal solution is reasonably approximated by the zero order solution, so that the addition of first or higher order corrections to the series solution (which usually is not convergent) results in an improvement in accuracy. The approach has had great success when applied to systems with small nonlinear terms [35, 36] so that the zero order problem is linear. Also, in certain applications a state transition matrix may be determined for the first and higher order corrections, further facilitating the solution process. The major limitation in guidance applications appears to be that significant nonlinearities, such as aerodynamic effects must be neglected in the zero order problem in order to obtain an analytic solution for the zero order problem, which is also nonlinear even in the absence of aerodynamic effects. It turns out in this case that the zero order problem is not sufficiently close to the original problem and the solution begins to diverge even when a first order correction is attempted (cf. Sec. 3.2b). A second drawback which is inherent in any attempt of analysis by model simplification is that a significant amount of re-analysis is required when even a minor change in the optimal control problem formulation is made.

Collocation [8, 37] is a general method for obtaining an approximate solution of differential equations. It involves choosing simple interpolating functions and enforcing the interpolatory constraints at specific points within finite elements to evaluate the unknown coefficients. Thus when applied to an optimal control problem, it reduces the associated two point boundary value problem to a set of coupled nonlinear algebraic equat-

ions. Collocation methods have the advantages that they are simple to use for a wide variety of optimization problems, and their accuracy can be improved by increasing the number of elements used in the approximation. The major disadvantages are that there is no general guarantee that the numerical methods employed will successfully solve the nonlinear programming problem under all circumstances, and the dimension of the problem increases proportionately with the number of elements.

It is apparent from the above discussion that the advantages of analytical and numerical methods are in many respects complementary in the sense that if the advantages can be combined in some way, then most of the important disadvantages (from the viewpoint of real time applications) can be reduced. In this chapter, two of possibly many ways to obtain such a hybrid methodology are presented, with the potential for use in the development of real time optimal guidance algorithms. The first approach uses the method of regular expansion to improve upon a collocation solution, thereby reducing the error for a given number of elements. The second approach improves upon the first by using both regular expansion and analytical methods to identify more intelligent interpolating functions in the collocation method, again with the objective of improving the level of accuracy without increasing the number of elements.

4.2 The Method of Collocation

Collocation is a method for constructing an approximate solution to a set of differential equations by using finite elements of polynomials or simple analytic interpolating functions. The unknown coefficients are determined by enforcing continuity at the nodes and that the time derivatives of the interpolating functions satisfy the differential equations at some specified points within each element. We consider an optimization problem with unperturbed (ie. $g(x, u, t) = 0$) dynamics $dx/dt = f(x, u, t)$ and Hamiltonian $H = \lambda^T f$. For simplicity, assume a first order polynomial approximation where the derivative constraints are enforced at the mid point of each element. These constraints can be expressed as:

$$p_j = \frac{x_j - x_{j-1}}{\hat{t}_j - \hat{t}_{j-1}} = \left.\frac{\partial H}{\partial \lambda}\right|_{\hat{t}=(\hat{t}_j+\hat{t}_{j-1})/2\ ;\ x=(x_j+x_{j-1})/2\ ;\ \lambda=(\lambda_j+\lambda_{j-1})/2}$$

$$q_j = \frac{\lambda_j - \lambda_{j-1}}{\hat{t}_j - \hat{t}_{j-1}} = -\left.\frac{\partial H}{\partial x}\right|_{\hat{t}=(\hat{t}_j+\hat{t}_{j-1})/2\ ;\ x=(x_j+x_{j-1})/2\ ;\ \lambda=(\lambda_j+\lambda_{j-1})/2}$$

$$x(\hat{t}) = x_{j-1} + p_j(\hat{t} - \hat{t}_{j-1}) \qquad ; j = 1, \ldots, N$$

$$\lambda(\hat{t}) = \lambda_{j-1} + q_j(\hat{t} - \hat{t}_{j-1}) \qquad ; \hat{t} \in [\hat{t}_{j-1}, \hat{t}_j]\ ;\ \hat{t}_0 = t_o\ ;\ \hat{t}_N = t_o + T_0 \qquad (4.1)$$

where N is the number of elements. The control is assumed to have been eliminated using the optimality condition. In practice, it is more convenient to directly evaluate the nodal values $(x_0, \lambda_0, ..., x_N, \lambda_N)$ rather than finding the coefficients of the interpolating functions. Though higher order polynomials such as Hermite's cubic are generally preferred (because of their smoothness properties), we consider a first order representation to simplify the presentation, although the approach applies equally well for higher order representations.

4.3 Regular Perturbation Formulation

A regular perturbation formulation may be introduced by rewriting the actual dynamics in the following form:

$$\dot{x} = p_j + \varepsilon(H_\lambda - p_j)$$

$$\dot{\lambda} = q_j + \varepsilon(-H_x - q_j)$$

$$H_u = 0 \qquad ; \hat{t} \in [\hat{t}_{j-1}, \hat{t}_j] \tag{4.2}$$

Note that ε has again been introduced as a bookkeeping parameter. The justification for this step is that if the collocation solution alone accurately approximates the true solution, then the second terms in Eq. 4.2 may be regarded as having a small perturbing effects on the state and costate derivatives, which is actually zero at the mid points of the elements. If the control cannot be eliminated explicitly in the collocation formulation in Eq. 4.1, then an analytic portion $\Pi(u, x, \lambda)$ of the optimality condition (for which it is possible to eliminate u) can be extracted such that

$$0 = \Pi + \varepsilon(H_u - \Pi) \tag{4.3}$$

Note that in the above equations H is the Hamiltonian corresponding to the original system without a perturbation parameter. As presented above, a collocation solution may be viewed as the zero order solution for the regular perturbation problem formulated in Eq. 4.2. Also, as will be shown by example in the next section, more intelligent choices of interpolating functions can be identified from the necessary conditions, by utilizing to the extent possible the analytically tractable portions of the solution. This results in a significant decrease in the computational requirements for a given level of accuracy.

Now we can apply the perturbation technique described in the Section 3.2 to improve the approximate zero order solution from collocation. For the higher order problems defined in Eqs. 3.29 - 3.31, we have:

$$A_{11_j} = \frac{\partial p_j}{\partial x} = \frac{\partial^2 H}{\partial x \partial \lambda}\bigg|_{\hat{t}=(\hat{t}_j+\hat{t}_{j-1})/2\ ;\ x=(x_j+x_{j-1})/2\ ;\ \lambda=(\lambda_j+\lambda_{j-1})/2}$$

$$A_{12_j} = \frac{\partial p_j}{\partial \lambda} = \frac{\partial^2 H}{\partial^2 \lambda}\bigg|_{\hat{t}=(\hat{t}_j+\hat{t}_{j-1})/2\ ;\ x=(x_j+x_{j-1})/2\ ;\ \lambda=(\lambda_j+\lambda_{j-1})/2}$$

$$A_{21_j} = \frac{\partial q_j}{\partial x} = -\frac{\partial^2 H}{\partial^2 x}\bigg|_{\hat{t}=(\hat{t}_j+\hat{t}_{j-1})/2\ ;\ x=(x_j+x_{j-1})/2\ ;\ \lambda=(\lambda_j+\lambda_{j-1})/2}$$

$$A_{22_j} = \frac{\partial q_j}{\partial \lambda} = -\frac{\partial^2 H}{\partial \lambda \partial x}\bigg|_{\hat{t}=(\hat{t}_j+\hat{t}_{j-1})/2\ ;\ x=(x_j+x_{j-1})/2\ ;\ \lambda=(\lambda_j+\lambda_{j-1})/2}$$

$$C_{1_j} = p_j + (\hat{t} - \hat{t}_{j-1})p_{t_j}$$

$$= \{\frac{\partial H}{\partial \lambda} + (\hat{t} - \hat{t}_{j-1})\frac{\partial^2 H}{\partial t \partial \lambda}\}\bigg|_{\hat{t}=(\hat{t}_j+\hat{t}_{j-1})/2\ ;\ x=(x_j+x_{j-1})/2\ ;\ \lambda=(\lambda_j+\lambda_{j-1})/2}$$

$$C_{2_j} = q_j + (\hat{t} - \hat{t}_{j-1})q_{t_j}$$

$$= \{-\frac{\partial H}{\partial x} - (\hat{t} - \hat{t}_{j-1})\frac{\partial^2 H}{\partial t \partial x}\}\bigg|_{\hat{t}=(\hat{t}_j+\hat{t}_{j-1})/2\ ;\ x=(x_j+x_{j-1})/2\ ;\ \lambda=(\lambda_j+\lambda_{j-1})/2} \qquad (4.4)$$

and for k = 1,

$$P_{11_j} = \frac{\partial H}{\partial \lambda}\bigg|_{\hat{t}\ ;\ x=x_{j-1}+p_j(\hat{t}-\hat{t}_{j-1})\ ;\ \lambda=\lambda_{j-1}+q_j(\hat{t}-\hat{t}_{j-1})} - p_j$$

$$P_{21_j} = -\frac{\partial H}{\partial x}\bigg|_{\hat{t}\ ;\ x=x_{j-1}+p_j(\hat{t}-\hat{t}_{j-1})\ ;\ \lambda=\lambda_{j-1}+q_j(\hat{t}-\hat{t}_{j-1})} - q_j \qquad (4.5)$$

where all the terms in Eq. 4.4 are constant* within an element, and are evaluated using the collocation solution. The matrix A_j is simply the perturbation of the original state and costate dynamics evaluated at the constraint point of each element. The expression in Eq. 3.32, which now corresponds to a piecewise constant system matrix A_j, can be written as

$$\begin{bmatrix} x_k(\hat{t}) \\ \lambda_k(\hat{t}) \end{bmatrix} = \Omega_A(\hat{t}, t_o)\begin{bmatrix} x_k(t_o) \\ \lambda_k(t_o) \end{bmatrix} + \frac{T_k}{T_0}\int_{t_o}^{\hat{t}} \Omega_A(\hat{t}, \tau)\begin{bmatrix} C_1 \\ C_2 \end{bmatrix} d\tau + \int_{t_o}^{\hat{t}} \Omega_A(\hat{t}, \tau)\begin{bmatrix} P_{1k} \\ P_{2k} \end{bmatrix} d\tau \qquad (4.6)$$

* If higher order interpolating polynomials are chosen, the dynamical system will be a time varying matrix polynomial with piecewise constant coefficients.

and for a constant system matrix A_j, it can be written as

$$\begin{bmatrix} x_k(\hat{t}) \\ \lambda_k(\hat{t}) \end{bmatrix} = \Omega_{A_j}(\hat{t},\hat{t}_{j-1}) \begin{bmatrix} x_k(\hat{t}_{j-1}) \\ \lambda_k(\hat{t}_{j-1}) \end{bmatrix} + \frac{T_k}{T_0} \Omega_{A_j}(\hat{t},\hat{t}_{j-1}) A_j^{-1} \left(\begin{bmatrix} p_j \\ q_j \end{bmatrix} + (\hat{t} - \hat{t}_{j-1}) \begin{bmatrix} p_{t_j} \\ q_{t_j} \end{bmatrix} \right.$$

$$\left. + A_j^{-1} \begin{bmatrix} p_{t_j} \\ q_{t_j} \end{bmatrix} \right) + \int_{\hat{t}_{j-1}}^{\hat{t}} \Omega_{A_j}(\hat{t},\tau) \begin{bmatrix} P_{1k}(\tau) \\ P_{2k}(\tau) \end{bmatrix} d\tau \; ; \; \hat{t} \in [\hat{t}_j, \hat{t}_{j-1}] \qquad (4.7)$$

where Ω_{A_j} is the state transition matrix and p_{t_j}, q_{t_j} are defined as in Eq. 4.4. Note that Ω_{A_j} is not the same as in Eqs. 3.32 and 3.33 because A is defined differently. The state transition matrix here may not have an analytic expression because the zero order solution is not necessarily analytic. If this is true, we can solve Eqs. 4.4 and 4.5 using the sensitivity functions and superposition property of linear systems. This is done by assigning a unit vector for the initial conditions, and numerically integrates the system from t_o to $t_o + T_0$. Thus by changing the position of the non-zero element in the unit vector, the sensitivity functions are obtained. This process can be done in parallel for different unit vector.

In the zero order solution, ε in Eq. 4.2 is set to zero, which means that the standard collocation constraints in Eq. 4.1 are employed and an approximate solution is obtained by solving the algebraic equations. Then first and higher order corrections may be computed by quadrature as explained in the earlier section on regular perturbation.

4.4 A Duffing's Equation Example

This investigation is carried out to demonstrate the hybrid approach outlined in the preceding section. The example is based on Duffing's equation presented in its first order form:

$$\begin{aligned} \dot{x} &= v && ; x(0) = x_o \\ \dot{v} &= -x - ax^3 + u && ; v(0) = v_o \end{aligned} \qquad (4.8)$$

and the objective is to

$$\min_u \left\{ S_x x^2(t_f) + S_v v^2(t_f) + \int_0^{t_f} (1 + \frac{u^2}{2}) dt \right\} \qquad (4.9)$$

with S_x, S_v being the weights on the terminal values and t_f is free. The problem can be converted to the Mayer's form in Eq. 3.17 (if desired) through the usual method of introdu-

cing an additional state equation whose right hand side is the integrand of Eq. 4.9. We investigate the problem in different levels of complexity according to how the dynamics of the full system are treated.

a) Level 0 formulation

This is the degenerate case in which there is an analytic zero order solution, and therefore collocation is not required (solely a regular perturbation approach as discussed in Sec. 3.2). Let $\varepsilon = a$, thus neglecting the hardening effect ax^3 in the original problem. The necessary conditions are:

$$\dot{x} = v \qquad ; x(0) = x_o$$

$$\dot{v} = -x + u - \varepsilon x^3 \qquad ; v(0) = v_o$$

$$\dot{\lambda}_x = \lambda_v + \varepsilon 3\lambda_v x^2 \qquad ; \lambda_x(t_f) = 2S_x x(t_f)$$

$$\dot{\lambda}_v = -\lambda_x \qquad ; \lambda_v(t_f) = 2S_v v(t_f)$$

$$H_u = u + \lambda_v = 0$$

$$\left\{H = \lambda_x v + \lambda_v(-x + u - \varepsilon x^3) + 1 + u^2/2\right\}\Big|_{t_f} = 0 \tag{4.10}$$

The zero order problem ($\varepsilon = 0$) is linear and time invariant, and can easily be solved as

$$\begin{bmatrix} x_0(\hat{t}) \\ v_0(\hat{t}) \\ \lambda_{x0}(\hat{t}) \\ \lambda_{v0}(\hat{t}) \end{bmatrix} = \begin{bmatrix} \cos\bar{t} & \sin\bar{t} & (\sin\bar{t} - \bar{t}\cos\bar{t})/2 & -\bar{t}\sin\bar{t}/2 \\ -\sin\bar{t} & \cos\bar{t} & \bar{t}\sin\bar{t}/2 & -(\sin\bar{t} + \bar{t}\cos\bar{t})/2 \\ 0 & 0 & \cos\bar{t} & \sin\bar{t} \\ 0 & 0 & -\sin\bar{t} & \cos\bar{t} \end{bmatrix} \begin{bmatrix} x_0(\hat{t}_o) \\ v_0(\hat{t}_o) \\ \lambda_{x0}(\hat{t}_o) \\ \lambda_{v0}(\hat{t}_o) \end{bmatrix} \tag{4.11}$$

where

$$\bar{t} = \hat{t} - \hat{t}_o \qquad ; \hat{t}_o, \hat{t} \in [0, T_0] \tag{4.12}$$

The above state transition matrix is also the state transition matrix $\Omega_A(\hat{t}, \hat{t}_o)$ for the higher order correction. Given the boundary conditions of $x_0(0) = x_o$, $v_0(0) = v_o$, $\lambda_{x0}(T_0) = 2S_x x_0(T_0)$, $\lambda_{v0}(T_0) = 2S_v v_0(T_0)$, the remaining unknowns $\lambda_{x0}(0)$, $\lambda_{v0}(0)$, $\lambda_{x0}(T_0)$, $\lambda_{v0}(T_0)$, T_0 can be solved with a Newton's method using Eq. 4.11 and the corresponding transversality condition

$$\left\{H_0 = \lambda_{x0}v_0 - \lambda_{v0}x_0 - \lambda_{v0}^2/2 + 1\right\}\Big|_{T_0} = 0 \tag{4.13}$$

From Eq. 3.29, the differential equations governing the higher order correction dynamics are

$$\frac{d}{d\hat{t}}\begin{bmatrix} x_k \\ v_k \\ \lambda_{xk} \\ \lambda_{vk} \end{bmatrix} = \begin{bmatrix} 0 & 1 & 0 & 0 \\ -1 & 0 & 0 & -1 \\ 0 & 0 & 0 & 1 \\ 0 & 0 & -1 & 0 \end{bmatrix}\begin{bmatrix} x_k \\ v_k \\ \lambda_{xk} \\ \lambda_{vk} \end{bmatrix} + \frac{T_k}{T_0}\begin{bmatrix} v_0(\hat{t}) \\ -x_0(\hat{t}) - \lambda_{v0}(\hat{t}) \\ \lambda_{v0}(\hat{t}) \\ -\lambda_{x0}(\hat{t}) \end{bmatrix} + \begin{bmatrix} P_{1k}(\hat{t}) \\ P_{2k}(\hat{t}) \\ P_{3k}(\hat{t}) \\ P_{4k}(\hat{t}) \end{bmatrix} \tag{4.14}$$

with the boundary conditions

$$x_k(0) = v_k(0) = 0 \; ; \; \lambda_{xk}(T_0) = 2S_x x_k(T_0) \; ; \; \lambda_{vk}(T_0) = 2S_v v_k(T_0) \tag{4.15}$$

In this case, we have for k = 1, 2:

$$P_{11} = 0 \qquad ; P_{21} = -x_0^3 \qquad ; P_{31} = 3\lambda_{v0}x_0^2 \qquad ; P_{41} = 0$$

$$P_{12} = v_1 T_1 / T_0 \qquad ; P_{22} = -(x_1 + \lambda_{v1} + x_0^3)T_1 / T_0 - 3x_0^2 x_1$$

$$P_{32} = (\lambda_{v1} + 3\lambda_{v0}x_0^2)T_1 / T_0 + 3\lambda_{v1}x_0^2 + 3\lambda_{v0}x_0 x_1 \qquad ; P_{42} = -\lambda_{x1}T_1 / T_0 \tag{4.16}$$

and the transversality conditions:

$$\left\{H_1 = \lambda_{x1}v_0 - \lambda_{v1}(x_0 + \lambda_{v0}) + \lambda_{x0}v_1 - \lambda_{v0}(x_1 + x_0^3)\right\}\Big|_{T_0} = 0$$

$$\left\{H_2 = \lambda_{x2}v_0 - \lambda_{v2}(x_0 + \lambda_{v0}) + \lambda_{x0}v_2 + \lambda_{v1}x_1 - 3\lambda_{v0}x_0^2 x_1 \right.$$
$$\left. -\lambda_{v1}(x_1 + \lambda_{v1} + x_0^3) + \lambda_{v1}^2/2\right\}\Big|_{T_0} = 0 \tag{4.17}$$

which are needed to compute the first and second order corrections by quadrature. The results are shown in Figs. 4.1 - 4.4 for $S_x = S_v = 100$, and a = 0.4. The first order state and costate histories are stored and later retrieved by linear interpolation to construct the second order solution. The optimal solution generated using a multiple shooting technique is also included for comparison. These results clearly show that the series is not convergent, and that the most accurate approximation is obtained using a first order solution. If we regard this level of accuracy as insufficient, then the conclusion must be that the nonlinear term (ax^3) is too large to be neglected in the zero order solution.

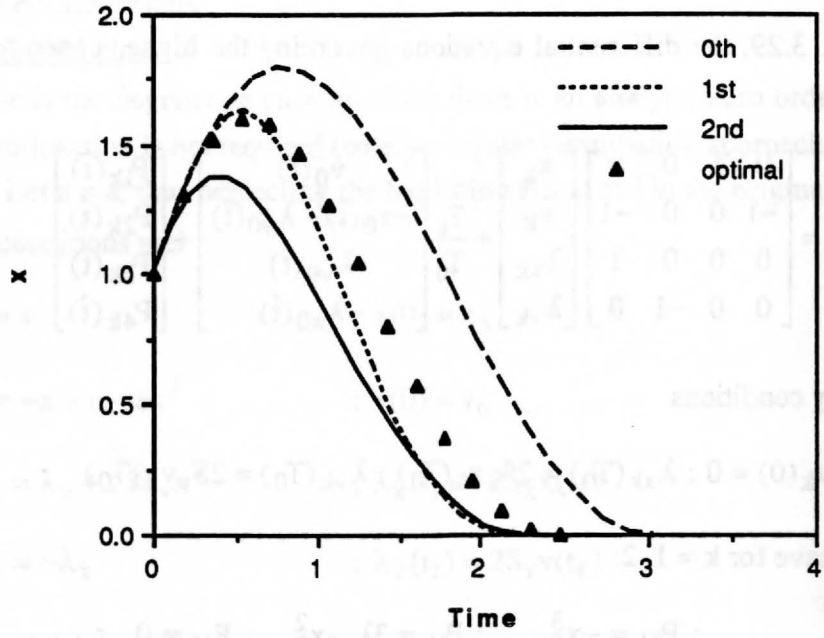

Figure 4.1. Level 0 Result in x.

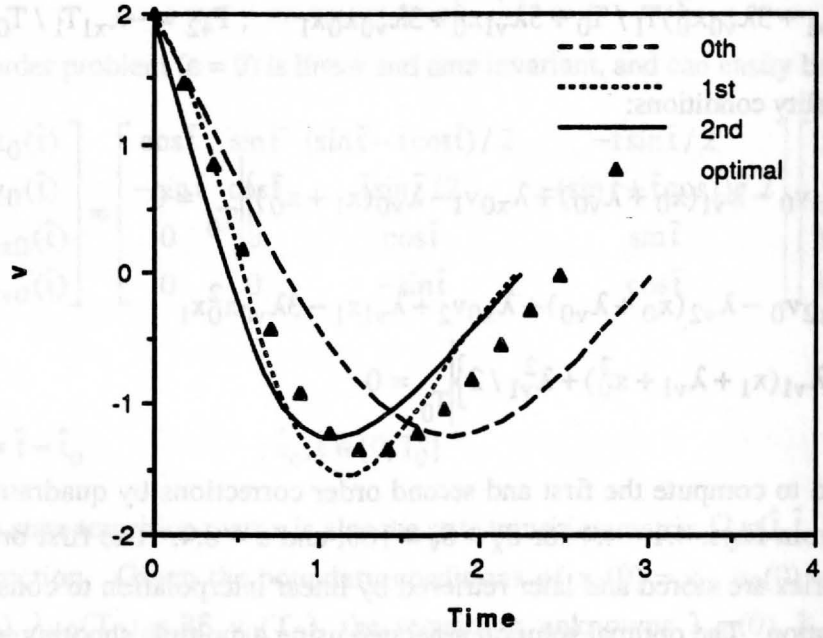

Figure 4.2. Level 0 Result in v.

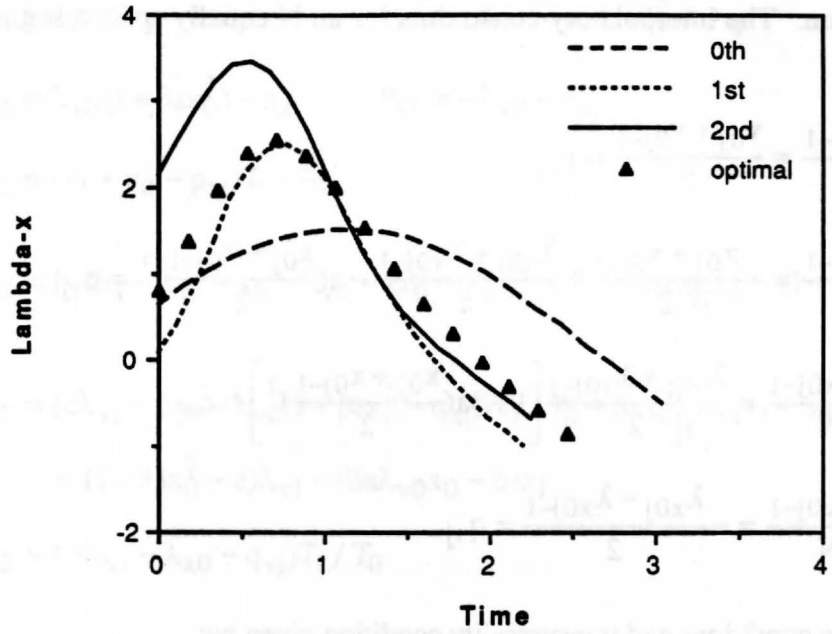

Figure 4.3. Level 0 Result in λ_x.

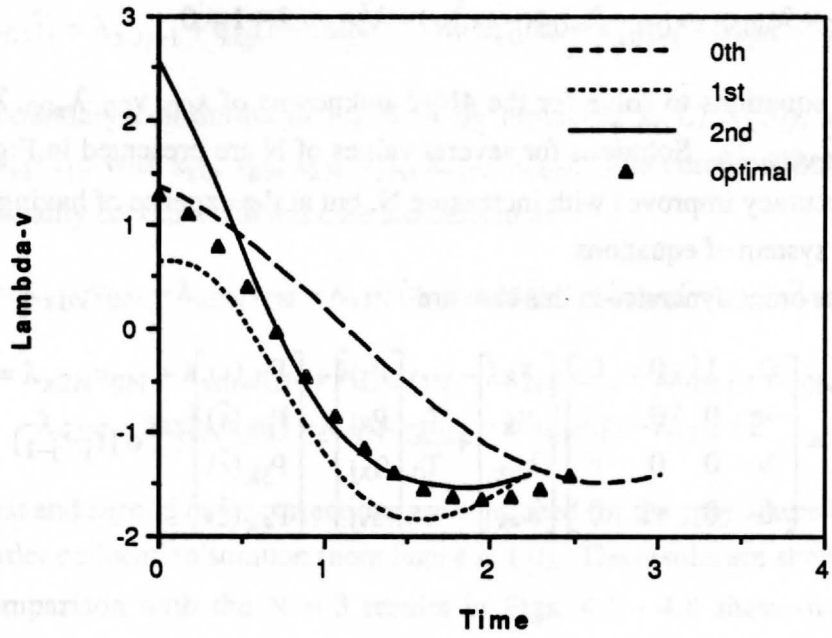

Figure 4.4. Level 0 Result in λ_v.

b) Level 1 formulation

This case illustrates the hybrid approach as outlined in the section on collocation, using a piecewise linear representation to approximate the states and the costates for the zero order solution. The interpolatory constraints for an N equally spaced segmentation are:

$$\frac{x_{0j}-x_{0j-1}}{T_0/N}=\frac{v_{0j}+v_{0j-1}}{2}=p_{xj}$$

$$\frac{v_{0j}-v_{0j-1}}{T_0/N}=-\frac{x_{0j}+x_{0j-1}}{2}-\frac{\lambda_{v0j}+\lambda_{v0j-1}}{2}-a\left(\frac{x_{0j}+x_{0j-1}}{2}\right)^3=p_{vj}$$

$$\frac{\lambda_{x0j}-\lambda_{x0j-1}}{T_0/N}=\frac{\lambda_{v0j}+\lambda_{v0j-1}}{2}\left[1+3a\left(\frac{x_{0j}+x_{0j-1}}{2}\right)^2\right]=q_{xj}$$

$$\frac{\lambda_{v0j}-\lambda_{v0j-1}}{T_0/N}=-\frac{\lambda_{x0j}-\lambda_{x0j-1}}{2}=q_{vj} \qquad (4.18)$$

with the boundary conditions and transversality condition given by:

$$x_{00}=x_o \quad ; v_{00}=v_o \quad ; \lambda_{x0N}=2S_x x_{0N} \quad ; \lambda_{v0N}=2S_v v_{0N}$$

$$\lambda_{x0N}v_{0N}+\lambda_{v0N}(-x_{0N}-\lambda_{v0N}-ax_{0N}^3)+\lambda_{v0N}^2/2+1=0 \qquad (4.19)$$

There are 4N+5 equations to solve for the 4N+5 unknowns of x_{00}, v_{00}, λ_{x00}, λ_{x00}, ... , x_{0N}, v_{0N}, λ_{x0N}, λ_{v0N}, T_0. Solutions for several values of N are presented in Figs. 4.5 to 4.8. Note that accuracy improves with increasing N, but at the expense of having to solve a large nonlinear system of equations.

The higher order dynamics in this case are

$$\frac{d}{d\hat{t}}\begin{bmatrix}x_k\\ v_k\\ \lambda_{xk}\\ \lambda_{vk}\end{bmatrix}=\begin{bmatrix}0 & 1 & 0 & 0\\ -c & 0 & 0 & -1\\ b & 0 & 0 & c\\ 0 & 0 & -1 & 0\end{bmatrix}\begin{bmatrix}x_k\\ v_k\\ \lambda_{xk}\\ \lambda_{vk}\end{bmatrix}+\frac{T_k}{T_0}\begin{bmatrix}p_{xj}\\ p_{vj}\\ q_{xj}\\ q_{vj}\end{bmatrix}+\begin{bmatrix}P_{1k}(\hat{t})\\ P_{2k}(\hat{t})\\ P_{3k}(\hat{t})\\ P_{4k}(\hat{t})\end{bmatrix} \; ; \hat{t}\in[\hat{t}_j,\hat{t}_{j-1}] \qquad (4.20)$$

where

$$c=1+3ax_0^2\Big|_{\bar{t}} \quad ; b=6a(\lambda_{v0}x_0)\Big|_{\bar{t}} \quad ; \bar{t}=(\hat{t}_j+\hat{t}_{j-1})/2 \qquad (4.21)$$

The state transition matrix expression for this case is given in Appendix C. For k = 1, 2, the forcing function terms in Eq. 4.20 are:

$$P_{11} = v_0 - p_{xj} \qquad ; P_{21} = -x_0 - \lambda_{v0} - ax_0^3 - p_{vj}$$

$$P_{31} = \lambda_{v0}(1 + 3ax_0^3) - q_{xj} \qquad ; P_{41} = -\lambda_{x0} - q_{vj}$$

$$P_{12} = (v_1 + v_0 - p_{xj})T_1 / T_0$$

$$P_{22} = \{-cx_1 - \lambda_{v1} - x_0 - \lambda_{v0} - ax_0^3 - p_{vj}\}T_1 / T_0 - 3ax_0\Big|_{\hat{t}} x_1^2 - (1 + 3ax_0^2 - c)x_1$$

$$P_{32} = \{c\lambda_{v1} + bx_1 + \lambda_{v0}(1 + 3ax_0^2 - q_{xj})\}T_1 / T_0 + 6ax_0\Big|_{\hat{t}} \lambda_{v1}x_1 + 3a\lambda_{v0}\Big|_{\hat{t}} x_1^2$$
$$+ (1 + 3ax_0^2 - c)\lambda_{v1} + (6a\lambda_{v0}x_0 - b)x_1$$

$$P_{42} = (-\lambda_{x1} - \lambda_{x0} - q_{vj})T_1 / T_0 \qquad (4.22)$$

where

$$x_0(\hat{t}) = x_{0j-1} + p_{xj}(\hat{t} - \hat{t}_{j-1}) \qquad ; v_0(\hat{t}) = v_{0j-1} + p_{vj}(\hat{t} - \hat{t}_{j-1})$$

$$\lambda_{x0}(\hat{t}) = \lambda_{x0j-1} + q_{xj}(\hat{t} - \hat{t}_{j-1}) \qquad ; \lambda_{v0}(\hat{t}) = \lambda_{v0j-1} + q_{vj}(\hat{t} - \hat{t}_{j-1}) \qquad (4.23)$$

plus the boundary conditions in Eq. 4.14 by replacing $x_k(0)$, $v_k(0)$, $x_k(T_0)$, $v_k(T_0)$, $\lambda_{xk}(T_0)$, $\lambda_{vk}(T_0)$ with x_{k0}, v_{k0}, x_{kN}, v_{kN}, λ_{xkN}, λ_{vkN}. The corresponding expansion of the transversality conditions in this case are defined as

$$0 = \lambda_{x1N}v_{0N} + \lambda_{x0N}v_{1N} - \lambda_{v1N}(x_{0N} + ax_{0N}^3) + \lambda_{v0N}(-x_{1N} - \lambda_{v0N} - ax_{0N}^3)$$

$$0 = \lambda_{x2N}v_{0N} + \lambda_{x0N}v_{2N} + \lambda_{x1N}v_{1N} - \lambda_{v2N}(x_{0N} + ax_{0N}^3) + \lambda_{v0N}(-x_{2N}$$
$$-\lambda_{v2N} - 3ax_{0N}^2x_{2N}) + \lambda_{v1N}(-x_{1N} - 3ax_{0N}^2x_1) - \lambda_{v1N}^2 / 2 \qquad (4.24)$$

First and second order corrections are computed for the case where N = 3 is used in the zero order collocation solution (note here ε is 1.0). The results are shown in Figs. 4.9 - 4.12. Comparison with the N = 3 results in Figs. 4.5 - 4.8 show that a significant improvement in accuracy is achievable without requiring a large number of elements. In Figs. 4.9 - 4.12 the second order solution is indistinguishable from the optimal solution. The discontinuity in slope (which is a consequence of using first order interpolation functions for the collocation solution) is also smoothed as the order of the correction

increases. Contrary to Level 0's results, the second order corrections do not diverge due to the fact that the nonlinear term has been accounted for in the zero order solution.

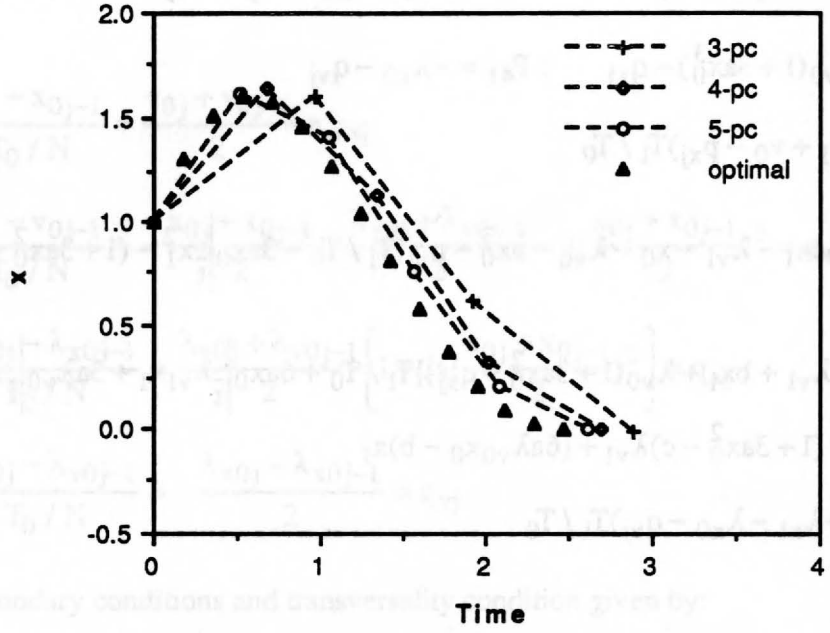

Figure 4.5. Level 1 Zero Order Results in x for Different N.

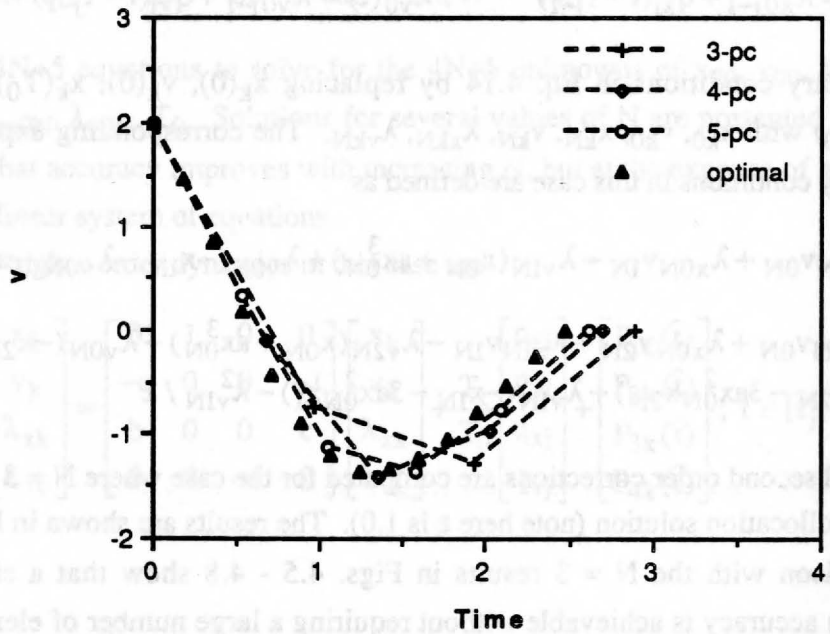

Figure 4.6. Level 1 Zero Order Results in v for Different N.

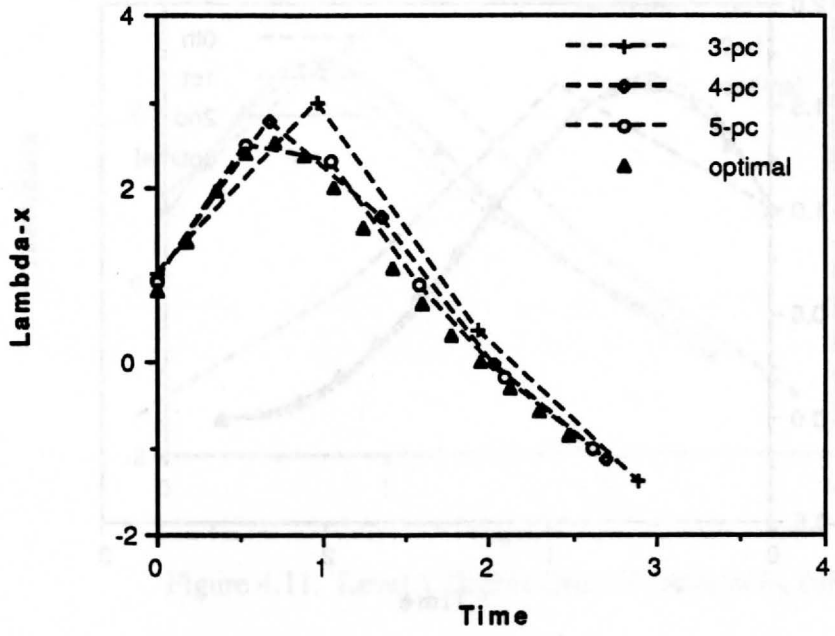

Figure 4.7. Level 1 Zero Order Results in λ_x for Different N.

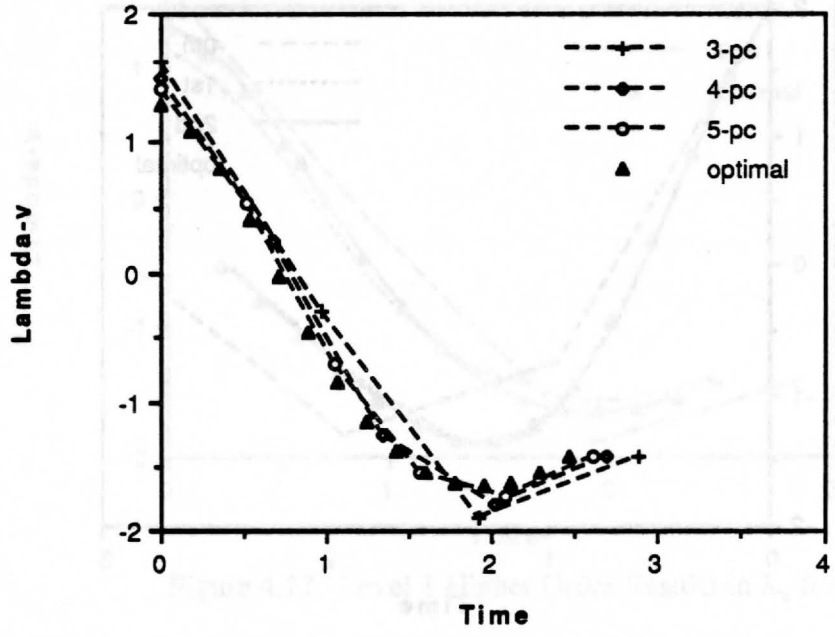

Figure 4.8. Level 1 Zero Order Results in λ_v for Different N.

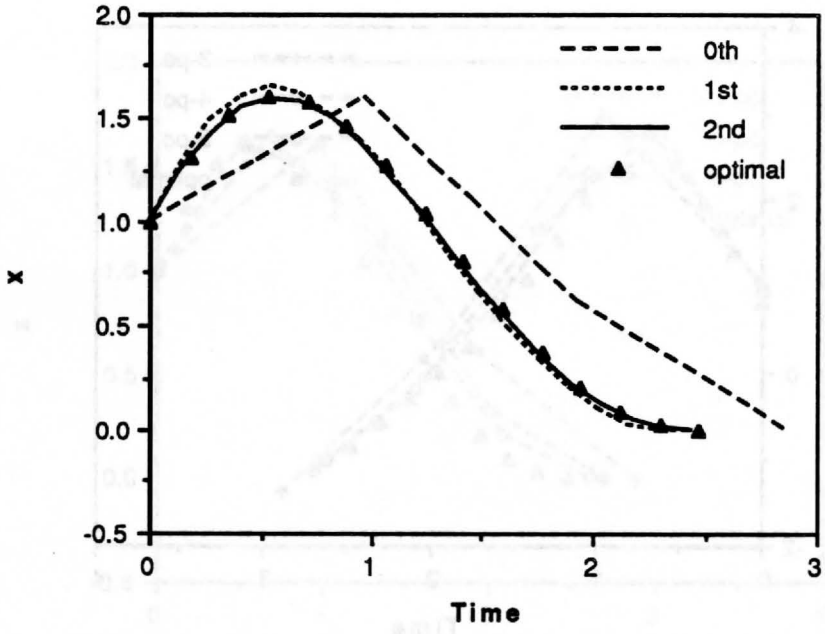

Figure 4.9. Level 1 Higher Order Results in x for N=3.

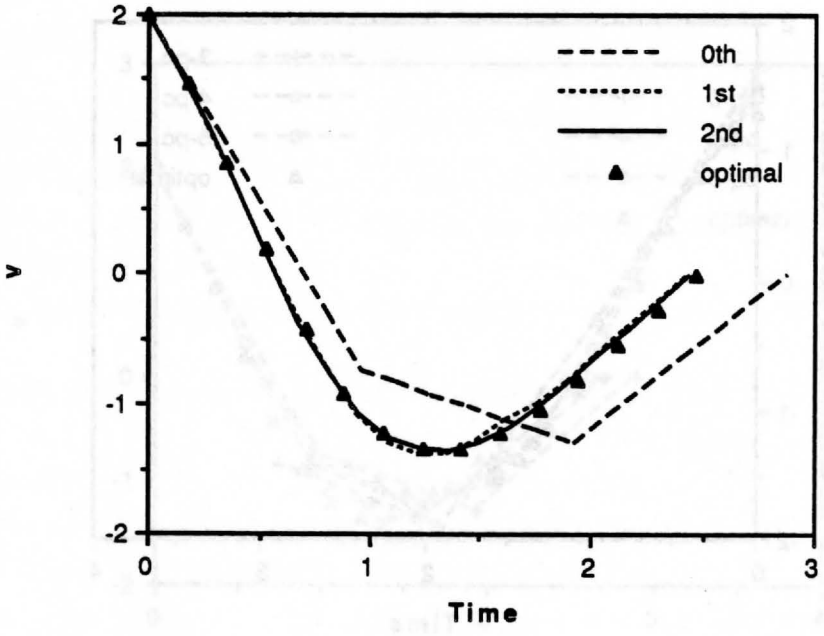

Figure 4.10. Level 1 Higher Order Results in v for N=3.

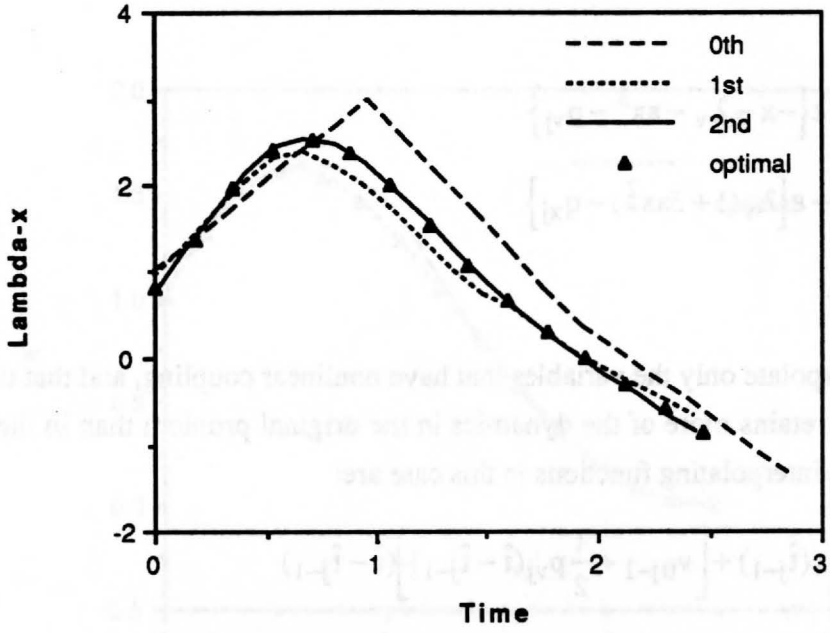

Figure 4.11. Level 1 Higher Order Results in λ_x for N=3.

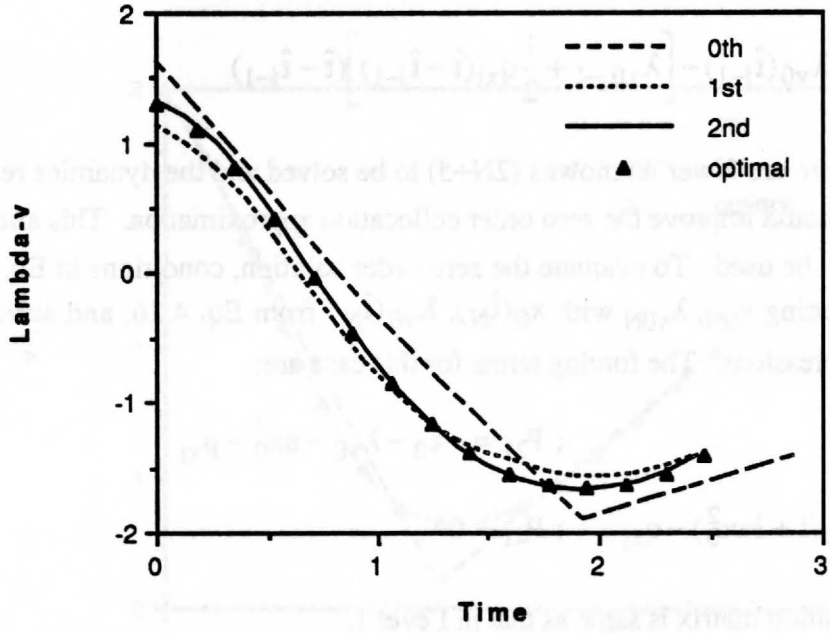

Figure 4.12. Level 1 Higher Order Results in λ_v for N=3.

c) Level 2 formulation

As a second illustration of a hybrid solution approach we retain a portion of the dynamics from the necessary conditions to identify a more intelligent interpolating function for the hybrid Level 1 formulation. Consider the following simple modification of the

regular perturbation formulation for this example:

$$\dot{x} = v$$

$$\dot{v} = p_{vj} + \varepsilon\left\{-x - \lambda_v - ax^3 - p_{vj}\right\}$$

$$\dot{\lambda}_x = q_{xj} + \varepsilon\left\{\lambda_v(1+3ax^2) - q_{xj}\right\}$$

$$\dot{\lambda}_v = -\lambda_x \qquad (4.25)$$

Note that we interpolate only the variables that have nonlinear coupling, and that the resulting interpolation retains more of the dynamics in the original problem than in the Level 1 formulation. The interpolating functions in this case are:

$$x_0(\hat{t}) = x_0(\hat{t}_{j-1}) + \left[v_{0j-1} + \frac{1}{2}p_{vj}(\hat{t} - \hat{t}_{j-1})\right](\hat{t} - \hat{t}_{j-1})$$

$$v_0(\hat{t}) = v_{0j-1} + p_{vj}(\hat{t} - \hat{t}_{j-1})$$

$$\lambda_{x0}(\hat{t}) = \lambda_{x0j-1} + q_{xj}(\hat{t} - \hat{t}_{j-1})$$

$$\lambda_{v0}(\hat{t}) = \lambda_{v0}(\hat{t}_{j-1}) - \left[\lambda_{x0j-1} + \frac{1}{2}q_{xj}(\hat{t} - \hat{t}_{j-1})\right](\hat{t} - \hat{t}_{j-1}) \qquad (4.26)$$

Consequently, there are fewer unknowns (2N+5) to be solved and the dynamics retained in the formulation should improve the zero order collocation approximation. This allows even fewer elements to be used. To evaluate the zero order solution, conditions in Eq. 4.19 are enforced by replacing x_{0N}, λ_{v0N} with $x_0(\hat{t}_N)$, $\lambda_{v0}(\hat{t}_N)$ from Eq. 4.26, and similarly for the first order expressions. The forcing terms for this case are:

$$P_{11} = 0 \qquad ; P_{21} = -x_0 - \lambda_{v0} - ax_0^3 - p_{vj}$$

$$P_{31} = \lambda_{v0}(1+3ax_0^2) - q_{xj} \qquad ; P_{41} = 0 \qquad (4.27)$$

and the state transition matrix is same as that in Level 1.

Figures 4.13 - 4.16 show the zero and first order state solutions for the case N = 2. The results show that the zero order solution is dramatically improved especially in the state variables in comparison to the zero order solution for N = 3 of the Level 1 formulation in Figs. 4.9 and 4.10. The accuracy of the first order solutions in Figs. 4.13 to 4.16 are very good and are almost riding on the exact solutions, even though a cruder segmentation has

been used. A similar trend is also prevailed on the costates histories.

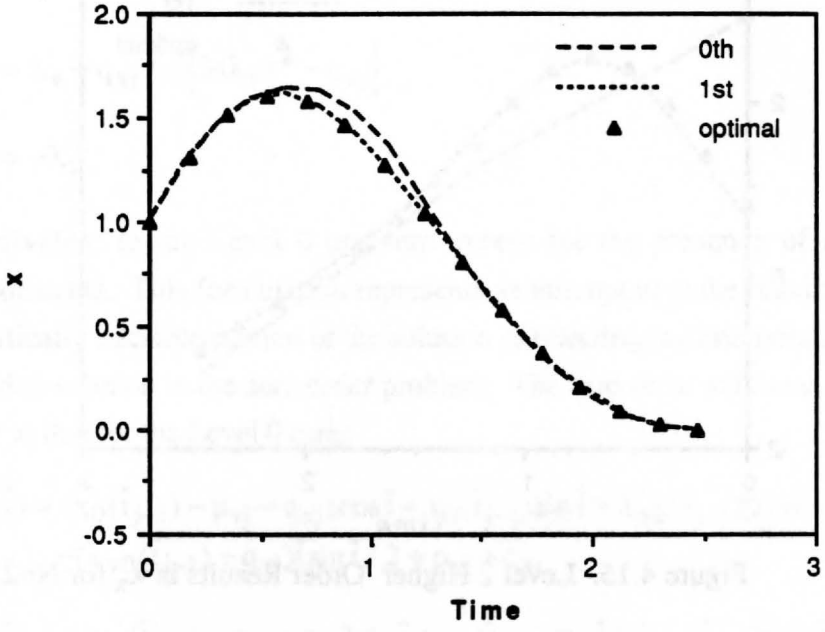

Figure 4.13. Level 2 Higher Order Results in x for N=2.

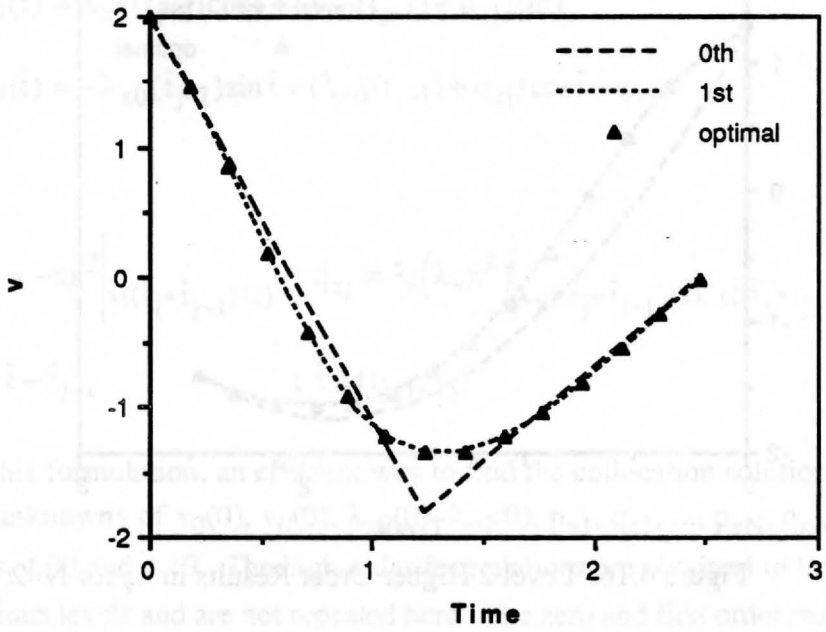

Figure 4.14. Level 2 Higher Order Results in v for N=2.

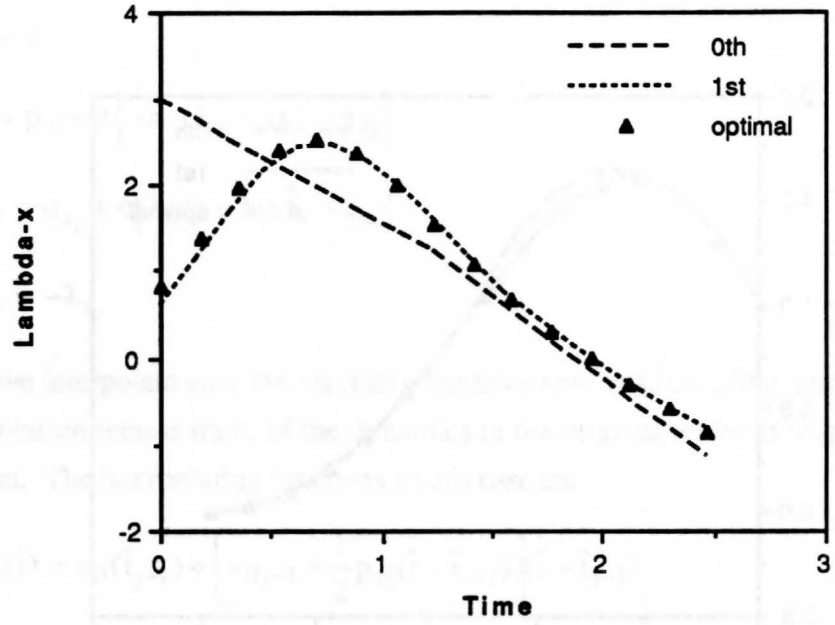

Figure 4.15. Level 2 Higher Order Results in λ_x for N=2.

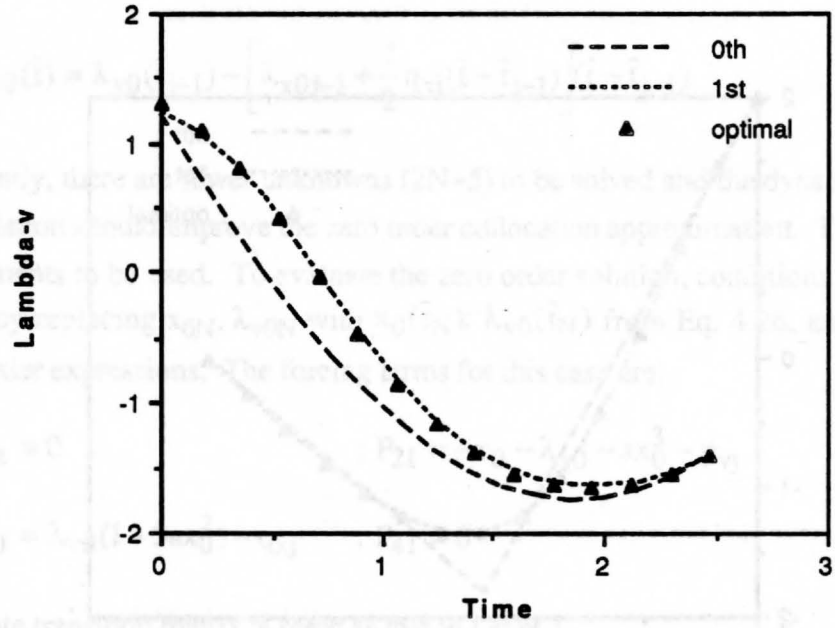

Figure 4.16. Level 2 Higher Order Results in λ_v for N=2.

d) Level 3 formulation

In this last demonstration, the Level 2 formulation is further enhanced. All the linear terms are retained in the zero order problem, and the nonlinear terms in the v and λ_v dynamics are approximated by piecewise constants. The resultant expressions become:

$$\dot{x} = v$$

$$\dot{v} = -x - \lambda_v + p_{vj} + \varepsilon\left\{-ax^3 - p_{vj}\right\}$$

$$\dot{\lambda}_x = \lambda_v + q_{xj} + \varepsilon\left\{3a\lambda_v x^2 - q_{xj}\right\}$$

$$\dot{\lambda}_v = -\lambda_x \qquad (4.28)$$

This is equivalent to the Level 0 problem except for the presence of two additional unknown constants. This formulation represents an attempt to make maximum utilization of the analytically tractable portion of the solution in selecting the interpolating function for the collocation solution in the zero order problem. The zero order solutions in this case are also similar to that for the Level 0 case:

$$x_0(\hat{t}) = (x_0(\hat{t}_{j-1}) - p_{vj} - q_{xj})\cos\bar{t} + v_0(\hat{t}_{j-1})\sin\bar{t} + \lambda_{x0}(\hat{t}_{j-1})[\sin\bar{t} - \bar{t}\cos\bar{t}]/2$$
$$-(\lambda_{v0}(\hat{t}_{j-1}) + q_{xj})\bar{t}\sin\bar{t}/2 + p_{vj} + q_{xj}$$

$$v_0(\hat{t}) = -(x_0(\hat{t}_{j-1}) - p_{vj} - q_{xj})\sin\bar{t} + v_0(\hat{t}_{j-1})\cos\bar{t} + \lambda_{x0}(\hat{t}_{j-1})\bar{t}\sin\bar{t}/2$$
$$-(\lambda_{v0}(\hat{t}_{j-1}) + q_{xj})[\sin\bar{t} + \bar{t}\cos\bar{t}]/2$$

$$\lambda_{x0}(\hat{t}) = \lambda_{x0}(\hat{t}_{j-1})\cos\bar{t} + (\lambda_{v0}(\hat{t}_{j-1}) + q_{xj})\sin\bar{t}$$

$$\lambda_{v0}(\hat{t}) = -\lambda_{x0}(\hat{t}_{j-1})\sin\bar{t} + (\lambda_{v0}(\hat{t}_{j-1}) + q_{xj})\cos\bar{t} - q_{xj} \qquad (4.29)$$

where

$$p_{vj} = -ax^3\Big|_{x((\hat{t}_j+\hat{t}_{j-1})/2)} \quad ; \; q_{xj} = 3a\left(\lambda_v x^2\right)\Big|_{\lambda_v((\hat{t}_j+\hat{t}_{j-1})/2);\, x((\hat{t}_j+\hat{t}_{j-1})/2)}$$

$$\bar{t} = \hat{t} - \hat{t}_{j-1} \qquad ; \; \hat{t} \in [t_{j-1}, t_j] \qquad (4.30)$$

In this formulation, an efficient way to find the collocation solution is to solve for the 2N+5 unknowns of $x_0(0)$, $v_0(0)$, $\lambda_{x0}(0)$, $\lambda_{v0}(0)$, p_{v1}, q_{x1}, ..., p_{vN}, q_{xN}, t_{f0} using Eq. 4.29 in Eqs. 4.30 and 4.19. The high order formulations are obtained in the same manner as the previous levels and are not repeated here. The zero and first order results using only one element are shown in Figs. 4.17 - 4.20. Though the first order results are not as accurate as those in Level 2 (because only one element is used), both zero and first order solutions are far superior than the Level 0 results (Figs. 4.1 - 4.4) which correspond to the degenerate case of only one element.

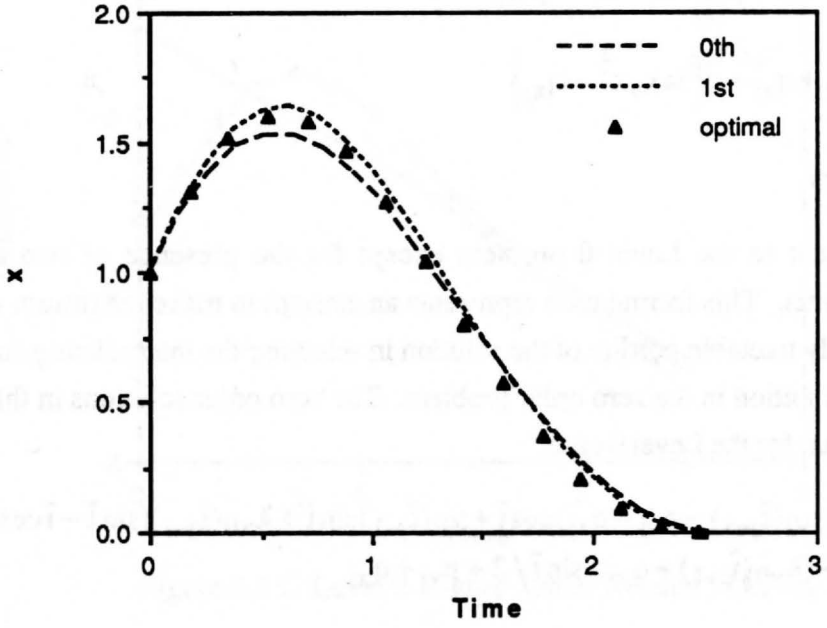

Figure 4.17. Level 3 Higher Order Results in x for N=1.

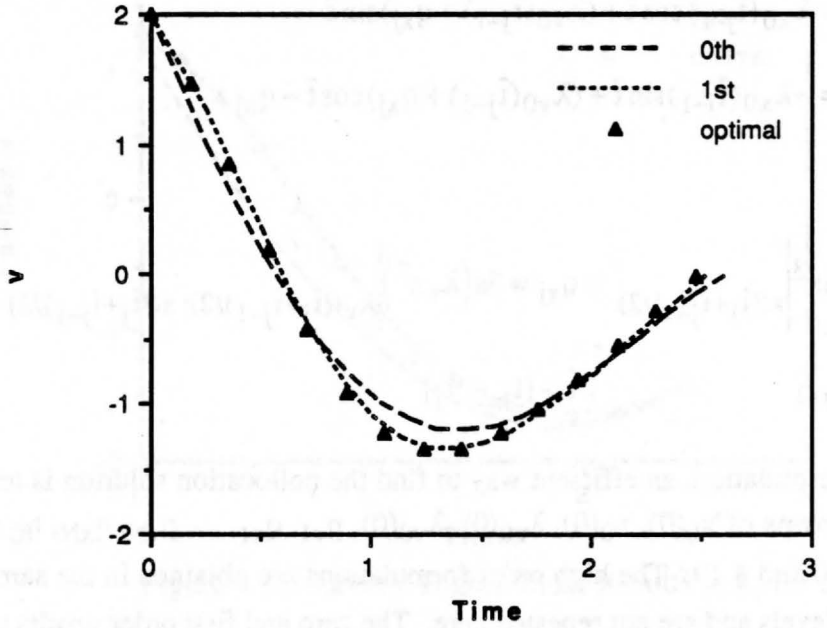

Figure 4.18. Level 3 Higher Order Results in v for N=1.

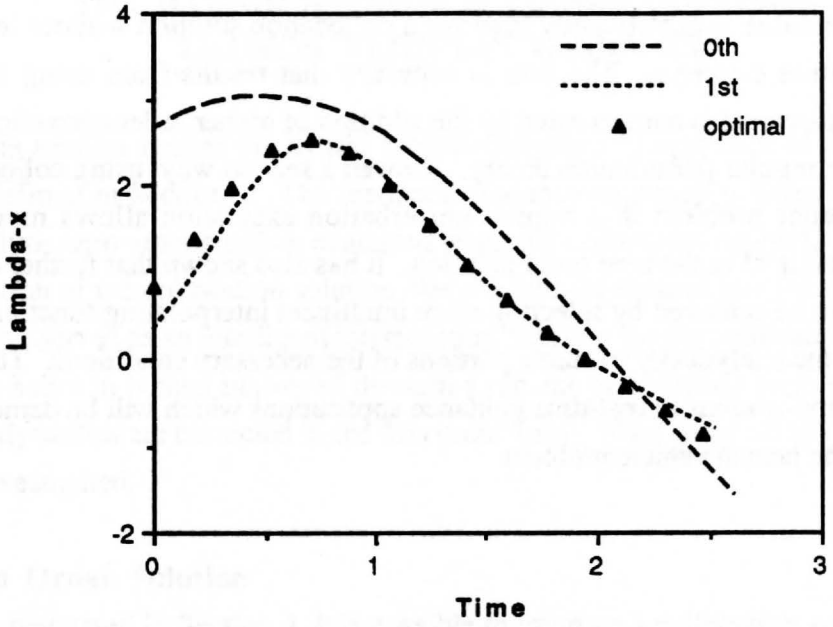

Figure 4.19. Level 3 Higher Order Results in λ_x for N=1.

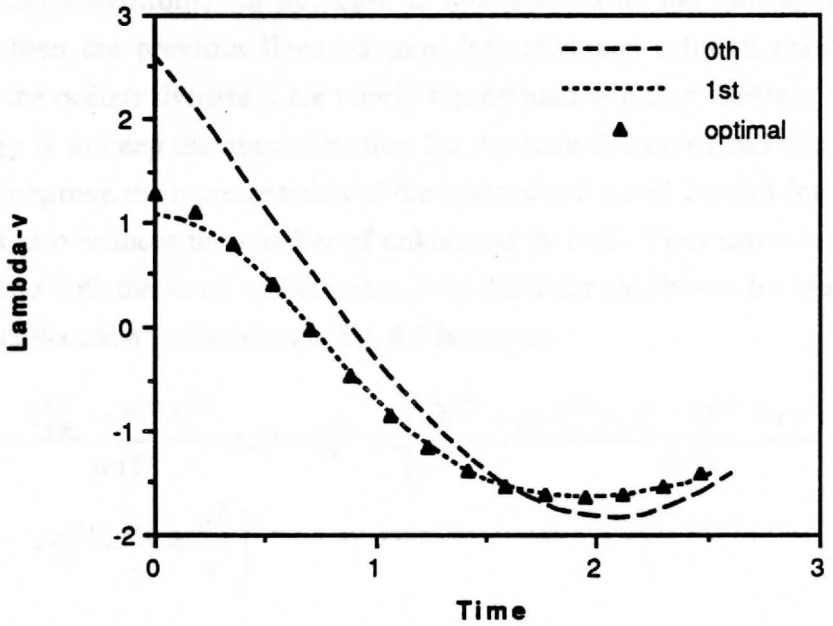

Figure 4.20. Level 3 Higher Order Results in λ_v for N=1.

4.5 Conclusions

A hybrid analytical/numerical approach for solving optimization problems using regular perturbation and collocation methods has been developed. The hybrid approach shows that it is possible to significantly improve a collocation solution without increasing the number of finite elements. The loss in accuracy that results from using a smaller number of finite elements is compensated by the addition of higher order corrections to the solution based on regular perturbation theory. Viewed a second way, using collocation to solve the zero order problem in a regular perturbation expansion allows more of the dynamics to be retained in the zero order solution. It has also shown that further dramatic improvements can be achieved by selecting more intelligent interpolating functions which are derived from the analytically tractable portions of the necessary conditions. The results show important implications in real-time guidance applications which will be demonstrated in Chapter 5 on the launch vehicle problem.

SECTION V

THE HYBRID APPROACH TO NEAR-OPTIMAL LAUNCH VEHICLES GUIDANCE

This section applies the hybrid analytical/numerical approach of Section 4 to the problem defined in Section 2. The feedback guidance approach is based on a piecewise nearly analytic zero order solution evaluated using the collocation method. Each piecewise representation of the collocation solution obeys a bilinear tangent law for the thrust vector angle, which serves as an intelligent interpolating function for the collocation method. The zero order solution is then improved through a regular perturbation analysis, wherein the neglected dynamics are corrected in the first order term. Wind shear effects and constraints are also investigated.

5.1 Zero Order Solution

As discussed in Section 4, it is possible to improve a collocation solution by using more intelligent interpolating functions than the first order representations in Eq. 4.1. The interpolating functions can be derived from analysis of the analytically tractable portions in the necessary conditions. In this case if spherical Earth and atmospheric effects are neglected then the previous linear tangent law guidance solution results (Sec. 3.2b). However, the costate dynamics are poorly represented as either constant or zero. Hence, the strategy is to keep the approximation for the state dynamics and use the collocation method to improve the representation of the costates (cf. Level 2 and 3 formulation in Sec. 4.3). This also reduces the number of unknowns by half. Thus instead of using Eq. 4.1 to interpolate both the states and costates, only the latter are chosen for interpolation. The perturbed collocation formulation in Eq. 4.2 becomes:

$$\dot{v} = \frac{T_{vac}^{(i)} - \bar{p}^{(i)} A_e^{(i)}}{m(t)} \sin\theta - \bar{g}_v^{(i)} + \varepsilon \left(\frac{(\bar{p}^{(i)} - p) A_e^{(i)} \sin\theta - D^{(i)} \sin\gamma + L^{(i)} \cos\gamma}{m(t)} + \bar{g}_v^{(i)} - \frac{\mu_e}{r^2} + \frac{u^2}{r} \right)$$

$$\dot{u} = \frac{T_{vac}^{(i)} - \bar{p}^{(i)} A_e^{(i)}}{m(t)} \cos\theta - \bar{g}_u^{(i)} + \varepsilon \left(\frac{(\bar{p}^{(i)} - p) A_e^{(i)} \cos\theta - D^{(i)} \cos\gamma - L^{(i)} \sin\gamma}{m(t)} + \bar{g}_u^{(i)} - \frac{uv}{r} \right)$$

$$\dot{r} = v$$

$$\dot{\lambda}_v = q_{vj} + \varepsilon(-\frac{\partial H}{\partial v} - q_{vj}) \quad ; \dot{\lambda}_u = q_{uj} + \varepsilon(-\frac{\partial H}{\partial u} - q_{uj}) \quad ; j = 1, \ldots, N$$

$$\dot{\lambda}_r = q_{rj} + \varepsilon(-\frac{\partial H}{\partial r} - q_{rj}) \quad ; \frac{\partial}{\partial \theta}(\lambda_v \dot{v} + \lambda_u \dot{u} + \lambda_r \dot{r}) = 0 \tag{5.1}$$

where

$$v = V\cos\gamma + W_i \quad ; u = V\sin\gamma + W_k$$

$$H = \lambda_v\left(\frac{(T_{vac}^{(i)} - pA_e^{(i)})\sin\theta - D^{(i)}\sin\gamma + L^{(i)}\cos\gamma}{m(t)} - \frac{\mu_e}{r^2} + \frac{u^2}{r}\right)$$
$$+\lambda_u\left(\frac{(T_{vac}^{(i)} - pA_e^{(i)})\cos\theta - D^{(i)}\cos\gamma - L^{(i)}\sin\gamma}{m(t)} - \frac{uv}{r}\right) + \lambda_r v \tag{5.2}$$

The terms $\bar{p}^{(i)}$, $\bar{g}_v^{(i)}$, $\bar{g}_u^{(i)}$ are approximations for the average values of the engine nozzle back-pressure and the spherical acceleration components for each flight stage. From previous investigation it is found that including partial terms for these effects improve the approximation, and for the present problem these parameters are chosen as:

$$\bar{p}^{(1)} = p(h_o)/2 \quad ; \bar{g}_v^{(1)} = \mu_e / r_o^2 - u_o^2 / r_o \quad ; \bar{g}_u^{(1)} = 0$$

$$\bar{p}^{(2)} = 0 \quad ; \bar{g}_v^{(2)} = \bar{g}_v^{(1)}/2 \quad ; \bar{g}_u^{(2)} = 0 \tag{5.3}$$

and they are assumed to be updated continuously in closed loop implementation.

In the following we make use of the analytic portion of the optimality condition in Eq. 5.1 to generate the zero order control, by using the form in Eq. 4.3. This amounts to regarding the dependence of aerodynamic forces on θ as a perturbation of the optimality condition, which results in the celebrated bilinear tangent law

$$\tan\theta_0(t) = \frac{\lambda_{v0j-1} + q_{vj}(t - t_{j-1})}{\lambda_{u0j-1} + q_{uj}(t - t_{j-1})} \tag{5.4}$$

With the above formulation and using the expression in Eq. 5.4 to eliminate the control, the zero order solution ($\varepsilon = 0$) can be expressed as:

$$v_0(t) = v_0(t_{j-1}) + \frac{FD}{k^{(i)}}\left\{\frac{\varsigma+\Delta}{\sqrt{1+\Delta^2}}\sinh^{-1}(\tan(\varphi+\eta)) - \sinh^{-1}(\tan\varphi)\right\}\Bigg|_{\varphi(t_{j-1})}^{\varphi(t)}$$
$$-(t-t_{j-1})\bar{g}_v^{(i)} \qquad ; t \in [t_{j-1}, t_j]$$

$$u_0(t) = u_0(t_{j-1}) + \frac{FE}{k^{(i)}}\left\{\frac{1+\Delta\xi}{\sqrt{1+\Delta^2}}\sinh^{-1}(\tan(\varphi+\eta)) - \xi\sinh^{-1}(\tan\varphi)\right\}\Bigg|_{\varphi(t_{j-1})}^{\varphi(t)}$$
$$-(t-t_{j-1})\bar{g}_u^{(i)}$$

$$r_0(t) = r_0(t_{j-1}) - \frac{FDC}{k^{(i)}A}\left\{(\Delta-\tan\varphi)\left[\frac{\varsigma+\Delta}{\sqrt{1+\Delta^2}}\sinh^{-1}(\tan(\varphi+\eta)) - \sinh^{-1}(\tan\varphi)\right]\right.$$
$$\left.\sec\varphi - \varsigma\sinh^{-1}(\tan\varphi)\right\}\Bigg|_{\varphi(t_{j-1})}^{\varphi(t)} + [v_0(t_{j-1}) - \bar{g}_v^{(i)}\frac{t-t_{j-1}}{2}](t-t_{j-1}) - G(t_{j-1})$$

$$\lambda_{v0}(t) = \lambda_{v0j-1} + q_{vj}(t-t_{j-1})$$

$$\lambda_{u0}(t) = \lambda_{u0j-1} + q_{uj}(t-t_{j-1})$$

$$\lambda_{r0}(t) = \lambda_{r0j-1} + q_{rj}(t-t_{j-1}) \qquad (5.5)$$

where

$$A = \sqrt{q_{vj}^2 + q_{uj}^2} \quad ; B = (c_v q_{vj} + c_u q_{uj})/A \quad ; C = \sqrt{c_v^2 + c_u^2 - B^2}$$

$$D = q_{vj}/A \quad ; E = (c_u A - q_{uj}B)/(AC) \quad ; F = T_{vac}^{(i)} - \bar{p}^{(i)}A_e^{(i)}$$

$$c_v = \lambda_{v0j-1} - q_{vj}t_{j-1} \; ; c_u = \lambda_{u0j-1} - q_{uj}t_{j-1} \quad ; c_m = m^{(i)} + k^{(i)}t_{j-1}$$

$$\varphi(t) = \tan^{-1}\left(\frac{At+B}{C}\right) \; ; \eta = \begin{cases} \tan^{-1}(1/\Delta) & , \Delta \geq 0 \\ \pi + \tan^{-1}(1/\Delta) & , \Delta < 0 \end{cases}$$

$$\Delta = \frac{c_m A + k^{(i)}B}{k^{(i)}C} \quad ; \xi = \frac{q_{uj}C}{c_u A - q_{uj}B} \quad ; \varsigma = \frac{c_v A - q_{vj}B}{q_{vj}C}$$

$$G(t_{j-1}) = \frac{FD}{k^{(i)}}\left\{\frac{\varsigma+\Delta}{\sqrt{1+\Delta^2}}\sinh^{-1}(\tan(\varphi+\eta)) - \sinh^{-1}(\tan\varphi)\right\}\Bigg|_{\varphi(t_{j-1})} \qquad (5.6)$$

The above expressions constitute a set of nonlinear interpolating functions and the zero order solution is now expressed in terms of the unknown costate nodal values. To evaluate

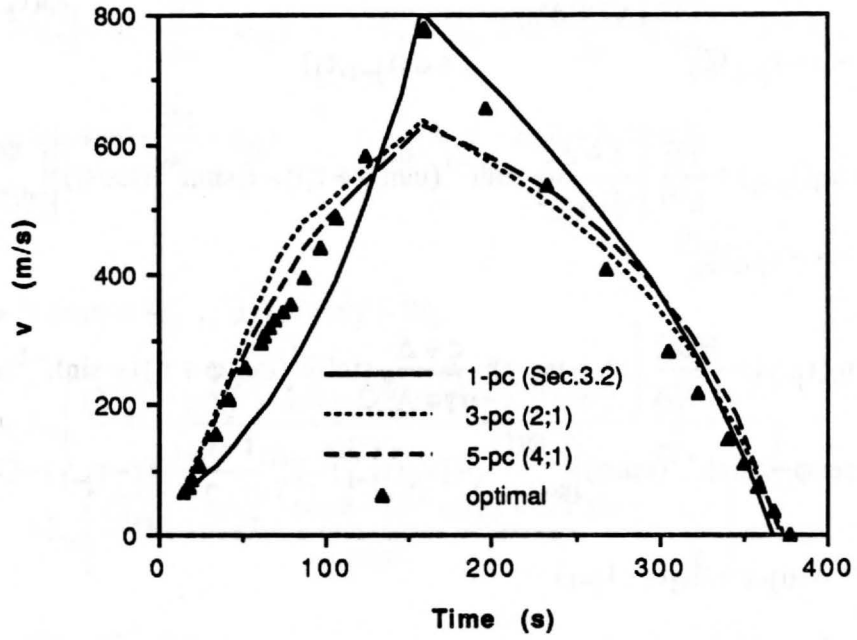

Figure 5.1. Open Loop v Profiles for Various N.

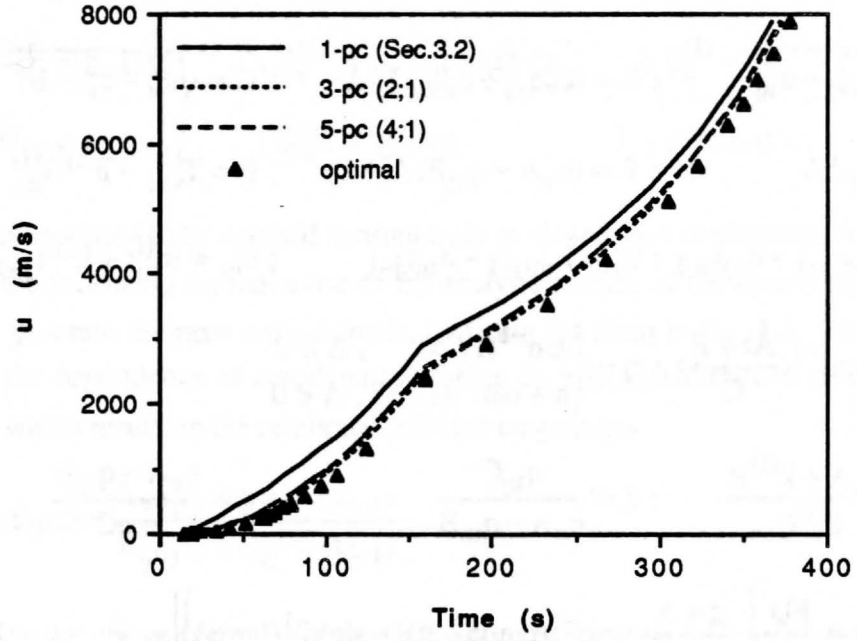

Figure 5.2. Open Loop u Profiles for Various N.

these values, the collocation constraints on the costate derivatives in Eq. 4.1 are enforced:

$$q_{vj} = \frac{\lambda_{v0j} - \lambda_{v0j-1}}{t_j - t_{j-1}} = -\frac{\partial H}{\partial v}\bigg|_{t=(t_j+t_{j-1})/2;\ \lambda_{v0}=(\lambda_{v0j}+\lambda_{v0j-1})/2;\ \lambda_{u0}=(\lambda_{u0j}+\lambda_{u0j-1})/2;\ \lambda_{r0}=(\lambda_{r0j}+\lambda_{r0j-1})/2}$$

$$q_{uj} = \frac{\lambda_{u0j} - \lambda_{u0j-1}}{t_j - t_{j-1}} = -\frac{\partial H}{\partial u}\bigg|_{t=(t_j+t_{j-1})/2;\ \ldots\ ;\ \lambda_{r0}=(\lambda_{r0j}+\lambda_{r0j-1})/2}$$

$$q_{rj} = \frac{\lambda_{r0j} - \lambda_{r0j-1}}{t_j - t_{j-1}} = -\frac{\partial H}{\partial r}\bigg|_{t=(t_j+t_{j-1})/2;\ \ldots\ ;\ \lambda_{r0}=(\lambda_{r0j}+\lambda_{r0j-1})/2} \qquad (5.7)$$

Since more control activity is expected inside the atmosphere, a denser segmentation is used for the first stage flight, whereas a 1-piece segment is sufficient for the subsequent more nearly exoatmospheric second stage flight. The total number of unknowns to be solved in the zero order problem are 3N+4. Open loop solutions in a stationary atmosphere for several increasing values of N are given in Figs. 5.1 to 5.6. The segmentation is N-1 elements for the first stage flight and one element for the second stage flight. Zero order results using only the regular perturbation approach as given in Sec. 3.2 are also included for comparison. Significant improvements are observed in the costate profiles with the hybrid approach because part of the aerodynamic effects are now accounted for in the zero order formulation. In particular, note from Figs. 5.4 - 5.6 that the zero order solution of Sec. 3.2 amounts to ignoring aerodynamic effects and invoking a flat, non rotating Earth approximation. This results in λ_u and λ_r being constant and λ_v being linear in time (see Figs. 5.4 - 5.6), which from Eq. 5.4 gives the linear tangent steering law. This largely accounts for the failure of the regular perturbation method when aerodynamic effects are included.

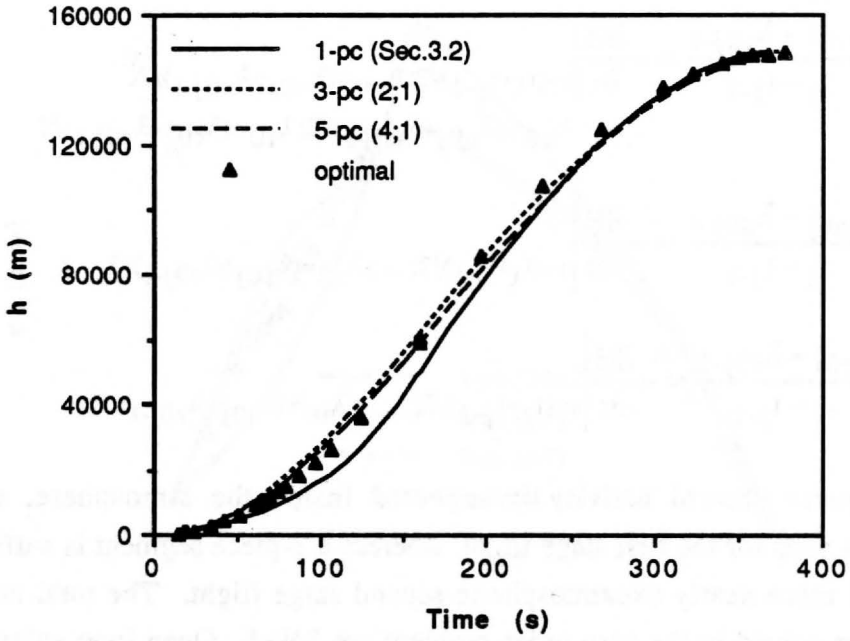

Figure 5.3. Open Loop h Profiles for Various N.

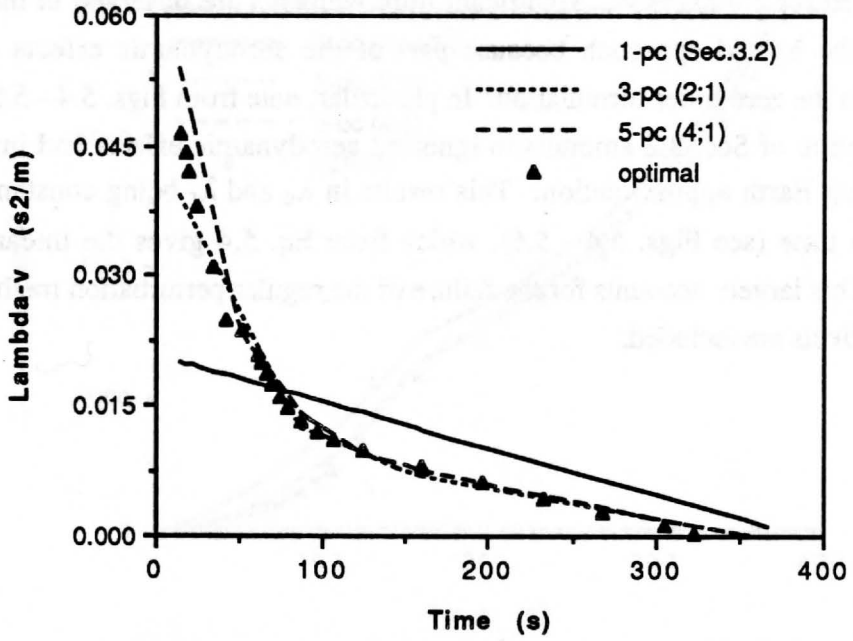

Figure 5.4. Open Loop λ_v Profiles for Various N.

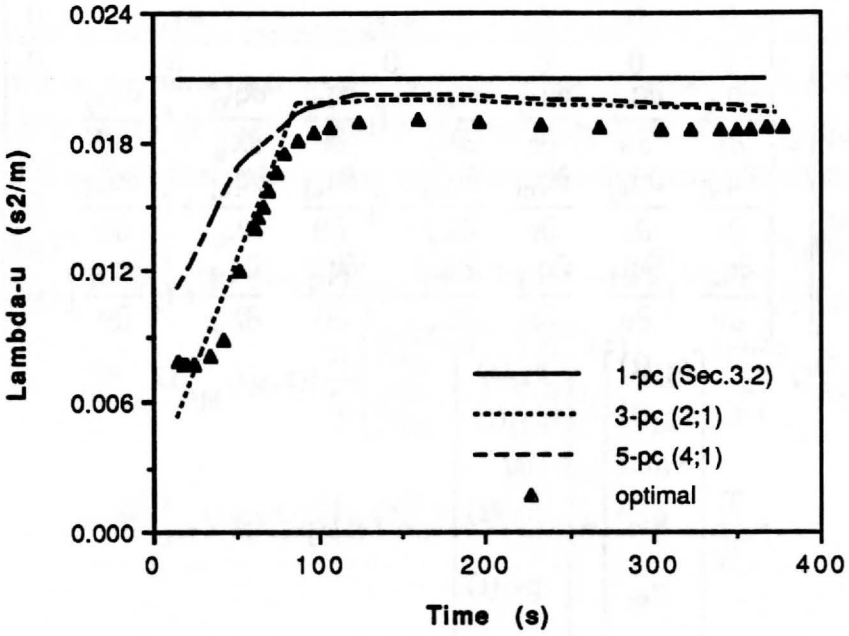

Figure 5.5. Open Loop λ_u Profiles for Various N.

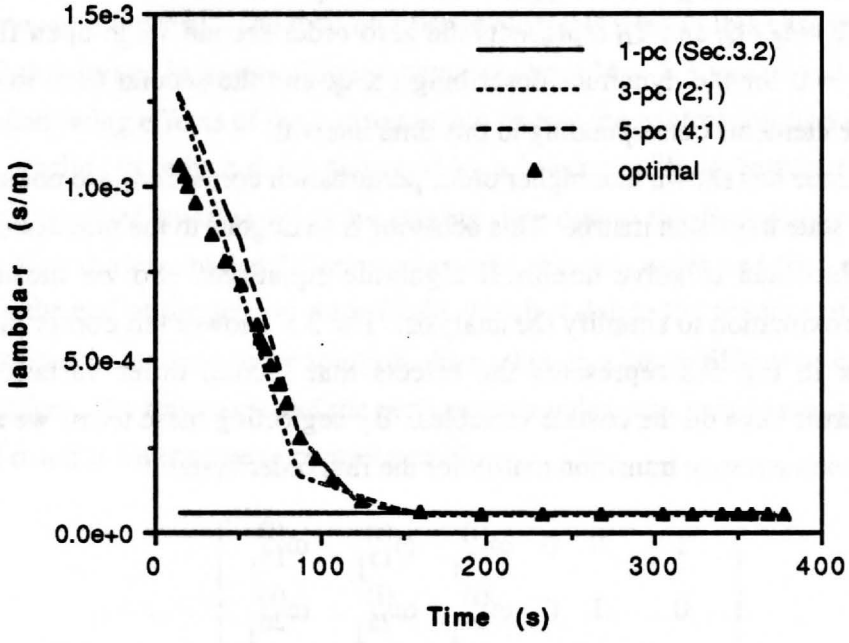

Figure 5.6. Open Loop λ_r Profiles for Various N.

5.2 First Order Solution

In this case, the linear differential equations satisfied by the first order terms have the following form:

$$\frac{d}{dt}\begin{bmatrix} v_1 \\ u_1 \\ r_1 \\ \lambda_{v1} \\ \lambda_{u1} \\ \lambda_{r1} \end{bmatrix} = \begin{bmatrix} 0 & 0 & 0 & a_{14j} & a_{15j} & 0 \\ 0 & 0 & 0 & a_{15j} & a_{25j} & 0 \\ 1 & 0 & 0 & 0 & 0 & 0 \\ \frac{\partial q_{vj}}{\partial v} & \frac{\partial q_{vj}}{\partial u} & \frac{\partial q_{vj}}{\partial r} & \frac{\partial q_{vj}}{\partial \lambda_v} + f_1\frac{\partial q_{vj}}{\partial \theta} & \frac{\partial q_{vj}}{\partial \lambda_u} + f_2\frac{\partial q_{vj}}{\partial \theta} & -1 \\ \frac{\partial q_{uj}}{\partial v} & \frac{\partial q_{uj}}{\partial u} & \frac{\partial q_{uj}}{\partial r} & \frac{\partial q_{uj}}{\partial \lambda_v} + f_1\frac{\partial q_{uj}}{\partial \theta} & \frac{\partial q_{uj}}{\partial \lambda_u} + f_2\frac{\partial q_{uj}}{\partial \theta} & 0 \\ \frac{\partial q_{rj}}{\partial v} & \frac{\partial q_{rj}}{\partial u} & \frac{\partial q_{rj}}{\partial r} & \frac{\partial q_{rj}}{\partial \lambda_v} + f_1\frac{\partial q_{rj}}{\partial \theta} & \frac{\partial q_{rj}}{\partial \lambda_u} + f_2\frac{\partial q_{rj}}{\partial \theta} & 0 \end{bmatrix}\begin{bmatrix} v_1 \\ u_1 \\ r_1 \\ \lambda_{v1} \\ \lambda_{u1} \\ \lambda_{r1} \end{bmatrix}$$

$$+\frac{T_1}{T_0}\begin{bmatrix} c_{1j}(t) \\ c_{2j}(t) \\ v_0(t) \\ q_{vj} \\ q_{uj} \\ q_{rj} \end{bmatrix} + \begin{bmatrix} p_{1j}(t) \\ p_{2j}(t) \\ 0 \\ p_{4j}(t) \\ p_{5j}(t) \\ p_{6j}(t) \end{bmatrix} \quad ; t \in [t_{j-1}, t_j] \tag{5.8}$$

Complete expressions are given in Appendix D. As explained earlier, the first stage flight time is fixed, $T = t_f - t_s$, and T_0 represents the zero order second stage open flight time. Therefore, $T_1 = 0$ for the dynamics describing $t \le t_s$, and the second term in Eq. 5.8 is dropped for the elements corresponding to this time interval.

Experience has shown that higher order perturbation corrections are not sensitive to using an exact state transition matrix. This behavior is analogous to the practice of using an approximate Jacobian to solve nonlinear algebraic equations. So we introduced the following approximation to simplify the analysis. The 3 x 5 lower left corner block of the system matrix in Eq. 5.8 represents the effects that second order variations of the atmospheric terms have on the costate variables. By neglecting these terms we are able to derive an approximate state transition matrix for the first order system:

$$\Omega^{(i)}_{A_j}(t, t_{j-1}) = \begin{bmatrix} 1 & 0 & 0 & \omega^{(i)}_{14_j} & \omega^{(i)}_{15_j} & \omega^{(i)}_{16_j} \\ 0 & 1 & 0 & \omega^{(i)}_{24_j} & \omega^{(i)}_{25_j} & \omega^{(i)}_{26_j} \\ t - t_{j-1} & 0 & 1 & \omega^{(i)}_{34_j} & \omega^{(i)}_{35_j} & \omega^{(i)}_{36_j} \\ 0 & 0 & 0 & 1 & 0 & t_{j-1} - t \\ 0 & 0 & 0 & 0 & 1 & 0 \\ 0 & 0 & 0 & 0 & 0 & 1 \end{bmatrix} ; t \in [t_{j-1}, t_j] \tag{5.9}$$

Appendix D details the ω terms in Eq. 5.9. The lower right hand block in Eq. 5.9 accounts for spherical Earth effects on the costate solution, neglected in the zero order solution. As will be shown in the numerical results section, this is an important correction for the exoatmospheric phase of flight. By successively applying Eq. 4.6 of N times, the perturbations at t_N for a first order system with piecewise representation are now given by

$$\begin{bmatrix} x_1(t_N) \\ \lambda_1(t_N) \end{bmatrix} = \Omega^{(2)}_{A_N}(t_N, t_{N-1})\Omega^{(1)}_{A_{N-1}}(t_{N-1}, t_{N-2}) \ldots \Omega^{(1)}_{A_1}(t_1, t_o)\begin{bmatrix} x_1(t_o) \\ \lambda_1(t_o) \end{bmatrix} +$$

$$\int_{t_{N-1}}^{t_N} \Omega^{(2)}_{A_N}(t_N, \tau)\{\frac{T_1}{T_0}\begin{bmatrix} C^{(2)}_{1_N}(\tau) \\ C^{(2)}_{2_N}(\tau) \end{bmatrix} + \begin{bmatrix} P^{(2)}_{1_N}(\tau) \\ P^{(2)}_{2_N}(\tau) \end{bmatrix}\}d\tau + \sum_{j=1}^{j=N-1} \Omega^{(2)}_{A_N}(t_N, t_{N-1}) \ldots$$

$$\ldots \Omega^{(1)}_{A_{j+1}}(t_{j+1}, t_j)\int_{t_{j-1}}^{t_j} \Omega^{(1)}_{A_j}(t_j, \tau)\begin{bmatrix} P^{(1)}_{1_j}(\tau) \\ P^{(1)}_{2_j}(\tau) \end{bmatrix} d\tau \qquad (5.10)$$

5.3 Numerical Results

Figures 5.7 to 5.10 show the closed loop results for the state variables expressed in the wind frame coordinates. The control is updated at every second and is held constant within each update interval. The total number of elements used in this case is N = 8. Note in Fig. 5.10 that jumps in angle of attack occur at about M = 1.3 and M = 2.3. These are due to the shadowing effects of the booster which causes the control solution to first follow a higher α profile (to reduce drag) followed by a lower profile to correct the trajectory. There is another third small jump at the staging time due to the discontinuous dynamics. This figure also shows a major difference between the zero order and first order solution for α during the end of the second stage flight, which is due to the absence of the spherical Earth corrections in the zero order solution. Even though a large difference exists between the two solutions, the trajectory and the performance index stay very close, and imply that the optimal result is insensitive to control variations.

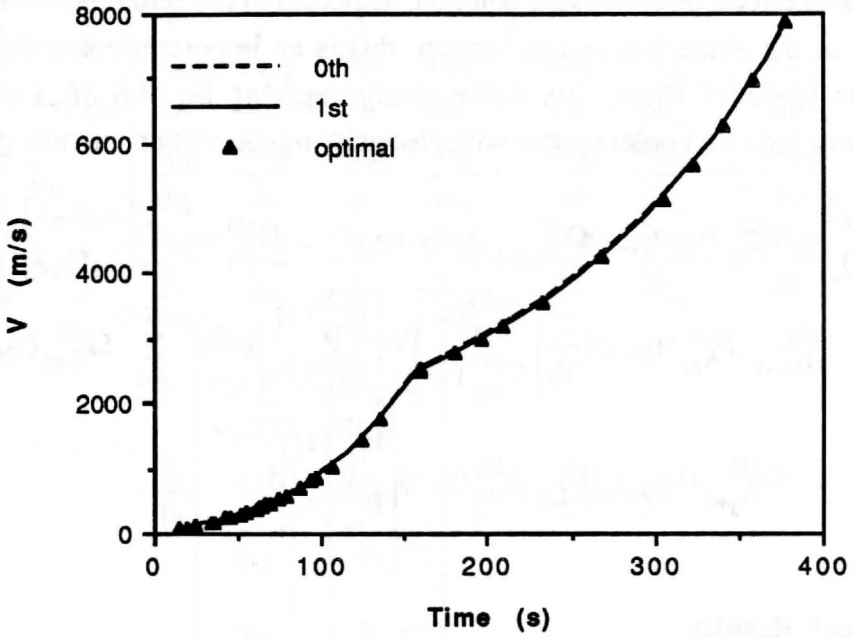

Figure 5.7. Closed Loop Velocity Profile for N=8.

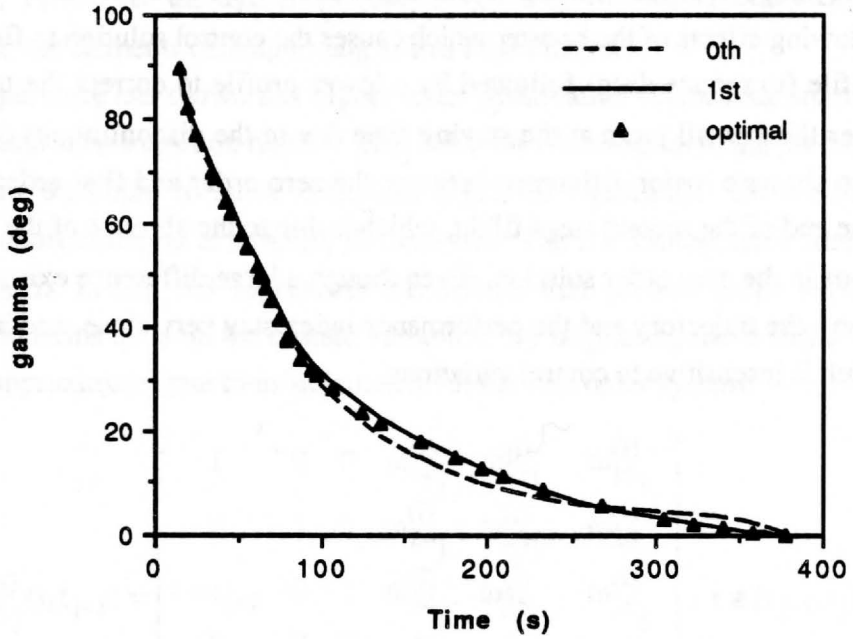

Figure 5.8. Closed Loop Flight-path Angle Profile for N=8.

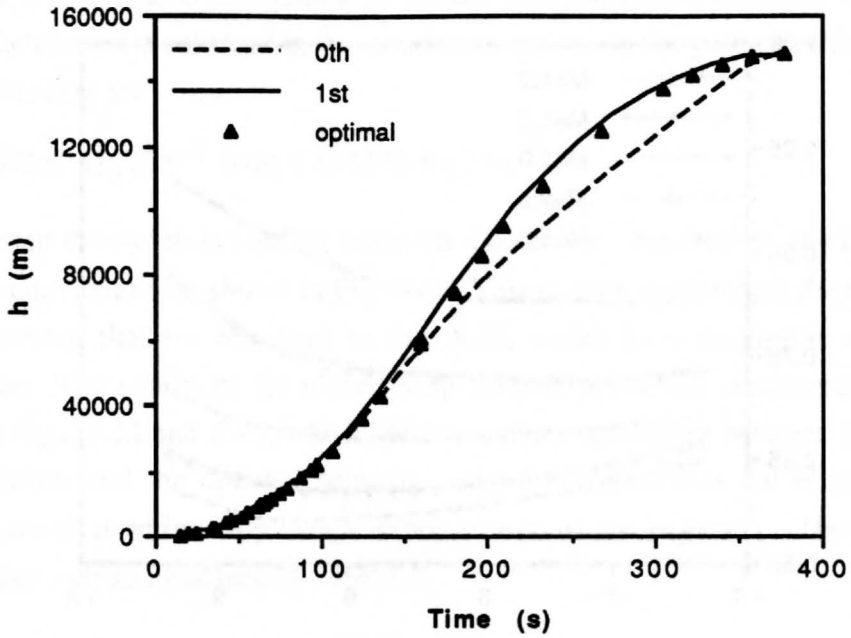

Figure 5.9. Closed Loop Altitude Profile for N=8.

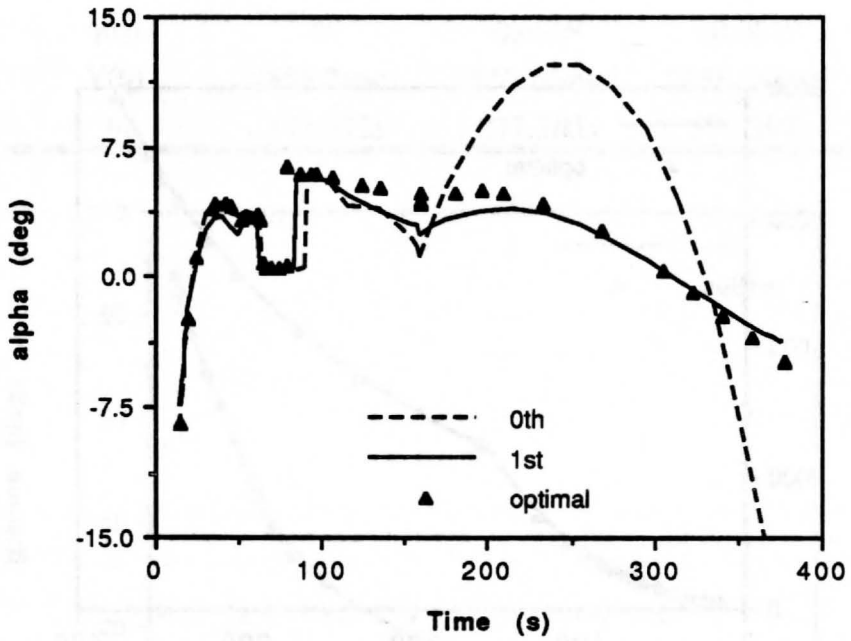

Figure 5.10. Closed Loop Angle of Attack Profile for N=8.

Next, we include the effects of non-stationary atmosphere on the solution. The wind profile used is the interpolated mean winter profile for Kennedy Space Center, shown in Fig. 2.11, and this profile is accounted for in the guidance solution. From earlier investigation it is learned that the performance is not sensitive to control variations, there-

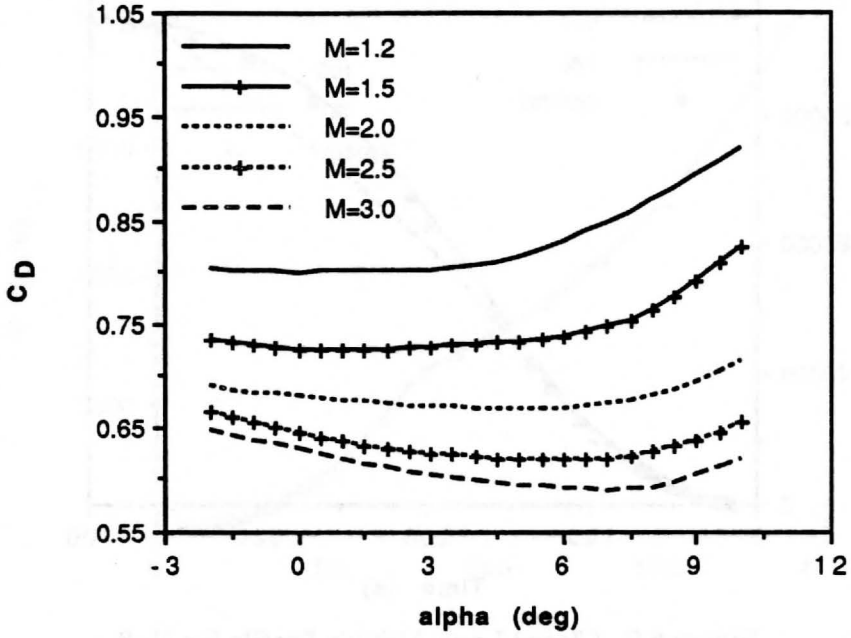

Figure 5.11. Convexized First Stage C_D Profile.

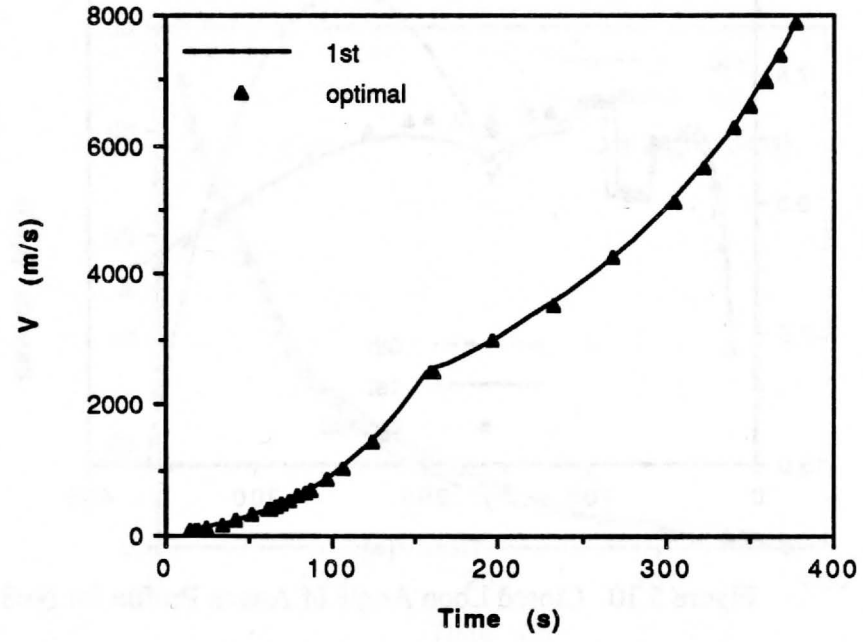

Figure 5.12. Closed Loop Velocity Profile Under Wind and αq Constraint.

fore attempt is not made to incorporate the control constraint in the analysis. Instead a hard bound on the control is enforced in the simulation, but not in the guidance derivation. The bounds in this case are

$$-167580\,\mathrm{deg\,Nm^{-2}} \le \alpha q \le 167580\,\mathrm{deg\,Nm^{-2}} \tag{5.11}$$

They represent the dynamic loading limits on the vehicle. In addition, the first stage C_D profile was convexized, as shown in Fig. 5.11. This is done to eliminate the objectionable jumps in control that are observed in Fig. 5.10, which have negligible effect on the performance. The results of the closed loop simulation for the unconstrained case are depicted in Figs. 5.12 and 5.15, which show excellent agreement between the first order guided solution and the optimal solution. Fig. 5.16 illustrates the effect of the αq constraint, which is active only over a minor portion of the trajectory. The performance results for this case summarized in Table 5.1.

Table 5.1. Performance Comparison for ALS Vehicle Guidance.

	optimal	1st-order	0th-order
$h(t_f)$	148160m	148160.0m	148160.0m
$\gamma(t_f)$	0^o	0.000^o	-0.001^o
$V(t_f)$	$7858.2ms^{-1}$	$7858.20ms^{-1}$	$7858.14ms^{-1}$
t_f	377.372s	377.382s	378.397s

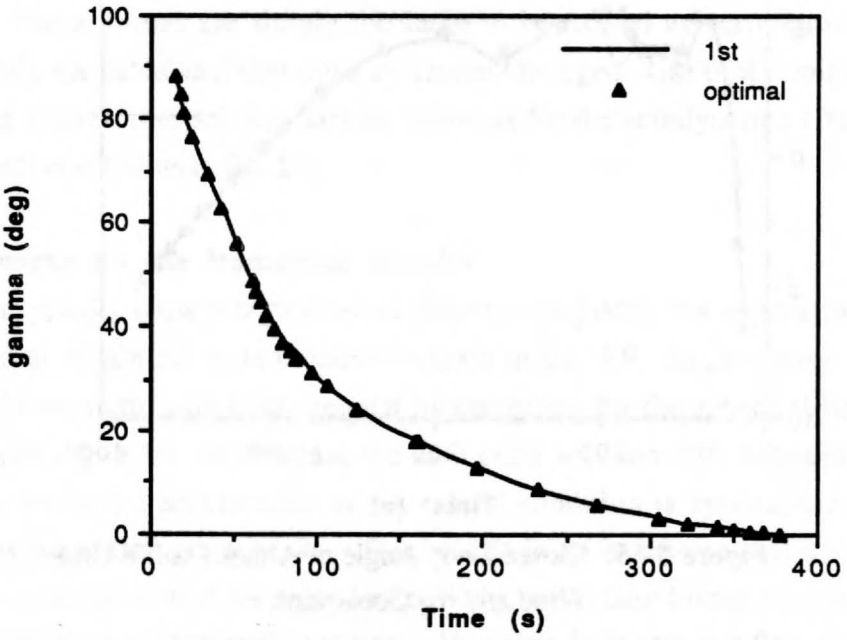

Figure 5.13. Closed Loop Flight-path Angle Profile Under Wind and αq Constraint.

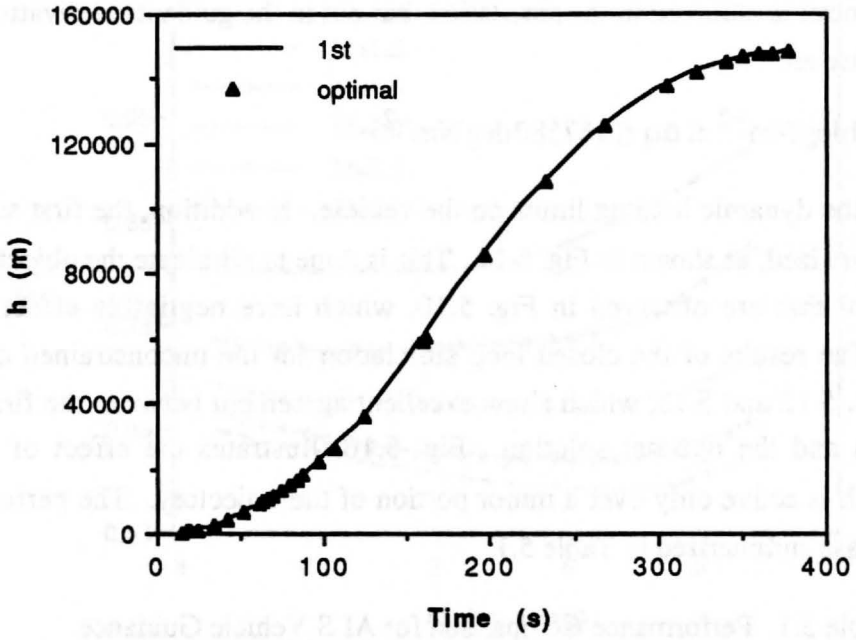

Figure 5.14. Closed Loop Altitude Profile Under Wind and αq Constraint.

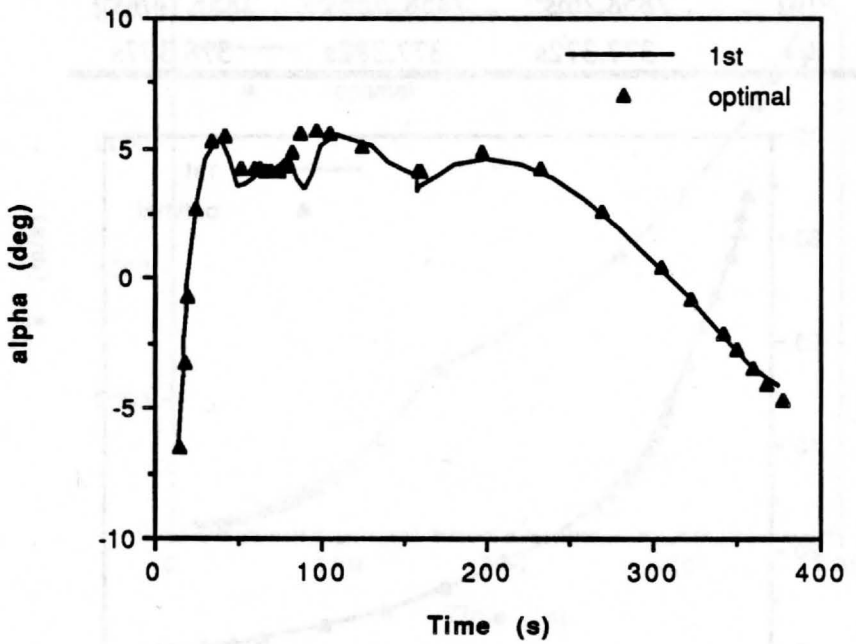

Figure 5.15. Closed Loop Angle of Attack Profile Under Wind and αq Constraint.

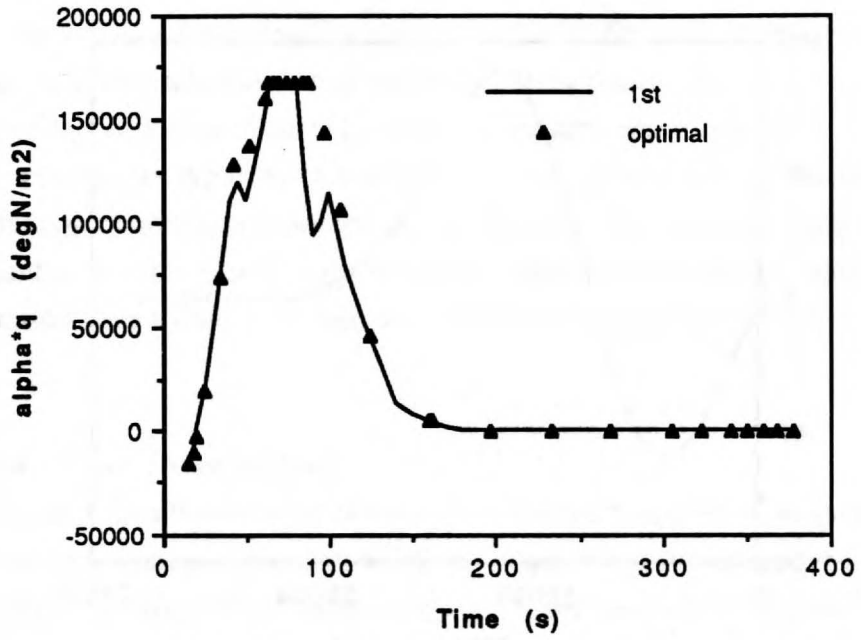

Figure 5.16. Closed Loop αq Profile Under Wind and αq Constraint.

In this example, the aerodynamic forces have a major effect in the middle portion of the first stage ascent. This is illustrated in Fig. 3.20 which shows the ratios of the lift and drag forces to the thrust components. This explains why the regular perturbation analysis in Sec. 3.2 is not able to correct for the effect of aerodynamic forces in the first order analysis. These forces are simply too large to be treated as perturbation effects, and consequently the calculated first order correction diverged. Use of the collocation method in forming a zero order solution largely accounts for the aerodynamic effect through the mid-element constraints in Eq. 5.7.

5.4 Remarks on the Numerical Results

The results show a high level of fidelity and justify the approximation we have introduced to obtain the state transition matrix in Eq. 5.9. In particular, the first order solution shows significant improvement by correcting for the spherical Earth effects, as illustrated in Fig. 5.10. In this case the zero order solution fails to anticipate the sharp change in the radial acceleration as the orbital condition is approached, even using a continuously updated guess of $\bar{g}_v$. This results in an excessive pull-up of the vehicle during the initial portion of the second stage flight, and is later forced to correct with a large negative α to meet the terminal conditions. However, both zero and first order results give extremely good orbit injection accuracy without requiring a high rate of control update.

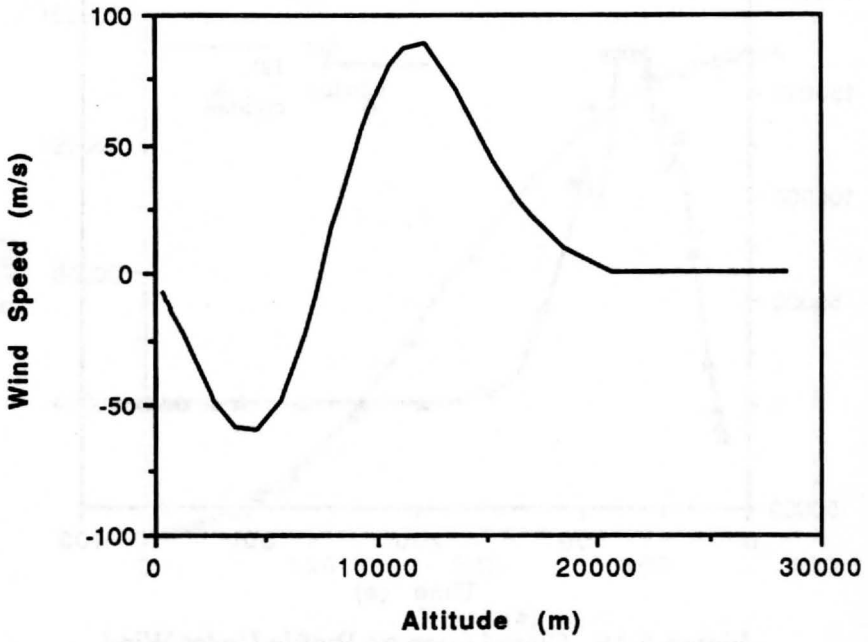

Figure 5.17. A Hypothetical Wind Shear Profile.

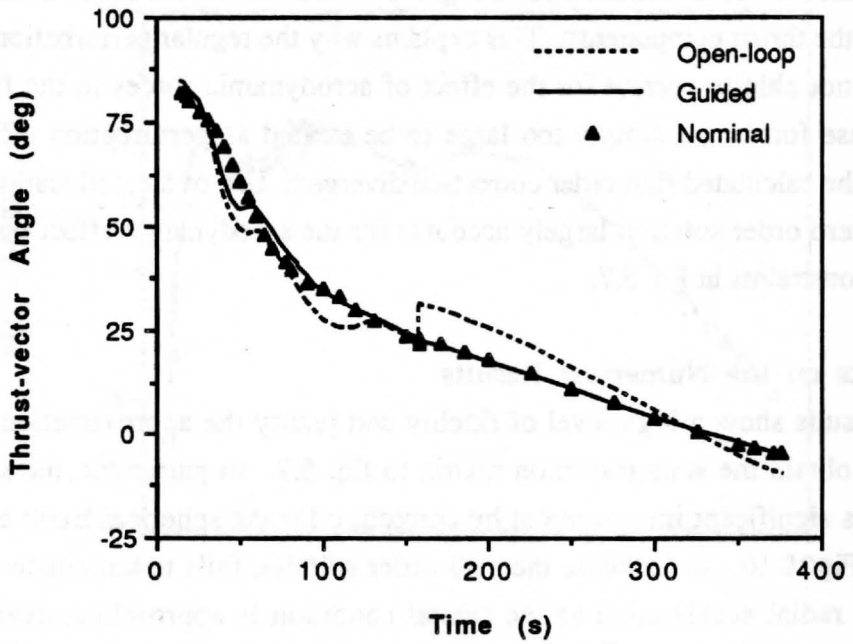

Figure 5.18. Comparison of the Thrust Vector Angle Profiles under Wind Shear.

The computations for the cases presented here are done on a SPARCstation 1. The CPU time needed for a control update ranges from 0.65s for an 8-element case to less than 0.15s for a 1-element solution during the second stage flight. The Newton's method with Broyden's update of the Jacobian [11] is used in the zero order collocation evaluation and the solution converges typically in 4 iterations. It is apparent from the numerical results that the first order correction is needed mainly to correct for spherical Earth effects which are dominant only in the second stage of flight. Therefore a significant additional savings in computation time would have resulted had we computed this correction only for that phase.

5.5 Wind Shear Investigation

To assess the effectiveness of the hybrid approach against wind shear, we show a typical scenario. First, an open loop trajectory using piecewise linear thrust vector angle program for the first stage flight, followed by the closed loop hybrid approach guidance for the second stage flight is simulated with a hypothetical wind shear (cf. Fig. 5.17). The open loop part of the guidance is derived from a linear interpolation of the previous results, which is based on the nominal mean wind profile. Second, a guided trajectory using closed loop guidance for both the first and second stage flight is simulated. This guided solution is assumed to have detected the wind shear, and is therefore included in the calculation. To assure structural integrity, both cases are incorporated with the αq constraints. The first case represents the approach for present launch vehicle operation, ie. an open loop guidance for the endoatmospheric flight using pre-flight atmospheric conditions, and compensated by a closed loop guidance for the exoatmospheric flight. The second case represents the proposed approach for ALS, ie. real-time near optimal guidance. Figs. 5.18 - 5.20 compare the 'Open loop' and the 'Guided' solutions. A point of interest, the 'Nominal' solution with the same linear piecewise control program flying under the nominal wind condition is also included. The 'Open-loop' solution gives poorer performance (cf. Table 5.2). The final time to orbit is 1.13s longer (equivalent to a loss of 4550lbs in payload) than the guided solution, and is also worse than the guided solution

Table 5.2. Performance Comparison under Wind Shear.

	Guided (1st)	Guided (0th)	Open loop
$h(t_f)$	148160.0m	148160.0m	148160.0m
$\gamma(t_f)$	0.000^o	-0.000^o	0.000^o
$V(t_f)$	$7858.20ms^{-1}$	$7858.18ms^{-1}$	$7858.20ms^{-1}$
$-J = t_f$	377.287s	378.243s	378.413s

using only a zero order solution. If the magnitude of the wind shear is further increased by 22%, then open-loop guidance will result in a catastrophic failure unless the αq limit is exceeded.

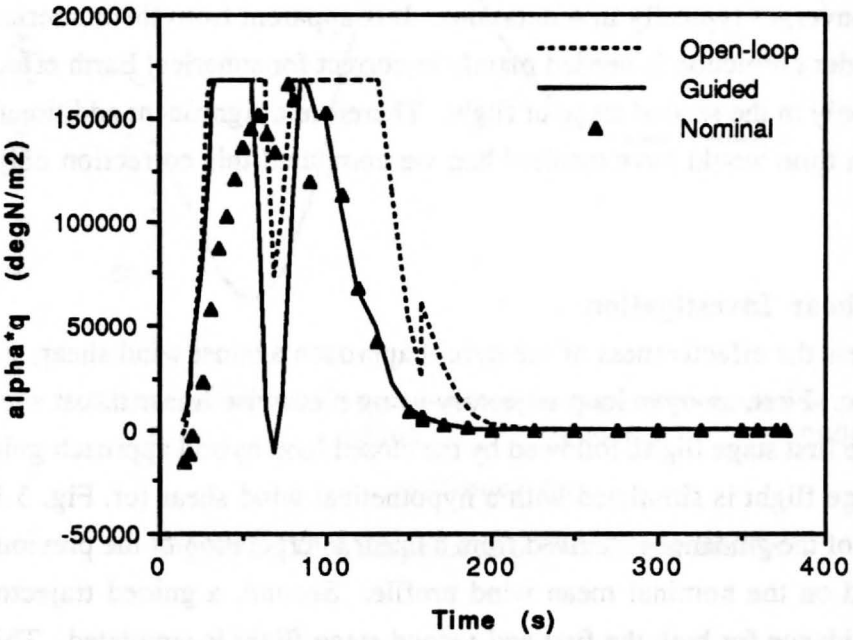

Figure 5.19. Comparison of the αq Profiles under Wind Shear.

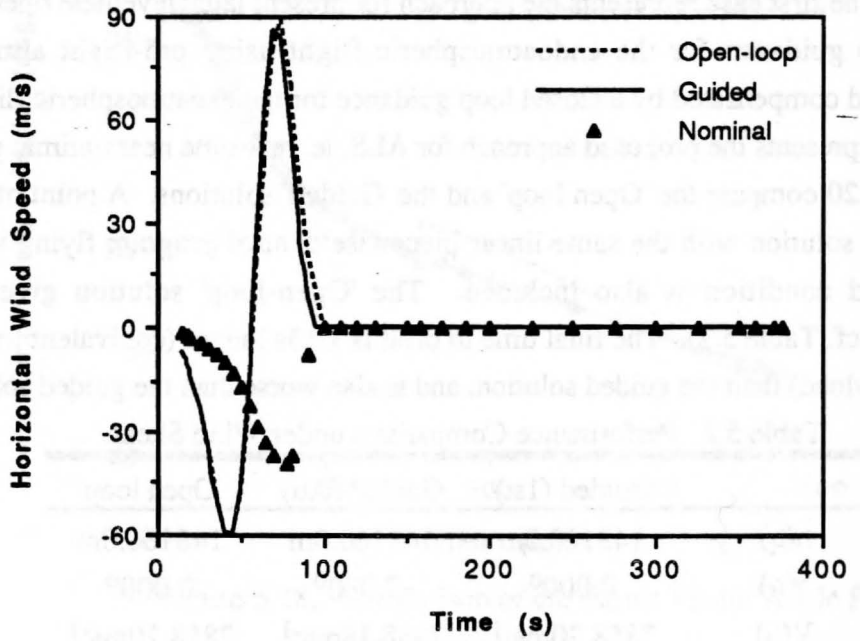

Figure 5.20. Experienced Horizontal Wind Speed for the 3 Different Simulations.

SECTION VI

CONCLUSIONS AND RECOMMENDATIONS

6.1 Conclusions

The fundamental problem in treating launch vehicle dynamics by singular perturbation methods relates to the inherent large value of longitudinal load factor. As a result, the zero order reduced solution gives a very poor approximation. A manifold solution was also attempted to account for flight path angle dynamics, but this method also fails due to the fact that the dynamics are not separable in the same manner throughout the ascent profile. Regular perturbation analysis gives a better solution in the absence of aerodynamic forces. However, the approach cannot handle guidance for the atmospheric flight phase, which is the main issue of this research. The neglected aerodynamic forces in the zero order solution are simply to large to be considered as a perturbation effect.

A new hybrid approach for the solution of nonlinear problems in optimal control has been developed for this application. This approach is hybrid because it combines the desirable features of numerical and analytical methods. The numerical method of collocation allows a simple formulation for solving a wide variety of optimization problems. The disadvantage of requiring a large number of approximation elements and solving a large dimension set of algebraic equations are compensated for by the analytical approach of regular perturbation. The regular perturbation approach provides higher order correction over the collocation solution without increasing the number of approximation elements. It can also be used to identify intelligent interpolating functions for the collocation solution, which results in a further substantial reduction in the number of finite elements needed for a given level of solution accuracy. These attractive features promise an enhanced real time capability in the solution of optimal control problems, which has been demonstrated in the launch vehicle guidance application. The main results on this problem are that a bilinear tangent steering law can be employed in all flight phases, including the atmospheric phase, and that the collocation solution can be obtained using a small number of elements.

6.2 Recommendations for Future Work

Many important issues remain for future research, and the following recommendations are made in increasing order of complexity:

Identifying More Intelligent Interpolating Functions - Though the zero order solution is capable of handling partial aerodynamic effects, spherical Earth effects were not directly

incormorpated in the analysis. This leads to a poor representation of the zero order solution as the vehicle approaches orbital speed. An investigation should be made to account for this effect in the formulation, and a proposed way to set up the problem is to add a constant perturbation term, similar to the Level 3 formulation in Sec. 4.3.

More Accurate Model - Improvements can be made in the launch vehicle problem by considering a more elaborate dynamic model. The rotating Earth effects and a more complex propulsion model should be considered. It may be necessary to modify the interpolating solution in the collocation approach, depending on the magnitudes of these nonlinearities.

Multi-flight Task Requirements - The hybrid guidance approach can be extended to handle various flight tasks such as deorbit and rendezvous. These requirements will pose terminal constraints on both the downrange and crossrange values, which can be included in a 3-D formulation. Such multi-flight task guidance capability would be very useful to manned vehicles like the Space Shuttle.

Constrained Problem Analysis - For the launch vehicle problem, it is coincidental that the performance is insensitive to control variations, thus allowing the exclusion of the control constraint in the analysis. However, it would be useful to complete the hybrid approach to include analysis of constrained optimization problems. To address the constrained problem requires a guess of the switching structure and a formulation of variable time intervals in which the constraint becomes active.

Launch Vehicles Range Safety Concerns - The range safety issues related to the launch vehicle ascent trajectory occur in the form of state constraints. To avoid potential disaster or to facilitate the retrieval of reusable boosters, the vehicle may be constrained to fly within a narrow corridor of air space. Present methods to handle this type of problem are not efficient and rely purely on numerical means. Future study should include a systematic and simplified formulation that is tractable by analytic methods such as the hybrid approach.

Hybrid Approach with the HJB Expansion - As demonstrated in [14, 38], the regular perturbation analysis can be carried out using the Hamilton-Jacobi-Bellman equation. In this formulation, the perturbation corrections are not represented by a set of linear O. D. E's., and the calculation of the state transition matrix or sensitivity functions are not required. Instead the perturbation corrections are evaluated simply by quadrature. Proposed future research should include a study of the relationships between these two types of formulations (the HJB and the state/costate expansion) and the hybrid approach using the HJB expansion, which promises a much simpler and more efficient evaluation of the perturbation corrections.

Manifold Investigation - The failure of the energy approximation analysis indicates that the zero order ($\varepsilon = 0$) reduced solution is far from satisfactory and a higher order approximation is needed. One distinguishing feature of Manifold Theory is the inclusion of ε in the manifold condition [24] which considers the fast variable as a function of the singular perturbation parameter in addition to the slow variable. Although this approach was not successful for this application, due to the varying role of the altitude state, it may be highly useful in other nonlinear optimization problems. A drawback in our analysis is that we had to numerically experiment to determine a solution close to the manifold. This has been accomplished by visual examination of the trajectories in Fig's. 3.5 and 3.6. It would be highly desirable to develop an algebraic test for when the initial condition lies on the manifold solution. An alternative would be to develop an iterative process that converges to the manifold solution.

APPENDIX A
Derivation of Eq. 3.32

We want to show that

$$\frac{T_k}{T_0}\int_{t_o}^{\hat{t}}\Omega_A(\hat{t},\tau)\begin{bmatrix}C_1(\tau)\\C_1(\tau)\end{bmatrix}d\tau = T_k\frac{t-t_o}{T_0}\begin{bmatrix}\dot{x}_0(\hat{t})\\\dot{\lambda}_0(\hat{t})\end{bmatrix} \tag{A.1}$$

in Eq. 3.32. Let $f_1 = \dot{x}_0(x_0,\lambda_0,\tau)$; $f_2 = \dot{\lambda}_0(x_0,\lambda_0,\tau)$, assuming u being eliminated and recall that

$$C_1 = f_1 + (\tau - t_o)\frac{\partial f_1}{\partial \tau} \qquad ; C_2 = f_2 + (\tau - t_o)\frac{\partial f_2}{\partial \tau} \tag{A.2}$$

The left hand side of (A.1) becomes

$$\frac{T_k}{T_0}\int_{t_o}^{\hat{t}}\Omega_A(\hat{t},\tau)\left\{\frac{d}{d\tau}\left((\tau-t_o)\begin{bmatrix}f_1\\f_2\end{bmatrix}\right)-(\tau-t_o)\begin{bmatrix}\partial f_1/\partial x_0 & \partial f_1/\partial \lambda_0\\ \partial f_2/\partial x_0 & \partial f_2/\partial \lambda_0\end{bmatrix}\begin{bmatrix}f_1\\f_2\end{bmatrix}\right\}d\tau \tag{A.3}$$

Using integration by parts on the first term in (A.3), we have

$$\frac{T_k}{T_0}\left\{(\tau-t_o)\Omega_A(\hat{t},\tau)\begin{bmatrix}f_1\\f_2\end{bmatrix}\right\}\Bigg|_{\tau=t_o}^{\tau=\hat{t}} - \frac{T_k}{T_0}\int_{t_o}^{\hat{t}}(\tau-t_o)\left(\frac{d}{d\tau}\Omega_A(\hat{t},\tau)\right)\begin{bmatrix}f_1\\f_2\end{bmatrix}d\tau$$
$$-\frac{T_k}{T_0}\int_{t_o}^{\hat{t}}(\tau-t_o)\Omega_A(\hat{t},\tau)\begin{bmatrix}\partial f_1/\partial x_0 & \partial f_1/\partial \lambda_0\\ \partial f_2/\partial x_0 & \partial f_2/\partial \lambda_0\end{bmatrix}\begin{bmatrix}f_1\\f_2\end{bmatrix}d\tau \tag{A.4}$$

Substituting the state transition matrix property

$$\frac{d}{d\tau}\Omega_A(\hat{t},\tau) = -\Omega_A(\hat{t},\tau)\begin{bmatrix}\partial f_1/\partial x_0 & \partial f_1/\partial \lambda_0\\ \partial f_2/\partial x_0 & \partial f_2/\partial \lambda_0\end{bmatrix} \tag{A.5}$$

into (A.4), the last two terms cancel and the result is demonstrated. The above state transition matrix is also used to derive Eq. 4.7.

APPENDIX B
State Transition Matrix Expression in Eq. 3.44

The state transition matrix used in the regular perturbation approach in Sec. 3.2 is

$$\Omega_A^{(i)}(t_2,t_1)=\begin{bmatrix} 1 & 0 & 0 & \omega_{14}^{(i)} & \omega_{15}^{(i)} & \omega_{16}^{(i)} \\ 0 & 1 & 0 & \omega_{24}^{(i)} & \omega_{25}^{(i)} & \omega_{26}^{(i)} \\ t_2-t_1 & 0 & 1 & \omega_{34}^{(i)} & \omega_{35}^{(i)} & \omega_{36}^{(i)} \\ 0 & 0 & 0 & 1 & 0 & t_1-t_2 \\ 0 & 0 & 0 & 0 & 1 & 0 \\ 0 & 0 & 0 & 0 & 0 & 1 \end{bmatrix} \tag{B.1}$$

where

$$\omega_{14}^{(i)}=\pi_{14}^{(i)}(t_2)-\pi_{14}^{(i)}(t_1)$$

$$\omega_{15}^{(i)}=\pi_{15}^{(i)}(t_2)-\pi_{15}^{(i)}(t_1)$$

$$\omega_{16}^{(i)}=\pi_{16}^{(i)}(t_2)-\pi_{16}^{(i)}(t_1)+t_1\omega_{14}^{(i)}$$

$$\omega_{24}^{(i)}=\omega_{15}^{(i)}$$

$$\omega_{25}^{(i)}=\pi_{25}^{(i)}(t_2)-\pi_{25}^{(i)}(t_1)$$

$$\omega_{26}^{(i)}=\pi_{26}^{(i)}(t_2)-\pi_{26}^{(i)}(t_1)+t_1\omega_{24}^{(i)}$$

$$\omega_{34}^{(i)}=\pi_{34}^{(i)}(t_2)-\pi_{34}^{(i)}(t_1)-(t_2-t_1)\pi_{14}^{(i)}(t_1)$$

$$\omega_{35}^{(i)}=\pi_{35}^{(i)}(t_2)-\pi_{35}^{(i)}(t_1)-(t_2-t_1)\pi_{15}^{(i)}(t_1)$$

$$\omega_{36}^{(i)}=\pi_{36}^{(i)}(t_2)-\pi_{36}^{(i)}(t_1)-(t_2-t_1)\pi_{16}^{(i)}(t_1)+t_1\omega_{16}^{(i)}$$

$$\pi_{14}^{(i)}(t)=A\left\{\frac{-\sinh^{-1}[\tan(\theta(t))-\eta)]}{(\Delta^2+1)^{3/2}}-\frac{\Delta\sin(\theta(t))+\cos(\theta(t))}{\Delta^2+1}\right\}$$

$$\pi_{15}^{(i)}(t)=A\left\{\frac{-\Delta\sinh^{-1}[\tan(\theta(t))-\eta)]}{(\Delta^2+1)^{3/2}}+\frac{\sin(\theta(t))-\Delta\cos(\theta(t))}{\Delta^2+1}\right\}$$

$$\pi_{16}^{(i)}(t) = B\left\{\frac{(p+\Delta)\sinh^{-1}[\tan(\theta(t))-\eta)]}{(\Delta^2+1)^{3/2}} + \frac{(p+\Delta)\cos(\theta(t))+(p\Delta-1)\sin(\theta(t))}{\Delta^2+1}\right\}$$

$$A = \frac{T_{vac}^{(i)}}{c_{u0}k^{(i)}} \quad ; B = \frac{A}{q}$$

$$\pi_{25}^{(i)}(t) = A\left\{\frac{-\Delta^2\sinh^{-1}[\tan(\theta(t))-\eta)]}{(\Delta^2+1)^{3/2}} + \frac{\Delta\sin(\theta(t))+\cos(\theta(t))}{\Delta^2+1}\right\}$$

$$\pi_{26}^{(i)}(t) = B\left\{\frac{\Delta(p+\Delta)\sinh^{-1}[\tan(\theta(t))-\eta)]}{(\Delta^2+1)^{3/2}} - \frac{(p+\Delta)\sin(\theta(t))-(p\Delta-1)\cos(\theta(t))}{\Delta^2+1}\right\}$$

$$\pi_{34}^{(i)}(t) = B\left\{\frac{[\Delta+\tan(\theta(t))]\sinh^{-1}[\tan(\theta(t))-\eta)]}{(\Delta^2+1)^{3/2}} + \frac{\Delta\sec(\theta(t))}{\Delta^2+1}\right\}$$

$$\pi_{35}^{(i)}(t) = B\left\{\frac{\Delta[\Delta+\tan(\theta(t))]\sinh^{-1}[\tan(\theta(t))-\eta)]}{(\Delta^2+1)^{3/2}} - \frac{\sec(\theta(t))}{\Delta^2+1}\right\}$$

$$\pi_{36}^{(i)}(t) = \frac{B}{q}\left\{\frac{-(p+\Delta)[\Delta+\tan(\theta(t))]\sinh^{-1}[\tan(\theta(t))-\eta)]}{(\Delta^2+1)^{3/2}} - \frac{(p\Delta-1)\sec(\theta(t))}{\Delta^2+1}\right\} \qquad (B.2)$$

All the variables are evaluated at the zero order values.

APPENDIX C

State Transition Matrix Expression of Level 1 Formulation in Sec. 4.3

The state transition matrix of Level 1 case for the Duffing's example is

$$\Omega_A(\hat{t},t_o)=\begin{bmatrix} a_{11} & a_{12} & a_{13} & a_{14} \\ a_{21} & a_{11} & -a_{14} & a_{24} \\ -ba_{24} & ba_{23} & a_{11} & -a_{21} \\ -ba_{23} & -ba_{13} & -a_{12} & a_{11} \end{bmatrix} \tag{C.1}$$

For $b > 0$:

$$\alpha = c-\sqrt{b} \quad ; \beta = c+\sqrt{b} \quad ; \bar{t} = \hat{t} - t_o$$

$$a_{11} = \frac{\alpha - c}{\alpha - \beta}\cos(\bar{t}\sqrt{\alpha}) + \frac{c-\beta}{\alpha-\beta}\cos(\bar{t}\sqrt{\beta})$$

$$a_{12} = \frac{\alpha - c}{(\alpha-\beta)\sqrt{\alpha}}\sin(\bar{t}\sqrt{\alpha}) + \frac{c-\beta}{(\alpha-\beta)\sqrt{\beta}}\sin(\bar{t}\sqrt{\beta})$$

$$a_{13} = \frac{-1}{(\alpha-\beta)\sqrt{\alpha}}\sin(\bar{t}\sqrt{\alpha}) + \frac{1}{(\alpha-\beta)\sqrt{\beta}}\sin(\bar{t}\sqrt{\beta})$$

$$a_{14} = \frac{1}{\alpha-\beta}\cos(\bar{t}\sqrt{\alpha}) - \frac{1}{\alpha-\beta}\cos(\bar{t}\sqrt{\beta})$$

$$a_{21} = \frac{c^2-\alpha c-b}{(\alpha-\beta)\sqrt{\alpha}}\sin(\bar{t}\sqrt{\alpha}) + \frac{b+c\beta-c^2}{(\alpha-\beta)\sqrt{\beta}}\sin(\bar{t}\sqrt{\beta})$$

$$a_{24} = \frac{-\sqrt{\alpha}}{\alpha-\beta}\sin(\bar{t}\sqrt{\alpha}) + \frac{\sqrt{\beta}}{\alpha-\beta}\sin(\bar{t}\sqrt{\beta}) \tag{C.2}$$

For $b < 0$:

$$\theta = (\sqrt{2\sqrt{c^2-b}-2c})/2 \quad ; \phi = \sqrt{(c+\sqrt{c^2-b})/2}$$

$$a_{11} = \cosh(\theta\bar{t})\cos(\phi\bar{t}) + \frac{c+\theta^2-\phi^2}{2\theta\phi}\sinh(\theta\bar{t})\sin(\phi\bar{t}) \; ; \; a_{14} = \frac{-1}{2\theta\phi}\sinh(\theta\bar{t})\sin(\phi\bar{t})$$

$$a_{12} = \frac{\theta^2+\phi^2-c}{2\theta(\theta^2+\phi^2)}\sinh(\theta\bar{t})\cos(\phi\bar{t}) + \frac{\theta^2+\phi^2+c}{2\phi(\theta^2+\phi^2)}\cosh(\theta\bar{t})\sin(\phi\bar{t})$$

$$a_{13} = \frac{-1}{2\theta(\theta^2+\phi^2)}\sinh(\theta\bar{t})\cos(\phi\bar{t}) + \frac{1}{2\phi(\theta^2+\phi^2)}\cosh(\theta\bar{t})\sin(\phi\bar{t})$$

$$a_{21} = \frac{c^2-b-c(\theta^2+\phi^2)}{2\theta(\theta^2+\phi^2)}\sinh(\theta\bar{t})\cos(\phi\bar{t}) + \frac{b-c^2-c(\theta^2+\phi^2)}{2\phi(\theta^2+\phi^2)}\cosh(\theta\bar{t})\sin(\phi\bar{t})$$

$$a_{24} = \frac{-1}{2\theta}\sinh(\theta\bar{t})\cos(\phi\bar{t}) - \frac{1}{2\phi}\cosh(\theta\bar{t})\sin(\phi\bar{t}) \qquad \text{(C.3)}$$

The state transition matrix has the same structure of that in Level 0 for $b = 0$.

APPENDIX D

System Matrix and State Transition Matrix Expression of the First-orderFormulation in Sec. 5.2

The terms defined in Eq. 5.8 have the following expressions:

$$a_{14j} = \frac{T_{vac}^{(i)} - \bar{p}A_e^{(i)}}{m(t)}\left[\frac{\lambda_{u0}^2}{(\lambda_{v0}^2 + \lambda_{u0}^2)^{3/2}}\right]$$

$$a_{15j} = \frac{T_{vac}^{(i)} - \bar{p}A_e^{(i)}}{m(t)}\left[\frac{-\lambda_{v0}\lambda_{u0}}{(\lambda_{v0}^2 + \lambda_{u0}^2)^{3/2}}\right]$$

$$a_{25j} = \frac{T_{vac}^{(i)} - \bar{p}A_e^{(i)}}{m(t)}\left[\frac{\lambda_{v0}^2}{(\lambda_{v0}^2 + \lambda_{u0}^2)^{3/2}}\right]$$

$$f_1 = \frac{-\cos\theta_0}{\lambda_{v0}\sin\theta_0 + \lambda_{u0}\cos\theta_0}$$

$$f_2 = \frac{\sin\theta_0}{\lambda_{v0}\sin\theta_0 + \lambda_{u0}\cos\theta_0}$$

$$c_{1j} = \frac{T_{vac}^{(i)} - \bar{p}A_e^{(i)}}{m(t)}\left[1 + \frac{(t - t_{j-1})k^{(i)}}{m(t)}\right]\frac{\lambda_{v0}}{\sqrt{\lambda_{v0}^2 + \lambda_{u0}^2}} - \bar{g}_v$$

$$c_{2j} = \frac{T_{vac}^{(i)} - \bar{p}A_e^{(i)}}{m(t)}\left[1 + \frac{(t - t_{j-1})k^{(i)}}{m(t)}\right]\frac{\lambda_{u0}}{\sqrt{\lambda_{v0}^2 + \lambda_{u0}^2}} - \bar{g}_u$$

$$p_{1j} = g_1 + \frac{\lambda_{u0}}{\lambda_{v0}^2 + \lambda_{u0}^2}\left\{\lambda_{v0}\frac{\partial g_1}{\partial\theta_0} + \lambda_{u0}\frac{\partial g_2}{\partial\theta_0}\right\}$$

$$p_{2j} = g_2 - \frac{\lambda_{v0}}{\lambda_{v0}^2 + \lambda_{u0}^2}\left\{\lambda_{v0}\frac{\partial g_1}{\partial\theta_0} + \lambda_{u0}\frac{\partial g_2}{\partial\theta_0}\right\}$$

$$P_{4_j} = -\frac{\partial H}{\partial v} - q_{vj} - \frac{\partial q_{vj}}{\partial\theta}\left\{\frac{\lambda_{v0}\partial g_1/\partial\theta_0 + \lambda_{u0}\partial g_2/\partial\theta_0}{(\lambda_{v0}\sin\theta_0 + \lambda_{u0}\cos\theta_0)(T_{vac}^{(i)} - \bar{p}A_e^{(i)})/m(t)}\right\}$$

$$P_{5_j} = -\frac{\partial H}{\partial u} - q_{uj} - \frac{\partial q_{uj}}{\partial\theta}\left\{\frac{\lambda_{v0}\partial g_1/\partial\theta_0 + \lambda_{u0}\partial g_2/\partial\theta_0}{(\lambda_{v0}\sin\theta_0 + \lambda_{u0}\cos\theta_0)(T_{vac}^{(i)} - \bar{p}A_e^{(i)})/m(t)}\right\}$$

$$P_{6_j} = -\frac{\partial H}{\partial r} - q_{rj} - \frac{\partial q_{rj}}{\partial \theta}\left\{\frac{\lambda_{v0}\partial g_1/\partial\theta_0 + \lambda_{u0}\partial g_2/\partial\theta_0}{(\lambda_{v0}\sin\theta_0 + \lambda_{u0}\cos\theta_0)(T_{vac}^{(i)} - \bar{p}A_e^{(i)})/m(t)}\right\}$$

$$\frac{\partial q_{vj}}{\partial \theta} = \left\{-\frac{\partial^2 H}{\partial\theta\partial v}\right\}\Bigg|_{t=(t_j+t_{j-1})/2;\ \ldots\ ;\ \lambda_{r0}=(\lambda_{r0j}+\lambda_{r0j-1})/2}$$

$$\frac{\partial q_{uj}}{\partial \theta} = \left\{-\frac{\partial^2 H}{\partial\theta\partial u}\right\}\Bigg|_{t=(t_j+t_{j-1})/2;\ \ldots\ ;\ \lambda_{r0}=(\lambda_{r0j}+\lambda_{r0j-1})/2}$$

$$\frac{\partial q_{rj}}{\partial \theta} = \left\{-\frac{\partial^2 H}{\partial\theta\partial r}\right\}\Bigg|_{t=(t_j+t_{j-1})/2;\ \ldots\ ;\ \lambda_{r0}=(\lambda_{r0j}+\lambda_{r0j-1})/2} \qquad \text{(D.1)}$$

where

$$g_1 = \frac{(p-p)A_e^{(i)}\sin\theta_0 - D^{(i)}\sin\gamma_0 + L^{(i)}\cos\gamma_0}{m(t)} + \bar{g}_v - \frac{\mu_e}{r_0} + \frac{u_0^2}{r_0}$$

$$g_2 = \frac{(p-p)A_e^{(i)}\cos\theta_0 - D^{(i)}\cos\gamma_0 - L^{(i)}\sin\gamma_0}{m(t)} + \bar{g}_u - \frac{u_0 v_0}{r_0} \qquad \text{(D.2)}$$

The remaining partial derivatives ($\partial q_{vj}/\partial v$, $\partial q_{vj}/\partial u$, ...) are similar to the last three expressions in (F.1).

The approximate state transition matrix in Eq. 5.9 can be obtained by taking the partial derivatives of the zero-order solution in Eq. 5.5 with respect to the initial conditions $\{v_0(t_{j-1}), u_0(t_{j-1}), r_0(t_{j-1}), \lambda_{v0}(t_{j-1}), \lambda_{u0}(t_{j-1}), \lambda_{r0}(t_{j-1})\}$. So we have:

$$\omega_{14} = \frac{\partial v_0(t)}{\partial\lambda_{v0}(t_{j-1})} = \frac{\partial v_0(t)}{\partial c_v} \qquad ; \omega_{15} = \frac{\partial v_0(t)}{\partial\lambda_{u0}(t_{j-1})} = \frac{\partial v_0(t)}{\partial c_u}$$

$$\omega_{16} = \frac{\partial v_0(t)}{\partial\lambda_{r0}(t_{j-1})} = -\frac{\partial v_0(t)}{\partial q_{vj}} \qquad ; \omega_{24} = \frac{\partial u_0(t)}{\partial\lambda_{v0}(t_{j-1})} = \frac{\partial u_0(t)}{\partial c_v}$$

$$\omega_{25} = \frac{\partial u_0(t)}{\partial\lambda_{u0}(t_{j-1})} = \frac{\partial u_0(t)}{\partial c_u} \qquad ; \omega_{26} = \frac{\partial u_0(t)}{\partial\lambda_{r0}(t_{j-1})} = -\frac{\partial u_0(t)}{\partial q_{vj}}$$

$$\omega_{34} = \frac{\partial r_0(t)}{\partial\lambda_{v0}(t_{j-1})} = \frac{\partial r_0(t)}{\partial c_v} \qquad ; \omega_{35} = \frac{\partial r_0(t)}{\partial\lambda_{u0}(t_{j-1})} = \frac{\partial r_0(t)}{\partial c_u}$$

$$\omega_{36} = \frac{\partial r_0(t)}{\partial\lambda_{r0}(t_{j-1})} = -\frac{\partial r_0(t)}{\partial q_{vj}} \qquad \text{(D.3)}$$

For example, using the chain rule, ω_{14} is given by

$$\omega_{14} = \frac{\partial v_0}{\partial D}\frac{\partial D}{\partial c_v} + \frac{\partial v_0}{\partial \Delta}\frac{\partial \Delta}{\partial c_v} + \frac{\partial v_0}{\partial \varsigma}\frac{\partial \varsigma}{\partial c_v} + \frac{\partial v_0}{\partial \varphi}\frac{\partial \varphi}{\partial c_v} + \frac{\partial v_0}{\partial \eta}\frac{\partial \eta}{\partial c_v} \qquad (D.4)$$

Symbolic manipulation programs such as *Mathematica*, *MACSYMA* can be used to obtain the analytic expressions of the above derivatives, and to write the subroutines needed for their computation.

REFERENCES

1. Brusch, R. G., Reed, T. E., "Real-time Launch Vehicle Steering Programme Selection, " *Journal of the British Interplanetary Society*, Vol. 26, 1973, pp. 279 - 290.
2. Chandler, D. C., Smith, I. E., "Development of the Iterative Guidance Mode with its Application to Various Vehicles and Missions, " *Journal of Spacecraft and Rockets*, Vol. 4, 1967, pp. 898 - 903.
3. McHenry, R. L., Brand, T. J., Long, A. D., Cockrell, B. F., Thibodeau, J. R. III, "Space Shuttle Ascent Guidance, Navigation and Control, " *Journal of the Astronautical Sciences*, Vol. XXVII, 1978, pp. 1 - 38.
4. Johnson, I. L., "Optimal Rocket Thrust Profile Shaping using Third-degree Spline Function Interpolation, " AIAA Paper No. 74-823, 1974.
5. Well, K. H., Tandon, S. R., "Rocket Ascent Trajectory Optimization via Recursive Quadratic Programming, " *Journal of the Astronautical Sciences*, Vol. XXX, 1982, pp. 101 - 116.
6. Well, K. H., "Ariane V Ascent Trajectory Optimization with a First-stage Splash Down Constraint, " *Proceedings of Control Application of Nonlinear Programming and Optimization Conference*, 1989.
7. Brusch, R., "Trajectory Optimization for the Atlas/Centaur Launch Vehicle, " *Journal of Spacecraft and Rockets*, Vol. 14, 1977, pp. 550 - 555.
8. Hargraves, C. R., Paris, S. W., "Direct Trajectory Optimization Using Nonlinear Programming and Collocation, " *AIAA Journal of Guidance, Control, and Dynamics*, Vol.10, 1987, pp. 338 - 342.
9. Pamadi, B. N., "Adaptive Guidance for an Aero-assisted Boost Vehicle, " *Proceedings of AIAA Guidance, Navigation & Control Conference*, 1988, pp. 995 - 1005.
10. Oberle, H. J., Grimm, W., "BNDSCO, A Program for Numerical Solution of Optimal Control Problems, " English Translation of DFVLR-Mitt. 85-05, 1985.
11. Broyden, C. G., "A Class of Methods for Solving Nonlinear Simultaneous Equations, " *Mathematics of Computation*, Vol. 19, 1965, pp. 577 - 583.
12. Breakwell, J. V., Rauch, H. E., "Optimum Guidance for a Low Thrust Interplanetary Vehicle, " *AIAA Journal*, Vol. 4, 1966, pp. 693 - 704.
13. Jacobson, R. A., Powers, W. F., "Iterative Explicit Guidance for Low Thrust Spacecraft, " *Journal of Spacecraft and Rockets*, Vol. 11, 1974, pp. 494 - 497.
14. Feeley, T. S., Speyer, J. L., "A Real-time Approximate Optimal Guidance Law for Flight in a Plane, " *Proceedings of American Control Conference*, 1990, pp. 2356 - 2361.

15. Leung, S. K., Calise, A. J., "An Approach to Optimal Guidance of an Advanced Launch Vehicle Concept, " *Proceedings of American Control Conference*, 1990, pp. 1824 - 1828.
16. Hodges, D. H., Calise, A. J., Bless, R. R., Leung, S. K., "A Weak Hamiltonian Finite Element method for Optimal Guidance of an Advanced Launch Vehicle," *Proceedings of American Control Conference*, 1989, pp. 2036 - 2043.
17. Leung, S. K., Calise, A. J., "A Hybrid Approach to Near-optimal Launch Vehicle Guidance, " *Proceedings of AIAA Guidance, Navigation & Control Conference*, to appear, 1992.
18. Hodges, D. H., Bless, R. R., Calise, A. J., Leung, S. K., "Finite Element Method for Optimal Guidance of an Advanced launch Vehicle, " *AIAA Journal of Guidance, Control, and Dynamics*, Vol. 15, No. 3, 1992, pp. 664 - 671.
19. Leung, S. K., Calise, A. J., "On the Use of Collocation Methods in Regular Perturbation Analysis of Optimal Control Problems, " Submitted for publication in *AIAA Journal of Guidance, Control, and Dynamics*, 1992.
20. Leung, S. K., Calise, A. J., "A Real-time Near-optimal Guidance Approach for Launch Vehices, " Submitted for publication in *AIAA Journal of Guidance, Control, and Dynamics*, 1992.
21. Calise, A. J., Hodges, D. H., Leung, S. K., Bless, R. R., "Optimal Guidance Law Development of an Advanced Launch System, " *NASA Interim Progress Report*, NASA Grant # NAG-1-939, Dec. 88. - May 89, 1989.
22. Calise, A. J., Hodges, D. H., Leung, S. K., Bless, R. R., "Optimal Guidance Law Development of an Advanced Launch System, " *NASA Interim Progress Report*, NASA Grant # NAG-1-939, Jun. 89 - Nov. 89, 1989.
23. Calise, A. J., Hodges, D. H., Leung, S. K., Bless, R. R., "Optimal Guidance Law Development of an Advanced Launch System, " *NASA Interim Progress Report*, NASA Grant # NAG-1-939, Dec. 89 - Jun. 90, 1990.
24. Calise, A. J., Hodges, D. H., Leung, S. K., Bless, R. R., "Optimal Guidance Law Development of an Advanced Launch System, " *NASA Interim Progress Report*, NASA Grant # NAG-1-939, Jun. 90 - Dec. 90, 1990.
25. Calise, A. J., Hodges, D. H., Leung, S. K., Bless, R. R., "Optimal Guidance Law Development of an Advanced Launch System, " *NASA Interim Progress Report*, NASA Grant # NAG-1-939, Dec. 90 - Jun. 91, 1991.
26. Bless, R. R., , "Time-Domain Finite Elements in Optimal Control With Application to Launch-Vehicle Guidance" NASA CR 4376, May 1991.

27. Pamadi, B., Duttion, K., "An Aerodynamic Model for the Advanced Launch System Vehicle," NASA TM, in preparation, 1992.
28. Marchal, C., "Survey Paper: Chattering Arcs and Chattering Controls," *Journal of Optimization Theory and Applications*, Vol. 11, 1973, pp. 441 - 468.
29. Press, W. H., Flannery, B. P., Teukolsky, S. A., Vetterling, W. T., *Numerical Recipes, the Art of Scientific Computing*, Cambridge University Press, 1986.
30. Minzer, R. A., et al., "U. S. Standard Atmosphere, 1975 (COESA 1975)," Goddard Space Flight Center, NASA TR-459, 1975.
31. Calise, A. J., Moerder, D. D., "Singular Perturbation Techniques for Real Time Aircraft Trajectory Optimization and Control," NASA CR-3597.
32. Ardema, M. D., "Singular Perturbations in Flight Mechanics," NASA TM X-62, 380.
33. Kokotovic, P., Khalil, K. H., O'Reilly, J., *Singular Perturbation Methods in Control: Analysis and Design*, Academic Press, 1986.
34. Bryson, A. E., Ho, Y. C., *Applied Optimal Control*, Hemisphere Publishing Corp., 1968.
35. Junkins, J. L., "An Asymptotic Perturbation Method for Non-linear Optimal Control Problems," *AIAA Journal of Guidance, Control, and Dynamics*, Vol. 9, 1986, pp. 357 - 367.
36. Baldwin, J. F., Williams, J. H. S., "The Use of a Method of Perturbations in the Synthesis of Closed Loop Optimal Control Laws for Nonlinear Systems," *Automatica*, Vol. 5., 1969, pp. 357 - 367.
37. Prenter, P. M., *Splines and Variational Methods*, Wiley, 1975.
38. Bensoussan A., *Perturbation Methods in Optimal Control*, John Wiley & Sons, 1982.